Title

I) The Development of Deoxycytidine Kinase Inhibitors with Nanomolar Affinity and Improved Metabolic Stability, II) The Synthesis of Ferrocene-Containing Monomers and Biodegradable Polymers Using Azide-Alkyne Click Chemistry and Ring Opening Polymeri...

Author

Gipson, Raymond Marshall

Publication Date

2015

Peer reviewed|Thesis/dissertation

UNIVERSITY OF CALIFORNIA

Los Angeles

I) The Development of Deoxycytidine Kinase Inhibitors with Nanomolar Affinity and Improved Metabolic Stability

II) The Synthesis of Ferrocene-Containing Monomers and Biodegradable Polymers Using Azide-Alkyne Click Chemistry and Ring Opening Polymerization

A dissertation submitted in partial satisfaction of the

requirements for the degree of Doctor of Philosophy

in Chemistry

by

Raymond Marshall Gipson

2015

ABSTRACT OF THE DISSERTATION

I) The Development of Deoxycytidine Kinase Inhibitors with Nanomolar Affinity and Improved Metabolic Stability

II) The Synthesis of Ferrocene-Containing Monomers and Biodegradable Polymers Using Azide-Alkyne Click Chemistry and Ring Opening Polymerization

by

Raymond Marshall Gipson

Doctor of Philosophy in Chemistry

University of California, Los Angeles, 2015

Professor Caius Gabriel Radu, Co-Chair

Professor Miguel A. Garcia-Garibay, Co-Chair

Small molecule dCK inhibitors, in combination with pharmacological perturbations of de novo dNTP biosynthetic pathways, can eliminate acute lymphoblastic leukemia cells in animal models. Our group's previous lead dCK inhibitors had a short half-life in vivo. Part I of this dissertation presents the development of new dCK inhibitors with improved pharmacokinetic properties. Guided by crystal structures of dCK in complex with the lead compound and with derivatives, we delineated the sites of the inhibitor for modification. Crystal structure of the complex between dCK and the racemic mixture of our new lead compound indicated that the *R*-isomer is responsible for kinase inhibition. This was corroborated by kinetic analysis of the purified enantiomers, which showed that the *R*-isomer has >60-fold higher affinity than the *S*-isomer for dCK. This new lead compound has significantly improved metabolic stability, making

it a prime candidate for dCK-inhibitor based therapies against hematological malignancies and, potentially, other cancers.

Part II presents a strategy for functionalizing biodegradable polymers with ferrocene. Small molecule drugs containing ferrocene play an important role in current cancer research, as these novel chemotherapeutics possess redox activity and have the ability to quench damaging free radicals. Current drugs that quench free radicals have adverse side effects, and dosage limits render them less effective in radiotherapy. In the search of more potent and/or selective radioprotective agents, ferrocene functionalized monomers were synthesized via azide-alkyne "click" cycloaddition. Potentially environmentally friendly ferrocene-containing polycarbonates were synthesized via ring opening polymerization (ROP), and they were characterized via NMR spectroscopy, gel permeation chromatography (GPC), thermal analysis, and electrochemical studies.

The dissertation of Raymond Marshall Gipson is approved.

Anastassia Alexandrova

Tatiana Segura

Miguel A. Garcia-Garibay, Committee Co-Chair

Caius Gabriel Radu, Committee Co-Chair

University of California, Los Angeles

2015

For my parents, David and Donna Gipson

And for my wife, Sarah

TABLE OF CONTENTS

LIST OF FIGURES

PART ONE

CHAPTER ONE

CHAPTER TWO

APPENDIX THREE

LIST OF SCHEMES

PART ONE

CHAPTER TWO

PART TWO

CHAPTER ONE

LIST OF TABLES

LIST OF ABBREVIATIONS

dCK	Deoxycytidine kinase
dNTP	Deoxyribonucleotide triphosphate
dC	Deoxycytidine
dA	Deoxyadenosine
dG	Deoxyguanosine
ATP	Adenosine triphosphate
UTP	Uridine triphosphate
PK	Pharmacokinetic
PET	Positron emission tomography
^{18}F-L-FAC	^{18}F-L-1-(2'-deoxy-2'-fluoroarabinofuranosyl) cytosine
PD	Pharmacodynamics
PEG	Polyethylene glycol
MPEG	Methoxy polyethylene glycol
DIBAL-H	Diisobutylaluminum hydride
Rochelle's salt	Sodium potassium tartrate
CBS	Corey–Bakshi–Shibata
TFA	Trifluoroacetate
DMAP	4-(*N,N*-dimethylamino)-pyridine

ACKNOWLEDGEMENTS

I would like to begin by thanking my doctoral advisor Professor Caius Radu. His guidance and support has helped me in many ways. I am also very thankful for Professor Nagichettiar Satyamurthy's support and guidance. I would like to thank Professors Miguel Garcia-Garibay, Anastassia Alexandrova, and Tatiana Segura for being members of my committee. I also owe a great deal of thanks to my undergraduate research advisors for inspiring me to begin a career in chemistry.

Part One of this dissertation is an adaptation of Nomme, J.; Li, Z.; Gipson, R. M.; Wang, J. et al. *J. Med. Chem.* **2014**, *57*, 9480–9494. Julian Nomme and Prof. Arnon Lavie are responsible for protein expression and purification, kinetic assays, crystallization, X-ray data collection, and refinement. Julian Nomme and Prof. Arnon Lavie also composed the majority of this *J. Med. Chem*. article. Tony Smith and Prof. Anastassia Alexandrova were responsible for computer modeling results. The biology subgroup in the lab of Prof. Caius Radu performed the IC_{50} determinations, PET studies, and in vivo plasma pharmacokinetic assays. I would like to acknowledge Professors Johannes Czernin, Michael Jung, and Nagichettiar Satyamurthy for their expert advice. Part One's abstract is adapted from the abstract in this *J. Med. Chem*. article. The group of Arnon Lavie composed Chapter One of Part One. The Radu lab wrote the chemistry and biology sections in Chapter Two of Part One, but the Lavie lab composed the rest. The Lavie lab composed the conclusion chapter of Part One. I would like to thank Jue Wang for providing me with compound **11i** for the synthesis shown in Scheme 6 of this dissertation. Other members of the Radu lab's chemistry subgroup carried out steps *d*, *e*, and *f* shown in Scheme 1 of Part One. Compound **S24d** shown in Scheme 6 of Part One was provided by my lab-mates in the Radu lab. Finally, I would like to thank Amanda L. Armijo, Thuc Le, and Soumya Poddar for all of their hard work with biology assays. I would like to thank Prof.

Jennifer Murphy and Zheng Li for synthesizing compounds **1**–**8** shown in Part One of this dissertation.

Part Two is a version of Upton, B. M.; Gipson, R. M.; Duhovic, S.; Lydon, B. R.; Matsumoto, N. M.; Maynard, H. D.; Diaconescu, P. L. *Inorg. Chem. Front.* **2014**, *1*, 271–277. Selma Duhovic conducted the cyclic voltammetry and chronoamperometry experiments reported in Part Two of this dissertation. The Diaconescu lab was responsible for Density Functional Theory (DFT) calculations. Nicolas M. Matsumonto and Heather Maynard provided Gel Permeation Chromatography data for all of the polycarbonates in Part Two. I would like to thank Briana Upton and the Diaconescu lab for synthesizing additional cyclic carbonate monomers and polycarbonates on display in the *Inorg. Chem. Front*. article (additional structures and data not presented in this dissertation).

BIOGRAPHICAL SKETCH

EDUCATION

Master of Science, Chemistry, University of California, Los Angeles • 2012
GPA: 3.82 / 4.00

Bachelor of Science, Chemistry, Kent State University, *Kent, Ohio* • 2009
Summa Cum Laude with University Honors; GPA 3.90 / 4.00
Senior Honors Thesis: The Synthesis of Novel Thieno[3,2-*b*]thiopene-2-carboxylate Liquid Crystals
Advisors: Professor Paul Sampson and Professor Alexander Seed

EXPERIENCE

UNIVERSITY OF CALIFORNIA – LOS ANGELES • Sep 2009 – Present
Teaching Assistant • Sep 2009 – Present

- Instructed groups of undergraduates, including students in pre-professional programs (dentistry, medicine, pharmacy) and some chemistry majors.
- Assisted in the instruction of the following courses:
  - Thermodynamics, Electrochemistry, Kinetics, and Organic Chemistry
  - Structure of Organic Molecules
  - General and Organic Chemistry Laboratory II
  - Organic Chemistry I: Structure and Reactivity
  - Organic Chemistry II: Reactivity, Synthesis, and Spectroscopy
  - Organic Chemistry Laboratory I and II

Graduate Student Researcher • Feb 2010 – Present

- Conducted work in medical chemistry that revealed a new inhibitor of the enzyme deoxycytidine kinase with improved metabolic stability, laying groundwork for advances in treatment of leukemia.
- Synthesized precursor with goal of radiolabeling AZD7762, collaborating with group led by Prof. Tobias Ritter.
- Discovered and developed novel synthetic route for functionalization of polycarbonate polymers with ferrocene.

KENT STATE UNIVERSITY, *Kent, Ohio* • Feb 2006 – Jun 2009
Undergraduate Researcher • Jan 2007 – Jun 2009

- Synthesized novel liquid crystals containing thieno[3,2-*b*]thiopenes mesogen.
- Participated in Kent State University's NSF REU program during Summer of 2007.

Math and Chemistry Tutor • Feb 2006 – May 2009

- Provided supplemental assistance to undergraduates taking various courses, such as Calculus I and II, Intuitive Calculus, Modeling Algebra, Algebra for Calculus, Trigonometry, Fundamental Math Concepts I and II, General Chemistry, and Organic Chemistry.
- Tutored as an employee of Kent State University's Academic Success Center.

CENTER ON POLYMER INTERFACES AND MACROMOLECULAR ASSEMBLIES (CIPMA), *Stanford, California* • Summer 2008
NSF REU Intern

- Gained polymer chemistry experience in the group of Prof. Robert Waymouth at Stanford University.

VOLUNTEER EXPERIENCE

UNIVERSITY CATHOLIC CENTER AT UCLA, *Los Angeles, California*
RCIA Team • Oct 2014 – Present

- Supporting the Campus Minister during weekly two-hour classes

HONORS AND AWARDS

UCLA Department of Pharmacology Retreat, Best Poster Presentation – Group D, 2013
Lubrizol Scholarship for Chemistry, Kent State University, 2009
Gary and Cynthia Scarmuzzi Bengier Senior Honors Thesis Fellowship, 2008
Akron Section of the American Chemical Society, Outstanding Chemistry Major Award, 2008
Division of Research and Graduate Studies, Research Grant Recipient, Kent State University, 2007
Honors Academic Achievement Award, Kent State University, 2007
Trustee Scholarship, Kent State University, 2005

PUBLICATIONS

Nomme, J.; Li, Z.; **Gipson, R. M.;** Wang, J.; Armijo, A. L.; Le, T.; Poddar, S.; Smith, T.; Santarsiero, B. D.; Ngyuen, H.-A.; Czernin, J.; Alexandrova, A. N.; Jung, M. E.; Radu, C. G. ; Lavie, A. "Structure-guided development of deoxycytidine kinase inhibitors with nanomolar affinity and improved metabolic stability" *J. Med. Chem*. **2014**, *57*, 9480–9494.

Upton, B. M.; **Gipson, R. M.;** Duhovic, S.; Lydon, B. R.; Matsumoto, N. M.; Maynard, H. D.; Diaconescu, P. L. "Synthesis of Ferrocene-Functionalized Monomers for Biodegradable Polymer Formation." *Inorg. Chem. Front*. **2014**, *1*, 271–277.

Gipson, R. M.; Sampson, P.; Seed, A. J. "The Synthesis and Mesogenic Behavior of the First Series of Low Molar Mass Thieno[3,2-b]thiophene-2-Carboxylate Ester-Based Mesogens." *Liq. Cryst.* **2010**, *37,* 101–108.

PART ONE

The Design and Development of Improved Deoxycytidine Kinase Inhibitors

Adapted from: Julian Nomme,* Zheng Li,* Raymond M. Gipson,* Jue Wang,* Amanda L. Armijo, Thuc Le, Soumya Poddar, Tony Smith, Bernard D. Santarsiero, Hien-Anh Nguyen, Johannes Czernin, Anastassia N. Alexandrova, Michael E. Jung, Caius G. Radu, and Arnon Lavie

J. Med. Chem. **2014**, *57*, 9480–9494.

CHAPTER 1: INTRODUCTION

1.1 Background

Deoxycytidine kinase (dCK) is a deoxyribonucleoside kinase capable of phosphorylating deoxycytidine, deoxyadenosine, and deoxyguanosine to their monophosphate forms using either ATP or UTP as phosphoryl donors.[1] Phosphorylation by dCK is responsible for converting salvaged deoxycytidine into deoxycytidine monophosphate (dCMP), a precursor for both dCTP and dTTP pools. Apart from the physiological role of generating dNTPs, dCK plays a crucial role in activating multiple nucleoside analog prodrugs that are widely used in anticancer and antiviral therapy.[2] Recently, we[3,4] and others[5] identified a requirement for dCK in hematopoiesis in lymphoid and erythroid progenitors. The kinase has also been implicated in regulating the G2/M transition in response to DNA damage in cancer cells.[6] More recently, we have shown that partial inhibition of dCK activity, combined with perturbations of nucleotide de novo synthesis pathways, was synthetically lethal to acute lymphoblastic leukemia cells but not to normal hematopoietic cells.[7] These aspects of dCK's biology, and its potential role as a new therapeutic target in cancer, prompted us to develop small molecule inhibitors of its enzymatic activity.

In earlier publications[8,9] we reported the discovery of hit compounds from a high

throughput screen and subsequent optimization of the molecules to lead compounds **1** and **2** (numbered **36** and **37**, respectively, in ref 8). Lead compounds **1** and **2** can be divided into four distinct structural parts (Figure 1A). Part A is the pyrimidine ring, which is connected by a linker (part B) to a 5-subsituted-thiazole ring (part C), which in turn is connected to a phenyl ring (part D). Conceptually, each of these parts can be modified to attain desired "druglike" properties. In previous work, we focused on the thiazole portion of the inhibitor. The crystal structure of dCK with one of the early compounds suggested that the ring 5-position could accommodate hydrophobic substituents, which led to the discovery that a propyl group at the 5-position is strongly favored over a methyl group.[8,9]

To guide and rationalize the medicinal chemistry efforts in other parts of the molecule, we solved the crystal structures of human dCK with several of the inhibitors we developed. The crystal structures illuminate the relationship between the enzyme structure, the small molecule structure, and its inhibition potency. The beginning of Part One will report the in vitro binding affinities (IC_{50}^{app} and K_i^{app}), cellular IC_{50} values, and crystal structures of dCK in complex with compounds that differ in the pyrimidine and phenyl rings. Unfortunately, despite nanomolar affinity for dCK, when tested in a liver microsomal assay, these compounds exhibited low metabolic stability (data not shown). This shortcoming was recapitulated by pharmacokinetic studies in mice.[7,8]

To identify inhibitors with improved in vivo properties, we set out to explore additional chemical modifications, specifically, those that maintain the low nanomolar binding affinity of the lead compounds. Part One will report novel chiral derivatives of our inhibitors. Crystal structures of these chiral compounds bound to dCK played a key role in elucidating the chirality of the active form of the inhibitor. By combining organic chemistry intuition with detailed structural information on the target−inhibitor complex, we have identified a lead compound that retains the nanomolar affinity for dCK but has gained significant in vivo metabolic stability. This compound could play a vital role in any therapeutic strategy based on induction of DNA replication stress

overload by perturbing a cancer cell's dNTP pools.

A

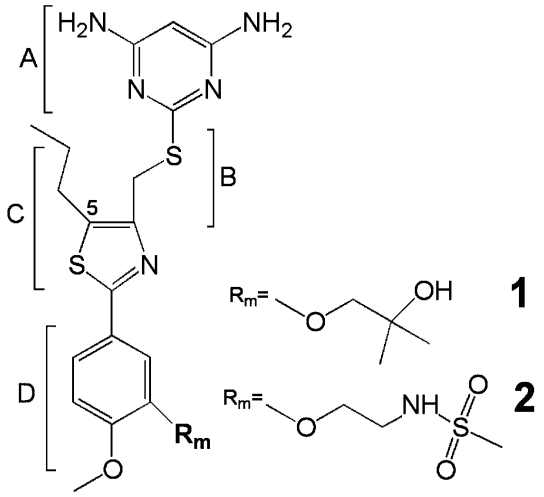

B

Compound	Steady state kinetics IC_{50}^{app} (nM)	K_i^{app} (nM)	CEM cells IC_{50} (nM)
1	14.5 ± 2.8	0.8 ± 0.7	1.4
2	14.1 ± 3.0	0.5 ± 0.5	4.9

Figure 1. dCK inhibitor lead compounds. (A) Schematic representation of lead compounds **1** and **2**. These compounds are composed of four parts. Part A indicates the pyrimidine ring, and part B is the linker connecting to a 5-substituted-thiazole ring (part C), which is followed by a phenyl ring (part D). Compounds **1** and **2** differ at the substituent present at the phenyl meta position (R_m). (B) In vitro (IC_{50}^{app} and K_i^{app}) and cell (IC_{50}) properties for **1** and **2**.

1.2 Optimizing the Interaction of the Inhibitor's Pyrimidine Ring with dCK

The pyrimidine ring (part A of the molecules, Figure 1A) was predicted to be the part of the molecule most difficult to improve. This is because, as observed in the crystal structures of dCK in complex with lead compounds **1** and **2** (PDB codes 4L5B and 4KCG, respectively), the inhibitor's pyrimidine ring binds to dCK at a position nearly identical to that adopted by the pyrimidine ring of the physiological substrate dC, making several hydrogen bonds, hydrophobic, and π−π stacking interactions (Figure 2A). This binding mode suggested an already quite optimized enzyme−pyrimidine ring interaction. For compounds **1** and **2**, both pyrimidine ring exocyclic amino groups formed hydrogen-bonding interactions with side chains of Glu53, Gln97,

and Asp133. Hence, not surprisingly, simultaneous removal of both amino groups resulted in complete loss of dCK inhibition.[8] In contrast, removal of a single amino group to generate compound **3** (Figure 2B), which is identical to **1** except for having a single exocyclic amino group in the pyrimidine ring (Figure 1A), resulted in similarly tight binding affinity as measured for **2** (Figures 1B and 2C). To explain how the affinity of **3** for dCK is maintained with only a single exocyclic amino group, we sought the crystal structure of the complex, but unfortunately, we were unable to obtain diffraction quality crystals. We speculate that the sole exocyclic amino group present in compound **3** is oriented in the dCK active site such that it maintains its interaction with Asp133, since only in that orientation can the neighboring pyrimidine ring nitrogen atom maintain its interaction with the side chain of Gln97 (Figure 2D). The conclusion here is that the interaction with Glu53 made by an exocyclic amino group, when present, provides only moderate additional binding energy. While a single exocyclic pyrimidine ring amino group is sufficient for a tight interaction with dCK, in our CEM cell-based assay, compound **3** exhibited a much-increased IC_{50} value (21.8 nM, Figure 2C) relative to compound **2** (4.9 nM, Figure 1B). This result showcases the importance of evaluating the interaction between an inhibitor and its target in using both an enzymatic in vitro assay and a cell-based assay. Because of the reduced inhibition of dCK activity of **3** in the cell-based assay, all future compounds contained the two exocyclic amino groups.

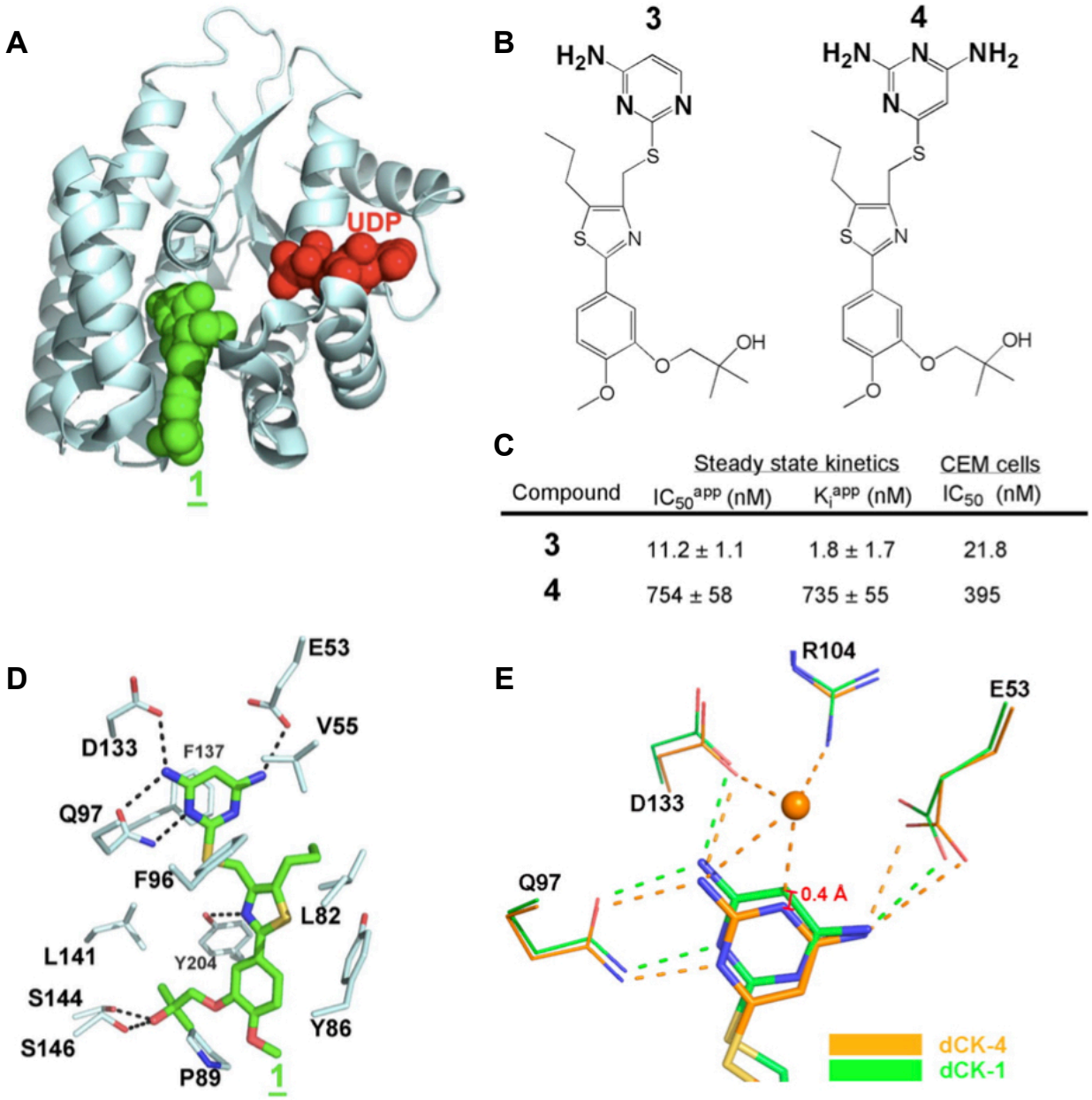

Figure 2. Modifications to the pyrimidine ring. (A) Ribbon diagram of a dCK monomer (light blue) with the observed molecule of **1** bound (green spheres) at the active site (PDB ID 4L5B). The nucleotide UDP (red) was also present in the complex. (B) Schematic representation of compound **3** that has a single exocyclic amino group, and of compound **4** that has a ring nitrogen atom between the two exocyclic amino groups. (C) In vitro (IC_{50}^{app} and K_i^{app}) and cell (IC_{50}) properties for **3** and **4**. (D) The interactions between **1** and dCK. dCK residues contributing to the interaction with **1** (green sticks) are represented as light blue sticks. Polar interactions are indicated as broken black lines. (E) Overlay of the dCK–**4** (orange, PDB code 4Q18) and dCK-**1** (green, PDB code 4L5B) structures with a focus on the pyrimidine ring. Note the ~0.4 Å shifted position of **4** relative to **1** that is due to the presence of a water molecule (orange sphere). Binding of this water molecule is made possible by the ring nitrogen atom in compound **4**.

Next, we assessed the importance of the position of the pyrimidine ring nitrogen atoms by synthesizing compound **4** (Figure 2A). This compound was measured to bind with ~50-fold

higher IC_{50}^{app} relative to the very similar lead compound **1** (Figure 1A), which only differs in the position of one pyrimidine ring nitrogen atom. We solved the 2.0 Å resolution crystal structure of the dCK−**4** complex to understand how this subtle change so drastically impacted the interaction with the enzyme (see Appendix 1 for the data collection and refinement statistics).

All of the examined compounds bind to the open state of the enzyme, which is also the catalytically incompetent state[10,11]. Inhibitors bind within a deep cavity, with the pyrimidine ring of the inhibitors positioned deepest and occupying the same position occupied by the pyrimidine ring of the nucleoside substrate.[8,9] While preventing the binding of the nucleoside substrate, our inhibitors do not interfere with binding of nucleotide to the phosphoryl donor-binding site. In fact, all crystal structures of dCK in complex with inhibitors also contained UDP at the donor site.

Despite significantly different IC_{50}^{app} values between compound **1** (14.5 nM) and compound **4** (754 nM), the pyrimidine ring of these related molecules interacts with the enzyme via very similar hydrophobic and polar interactions. The latter include Glu53, Gln97, and Asp133. However, the entire molecule **4** is displaced about 0.4 Å away from the floor of the binding cavity relative to compound **1** (Figure 2E). The crystal structure suggests that the factor responsible for this shift is the recruitment of a water molecule (orange sphere, Figure 2E) by the pyrimidine ring N present in compound **4**. In contrast, for compound **1** the CH group in this position eliminates the potential for a hydrogen bond. This water molecule is also held in place through interactions with Arg104 and Asp133. Hence, despite formation of this additional water-mediated interaction with the enzyme, the displacement away from the enzyme caused by allowing the water molecule to bind at that position ultimately reduces the binding affinity of **4**.

On the basis of these results, we decided to maintain the original structure of the pyrimidine ring and to focus on the other parts of the molecule as potential modification sites. We next examined the effect of various substituents at different phenyl group positions (part D of the molecule, Figure 1A).

1.3 Increasing Binding Affinity at the Phenyl Meta Position

Previously, we reported that a compound with no phenyl ring substituents, but otherwise identical to compound **1**, showed very modest potency in our CEM cell based assay (IC_{50} = 37 nM[8]). Adding a hydroxyl group at the meta position decreased the IC_{50} in that assay by about half (compound **5**, previously compound **31**,[3] Figure 3). The effect of adding the longer hydroxyethoxy group at that position (compound **6**, previously compound **32**[3]) was more impressive, yielding an IC_{50} of ~1 nM (Figure 3). We are aware that primary hydroxyls as in **6** are prone to oxidation or glucuronidation,[12] but these studies do inform us as to the importance of the type of substituent at the phenyl meta position.

A

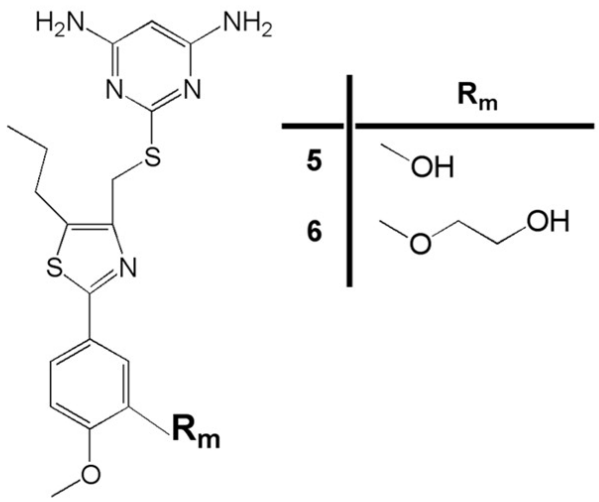

B

Compound	Steady state kinetics IC_{50}^{app} (nM)	Steady state kinetics K_i^{app} (nM)	CEM cells IC_{50} (nM)
5	26.1 ± 4.0	8.9 ± 0.9	18.6
6	14.6 ± 3.6	0.5 ± 0.4	1.15

C

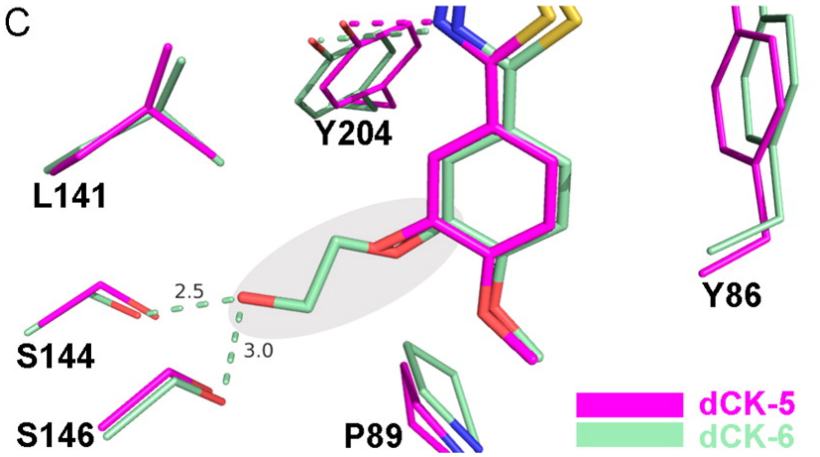

Figure 3. Modifications to the phenyl ring meta position. (A) Schematic representation of compounds **5** and **6** that differ by the nature of the meta position substituent. (B) In vitro (IC_{50}^{app} and K_i^{app}) and cell (IC_{50}) properties for **5** and **6**. (C) Overlay of the dCK−**5** (magenta, PDB code 4Q19) and dCK−**6** (pale green, PDB code 4Q1A) structures with a focus on the phenyl ring meta position. The tighter binding of **6** relative to **5** can be rationalized by the interaction of the longer meta substituent (position highlighted with a gray background) with S144/S146 of dCK.

To understand the difference in affinities to dCK between compounds **5** and **6**, we determined the structures of dCK in complex with these molecules, solved at 2.09 and 1.9 Å resolution, respectively (Appendix 1). The structure of dCK in complex with compound **5** reveals

that the hydroxyl group at the phenyl group meta position does not make any inhibitor−enzyme interactions. In contrast, the structure of dCK in complex with compound **6** shows that the hydroxyethoxy at this position is able to interact with the side chains of Ser144 and Ser146 (Figure 3C). We attribute this added interaction to the superior binding of compound **6** versus compound **5**.

In terms of the importance of substituents at the phenyl meta position, it is clear that having none or a short one such as a hydroxyl (compound **5**) diminishes the interaction with dCK. On the other hand, the binding affinity measured by both the in vitro kinetic assay and by the cell-based CEM assay of larger substituents (as present in compounds **1**, **2**, and **6**) are comparable. Previous crystal structures of dCK in complex with compound **1** (PDB code 4L5B) and **2** (PDB code 4KCG) also show an interaction between the substituent at the phenyl meta position and the enzyme, this time to Ser144. Additional side chains such as 2-fluoroethoxy poly(ethylene glycol) (n=2) $(PEG)_2$ (**S16**, **S17**, **S19**), 2-hydroxyethyl $(PEG)_2$ (**S11**), 2-methoxyethyl $(PEG)_2$ (**S20**, **S22**, **S23**, **S25−S29**), and 2-(4,6-diaminopyrimidine-2-thio)ethyl $(PEG)_2$ (**S10**) substituents were well tolerated at the meta position (see Appendix 2 for data).

We conclude that the precise nature of the substituent at the phenyl meta position is not critical as long as it contains a polar group that can extend to the proximity of Ser144/Ser146.

1.4 The Substituent at the Phenyl Group Para Position Plays a Minor Role in Binding

To determine the importance of substituents at the phenyl group para position, we prepared compound **7** (previously compound **28**[3]), which only differs from compound **2** by lacking a para position substituent (Figure 4A). The in vitro measured binding affinity values (IC_{50}^{app}; K_i^{app}) of compound **7** are nearly identical to that of **2** (Figure 4B), indicating that substituents at the para position are not required for tight binding. This is explained by the crystal structures of dCK in complex with compounds **7** and **8** (previously compound **30**[3]), which show a nearly identical binding mode, very similar to that observed for compound **2** (Figure 4C).

The crystal structures also reveal that no significant inhibitor−enzyme interactions occur via the para substituent, if present. This conclusion is supported by the properties of compound **8**, which in contrast to the methoxy group in compounds **1** and **2** has the longer hydroxyethoxy group but similar binding affinity. Hence, the in vitro binding affinities are largely unchanged between having no substituent at the phenyl group para position, having a methoxy, or the longer hydroxyethoxy. However, we did notice a ∼10-fold difference between compounds **7** and **8** in the CEM cell-based assay, with compound **7** being less potent. Furthermore, substituents at the phenyl ring's para position such as 2-fluoroethoxy (**S4**, **S14**, **S18**), fluoro (**S5**, **S6**), methoxymethyl terminated $(PEG)_2$ (**S21**, **S24**), and N-substituted methanesulfonamide (**S29**, **S30**) were relatively well tolerated (Appendix 2). Groups attached to the thiazole like 4-pyridinyl (**S7**), meta monosubstituted phenyl (**S17**), and 3,5-disubstituted phenyl ring (**S31**) substituents were also tolerated (Appendix 2). Therefore, while not directly important for the binding affinity, having even a small substituent at the phenyl group para position improves the relevant cell-based measurements. As a result, most subsequent compounds contained the methoxy group at that position.

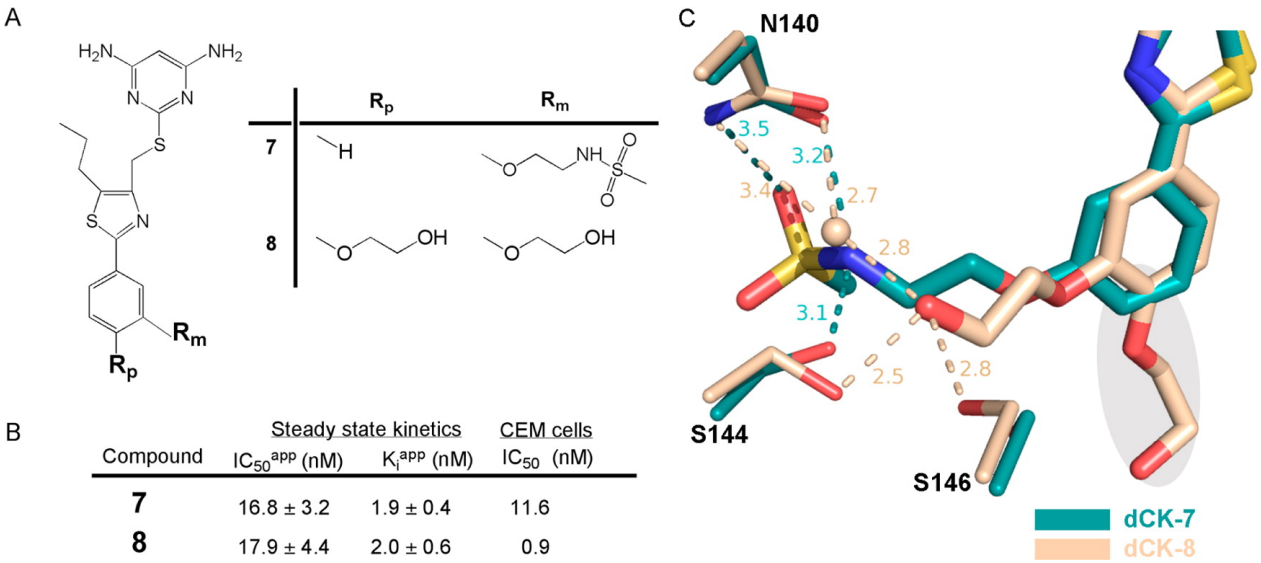

Figure 4. Modifications to the phenyl ring para position. (A) Schematic representation of compounds **7** and **8** that differ by the nature of the para position substituent. (B) In vitro (IC_{50}^{app} and K_i^{app}) and cell (IC_{50}) properties for **7** and **8**. (C) Overlay of the dCK−**7** (teal, PDB code 4Q1B) and dCK−**8** (beige, PDB code 4Q1C) structures with a focus on the phenyl ring para position. The inhibitors bind very similarly; the meta position substituents make a direct interaction with the enzyme, but the para substituent does not. The very similar IC_{50}^{app} and K_i^{app} values of **7** and **8** are explained by the lack of direct interactions to the enzyme via the para position. In contrast, the presence of a para position substituent lowers the cell-based determined IC_{50} value.

Table 1: Human Microsomal Intrinsic Clearance Assay.[a]

Compound	NADPH-dependent C_{lint}[a] (μL min^{-1} mg^{-1})	NADPH-dependent $T_{1/2}$ (min)	Comment
Verapamil	201	11.5	High clearance control
Warfarin	0	>240	Low clearance control
1	561	4.1	
2	870	2.7	
15a (Murphy et al.)	142	16.3	
9 (**R/S**)	419	5.5	
10 (**R/S**)	254	9.1	
12R	22.7	102	

[a]Test concentration of compounds was 1 μM

1.5 The Nature of the Thiazole Ring Substituent Dictates Metabolic Stability

In previous work we demonstrated that the nature of the substituent at the thiazole ring 5-position (part C of the molecule, Figure 1A) plays a crucial role in binding affinity.[9] In short, we compared having no substituent at that position to having a methyl, ethyl, or propyl. We found that propyl dramatically improved the binding affinity, and as a result, compounds with a propyl at the 5-position became our lead compounds (i.e., compounds **1** and **2**, Figure 1). Interestingly, compounds with a small/no substituent at the thiazole 5-position were observed to bind two inhibitor molecules per dCK active site, to binding sites that we refer to as position 1 and

position 2. In contrast, the tighter binding propyl-containing molecules were observed to bind with a single inhibitor molecule, at position 1, per dCK active site.[9] This revealed that binding of two molecules is not required for high affinity. In our previous report, we analyzed the implication of single versus double binding of inhibitor molecules to dCK and concluded that inhibition of dCK is primarily caused by the binding of the inhibitor at position 1, whereas the molecule bound at position 2 does not appreciably enhance the inhibition.

However, when tested for metabolic stability, we discovered that the propyl-group-containing compounds **1** and **2** are less stable relative to those having the shorter methyl group, e.g., compound **15a** as reported by Murphy et al. (Table 1). We also explored the activity of cyclopropyl and phenyl groups at the thiazolyl 5-position (Appendix 2). The cyclopropyl analog (**S27**) had a good IC_{50} value, but it failed in the PET L-FAC assay.[8] The phenyl analog (**S28**) demonstrated poor affinity. Hence we were forced to revert to the methylthiazole ring substituent despite a weaker interaction with dCK. To compensate for the loss of affinity provided by the thiazole propyl group, we searched for a compensating modification that would restore the in vitro binding affinity while maintaining acceptable metabolic stability. For that purpose, we decided to explore modifications on the linker moiety (part B of the compounds, Figure 1A).

CHAPTER 2: RESULTS AND DISCUSSION

2.1 Chemistry of Racemic Linker Modified Compounds

The $-SCH_2-$ group acts to link the pyrimidine and thiazole rings of our compounds. We tested a variety of alternatives to this linker, such as its deuterated analog ($-SCD_2-$), for the purpose of a kinetic isotope study. We reasoned that if the linker was implicated in hydrolytic metabolism, then, because of the kinetic isotope effect, a deuterated ($-SCD_2-$) analog would show an improvement in metabolic stability. The deuterium analogs (**S1**, **S8**, **S9**, **S13**) had affinity similar to their isotopologues, as expected (Appendix 2). However, the deuterated compounds failed to show an improvement in the PET L-FAC liver assay, indicating that a hydrolytic mechanism is probably not involved in the metabolism of the $-SCH_2-$ linker. We also tested the replacement of the sulfur atom of the $-SCH_2-$ group with a methylene group ($-CH_2CH_2-$). Replacing the sulfur atom of the linker with a carbon atom resulted in a considerable decrease in dCK affinity and metabolic stability (**S15**, Appendix 2). We next tested a linker in which the methylene was substituted to contain a methyl group ($-SCH(CH_3)-$). These racemic methyl-linker compounds showed very promising biological results and increased metabolic stability (see Section 2.7 for synthesis and Appendix 2 for data). Therefore, we carefully examined the synthetic route in an attempt to reduce the synthetic steps and improve the total yield. We succeeded in developing a six-step synthetic route toward **11** in an overall yield of 43% (Scheme 1). Commercially available 3-hydroxy-4-methoxybenzonitrile **11a** was subjected to an aqueous ammonium sulfide solution under basic conditions to provide thioamide **11b**. Cyclization to form the thiazole core of **11c** was achieved via condensation of thioamide **11b** with 4-bromopentane-2,3-dione[13] in refluxing ethanol. Introduction of a PEG chain into the phenyl ring of compound **11d** with 13-chloro-2,5,8,11-tetraoxatridecane[14] under basic conditions was achieved in 89% yield. Reduction of the resulting ketone-containing compound with diisobutylaluminum hydride (DIBAL-H) afforded racemic secondary alcohol **11e** in high yield. Alcohol **11e** was converted to the respective chloride **11f** with thionyl chloride. The chloride was

reacted in crude form with 4,6-diamino-2-mercaptopyrimidine to generate product **11R/S**.

Scheme 1. Synthetic Route for Methyl Linker Compound **11** (R/S)[a]

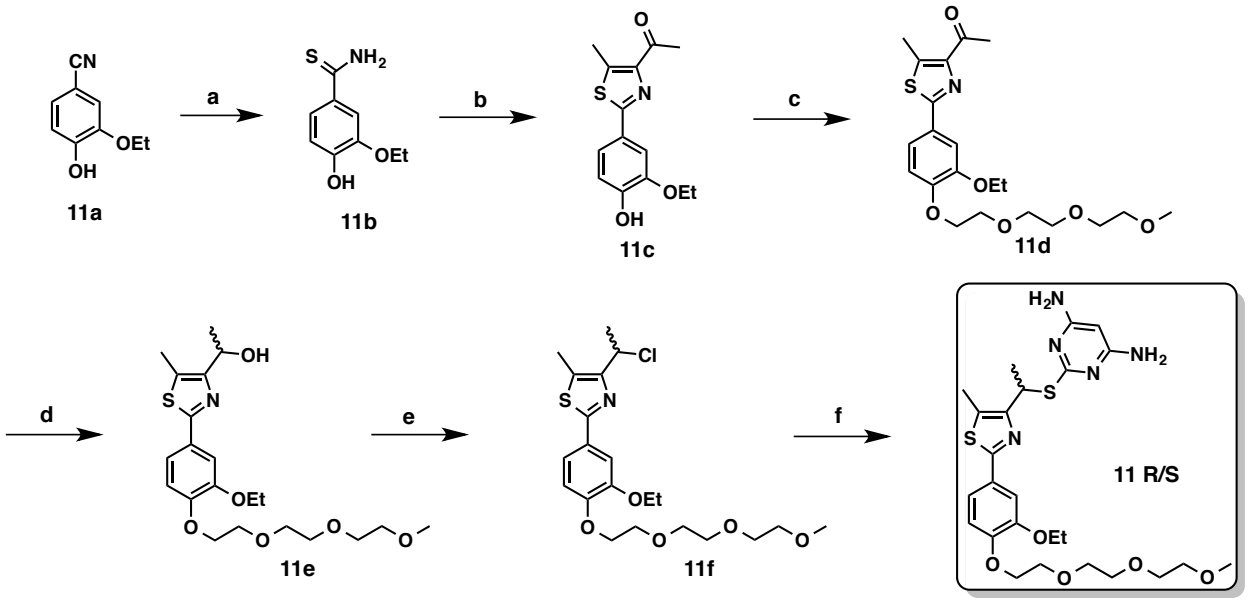

[a]Reagents and conditions: (a) $(NH_4)_2S$ (20% in H_2O), pyridine, Et_3N, 60 °C, 85%; (b) 4-bromopentane-2,3-dione, Ethanol, reflux, 95%; (c) 13-chloro-2,5,8,11-tetraoxatridecane, cesium carbonate, *N*,*N*-dimethylformamide, 50 °C, 89%; (d) Diisobutylaluminium hydride, dichloromethane, −78 °C, 92%; (e) $SOCl_2$, dichloromethane, 0 °C to rt; (f) 4,6-diamino-2-mercaptopyrimidine, K_2CO_3, *N*,*N*-dimethylformamide, 75 °C, 65% over two steps.

2.2 The Chirality of the Linker Methyl Group as a Determinant of Binding Affinity

The −SCH(CH_3)− linker was introduced to a compound that contained the propyl group at the thiazole ring 5-position (compound **9**) and to a compound that, instead of the propyl group, contained a methyl (compound **10**) (Figure 5A). As mentioned above, the rationale for compound **10** was the predicted improvement in metabolic stability. Interestingly, whereas compounds with a propylthiazole ring previously showed tighter binding to dCK compared to the analogous methylthiazole compounds, we now measured better binding with the methyl-containing compound **10** to the propyl-containing compound **9** (Figure 5B). Hence, the proximity of the thiazole-ring substituent (propyl or methyl) to the methyl-linker substituent resulted in the larger propyl group being not as accommodating in the dCK active site. Despite the improved in vitro binding parameters for **10** over **9**, the cell-based assay yielded similar IC_{50} values, yet consistent with **10** being superior (Figure 5B).

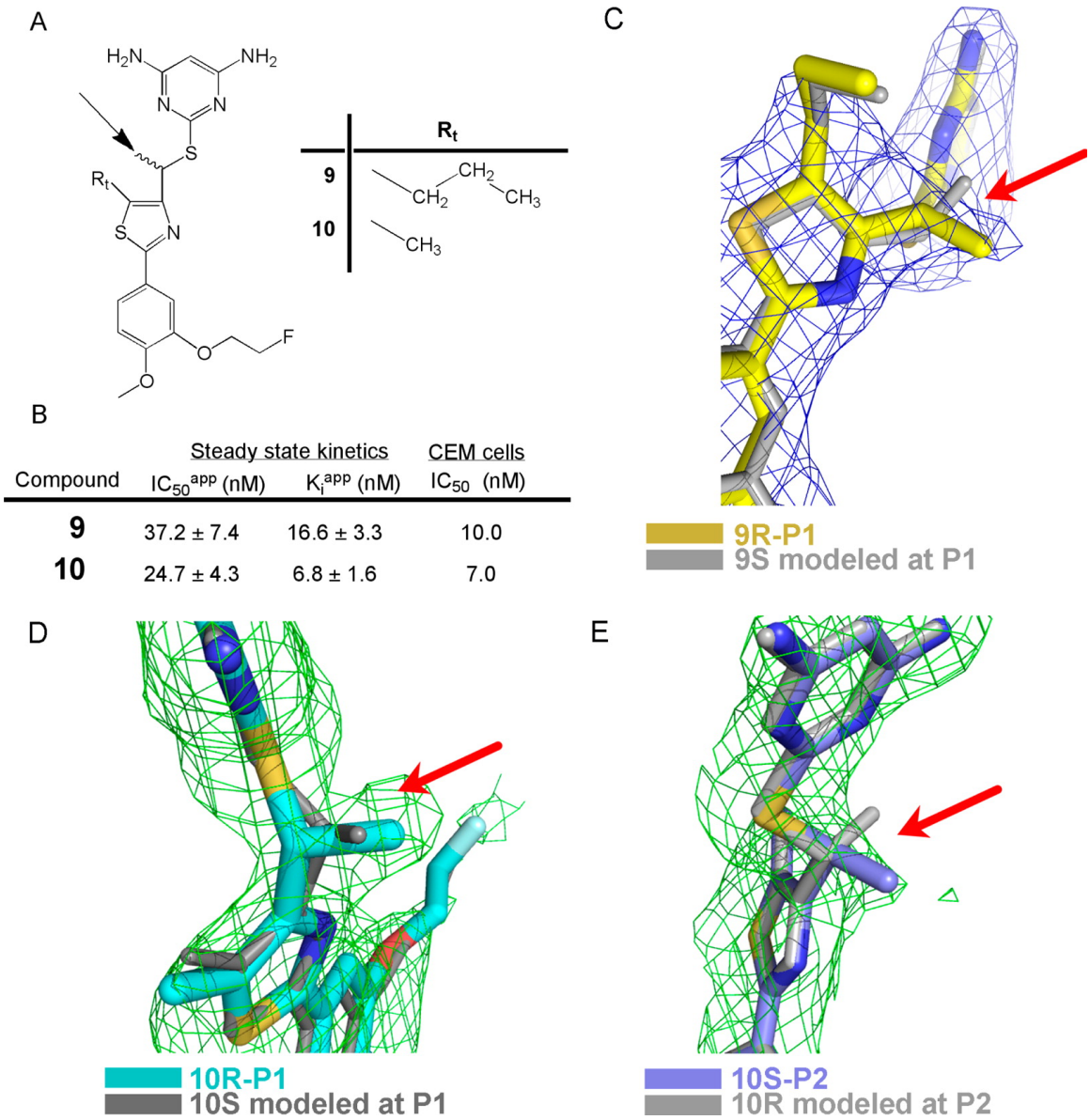

Figure 5. Modifications to the linker. (A) Schematic representation of compounds **9** and **10**. Both compounds were synthesized as the racemic mixture (R/S); the addition of a methyl group (arrow) to the methylene linker group makes these compounds chiral. Whereas **9** has a propyl group at the thiazole ring 5-position (R_t), **10** has a methyl group. (B) In vitro (IC_{50}^{app} and K_i) and cell (IC_{50}) properties for **9** and **10**. (C) The propyl group at the thiazole ring makes **9** bind as a single molecule to binding site position 1 of dCK (see text for details). Notably, despite forming the enzyme−inhibitor with racemic **9**, in the crystal structure we observe only the *R*-isomer (compound **9** in yellow, PDB code 4Q1D, $F_o - F_c$ omit map in blue contoured at 2σ). A theoretical model of the *S*-isomer (gray) demonstrates that only the *R*-isomer fits the electron density. (D) The methyl group at the thiazole ring permits two molecules of **10** to bind to dCK: one to position 1 and one to position 2. In position 1 we observe only the *R*-isomer (**10R**-P1, cyan, PDB code 4Q1E; $F_o - F_c$ omit map contoured at 2σ in green). A theoretical model of the *S*-isomer at position 1 (gray) clearly demonstrates that only the *R*-isomer fits the electron density (red arrow). (E) In position 2 we observe only the *S*-isomer (**10S**−P2, plum, PDB code 4Q1E; $F_o - F_c$ omit map contoured at 1.5σ in green). A theoretical model of the *R*-isomer at position 2 (gray) clearly demonstrates that only the *S*-isomer fits the electron density (red arrow).

Both compounds **9** and **10** were prepared as racemic mixtures; the introduced linker-methyl group makes that position a new chiral center (arrow, Figure 5A). To elucidate which of the two enantiomers is the active dCK inhibitor, we determined the crystal structure of dCK in complex with compounds **9** and **10** (solved at 2.0 and 1.85 Å resolution, respectively, Appendix 1). As expected, compound **9** binds as a single molecule to dCK, specifically at position 1, because of the presence of the propyl group in the thiazole ring. Interestingly, despite the fact that a racemic mixture of **9** was used to form the complex to dCK, the crystal structure provides unambiguous evidence for the *R*-isomer binding at position 1 (Figure 5C and Figure 6). Likewise, inspection of the structure of the complex between racemic **10** and dCK shows that the *R*-isomer occupies the most relevant position 1 binding site (Figure 5D and Figure 6). Since compound **10** contains the methyl substituent in the thiazole ring, which allows for a molecule to also occupy position 2, we observe compound **10** at that position as well. However, whereas it is the *R*-isomer of **10** that binds to position 1, it is the *S*-isomer that binds to position 2 (Figure 5E and Figure 6).

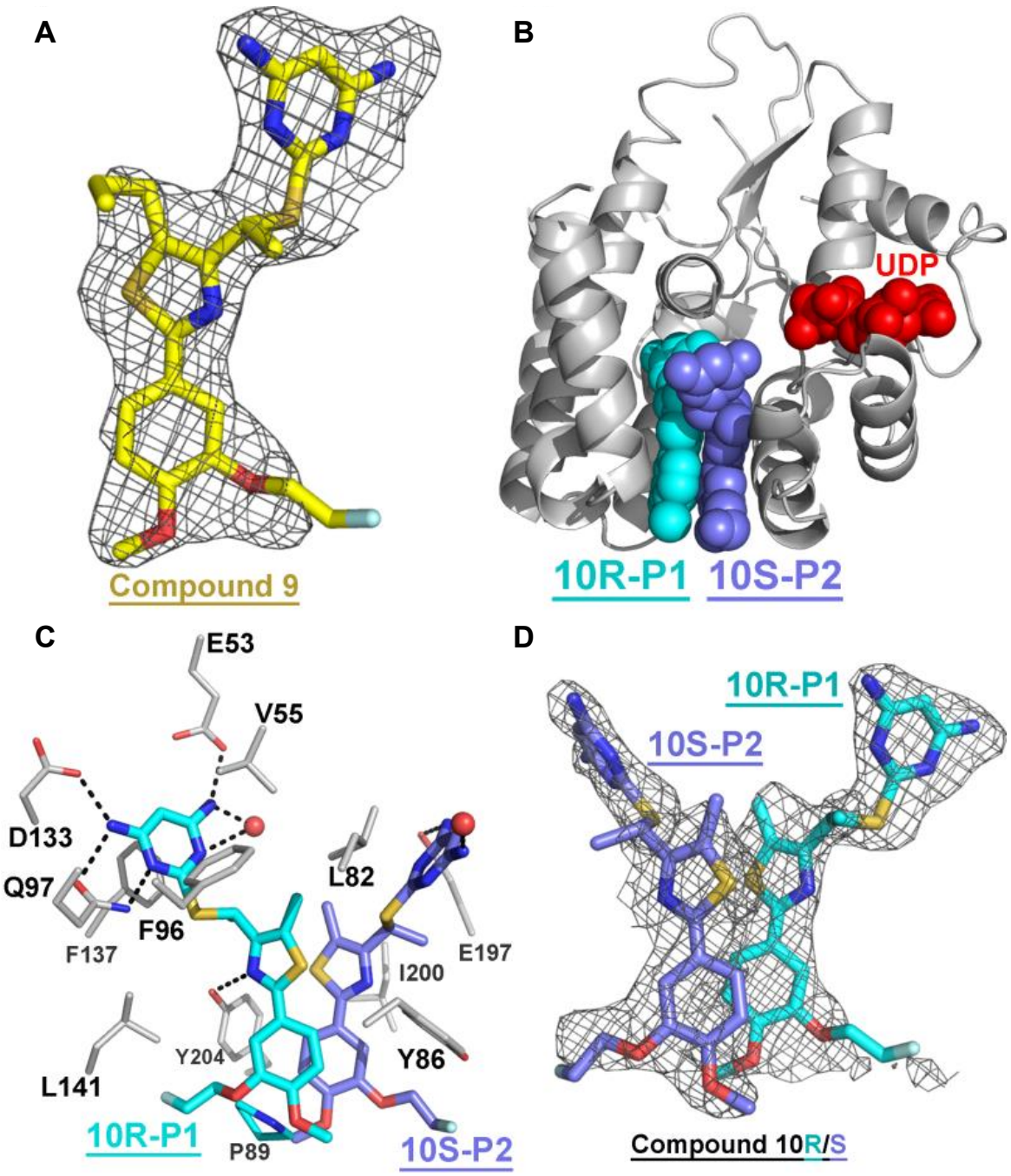

Figure 6. F_o-F_c map contoured at 2.0 sigma around compounds **9** and **10** from protomer A and binding of **10** to human dCK. A) Compound **9** was removed from the model that then underwent several rounds of refinement to eliminate model bias (PDB ID 4Q1D). B) Ribbon diagram of a dCK monomer (light gray) with the observed molecules of **10** bound at the active site (cyan and plum spheres). This inhibitor binds two molecules at the active site of dCK. Due to the presence of a chiral carbon within the linker and the use of a racemic mixture, we observe the *R* enantiomer binding at Position-1 (**10R**-P1 in cyan) and the *S* enantiomer binding at Position-2 (**10S**-P2 in plum), (PDB ID 4Q1E). The nucleotide UDP (red) was also present in the complex. C) The interactions between **10R** and **10S** and dCK. dCK residues contributing to the interaction with **10** (**10R** and **10S** as cyan and plum sticks respectively) are represented as light gray sticks. Polar interactions are indicated as broken black lines. D) Same as A) for compound **10**.

We previously concluded that position 1 is the critical binding site for this family of inhibitors. This would suggest that the measured in vitro inhibition values of racemic **10** are reflecting the preferential binding of the *R*-isomer. To test this, we synthesized compound **11**, which is a slight modification of **10** (the nature of the phenyl group substituents) but notably had the racemic mixture separated to yield the pure isomers **11R** and **11S** (Figure 7A). We determined the in vitro binding affinities of the enantiomerically pure compounds and observed that **11S** has ~400-fold weaker binding affinity relative to **11R** (Figure 7B). This result provides clear evidence that the *R*-form is responsible for the tight interaction with dCK. This result also validates our structure-based interpretation that position 1 is the one most relevant inhibitor binding site for dCK inhibition and that position 2 is occupied because of the high concentration of the inhibitor used in the crystallization setups.

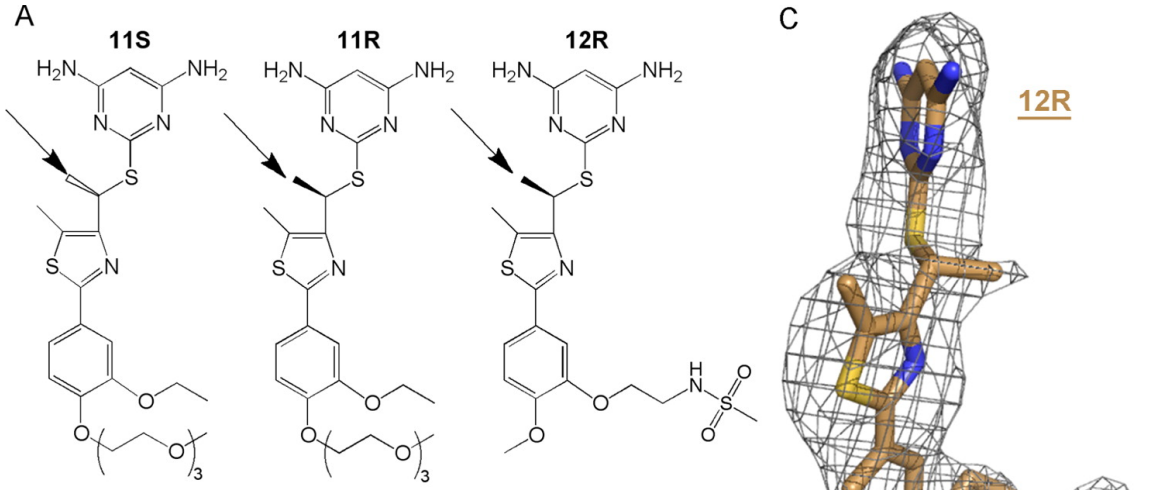

B

Compound	Steady state kinetics IC_{50}^{app} (nM)	Steady state kinetics K_i^{app} (nM)	CEM cells IC_{50} (nM)
11S	5632 ± 785	5607 ± 781	429.5 ± 34.1
11R	31.7 ± 4.1	14.0 ± 1.5	1.25 ± 0.09
12S	605 ± 108	585 ± 104	94.0 ± 14.4
12R	27.8 ± 3.5	9.2 ± 1.1	3.7 ± 0.8

Figure 7. The *R*-isomer is the relevant isomer regarding dCK inhibition. (A) Schematic representation of compounds **11S**, **11R**, and **12R** (*R* or *S* designate the chirality of the linker methylene carbon; arrows point at the added methyl group). (B) In vitro (IC_{50}^{app} and K_i^{app}) and cell (IC_{50}) properties for **11S**, **11R**, and **12R**. The *R*-isomer of both **11** and **12** is responsible for the observed inhibition of the enzyme. (C) dCK was crystallized in the presence of enantiomerically pure **12R**, and the enzyme−inhibitor complex structure was solved (PDB code 4Q1F). F_o−F_c omit map (1.6σ) for the position 1 binding site clearly shows the presence of **12R** (brown). Despite the thiazole methyl

group in **12R** (which is compatible with molecules also binding to position 2), we do not observe a second **12R** molecule at position 2. This is consistent with the results with compound **10** (Figure 5) that showed that only the *S*-isomer binds to positon 2.

2.3 Enantioselective Synthesis of Chiral Molecules

Having discovered that the *R*-isomers of compounds **9**, **10**, and **11** are responsible for the dCK inhibition, we set out to develop an asymmetric synthesis (Scheme 2). The chiral synthesis developed by our group for compound **12R**, which is a close analog of **10**, features a chiral Corey−Bakshi−Shibata (CBS) reaction of ketone **12d**. Chiral alcohol **12e** was synthesized according to this method with an enantiomeric excess of 96%, as determined via chiral HPLC. Employing mesic or tosic anhydride to give the sulfonates under different basic conditions such as Et_3N, pyridine, or DMAP resulted in elimination to the alkene, presumably due to the stability of the secondary benzylic-like carbocation. The use of trifluoroacetic anhydride (TFAA) at 0 °C converted alcohol **12e** into the corresponding trifluoroacetate (TFA) **12f** without a significant decrease in the % ee of the ester.

Finally, compound **12f** was reacted with 4,6-diamino-2-mercaptopyrimidine to generate **12R** in 61% yield over two steps with an enantiomeric excess of 40%. Presumably, a portion of the reaction occurs via a direct S_N2 pathway, while another part occurs via an S_N1 pathway, and thereby racemized material was obtained. Chiral resolution via recrystallization generated **12R** with an enantiomeric excess of over 90%. Likewise, (*S*)-(−)-2-methyl-CBS-oxazaborolidine was used in the CBS reduction to synthesize **12S** as a major product.

Scheme 2. Asymmetric Synthesis Route of **12R**[a]

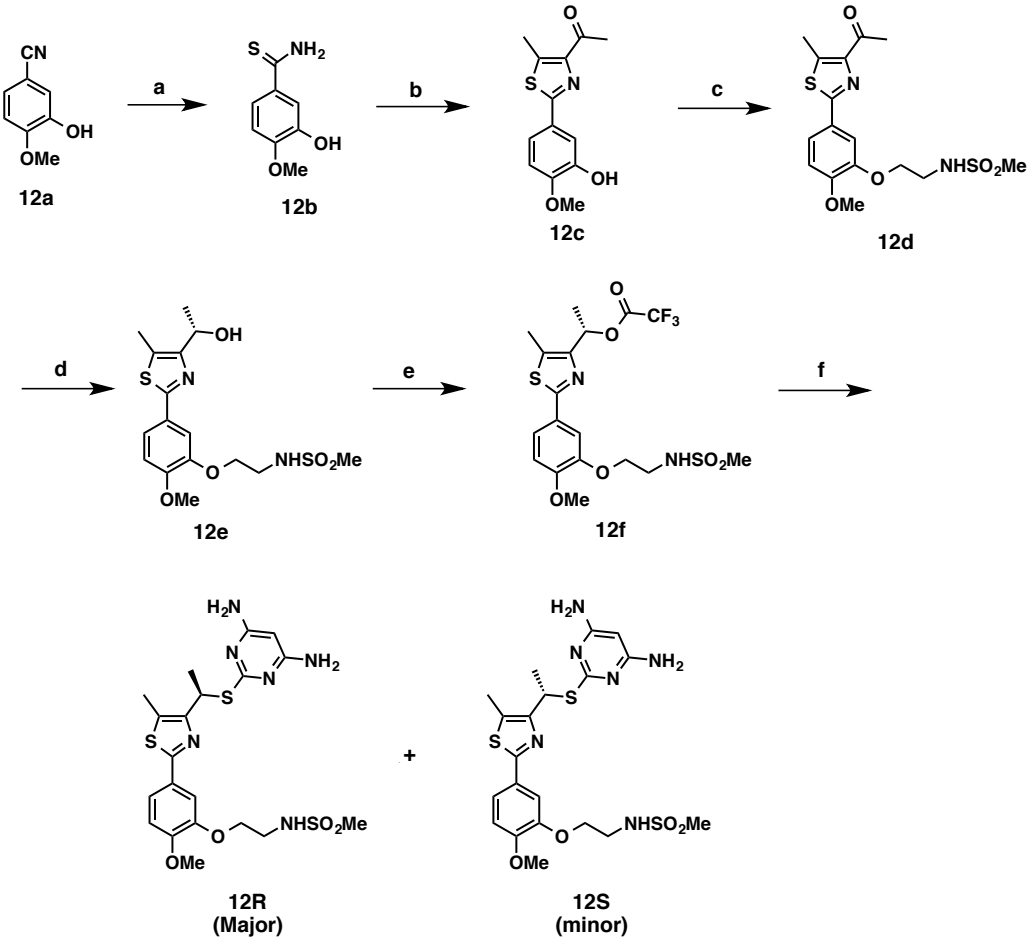

[a]Reagents and conditions: (a) $(NH_4)_2S$ (20% in H_2O), pyridine, Et_3N, 60 °C, 85%; (b) 4-bromopentane-2,3-dione, Ethanol, reflux, 96%; (c) N-(2-bromoethyl)methanesulfonamide, Cesium carbonate, *N*,*N*-dimethylformamide, 50 °C, 82%; (d) (*R*)-(+)-2-methyl-CBS-oxazaborolidine, BH_3−THF complex, THF, −78 °C, 77%, (96% ee); (e) TFAA, dichloromethane, 0 °C; (f) 4,6-diamino-2-mercaptopyrimidine, *N*,*N*-dimethylformamide, 80 °C, 61% in last two steps.

2.4 Characterization of Enantiomerically Pure 12R

Compound **12R** (Figure 7A) was measured to have very similar in vitro binding affinities to **11R** (Figure 7B). Significantly, just as the affinity of **11S** was much reduced relative to **11R**, the affinity to dCK of **12S** was much reduced relative to **12R**. This reiterated the preference of dCK for compounds that contain the *R*-isomer of the linker.

We solved the dCK−**12R** complex crystal structure. We expected **12R** to bind only at position 1 based on the previous structure with compound **10** (observing **10R** bound at position 1) and the kinetic results using enantiomerically pure **11S**, **11R**, **12S**, and **12R** (observing higher

affinities for the *R*-isomers) and since the crystals were formed with the enantiomerically pure **12R**. Additionally, lacking the *S*-isomer, we expected a vacant position 2 binding site. Indeed, the crystal structure of the dCK−**12R** complex revealed a single inhibitor molecule at position 1 (Figure 7C). This result suggests that the *R*-isomer has very low affinity to the binding site at position 2. Notably, while the interaction between the *R*-isomer and dCK is limited to the position 1 binding site, this does not diminish the binding affinity for the enzyme.

2.5 Determinant of Chiral Selectivity

The reason for the dramatic selectivity of the dCK position 1 binding site for the *R*-isomers of the inhibitors needed to be determined. Likewise, we needed to understand why position 2 only binds to the *S*-isomers of the inhibitors. The simple explanation would involve steric considerations relating the inhibitor and enzyme, where the chiral methyl group of the linker clashes with enzyme residues in the case of one isomer but not the other. However, inspection of the crystal structures solved with compounds **10**(**R**/**S**) and **12R** does not support this interpretation; we could model the *S*-isomer bound to position 1 (Figure 5D) and the *R*-isomer bound at position 2 (Figure 5E) with no apparent clashes.

Comparison of the binding mode between **10R** and **10S** reveals that the relative orientation of the pyrimidine ring to the thiazolephenyl part is strikingly different between the *R* and *S* isomers (Figure 8A and Figure 8B). That is, by a change of the angles of the linker that connects the pyrimidine ring to the thiazole ring, each isomer has adjusted its conformation to best fit its binding site (i.e., induced fit). This demonstrates that the enzyme dictates the relative orientations between the pyrimidine ring, linker, and the thiazolephenyl rings. It also shows that the relative orientation between thiazole and phenyl rings (being coplanar) is largely unchanged, not surprising because of the resonance between the rings.

To further probe the observed chiral selectivity, we constructed a theoretical model of **10S** binding at position 1 with the same orientation as **10R**. Whereas the observed distance

between the chiral methyl of the linker and the thiazole ring methyl group for **10R** in position 1 is 4.2 Å (Figure 8C), for the modeled **10S** bound to position 1, that distance would be an unfavorable 2.5 Å (Figure 8D). Likewise, whereas the observed distance between the chiral methyl and the thiazole methyl for **10S** in position 2 is 4.4 Å (Figure 8E), for the modeled *R*-isomer adopting the same conformation as **10S**, that distance would be an unfavorable 2.6 Å (Figure 8F). Hence, the strict chiral selection to either position 1 or position 2 is due to the enzyme dictating a particular inhibitor orientation that is vastly different between the binding sites. In the case of position 1, that orientation is not compatible with the *S*-isomer, and for position 2, that orientation is not compatible with the *R*-isomer.

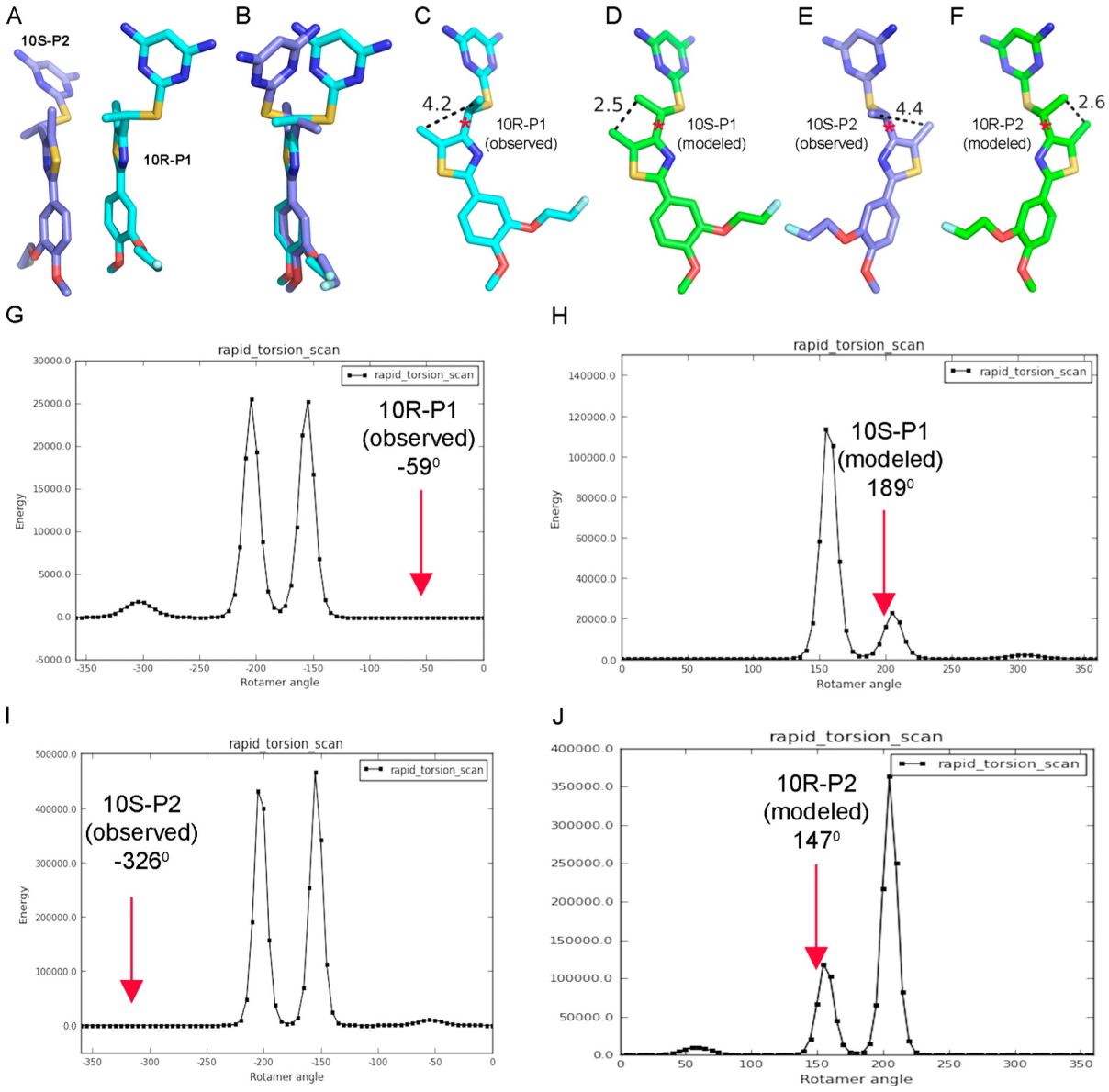

Figure 8. Chiral selectivity is due to conformational selection by the enzyme's binding site. (A) Observed orientation of **10R** (cyan) at position 1 (**10R**-P1, PDB code 4Q1E) and **10S** (plum) at position 2 (**10S**-P2) upon dCK binding. (B) **10S** overlaid on **10R** based on the thiazole ring. Note the different relative orientations of the thiazole and pyrimidine rings between **10R** and **10S**. (C) The conformation of **10R** (**10R**-P1) is dictated by the position 1 binding site. In this conformation the distance between the chiral linker methyl group and the thiazole ring methyl group is 4.2 Å. (D) The theoretical model of **10S** binding with the same conformation as **10R** in position 1 (**10S**-P1) shows that the homologous distance is reduced to 2.5 Å. (E) The conformation of **10S** (**10S**-P2) is dictated by the position 2 binding site. In this conformation the distance between the chiral linker methyl group and the thiazole ring methyl group is 4.4 Å. (F) The theoretical model of **10R** binding with the same conformation as **10S** in position 2 (**10R**-P2) shows that the homologous distance is reduced to 2.6 Å. (G) For **10R**-P1, the observed torsion angle between the thiazole ring and the linker is −59°. Scanning possible torsion angles shows that this value represents a low energy conformation of **10R**. (H) For **10S**-P1, the observed torsion angle is 189°. This value corresponds to a high-energy conformation. (I) For **10S**-P2, the observed torsion angle is −326°. Scanning possible torsion angles shows that this value is at a low energy conformation of **10S**. (J) For **10R**-P2, the observed torsion angle is 147°. This value corresponds to a high-energy conformation.

Using computer simulations, we obtained a qualitative estimate of the conformational penalty incurred by **10R** and **10S** upon binding with the protein. The conformational penalty is the energy difference between the preferred solution-phase geometry of a substrate and the geometry that it assumes upon binding: $\Delta E = E_{solution} - E_{bound}$. Each enantiomer was docked with the solvated protein at position 1 and allowed to equilibrate (Figure 9). The equilibrated, docked inhibitor structures were removed from the protein, and their energies were assessed with the semiempirical PDDG/PM3 method.[15-20] Unbound structures of **10R** and **10S** were optimized in implicit solvent to determine their low-energy solution-phase conformations. As with the bound structures, energies of the unbound structures were assessed with PDDG/PM3. The resulting energies were used to obtain qualitative conformational penalties for each enantiomer. The conformational penalty for **10S** was almost twice the conformational penalty for **10R** (45 kcal/mol larger penalty for **10S**), further demonstrating that **10R** needs to undergo a much less unfavorable structural rearrangement in order to bind with the protein at position 1.

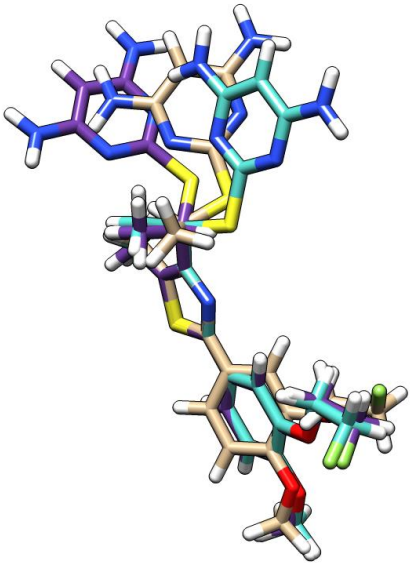

Figure 9. Relative orientation of **10R** (cyan) and **10S** (plum) optimized in solution, compared to the pose of **10R** bound at Position 1 in crystal structure (tan). The structures are aligned according to the thiazole rings. This illustrates the conformational change that must occur for the molecule to move out of solution and bind with the protein. Both **10R** and **10S** incur an energy penalty in undergoing this conformational change, but the penalty for **10R** is much less than the penalty for **10S**.

Another way of considering this issue is to examine the energy of the inhibitor as a function of rotation around the bond that connects the thiazole ring to the chiral linker atom (bond marked with ∗ in Figure 8C−F). For **10R** bound to dCK at position 1, the observed dihedral angle that specifies this rotation is −59° and fits a low energy conformation (Figure 8G). In contrast, the modeled *S*-isomer at this binding site would have a torsion angle of 189°, which is clearly a high-energy conformation (Figure 8H). The same pattern is observed for position 2, with the *S*-isomer binding to dCK with a torsion angle of −326°, which is a low energy conformation, while the modeled *R*-isomer at that position is a high-energy conformation (Figure 8I and Figure 8J). Hence, the chiral selectivity does not come directly from the enzyme sterically favoring one isomer over the other. Rather, the enzyme dictates a particular conformation, and the selectivity comes from one isomer being able to adopt that particular conformation, whereas the energy penalty for the other isomer precludes its binding.

In addition to explaining the chiral selectivity for the compounds discussed here, this understanding can be used for the design of chiral molecules that bind to either binding site. Specifically, the prediction would be that replacing the thiazole methyl group with a hydrogen atom would eliminate any steric clash to the chiral methyl group, and hence either isomer could bind to either inhibitor binding-site.

2.6 Improved Metabolic Stability of 12R

We first determined the metabolic stability of **12R** in a standard microsomal liver clearance assay. The NADPH-dependent $T_{1/2}$ of **12R** was ∼37-fold longer than that of our previous lead compound **2** (Table 1). We then tested compound **12** in mice, using our previously described positron emission tomography (PET) assay.[8] Whereas our earlier lead compound **2** retained only ∼25% inhibition of dCK activity 4 hours after dosing by intraperitoneal injection,[3] compound **12** (given as the racemic mixture) exhibited >50% inhibition of dCK activity at this time point (Figure 10A). Furthermore, 8 hours after treatment with compound **12**, dCK inhibition

was still above 30%. We then determined the pharmacokinetic properties of compound **12** to compare with our previous lead compounds **1** and **2**. As shown in Figure 10B, the pharmacokinetic properties of compound **12** were significantly improved relative to the previously published values for compounds **1** and **2**. Collectively, these findings demonstrate that introduction of the chiral linker plus replacement of the thiazole ring propyl substituent by a methyl group yields a dCK inhibitor with improved metabolic stability.

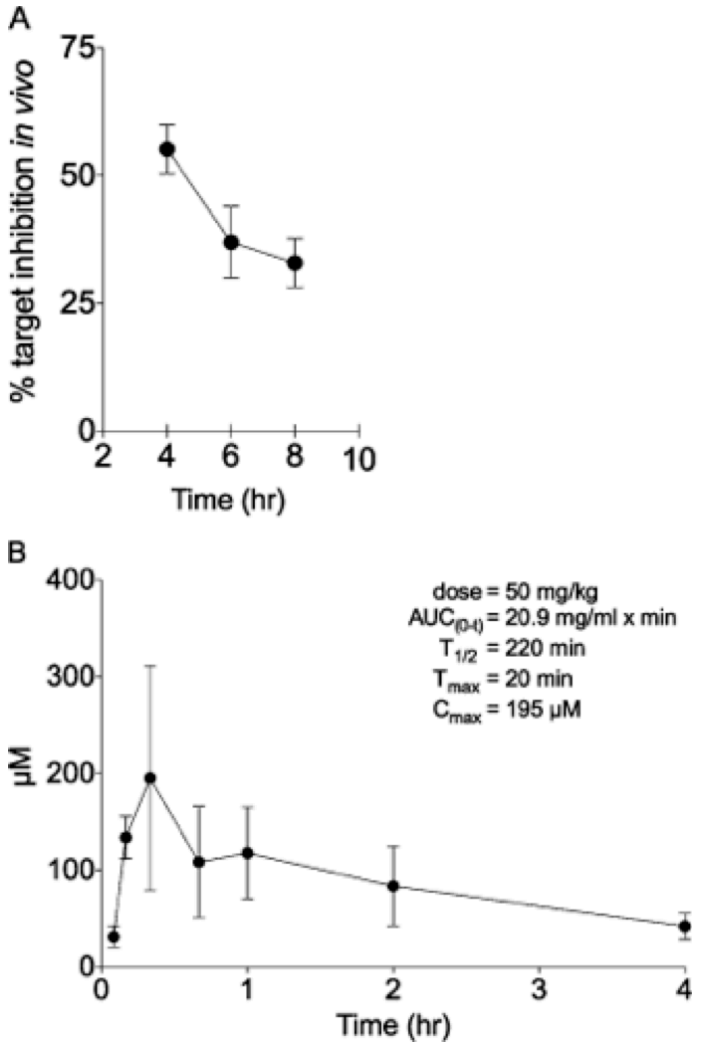

Figure 10. In vivo evaluation of compound **12**. (A) Quantification of PET probe, ^{18}F-L-FAC, uptake in the liver of C57Bl/6 female mice treated with compounds **12** (25 mg/kg) via intraperitoneal injection. Dose formulation: 50% PEG/Tris, pH 7.4. Data are mean values ± SEM for at least n = 5 mice/time point. (B) Plasma pharmacokinetic profile of compound **12**. C57Bl/6 female mice were dosed via intraperitoneal injection with 50 mg/kg compound **12** formulated in 50% PEG/Tris, pH 7.4. Data are mean values ± SEM for n = 4 mice/time point.

2.7 Synthetic Chemistry Routes for the Preparation of dCK Inhibitors

Compounds **9** and **10** were synthesized according to the route shown in Scheme 3. Each of the syntheses started with a previously reported alcohol-containing compound (**9a** and **10a**). Alcohol **9a** was oxidized with Dess-Martin Periodinane (DMP) to yield aldehyde **9b**. This aldehyde could not be accessed directly from the reduction of an ester functional group using DIBAL. Next, the reaction of **9b** with methyl magnesium iodide generated a racemic secondary alcohol (**9c**). Treatment of **9c** with thionyl chloride gave alkyl chloride **9d**. Alkyl chloride **9d** could not be purified by column chromatography due to its instability, so **9d** was used for the next step immediately after aqueous work-up. The reaction of **9d** with diamino-2-mercaptopyrimidine under basic conditions produced the desired racemic target (**9**). The synthesis of compound **10** was the same as the route used for the preparation of **9**, as shown below. Attempts to synthesize a difluoro-linker ($–CF_2S–$) and a dimethyl-linker ($–C(CH_3)_2S–$) were unsuccessful, but an inhibitor with a $–CH_2CH_2–$ was isolated.

Scheme 3. The synthesis for compounds **9** and **10** as racemic mixtures[a]

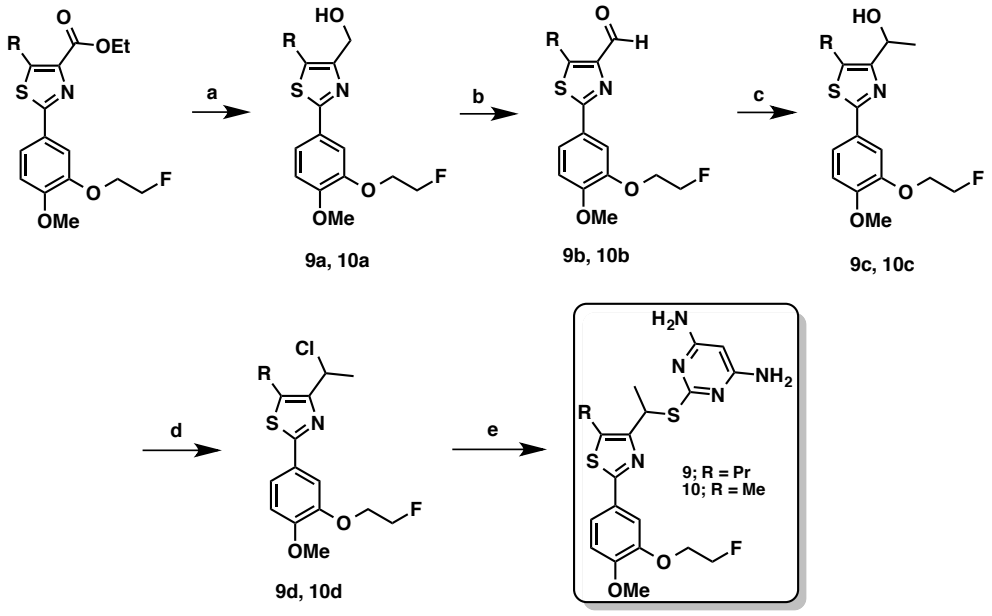

[a]Reagents and conditions: (a) Diisobutylaluminium hydride, tetrahydrofuran, (previous work); (b) Dess–Martin

periodinane, dichloromethane, 23 °C (80% yield for **9b**, 70% yield for **10b**); (c) Methylmagnesium iodide, tetrahydrofuran, 0 °C (86% yield **9c**, 68% yield for **10c**); (d) Thionyl chloride, dichloromethane, 23 °C (96% crude yield for **9d**, 94% crude yield for **10d**); (e) 4,6-Diamino-2-mercaptopyrimidine, potassium carbonate, *N*,*N*-dimethylformamide, 80 °C (66% yield for **9**, 64% yield for **10**).

Section 2.1 gave a rational for synthesizing an inhibitor in which the sulfur atom of the –SCH_2– linkage was replaced with a methylene carbon. The synthesis of this methyl linker analog (**S15**) is shown below in Scheme 4. The synthesis of **S15** begins from a primary alcohol that was previously reported by our group. Alcohol **9a** was used as an alkylating agent in a low-yielding ruthenium catalyzed decarboxylation to yield ester **S15a**.[21] In the next step, commercially available malondiamidine hydrochloride was used to construct the 2,4-diaminopyrimidine ring of **S15**.[22] As stated in Section 2.1, **S15**'s affinity for dCK and in vitro metabolic stability showed no improvement relative to our other lead compounds. The SAR of the phenyl ring's substituents was the next area of interest.

Scheme 4. The synthetic route for the inhibitor with a –CH_2CH_2– linkage between the thiazole and pyrimidine rings (**S15**).

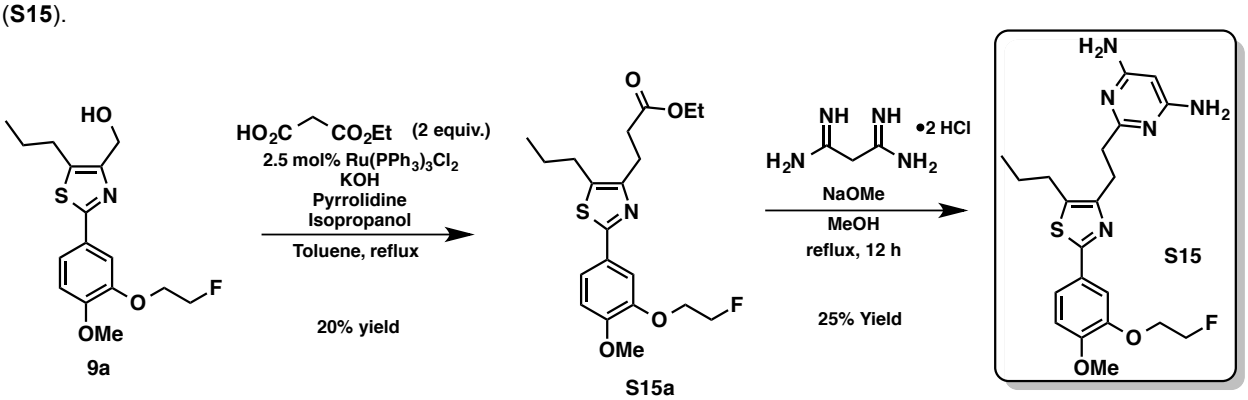

Compounds **S24** and **11** were discussed in Section 1.4 as analogs in which the phenyl ring's para position bears a PEG chain. Scheme 5 presents the synthetic route for compound **24** in addition to an alternative synthesis for inhibitor **11**. Each reaction sequence begins with a Hantzsch thiazole synthesis.[23] Afterwards, the phenol ring was alkylated with 13-chloro-2,5,8,11-tetraoxatridecane in order to install the PEG chain. The subsequent DIBAL reduction, DMP oxidation, Grignard reaction, chlorination, and substitution reactions resemble the synthetic route for compounds **9** and **10** shown in Scheme 3. As predicted, the introduction of

the PEG chain increased aqueous solubility in aqueous PEG/Tris solution.

Scheme 5. The synthetic route for para-PEG$_3$ compounds **S24,** and an alternative route for the preparation of compound **11**.[a]

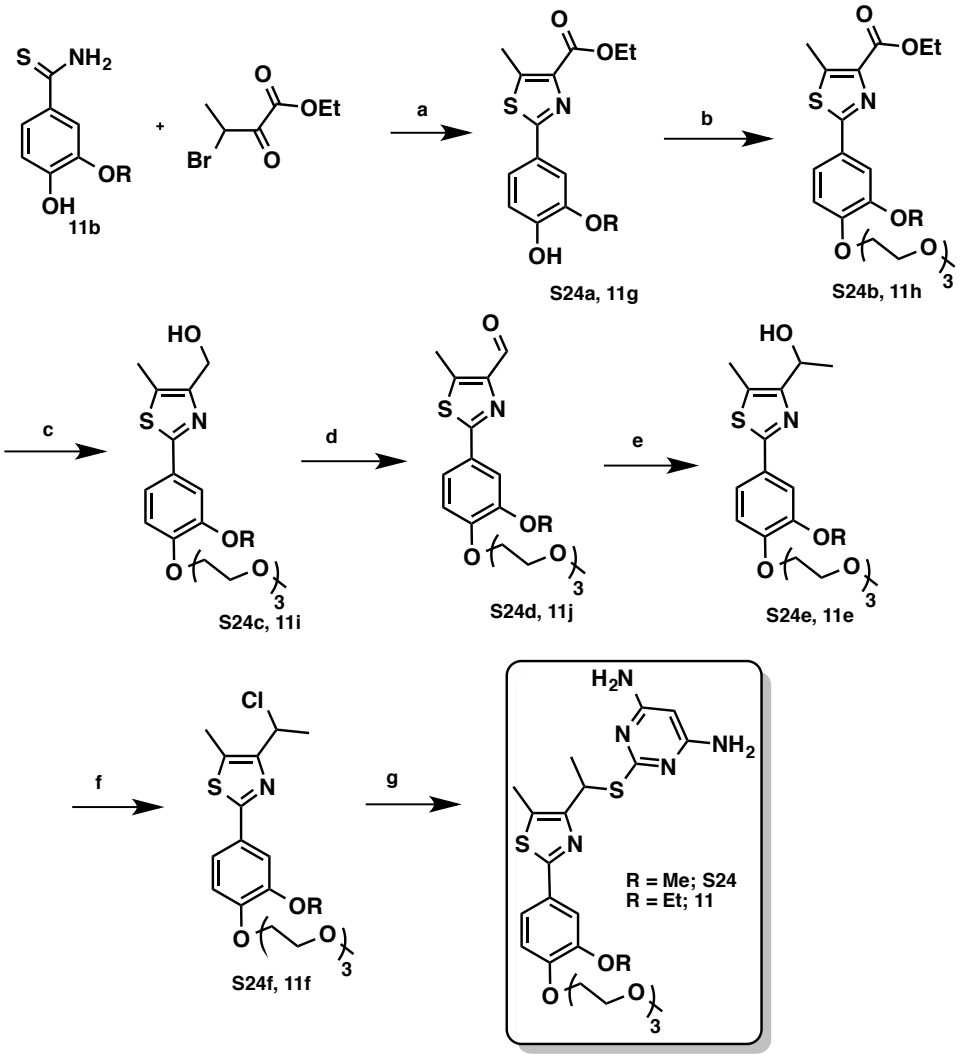

[a]Reagents and conditions: (a) Ethanol, reflux (87% yield for **S24a**); (b) 13-Chloro-2,5,8,11-tetraoxatridecane, Cesium carbonate, *N*,*N*-dimethylformamide (93% yield for **S24b**); (c) Diisobutylaluminium hydride, dichloromethane, −78 °C (92% yield for **S24c**); (d) Dess–Martin periodinane, dichloromethane, 23 °C (86% yield for **S24d,** 78% yield for **11j**); (e) Methylmagnesium iodide, tetrahydrofuran (85% yield for **S24e**, **86%** yield for **11e**); (f) Thionyl chloride, dichloromethane, 23 °C; (g) 4,6-Diamino-2-mercaptopyrimidine, potassium carbonate, *N*,*N*-dimethylformamide, 80 °C (70% yield for **S24**).

The synthetic route presented in Scheme 5 was also used for the preparation of compounds **S22**, **S23**, and **S28** (Scheme 6). Schemes 5 and 6 each utilize ethyl 3-bromo-2-oxobutanoate as a reactant in the initial Hantzsch cyclization. As a result, the syntheses are

inefficient. An optimized synthesis was developed where 4-bromopentane-2,3-dione was used in place of ethyl 3-bromo-2-oxobutanoate in the Hantzsch cyclization. Scheme 7 illustrates the optimized route that uses the former reagent.

Scheme 6. The synthetic route for meta-PEG$_3$ compounds **S22**, **S23**, and **S28**.[a]

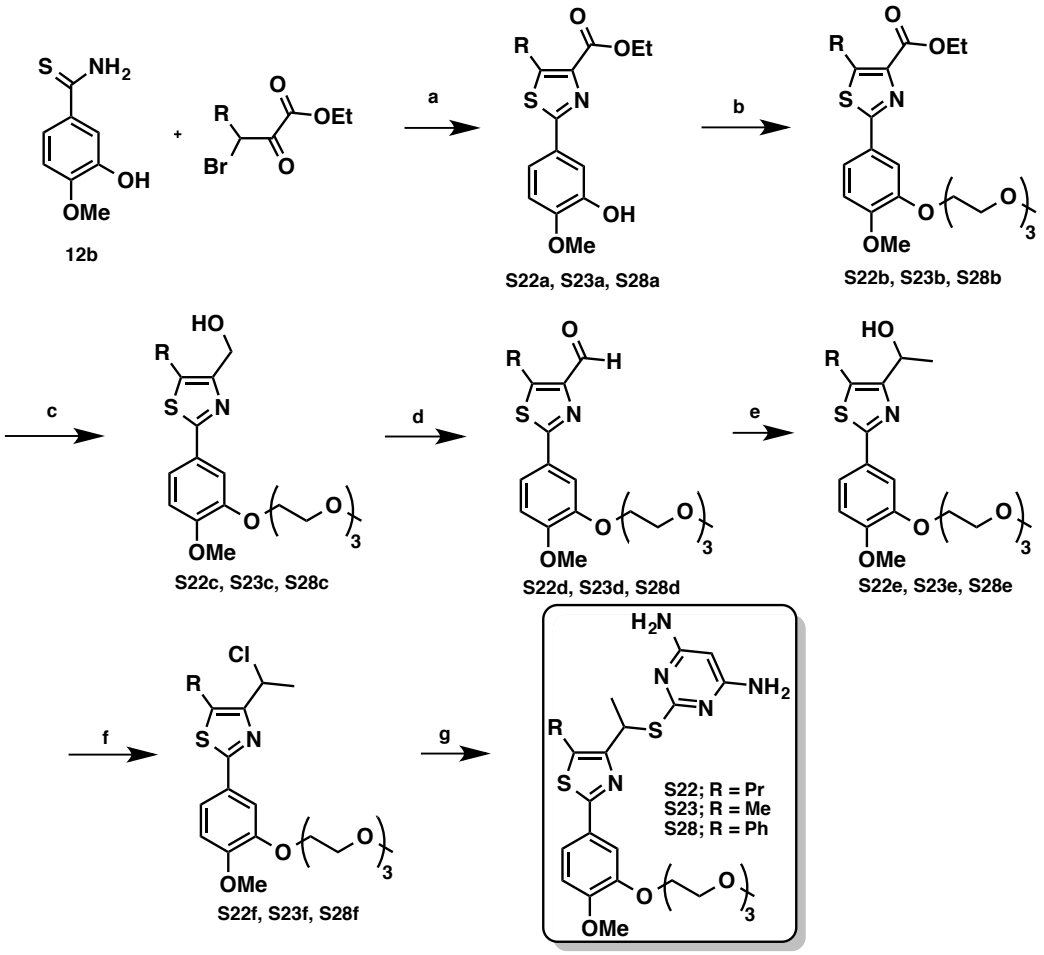

[a]Reagents and conditions: (a) Ethanol, reflux (60% yield for **S22a**, 55% yield for **S23a**, and 33% yield for **S28a**); (b) 13-chloro-2,5,8,11-tetraoxatridecane, cesium carbonate, *N*,*N*-dimethylformamide (45% yield for **S22b**, 47% yield for **S23b**, and 90% yield for **S28b**); (c) Diisobutylaluminium hydride, dichloromethane, −78 °C (93% yield for **S22c**, 95% yield for **S23c**, and 89% yield for **S28c**); (d) Dess–Martin periodinane, dichloromethane, 23 °C (82% yield for **S22d**, 93% yield for **S23d**, and 83% yield for **S28d**); (e) Methylmagnesium iodide, tetrahydrofuran (67% yield for **S22e**, 87% yield for **S23e**); (f) Thionyl chloride, dichloromethane, 23 °C (93% crude yield for **S22f**, and 98% crude yield for **S28f**); (g) 4,6-Diamino-2-mercaptopyrimidine, potassium carbonate, *N*,*N*-dimethylformamide, 80 °C (76% yield for **S22**, 60% yield for **S23**, and 58% yield for **S28**).

Scheme 7 illustrates the optimized route that uses 4-bromopentane-2,3-dione in the place of ethyl 3-bromo-2-oxobutanoate. 4-Bromopentane-2,3-dione was synthesized in one step from commercially available pentane-2,3-dione.[24] Chirality was introduced via Corey-Bakshi-

Shibata (CBS) reduction of ketone **S23h** to afford secondary alcohol **S23e**. Percent enantiomeric excess (%ee) values of 98% could be achieved via the CBS reduction (determined via chiral HPLC). Alcohol **S23e** was converted to the corresponding trifluoroacetate (TFA) (**S23i**) successfully.[25] The TFA ester served as a suitable leaving group in the subsequent S_N2 reaction. The conversion of compound **S23e** to **S23i** did not result in a significant attrition of %ee, but the %ee decreased to approximately 40% when converting **S23i** to (*R*)-S23 or (*S*)-S23. However, chiral resolution via recrystallization increased the %ee of the optically enriched dCK inhibitor to values up to approximately 90%, albeit in a low yield. An achiral synthesis for **S23** was performed using this strategy when DIBAL-H and thionyl chloride were used in place of the CBS-reduction method and trifluoroacetic anhydride, respectively.

Scheme 7. The chiral synthetic route for meta-PEG_3 compound **S23**.[a]

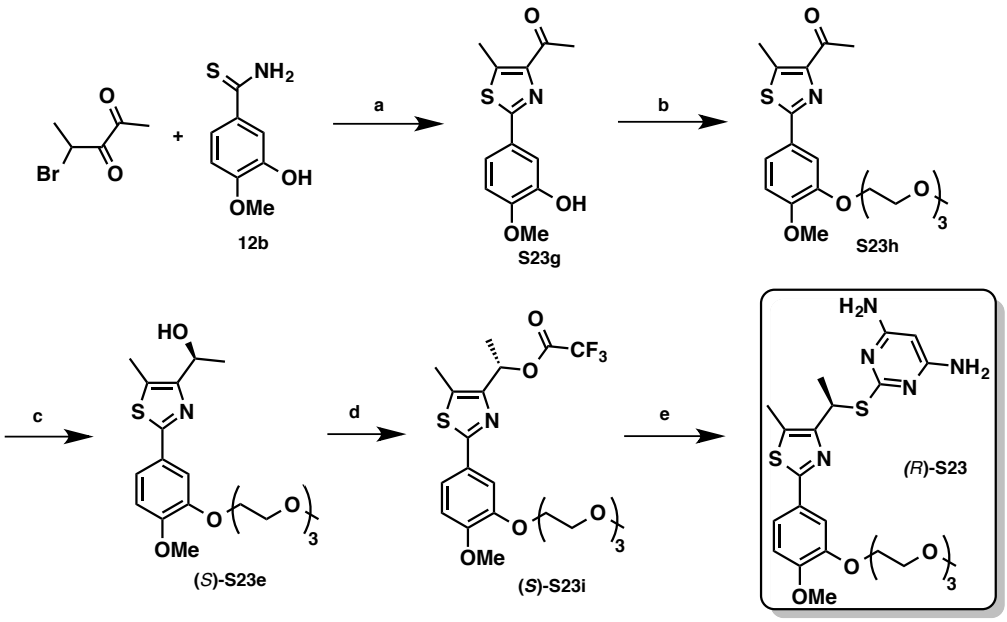

[a]Reagents and conditions: (a) Ethanol, reflux, 95%; (b) 13-chloro-2,5,8,11-tetraoxatridecane, cesium carbonate (68% yield); (c) CBS-catalyst, BH_3-THF complex, tetrahydrofuran, –78 °C (60% yield); (d) TFAA, dichloromethane, 0 °C (93% crude yield); (e) 4,6-Diamino-2-mercaptopyrimidine, potassium carbonate, *N*,*N*-dimethylformamide, 80 °C (57% yield).

Similarly, we synthesized the *R*-isomer of Compound **11** with a percent enantiomeric excess of 88%, albeit in low yield. Scheme 8 displays the three-step reaction sequence for preparing **11R**. This series of reactions matches the sequence of transformations used for the

preparation of **12R** (see Scheme 2 for the preparation of **12R**). A CBS-reduction produced (***S***)-**11e** from ketone **11d.** Next, **11g** was synthesized because the alcohol functionality of (***S***)-**11e** needed to be converted into a suitable leaving group. Utilizing the trifluoroacetate leaving-group allowed us to retain optical purity and to avoid decomposition reaction pathways. Finally, substituting the TFA group with the appropriate thiol gave **11R.** The percent yield over the three steps shown in Scheme 8 was approximately 35%. The %ee of the final step of the reaction sequence was initially low, however after three recrystallizations the %ee value was increased to approximately 88% (determined via chiral HPLC).

Scheme 8. The Chiral Synthetic Route for para-PEG$_3$ Compound **11R**.[a]

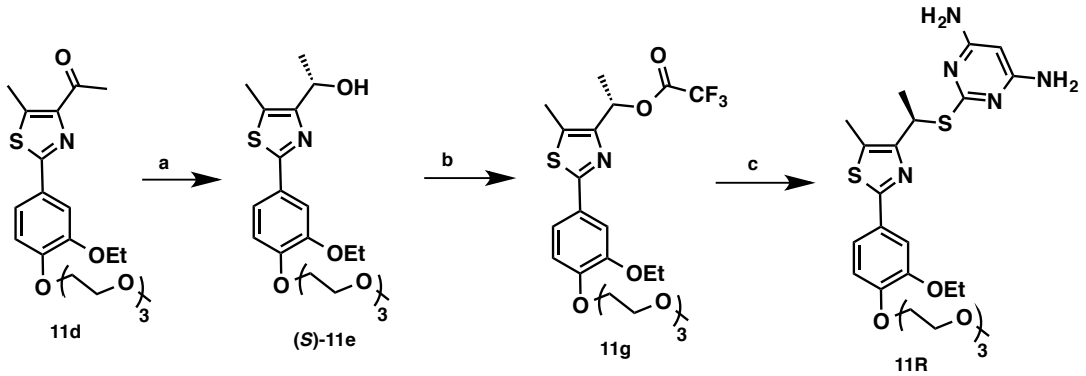

[a]Reagents and Conditions: (a) (*R*)-(+)-2-methyl-CBS-oxazaborolidine, BH_3−THF complex, THF, −78 °C; (b) TFAA, dichloromethane, 0 °C; (c) 4,6-diamino-2-mercaptopyrimidine, *N*,*N*-dimethylformamide, 80 °C, 34% over three steps.

The synthesis of an analog containing a 1,3,4-oxadiazole ring was accomplished according to the synthetic route shown in Scheme 9. This type of analog was targeted because we predicted that an oxadiazole ring would impart improved solubility and formulation. Commercially available 2-(chloromethyl)-5-phenyl-1,3,4-oxadiazole was coupled with **12c**, and the conversion of **12c** to inhibitor **S32** proceeded via the routine reduction-chlorination-substitution reaction sequence. Unfortunately, inhibitor **S32** performed poorly in comparison to our lead dCK inhibitors.

Scheme 9: The synthetic route for oxadiazole-containing compound **S32**.[a]

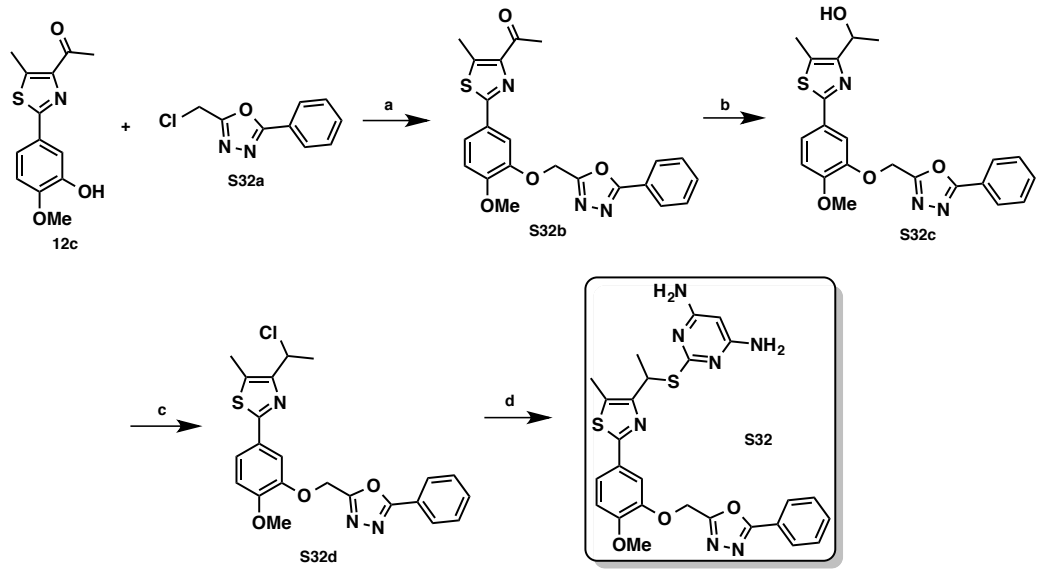

[a]Reagents and conditions: (a) Cesium carbonate, *N*,*N*-dimethylformamide; (b) Diisobutylaluminium hydride, CH_2Cl_2, –78 °C; (d) Thionyl chloride, dichloromethane, 23 °C; (d) 4,6-Diamino-2-mercaptopyrimidine, potassium carbonate, *N*,*N*-dimethylformamide, 80 °C.

CHAPTER 3: CONCLUSION

Structural and inhibition studies of the compounds discussed here, performed using both the purified recombinant enzyme and a cell-based assay, revealed and rationalized the essential determinants for binding to dCK and also guided the type and placement of substituents. This informed the development of the initial leads, compounds **1** and **2**. These compounds contain a propyl group at the 5-position of the thiazole ring, since, as shown earlier, the propyl substituent provides improved affinity for dCK compared to compounds with a methyl group at that position. Unfortunately, this affinity-strengthening propyl group compromised the metabolic stability relative to compounds containing a methyl group at that position. This forced us to revert to the weaker-binding, but more metabolically stable, scaffold of a methyl group at the thiazole ring. With the goal of improving metabolic stability, we tested a chiral methylene methyl sulfur linker between the thiazole and pyrimidine moieties. This linker was found to

confer two positive effects: (1) in terms of affinity for dCK, the modified linker compensated for the lack of the thiazole propyl group, and (2) the compounds exhibited improved metabolic stability. The interaction of dCK with compounds containing this linker is specific to the *R*-isomer. This was proven by the dCK-inhibitor crystal structure and by comparing the binding affinities of the *R* versus *S* enantiomers. The new lead compound **12R** is a promising dCK inhibitor, which by perturbing the dNTP pools and inducing DNA replication stress overload could be used in combination with other drugs to specifically trigger synthetic lethality in cancer cells.

CHAPTER 4: EXPERIMENTAL SECTION

4.1 Methods and Materials

Materials: General laboratory reagents were purchased from Fisher (Pittsburgh, PA, USA) and Sigma-Aldrich (St. Louis, MO, USA). Nucleotides were obtained from Sigma. All inhibitors were synthesized at UCLA. Chiral Technologies Inc. (800 North Five Points Road, West Chester, PA 19380, USA) performed the separation of *R* and *S* enantiomers.

General Chemistry Procedures: Unless otherwise noted, reactions were carried out in oven-dried glassware under an atmosphere of nitrogen using commercially available anhydrous solvents. Solvents used for extractions and chromatography were not anhydrous. 4,6-Diamino-2-mercaptopyrimidine was obtained from drying the hydrate over dynamic vacuum at 110 °C for 20 h. All other reagents obtained from commercial suppliers were reagent grade and used without further purification unless specified. Reactions and chromatography fractions were analyzed by thin-layer chromatography (TLC) using Merck precoated silica gel 60 F_{254} glass plates (250 μm). Visualization was carried out with ultraviolet light, vanillin stain, permanganate stain, or p-anisaldehyde stain. Flash column chromatography was performed using E. Merck silica gel 60 (230−400 mesh) with compressed air. ^{1}H and ^{13}C NMR spectra were recorded on a ARX500 (500 MHz), Avance 500 (500 MHz), or Avance 300 (300 MHz) spectrometers. Chemical shifts are reported in parts per million (ppm, δ) using the residual solvent peak as the reference. The coupling constants, J, are reported in hertz (Hz), and the resonance patterns are reported with notations as the following: br (broad), s (singlet), d (doublet), t (triplet), q (quartet), and m (multiplet). Electrospray mass spectrometry data were collected with a Waters LCT Premier XE time-of-flight instrument controlled by MassLynx 4.1 software. Samples were dissolved in methanol and infused using direct loop injection from a Waters Acquity UPLC into the multimode ionization source. Analytical HPLC analysis was performed on a Knauer Smartline HPLC system with a Phenomenex reverse-phase Luna column (5 μm, 4.6 mm × 250 mm) with inline Knauer UV (254 nm) detector. Mobile phase: A, 0.1% TFA in H_2O; B, 0.1% TFA

in MeCN. Eluent gradient is specified for each described compound. Percent enantiomeric excess (% ee) values were determined via chiral HPLC with a CHIRALPAK IA-3/IA polysaccharide-based immobilized type column (3 μm, 4.6 mm × 150 mm) with inline Knauer UV (310 nm) detector. Mobile phase: A, 0.1% TFA in hexanes; B, 0.1% TFA in propanol. Eluent gradient: 50% phase A and 50% phase B. Chromatograms were collected by a GinaStar (Raytest USA, Inc.; Wilmington, NC, USA) analog to digital converter and GinaStar software (Raytest USA, Inc.).

Protein Expression and Purification: Protein expression and purification were performed exactly as described by us.[9] In brief, we used the S74E-C4S-dCK variant, which is the human dCK protein where four solvent-exposed cysteines are mutated into serines (C4S). We showed that the C4S mutant generates better quality crystals without altering the three-dimensional conformation of the enzyme or its enzymatic activity.[26] Additionally, the enzyme contained the mutation of Ser74 to glutamic acid (S74E); this mutation serves to mimic the phosphorylated state of this residue. When we refer to dCK in this report, we mean the C4S-S74E-dCK variant. dCK was expressed in Escherichia coli BL21 C41(DE3) cells using a pET-14b vector; the cells were grown in 2xYT medium and induced with 0.1 mM IPTG for 4 h at 310 K. The cells were harvested, and the pellet was lysed by sonication. The lysate was cleared by centrifugation at 30 000 rev/min for 1 h at 277 K, and the supernatant was loaded onto a 5 mL HisTrap nickel-affinity column (GE Healthcare). The column was washed with 300 mL of a buffer composed of 25 mM Tris-HCl, pH 7.5, 500 mM NaCl, 30 mM imidazole. The bound protein was eluted with the same buffer but containing 250 mM imidazole and was further purified by gel filtration using an S-200 column in a buffer consisting of 25 mM HEPES, pH 7.5, 200 mM sodium citrate, 2 mM EDTA, 3 mM DTT. The protein fractions were pooled, concentrated, aliquoted, flash-frozen in liquid nitrogen, and stored at 193 K until use.

Kinetic Assay: The phosphorylation activity of dCK was determined using a spectroscopic NADH-dependent enzyme-coupled assay.[2,27] All measurements were taken in triplicate at 310 K in a buffer consisting of 100 mM Tris, pH 7.5, 200 mM KCl, 5 mM $MgCl_2$, 0.5 mM EDTA, 0.8 mM phosphoenolpyruvate, 0.4 mM NADH with 50 nM dCK, and 1 mM ATP. IC_{50}^{app} and K_i^{app} were determined as described by us,[9] and all data were fitted using the KaleidaGraph software.

IC_{50} Determinations: These were performed in CCRF-CEM acute lymphoblastic leukemia cells as previously described.[8,9]

PET Studies: PET studies to determine % inhibition of dCK activity in vivo were performed as previously described:[8,9] Animal studies were approved by the UCLA Animal Research Committee and were carried out according to the guidelines of the Department of Laboratory Animal Medicine at UCLA. For the PET liver assay, C57BL/6 mice were intraperitoneally (i.p.) injected with the indicated amounts of dCK inhibitor (re-suspended in 40% Captisol) 4 hours prior to intravenous injection of 70 μCi of ^{18}F-L-FAC. For the tumor xenograft assay, NOD scid IL-2 receptor gamma chain knockout (NSG) bearing subcutaneous CCRF-CEM tumor xenografts were injected with 50 mg/kg of compound **1** or vehicle. Four hours post-treatment mice were injected intravenously with 70 μCi of ^{18}F-L-FAC. For all mPET/CT studies, a 1 h interval was allowed between probe administration and mPET/CT scanning (Inveon, Siemens Medical Solutions USA Inc.; microCAT, Imtek Inc.). Static mPET images were acquired for 600 s. Images were analyzed using OsiriX Imaging Software Version 3.8.

Human Microsomal stability Assays: These assays were performed by Cyprotex (Watertown, MA) according to standard operating protocols.

Plasma Pharmacokinetics of Compounds 10 and 12 in Mice: These measurements were performed as previously described.[8,9] Briefly, C57Bl/6 female mice were treated with the dCK inhibitors via intraperitoneal injection. The drugs were administered in 50% polyethylene glycol

(PEG 400)/50 mM Tris-HCl, pH 7.5. Five minutes after drug injection, whole blood (~75 μL) was obtained at various time points from the retro-orbital sinus using hematocrit capillary tubes. Samples were centrifuged at 20 000g for 5 min, and the supernatant (5 μL) was transferred into a clean tube. Calibration standards were prepared by spiking various amounts of **11** and **12** in 5 μL of supernatant from the plasma of untreated mice to obtain final concentrations between 0.001 to 100 pmol/μL. Samples and the calibration standards were mixed with 500 μL ice-cold acetonitrile/water (50/50, v/v) containing an internal standard (1). All of the samples were evaporated to dryness in a vacuum centrifuge. The residue was reconstituted in 100 μL of acetonitrile/water (50/50, v/v). Samples (5 μL) were injected onto a reverse phase column (Agilent ZORBAX rapid resolution high definition Eclipse Plus C18, 2.1 mm × 50 mm, 1.8 μm) equilibrated in water acetonitrile/formic acid, 95/5/0.1, and eluted (200 μL/min) with an increasing concentration of solvent B (acetonitrile/formic acid 100/ 0.1, v/v: min/% acetonitrile; 0/5, 2/5, 8/80, 9/80, 10/5, 12/5). The effluent from the column was directed to an electrospray ion source (Agilent Jet Stream) connected to a triple quadrupole mass spectrometer (Agilent 6460 QQQ) operating in the positive ion MRM mode. The ion transitions for **1**, **11**, and **12** are 476.2−334.5, 550.2−408.2, and 511.1−369.1 respectively. The peak areas for **11** and **12** were normalized to the peak area of the internal standard, and the plasma concentrations were computed using the standard curves generated by calibration standards spiked in plasma from untreated mice. Approximated values of the area under the curve (AUC), half-life ($T_{1/2}$), maximum concentration in the plasma (C_{max}), and time to reach the maximum concentration (T_{max}) were calculated using Boomer/ Multi-Forte PK functions from Microsoft Excel.[28,29]

Crystallization, X-ray Data Collection, and Refinement: Crystals of human dCK in complex with inhibitors and UDP were grown at 285 K using the hanging-drop vapor-diffusion method. All dCK-inhibitor complexes were prepared as follows: 1 μL of dCK protein at 10−17 mg/mL in complex with a 2.5-fold molar excess of inhibitor, and 2 mM UDP and 5 mM $MgCl_2$ were mixed

with 1 μL of reservoir buffer solution. The reservoir solution consisted of 0.9−1.5 M trisodium citrate dehydrate and 25 mM HEPES, pH 7.5. Prior to data collection, crystals were soaked in mineral oil for cryoprotection. Diffraction data for dCK in complex with compounds **4−8** were collected on the Life Sciences Collaborative Access Team (LS-CAT) beamline 21-ID-G. Data for all other complexes (compounds **9−12**) were collected using the in-house X-ray source (Rigaku RU-200 rotating anode) with a R-AXIS IV++ image plate detector. Data were processed and scaled with XDS and XSCALE.[30] Structures were determined by molecular replacement with MOLREP[31] using the dCK structure (PDB entry 4JLN[9]) as a search model. Refinement was conducted using REFMAC,[32] and model building was conducted using Coot.[33] All inhibitor coordinates and library descriptions were generated using the PRODRG server.[34] All data sets were perfectly twinned, and iterative refinements were carried out using REFMAC with the Twin option active. Data collection and refinement statistics are listed in Appendix 1. Structural figures were prepared using the PyMOL Molecular Graphics System (version 1.6.0, Schrödinger).

Modeling: The *S*-isomer in position 1 and the *R*-isomer in position 2 were generated by flipping the chirality of the linker carbon using Maestro, version 9.1, Schrödinger, LLC, 2010. This program was also used to generate the torsion scans around the bond connecting the chiral linker carbon and the thiazole ring (torsion angle defined by CAC−CBC−CBB−NAO). Equilibration simulations were performed using the MCPRO 2.0 software package[17] with the OPLS-AA[16] force field. The protein was solvated in a 30 Å cap of TIP4P water molecules.[15] The protein backbone and all bond lengths within the protein were held fixed. Angles and torsions within 11 Å of the center of the bound molecule were allowed to vary. All degrees of freedom of the bound molecule were sampled. Equilibration began with 5 × 106 configurations of solvent-only moves, followed by 10 × 106 configurations in which the protein and bound molecule were sampled, with additional solvent sampling at every tenth configuration. Equilibrations were

performed using Metropolis Monte Carlo in the NPT ensemble at 1 atm and 25 °C. For the unbound structures, optimizations were performed using OPLS-AA. Implicit solvent was simulated with the generalized Born/surface area (GB/SA) method.[18,20] Energies were assessed using the PDDG/PM3 method[35] in the BOSS software package.[17]

4.2. Experimental Procedures

4.2.1 Experimental Procedures Relevant to Compound 11

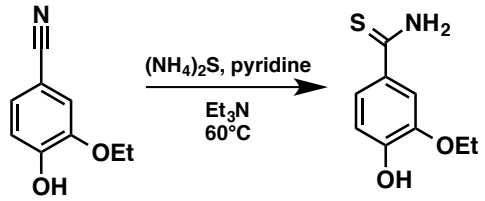

3-Ethoxy-4-hydroxybenzothioamide (**11b**). To a mixture of 3-ethoxy-4-hydroxybenzonitrile **11a** (2.50 g, 15.3 mmol) in pyridine (35 mL) and triethylamine (2.5 mL) was added ammonium sulfide solution (20 wt % in H_2O, 15.65 mL, 46.0 mmol). The mixture was stirred for 18 h at 60 °C. The reaction mixture was cooled and concentrated in vacuo to remove residual solvent. The resulting residue was washed with brine and extracted with ethyl acetate. The organic layer was dried over anhydrous Na_2SO_4, concentrated in vacuo, and purified by flash column chromatography over silica gel (3:1 ethyl acetate/hexanes) to yield **11b** (2.56 g, 13.0 mmol, 85% yield) as a yellow solid. ^{1}H NMR (300 MHz, $CDCl_3$) δ 7.68 (d, *J* = 2.1 Hz, 1H), 7.48 (br s, 1H), 7.28 (dd, *J* = 8.5, 2.1 Hz, 1H), 7.11 (br s, 1H), 6.89 (d, *J* = 8.5 Hz, 1H), 6.03 (s, 1H), 4.21 (q, *J* = 6.9 Hz, 2H), 1.47 (t, *J* = 6.9 Hz, 3H); ^{13}C NMR (125 MHz, acetone-d_6) δ 200.5, 150.3, 145.8, 131.0, 121.0, 114.0, 112.6, 64.3, 14.1.

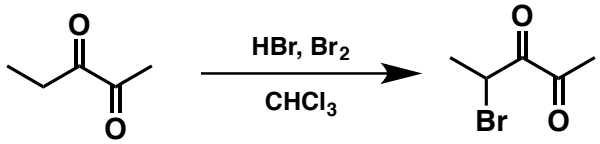

4-Bromopentane-2,3-dione. Pentane-2,3-dione (5.2 mL, 0.050 mol) was stirred in chloroform (75 mL) at 50 °C. To this solution was added another solution consisting of bromine (2.57 mL, 0.0499 mol) and chloroform (50 mL) over approximately 1 hr. After approximately 4.5 h the organic layer was separated in a separatory funnel, and the solvent was removed using a Rotavapor. The crude sample was subjected to column chromatography (silica gel, 10% ethyl acetate in hexane). Afterwards, fractional distillation using a Vigreux column (bp: 54°C – 56°C at 20 mbar) gave the product in high purity (2.803 g, 31% yield). ^{1}H NMR (500 MHz, $CDCl_3$) δ 5.23 (q, *J* =7.0 Hz, 1H), 2.43 (s, 3H), 1.75 (d, *J* = 7.0 Hz, 3H); ^{13}C NMR (125 MHz, $CDCl_3$) δ 197.20, 190.53, 39.70, 25.07, 18.38.

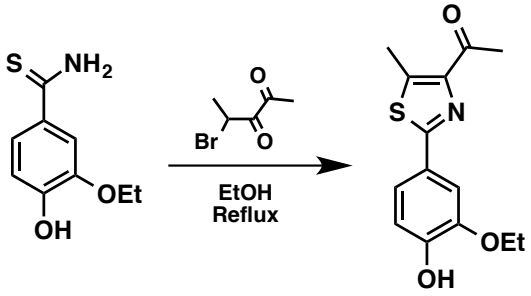

1-(2-(3-Ethoxy-4-hydroxyphenyl)-5-methylthiazol-4-yl)-ethan-1-one (**11c**)**.** A mixture of thioamide **11b** (1.50 g, 7.6 mmol) and 4-bromopentane-2,3-dione (2.04 g, 11.4 mmol) in ethanol (40 mL) was stirred under refluxing conditions for 4 h. The resulting mixture was cooled and concentrated in vacuo to remove residual solvent. The crude residue was purified by flash column chromatography over silica gel (10:3 hexanes/ethyl acetate) to yield the desired thiazole intermediate **11c** (2.00 g, 7.2 mmol, 95% yield) as a white solid. ^{1}H NMR (300 MHz, $CDCl_3$) δ 7.47 (d, *J* = 1.8 Hz, 1H), 7.35 (dd, *J* = 8.2, 1.8 Hz, 1H), 6.96 (d, *J* = 8.1 Hz, 1H), 5.93 (s, 1H), 4.23 (q, *J* = 7.2 Hz, 2H), 2.77 (s, 3H), 2.71 (s, 3H), 1.50 (t, *J* = 6.9 Hz, 3H); ^{13}C NMR (75 MHz,

$CDCl_3$) δ 196.0, 162.8, 148.9, 148.0, 146.3, 142.9, 125.9, 120.5, 114.8, 109.4, 64.9, 29.5, 14.9, 13.6. HRMS-ESI (m/z) $[M + H]^+$ calcd for $C_{14}H_{16}NO_3S$, 278.0851; found 278.0023.

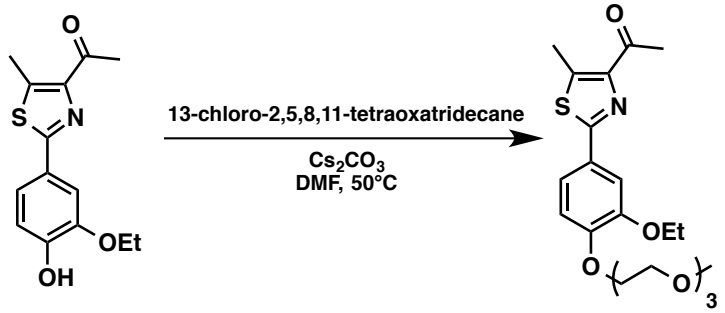

1-(2-(3-Ethoxy-4-(2-(2-(2-methoxyethoxy)ethoxy)ethoxy)-phenyl)-5-methylthiazol-4-yl)ethan-1-one (**11d**). To a solution of thiazole intermediate **11c** (1.66 g, 6.0 mmol) in DMF (35 mL) was added Cs_2CO_3 (3.13 g, 9.6 mmol) and 13-chloro-2,5,8,11-tetraoxatridecane (2.19 g, 12.0 mmol). The mixture was stirred for 18 h at 50 °C. After concentration to remove residual solvent, the resulting residue was washed with brine and extracted with ethyl acetate. The organic layer was washed with water three times, dried over anhydrous Na_2SO_4, concentrated in vacuo, and the crude residue was purified by flash column chromatography over silica gel (1:1 ethyl acetate/hexanes) to yield the desired ketone (2.26 g, 5.3 mmol, 89% yield) as a white solid. ^{1}H NMR (500 MHz, $CDCl_3$) δ 7.48 (d, *J* = 2.0 Hz, 1H), 7.38 (dd, *J* = 8.5, 2.0 Hz, 1H), 6.94 (d, *J* = 8.5 Hz, 1H), 4.24−4.20 (m, 2H), 4.17 (q, *J* = 7.0 Hz, 2H), 3.93−3.89 (m, 2H), 3.79−3.75 (m, 2H), 3.70−3.63 (m, 4H), 3.57−3.53 (m, 2H), 3.37 (s, 3H), 2.77 (s, 3H), 2.71 (s, 3H), 1.47 (t, *J* = 7.0 Hz, 3H); ^{13}C NMR (125 MHz, $CDCl_3$) δ 196.0, 162.5, 150.8, 149.4, 149.0, 143.1, 126.9, 119.8, 114.0, 111.4, 72.1, 71.1, 70.8, 70.7, 69.7, 69.0, 64.9, 59.2, 29.5, 15.0, 13.6.

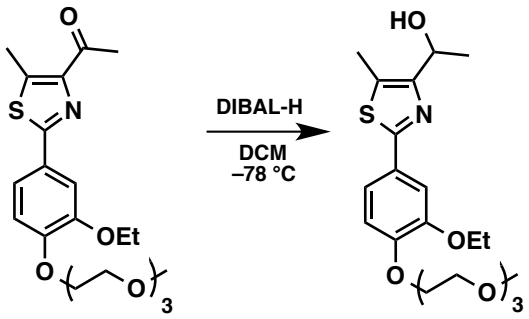

1-(2-(3-Ethoxy-4-(2-(2-(2-methoxyethoxy)ethoxy)ethoxy)-phenyl)-5-methylthiazol-4-yl)ethan-1-ol (**11e**)**.** To a stirred solution of ketone **11d** (1.06 g, 2.5 mmol) in CH_2Cl_2 (35 mL) cooled to −78 °C was slowly added diisobutylaluminum hydride (1.0 M in THF, 10 mmol, 10 mL). The mixture was allowed to warm to 23 °C and stirred for 1 h. The mixture was cooled to 0 °C and slowly quenched with a saturated aqueous solution of Rochelle's salt. The cloudy solution was stirred for 1 h at 23 °C until the solution became clear again. The resulting solution was extracted with ethyl acetate, washed with brine, dried over anhydrous Na_2SO_4, and concentrated in vacuo to give the desired alcohol **11e** (978 mg, 2.3 mmol, 92% yield) as a pale yellow solid. ^{1}H NMR (500 MHz, $CDCl_3$) δ 7.44 (d, *J* = 2.0 Hz, 1H), 7.33 (dd, *J* = 8.5, 2.0 Hz, 1H), 6.89 (d, *J* = 8.5 Hz, 1H), 4.91 (q, *J* = 6.5 Hz, 1H), 4.22−4.17 (m, 2H), 4.13 (q, *J* = 7.0 Hz, 2H), 3.91−3.86 (m, 2H), 3.76−3.72 (m, 2H), 3.69− 3.61 (m, 4H), 3.55−3.51 (m, 2H), 3.35 (s, 3H), 2.37 (s, 3H), 1.52 (d, *J* = 6.0 Hz, 3H), 1.44 (t, *J* = 7.0 Hz, 3H); ^{13}C NMR (125 MHz, $CDCl_3$) δ 164.3, 155.1, 150.0, 149.0, 127.2, 125.8, 119.3, 113.8, 111.0, 71.8, 70.8, 70.6, 70.4, 69.5, 68.7, 64.6, 64.4, 58.9, 24.0, 14.7, 10.7. HRMS-ESI (m/z) $[M + H]^+$ calcd for $C_{21}H_{32}NO_6S$, 426.1950; found 426.1958.

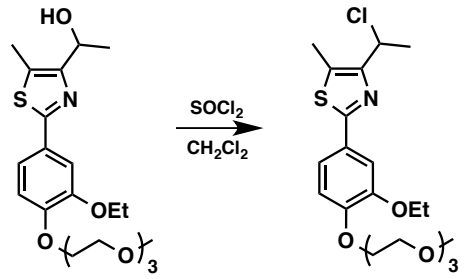

4-(1-Chloroethyl)-2-(3-ethoxy-4-(2-(2-(2-methoxyethoxy)-ethoxy)ethoxy)phenyl)-5-methylthiazole (**11f**)**.** To a stirred solution of alcohol **11e** (425 mg, 1.0 mmol) in CH_2Cl_2 (8 mL) was added thionyl chloride (0.78 mL, 10.0 mmol) slowly at 0 °C. The mixture was allowed to warm to 23 °C and stirred for 1 h. After concentration in vacuo to remove residual solvent, the resulting crude residue was used directly for next step without any further purification because of the instability of chloride **11f**. ^{1}H NMR (500 MHz, $CDCl_3$) δ 7.49 (d, *J* = 2.1 Hz, 1H), 7.37 (dd, *J* = 8.4, 2.1 Hz, 1H), 6.91 (d, *J* = 8.3 Hz, 1H), 5.26 (q, *J* = 6.7 Hz, 1H), 4.25 – 4.11 (m, 4H), 3.90 (dd, *J* = 5.6, 4.6 Hz, 2H), 3.80 – 3.74 (m, 2H), 3.71 – 3.62 (m, 4H), 3.58 – 3.52 (m, 2H), 3.37 (s, 3H), 2.48 (s, 3H), 1.99 (d, *J* = 6.7 Hz, 3H), 1.51 – 1.41 (m, 3H). ^{13}C NMR (126 MHz, $CDCl_3$) δ 164.44, 152.00, 150.41, 149.24, 129.59, 127.39, 119.68, 114.00, 111.50, 72.06, 71.05, 70.82, 70.68, 69.74, 68.94, 64.87, 59.17, 51.89, 24.55, 14.97, 11.34.

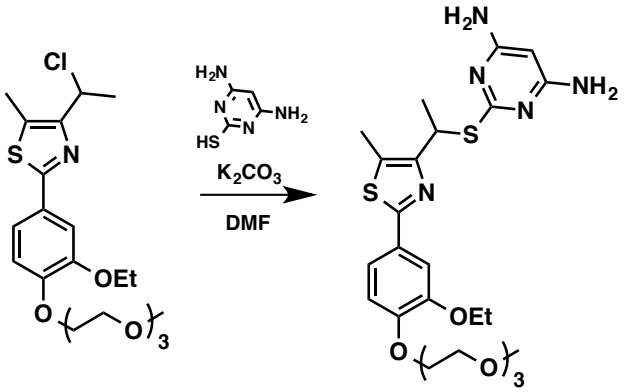

2-((1-(2-(3-Ethoxy-4-(2-(2-(2-methoxyethoxy)ethoxy)-ethoxy)phenyl)-5-methylthiazol-4-yl)ethyl)thio)pyrimidine- 4,6-diamine (**11 R/S**). A mixture of crude chloride **11f** from the previous step, 4,6-diamino-2-mercaptopyrimidine (625 mg, 4.0 mmol), and K_2CO_3 (552 mg, 4.0 mmol) in DMF (7 mL) was stirred at 70 °C for 1 h. The solution was cooled, concentrated in

vacuo, and purified by flash column chromatography over silica gel (25:1 dichloromethane/methanol) to give the desired product **11 R/S** (357 mg, 0.65 mmol, 65% yield over two steps) as a white solid. ^{1}H NMR (500 MHz, $CDCl_3$) δ 7.49 (d, *J* = 2.0 Hz, 1H), 7.35 (dd, *J* = 8.5 Hz, 2.0 Hz, 1H), 6.90 (d, *J* = 8.5 Hz, 1H), 5.24 (s, 1H), 5.02 (q, *J* = 7.0 Hz, 1H), 4.58 (s, 4H), 4.22−4.18 (m, 2H), 4.15 (q, *J* = 7.0 Hz, 2H), 3.91−3.87 (m, 2H), 3.78−3.75 (m, 2H), 3.69−3.63 (m, 4H), 3.56−3.53 (m, 2H), 3.37 (s, 3H), 2.50 (s, 3H), 1.81 (d, *J* = 7.0Hz, 3H), 1.46 (t, *J* = 7.0 Hz, 3H); ^{13}C NMR (125MHz, $CDCl_3$) δ 170.7, 163.8, 163.2 (2), 153.3, 149.9, 149.1, 127.9, 126.8, 119.4, 114.0, 111.3, 80.6, 71.9, 70.9, 70.7, 70.6, 69.7, 68.9, 64.7, 59.1, 37.7, 22.0, 14.8, 11.6; HRMS-ESI (m/z) $[M + H]^+$ calcd for $C_{25}H_{35}N_5O_5S_2H$, 550.2158; found 550.2169.

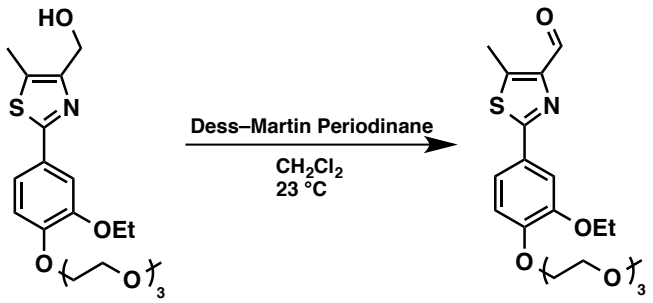

2-(3-ethoxy-4-(2-(2-(2-methoxyethoxy)ethoxy)ethoxy)phenyl)-5-methylthiazole-4-carbaldehyde (**11j**). Dess-Martin Periodinane (222 mg, 0.525 mmol) was added to a solution of alcohol **11i** (108 mg, 0.262 mmol) in dry dichloromethane (5 mL) at room temperature while under a nitrogen atmosphere. After 1.75 hours, another 110 mg of DMP was added. The reaction was monitored via TLC (ethyl acetate), and after 1 hour it was diluted with ether, washed with aqueous sodium hydroxide (1 M), and washed with saturated sodium thiosulfate. The organic layer was washed with saturated sodium bicarbonate, washed with brine, and dried with magnesium sulfate. The drying agent was filtered off, and the solvent was removed under reduced pressure. Column chromatography (silica gel, gradient elution: 75% to 100% ethyl acetate in hexane) afforded the aldehyde (84 mg, 78% yield). ^{1}H NMR (500 MHz, $CDCl_3$) δ 7.49 (d, *J* = 2.1 Hz, 1H), 7.34 (dd, *J* = 8.4, 2.2 Hz, 1H), 4.24 – 4.18 (m, 2H), 4.18 – 4.12 (m, 2H),

3.91 – 3.88 (m, 2H), 3.77 – 3.73 (m, 2H), 3.69 – 3.61 (m, 4H), 3.55 – 3.51 (m, 2H), 3.35 (s, 3H), 2.78 (s, 3H), 1.45 (t, *J* = 7.0 Hz, 3H). ^{13}C NMR (126 MHz, $CDCl_3$) δ 186.53, 164.85, 150.89, 149.36, 149.26, 144.78, 126.33, 119.97, 113.78, 111.11, 72.00, 71.00, 70.76, 70.62, 69.64, 68.87, 64.82, 59.11, 14.87, 12.42. HRMS-ESI (m/z) $[M + H]^+$ calcd for $C_{20}H_{28}NO_6S$, 410.1637; found 410.1622.

4.2.2 Experimental Procedures Relevant to Compound 12

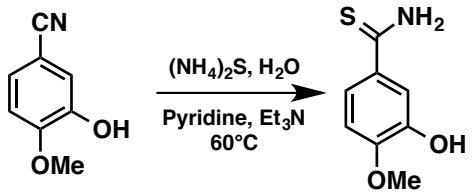

3-Hydroxy-4-methoxybenzothioamide (**12b**). To a mixture of 3-hydroxy-4-methoxybenzonitrile **12a** (3.00 g, 20.11 mmol) in pyridine (30 mL) and triethylamine (3 mL) was added ammonium sulfide solution (20 wt % in H_2O, 20.7 mL, 60.3 mmol). The mixture was stirred for 18 h at 60 °C. The reaction mixture was cooled and concentrated under reduced pressure to remove residual solvent. The resulting residue was mixed with brine and ethyl acetate, and the product was extracted with ethyl acetate. The organic layer was dried over anhydrous Na_2SO_4 and concentrated in vacuo. The crude product was purified by flash column chromatography (silica gel, 3:1 ethyl acetate/hexanes) to yield **12b** (3.13 g, 17.1 mmol, 85% yield) as a yellow solid. ^{1}H NMR (500 MHz, acetone-d_6) δ 8.77 (br s, 1H), 8.65 (br s, 1H), 7.85 (s, 1H), 7.59 (d, *J* = 2.5 Hz, 1H), 7.56 (dd, *J* = 8.5, 2.3 Hz, 1H), 6.94 (d, *J* = 8.5 Hz, 1H), 3.88 (s, 3H); 13C NMR (125 MHz, acetone-d_6) δ 200.7, 150.5, 145.7, 132.4, 119.5, 114.8, 110.2, 55.5.

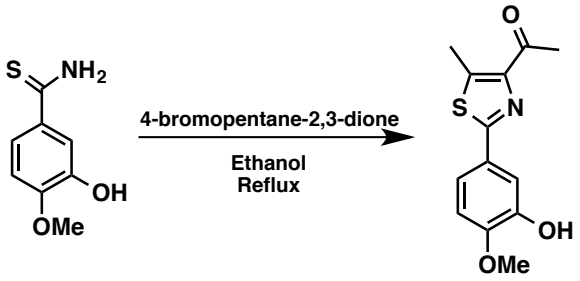

1-(2-(3-Hydroxy-4-methoxyphenyl)-5-methylthiazol-4-yl)-ethan-1-one (**12c**). A mixture of thioamide **12b** (2.75 g, 15.0 mmol) and 4-bromopentane-2,3-dione (4.03 g, 22.5 mmol) in ethanol (70 mL) was stirred under refluxing conditions for 4 h. The resulting mixture was cooled and concentrated under reduced pressure. The crude residue was purified by flash column chromatography (silica gel, 10:3 hexanes/ethyl acetate) to yield the desired thiazole intermediate **12c** (3.79 g, 14.4 mmol, 96% yield) as a white solid. ^{1}H NMR (500 MHz, DMSO-d_6) δ 9.53 (brs, 1H), 7.34 (d, *J* = 2.0 Hz, 1H), 7.26 (dd, *J* = 8.5, 2.0 Hz, 1H), 6.98 (d, *J* = 8.5 Hz, 1H), 3.80 (s, 3H), 2.66 (s, 3H), 2.57 (s, 3H); ^{13}C NMR (125 MHz, DMSO-d_6) δ 195.2, 162.5, 150.1, 148.5, 147.1, 142.7, 125.6, 118.2, 112.9, 112.5, 55.9, 29.4, 13.2.

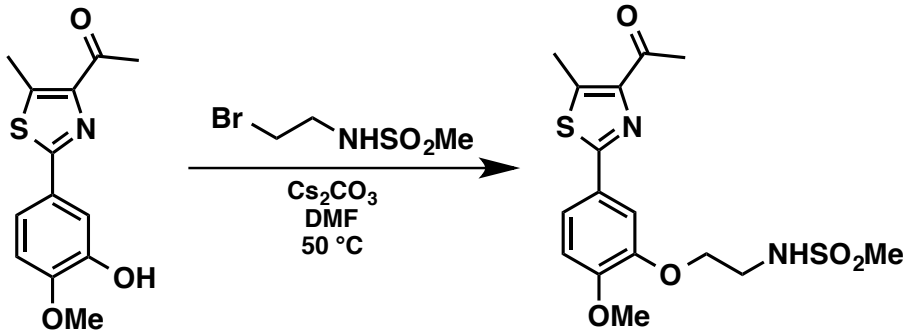

N-(2-(5-(4-Acetyl-5-methylthiazol-2-yl)-2-methoxyphenoxy)-ethyl)methanesulfonamide (**12d**). To a solution of thiazole intermediate **12c** (1.58 g, 6.0 mmol) in DMF (35 mL) were added Cs_2CO_3 (3.13 g, 9.6 mmol) and *N*-(2-bromoethyl)methanesulfonamide (2.18 g, 10.8 mmol). The mixture was stirred for 72 h at 50 °C. After concentration to remove residual solvent, the resulting residue was washed with brine and extracted with ethyl acetate. The organic layer was washed with water three times and dried over anhydrous Na_2SO_4. The solvent was moved on a rotary evaporator, and the crude product was purified by flash column chromatography (silica

gel, 3:2 ethyl acetate/hexanes) to yield the desired ketone (1.89 g, 4.9 mmol, 82% yield) as a white solid. ^{1}H NMR (500 MHz, $CDCl_3$) δ 8.00 (s, 1H), 7.51 (d, *J* = 2.0 Hz, 1H), 7.46 (dd, *J* = 8.5, 2.0 Hz, 1H), 6.92 (d, *J* = 8.5 Hz, 1H), 4.25−4.20 (m, 2H), 3.90 (s, 3H), 3.60−3.55 (m, 2H), 3.03 (s, 3H), 2.76 (s, 3H), 2.70 (s, 3H); ^{13}C NMR (125 MHz, $CDCl_3$) δ 195.8, 162.5, 151.5, 148.9, 147.8, 143.1, 126.4, 121.1, 112.4, 111.7, 69.1, 55.9, 42.7, 40.6, 29.4, 13.4.

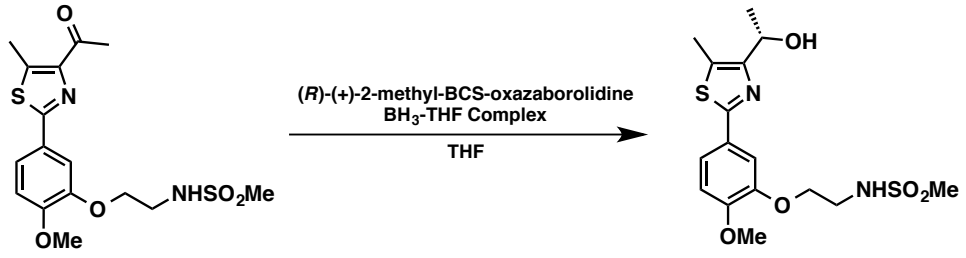

(*S*)-N-(2-(5-(4-(1-Hydroxyethyl)-5-methylthiazol-2-yl)-2-methoxyphenoxy)ethyl)methanesulfonamide (**12e**). To a stirred solution of (*R*)-(+)-2-methyl-CBS-oxazaborolidine (6.7 mL of a 1.0 M solution in toluene, 6.7 mmol) in THF (26 mL) at −78 °C under Ar was added borane−tetrahydrofuran complex (4.4 mL of a 1.0 M solution in THF, 4.4 mmol) followed by a solution of **12d** (284 mg, 0.74 mmol) in THF (14 mL). After the addition of **12d** with a syringe pump over the course of 6 hours, the reaction mixture was stirred for another 20 min at −78 °C. Water (10 mL) and methanol (5 mL) were added, and the mixture was allowed to warm to room temperature. After removal of the solvent under reduced pressure, the crude product was mixed with ethyl acetate and washed with brine. The organic layer was washed with water three times, dried over anhydrous Na_2SO_4, and concentrated in vacuo. The crude residue was purified by flash column chromatography twice over silica gel with 3:2 ethyl acetate/hexanes and 40:1 dichloromethane/methanol to yield alcohol **12e** (221 mg, 0.57 mmol, 77% yield, 96% ee) as a white solid. ^{1}H NMR (500 MHz, acetone-d_6) δ 7.57 (d, *J* = 2.0 Hz, 1H), 7.46 (dd, *J* = 8.5, 2.0 Hz, 1H), 7.05 (d, *J* = 8.5 Hz, 1H), 6.26 (br s, 1H), 5.02−4.95 (m, 1H), 4.21 (t, *J* = 5.5 Hz, 2H), 3.88 (s, 3H), 3.57 (dt, *J* = 5.5, 5.5 Hz, 2H), 3.04 (s, 3H), 2.48 (s, 3H), 1.50 (d,

J = 6.0 Hz, 3H); ^{13}C NMR (125 MHz, acetone-d_6) δ 162.9, 156.1, 151.3, 148.4, 127.1, 126.8, 119.7, 112.1, 111.4, 68.6, 64.1, 55.3, 42.6, 39.6, 23.0, 10.0.

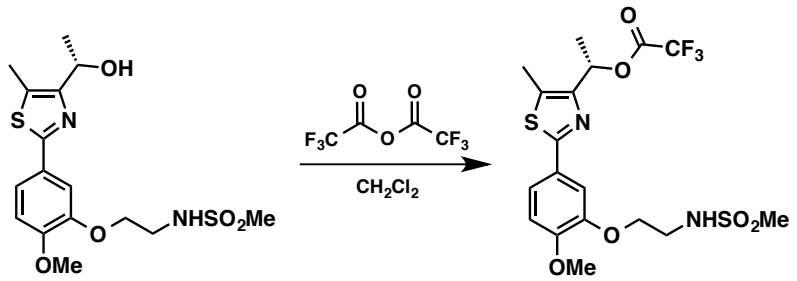

(*S*)-1-(2-(4-Methoxy-3-(2-(methylsulfonamido)ethoxy)-phenyl)-5-methylthiazol-4-yl)ethyl 2,2,2-Trifluoroacetate (**12f**). To a stirred solution of alcohol **12e** (221 mg, 0.57 mmol) in CH_2Cl_2 (13 mL) was added trifluoroaceticanhydride (0.66 mL, 2.9 mmol) slowly at 0 °C. After being stirred at 0 °C for 30 min, the mixture was allowed to warm to 23 °C and stirred for another 30 min. After removing the solvent under reduced pressure, the crude product was used directly in the next step without further purification due to its instability.

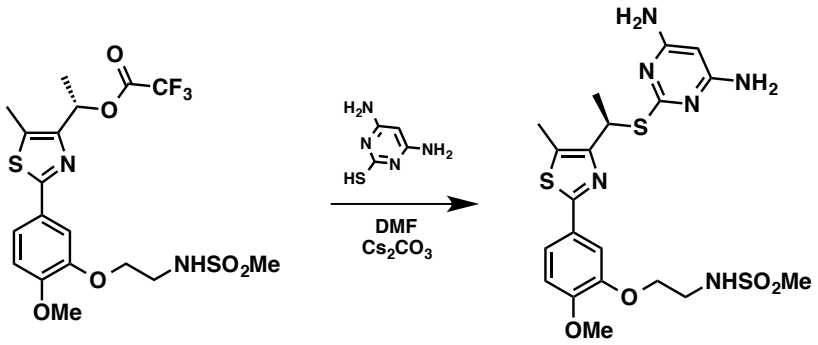

(*R*)-N-(2-(5-(4-(1-((4,6-Diaminopyrimidin-2-yl)thio)ethyl)-5-methylthiazol-2-yl)-2-methoxyphenoxy)ethyl)methane-sulfonamide (**12R**). A mixture of **12f** from the previous step and 4,6-diamino-2-mercaptopyrimidine (112 mg, 0.86 mmol) in DMF (5 mL) was stirred at 80 °C for 1 h. The solution was cooled, concentrated in vacuo, and purified by flash column chromatography (silica gel, 25:1 dichloromethane/methanol) to give a mixture of enantiomers **12R** and **12S** (178 mg, 0.35 mmol, 61% total yield over two steps, 40% ee of the *R*-isomer) as a

white solid. Recrystallization of the enantiomers (MeOH/acetone) gave **12R** with >93% ee. ^{1}H NMR (500 MHz, acetone-d_6) δ 7.55 (d, J = 2.0 Hz, 1H), 7.48 (dd, *J* = 8.5, 2.0 Hz, 1H), 7.06 (d, *J* = 8.5 Hz, 1H), 6.26 (br s, 1H), 5.60−5.55 (m, 4H), 5.37 (s, 1H), 5.30 (q, *J* = 7.0 Hz, 1H), 4.23 (t, *J* = 5.5 Hz, 2 H), 3.89 (s, 3H), 3.58 (dt, *J* = 5.5, 5.5 Hz, 2H), 3.05 (s, 3H), 2.52 (s, 3H), 1.74 (d, *J* = 7.0 Hz, 3H); ^{13}C NMR (125 MHz, DMSO-d_6) δ 168.0, 163.5, 162.9, 153.6, 150.6, 147.8, 126.6, 126.2, 119.5, 112.3, 110.4, 79.0, 67.9, 55.7, 41.9, 36.1, 30.7, 22.2, 11.2; HRMS-ESI (m/z) [M + H]$^+$ calcd for $C_{20}H_{26}N_6O_4S_3H$, 511.1256; found 511.1259; **12R** $[\alpha]^{19}_D$ +340.0 (c 0.12, acetone) (93% ee).

4.2.3 Experimental Procedures Relevant to Compound S24

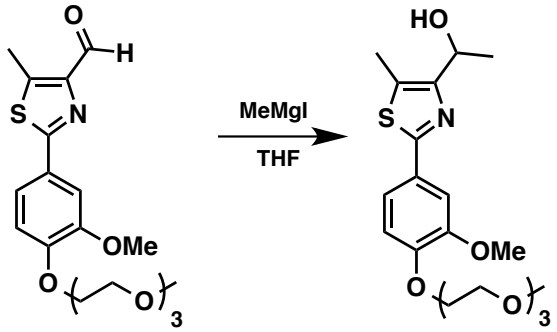

1-(2-(3-methoxy-4-(2-(2-(2-methoxyethoxy)ethoxy)ethoxy)phenyl)-5-methylthiazol-4-yl)ethan-1-ol (**S24e**). While at 0 °C, a solution of methyl magnesium iodide (3M, 0.40 mmol) was added to a solution of aldehyde (**S24d**) (63 mg, 0.16 mmol) in dry tetrahydrofuran (1.0 mL). The reaction was slowly warmed to room temperature and monitored by TLC (30% ethyl acetate in hexane). After 15 minutes, the reaction was quenched via addition of acetic acid (80% in water, 0.15 mL) at 0 °C. Water (5 mL) was added, and the product was extracted with dichloromethane. Column chromatography (silica gel, gradient elution: 100% ethyl acetate to 1% methanol in dichloromethane) gave the desired alcohol (55 mg, 85% yield). ^{1}H NMR (500 MHz, $CDCl_3$) δ 7.46 (d, *J* = 2.1 Hz, 1H), 7.35 (dd, *J* = 8.3, 2.1 Hz, 1H), 6.91 (d, *J* = 8.3 Hz, 1H), 4.93 (p, *J* = 6.6 Hz, 1H), 4.22 (dd, *J* = 5.7, 4.6 Hz, 2H), 3.93 (s, 3H), 3.90 (dd, *J* = 5.7, 4.5 Hz,

2H), 3.77 – 3.72 (m, 2H), 3.72 – 3.62 (m, 4H), 3.57 – 3.51 (m, 2H), 3.37 (s, 3H), 2.89 (d, *J* = 7.5 Hz, 1H), 2.41 (s, 3H), 1.54 (d, *J* = 6.5 Hz, 3H). ^{13}C NMR (126 MHz, $CDCl_3$) δ 164.56, 155.34, 149.94, 149.81, 127.39, 125.98, 119.44, 113.42, 109.50, 72.07, 71.00, 70.78, 70.69, 69.69, 68.64, 64.75, 59.18, 56.22, 24.30, 11.03. HRMS-ESI (m/z) $[M + H]^+$ calcd for $C_{20}H_{30}NO_6S$, 412.1794; found 412.1799.

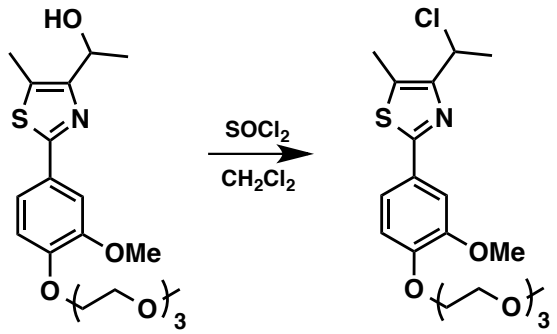

4-(1-chloroethyl)-2-(3-methoxy-4-(2-(2-(2-methoxyethoxy)ethoxy)ethoxy)phenyl)-5-methylthiazole (**S24f**) To a stirred solution of alcohol **S24e** (55.3 mg, 0.134 mmol) and CH_2Cl_2 (0.2 mL) was added thionyl chloride (0.48 mL, 6.7 mmol) slowly at room temperature. The mixture was stirred for 2.5 hours under a balloon of nitrogen. The reaction was cooled to 0 °C, and cold saturated sodium bicarbonate (1.0 mL) was added. The product was extracted with dichloromethane after adding an additional 3 mL of water. The organic fractions were dried with magnesium sulfate, the drying agent was filtered off, and the solvent was removed under reduced pressure. The crude product was used for the next step without further purification. ^{1}H NMR (500 MHz, $CDCl_3$) δ 7.49 (d, *J* = 2.1 Hz, 1H), 7.36 (dd, *J* = 8.4, 2.1 Hz, 1H), 6.90 (d, *J* = 8.3 Hz, 1H), 5.26 (q, *J* = 6.7 Hz, 1H), 4.21 (dd, *J* = 5.7, 4.6 Hz, 2H), 3.93 (s, 3H), 3.89 (dd, *J* = 5.7, 4.5 Hz, 2H), 3.76 – 3.71 (m, 2H), 3.71 – 3.61 (m, 4H), 3.56 – 3.51 (m, 2H), 3.36 (s, 3H), 2.47 (s, 3H), 1.99 (d, *J* = 6.7 Hz, 3H). ^{13}C NMR (126 MHz, $CDCl_3$) δ 164.39, 151.92, 150.03, 149.75, 129.60, 127.18, 119.57, 113.31, 109.68, 72.02, 70.95, 70.72, 70.64, 69.64, 68.57, 59.13, 56.19, 51.81, 24.52, 11.31.

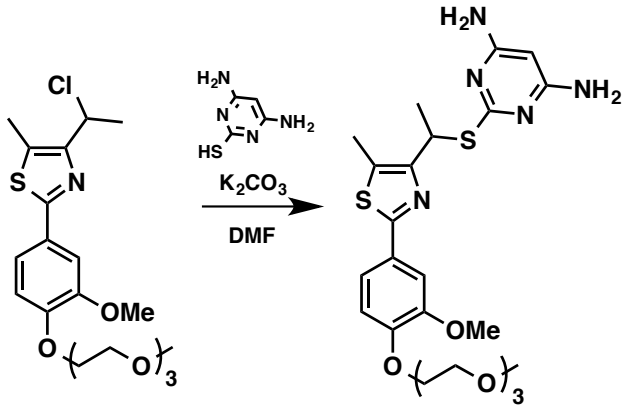

2-((1-(2-(3-methoxy-4-(2-(2-(2-methoxyethoxy)ethoxy)ethoxy)phenyl)-5-methylthiazol-4-yl)ethyl)thio)pyrimidine-4,6-diamine (**S24**)**.** A mixture of chloride **S24f** (60 mg) from the previous step, 4,6-diamino-2-mercaptopyrimidine (28 mg, 0.20 mmol), and K_2CO_3 (77 mg, 0.56 mmol) in DMF (1.0 mL) was stirred at 80 °C for 2.5 hours while under a nitrogen atmosphere. The solution was concentrated under reduced pressure, water was added, and the product was extracted with dichloromethane. After drying with magnesium sulfate and filtering off the drying agent, the solvent was removed under reduced pressure. Column chromatography (silica gel, gradient elution: 5% to 10% methanol in dichloromethane) gave the desired product (52 mg, 0.097 mmol, 72% yield over two steps) as a white solid. ^{1}H NMR (500 MHz, $CDCl_3$) δ 7.50 (d, *J* = 2.0 Hz, 1H), 7.35 (dd, *J* = 8.3, 2.1 Hz, 1H), 6.90 (d, *J* = 8.4 Hz, 1H), 5.27 – 5.19 (m, 2H), 4.56 (s, 4H), 4.21 (dd, *J* = 5.7, 4.6 Hz, 2H), 3.95 – 3.87 (m, 5H), 3.77 – 3.71 (m, 2H), 3.71 – 3.62 (m, 4H), 3.58 – 3.52 (m, 2H), 3.37 (s, 3H), 2.50 (s, 3H), 1.81 (d, *J* = 7.0 Hz, 3H). ^{13}C NMR (126 MHz, $CDCl_3$) δ 170.84, 163.87, 163.29, 153.48, 149.76, 149.68, 127.88, 127.01, 119.41, 113.42, 109.72, 80.68, 72.07, 71.00, 70.78, 70.69, 69.68, 68.57, 59.21, 56.24, 37.90, 22.08, 11.70. HRMS-ESI (m/z) $[M + H]^+$ calcd for $C_{24}H_{34}N_5O_5S_2$, 536.2001; found 536.2004.

4.2.4 Experimental Procedures Relevant to Compound 9

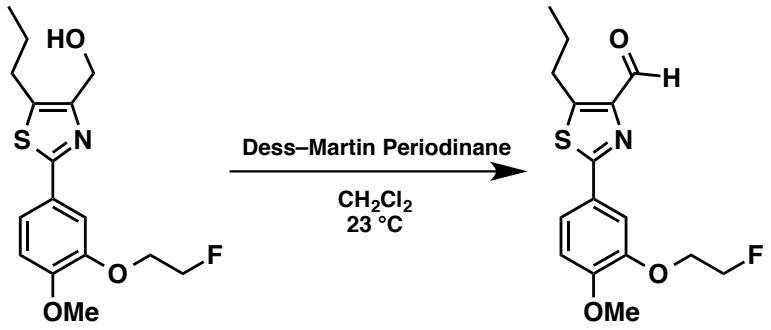

2-(3-(2-fluoroethoxy)-4-methoxyphenyl)-5-propylthiazole-4-carbaldehyde (**9b**)**.** Dess-Martin Periodinane (93 mg, 0.21 mmol) was added to a solution of alcohol **9a** (50 mg, 0.15 mmol) in dry dichloromethane (4 mL) at room temperature while under a nitrogen atmosphere. A precipitate formed 5 minutes into the reaction. The reaction was monitored via TLC, and after 30 minutes it was diluted with ether (50 mL), washed with aqueous sodium hydroxide (10 mL, 1 M), and washed with saturated sodium thiosulfate (5 mL). The organic layer was washed with saturated sodium bicarbonate (20 mL), washed with brine, and dried with magnesium sulfate. The drying agent was filtered off, and the solvent was removed under reduced pressure. Column chromatography (30% ethyl acetate in hexane) afforded the aldehyde (80% yield)**.** ^{1}H NMR (500 MHz, $CDCl_3$) δ 10.15 (s, 1H), 7.56 (d, *J* = 2.1 Hz, 1H), 7.44 (dd, *J* = 8.4, 2.1 Hz, 1H), 6.91 (d, *J* = 8.5 Hz, 1H), 4.89 – 4.81 (m, 1H), 4.79 – 4.72 (m, 1H), 4.42 – 4.36 (m, 1H), 4.39 – 4.29 (m, 1H), 3.91 (s, 3H), 3.22 (t, *J* = 7.6 Hz, 2H), 1.82 – 1.71 (m, 2H), 1.02 (t, *J* = 7.3 Hz, 3H). ^{13}C NMR (126 MHz, $CDCl_3$) δ 186.21, 164.74, 151.89, 151.15, 149.12, 148.37, 125.99, 120.98, 111.86, 111.67, 82.57, 81.21, 68.70, 68.53, 56.18, 28.70, 25.05, 13.79. HRMS-ESI (m/z) $[M + H]^+$ calcd for $C_{16}H_{19}FNO_3S$, 324.1070; found 324.1049.

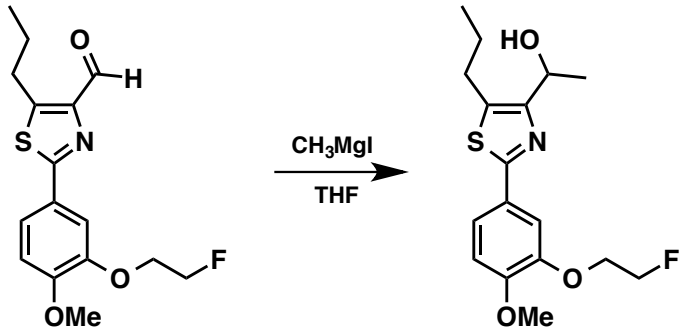

1-(2-(3-(2-fluoroethoxy)-4-methoxyphenyl)-5-propylthiazol-4-yl)ethan-1-ol (**9c**). While at room temperature, a solution of methyl magnesium iodide (3M, 0.23 mmol) was added to a solution aldehyde **9b** (37.6 mg, 0.116 mmol) in dry tetrahydrofuran (0.5 mL). The reaction was monitored via TLC (30% ethyl acetate in hexane), and after 30 minutes the reaction was quenched via addition of acetic acid (80% in water, 0.05 mL). Water (10 mL) was added, and the product was extracted with ethyl acetate. More product could be extracted by washing the aqueous layer with dichloromethane. The combined organic layers were dried with magnesium sulfate, the drying agent was filtered off, and the solvent was removed under reduced pressure. Column chromatography (silica gel, gradient elution: 30% to 50% ethyl acetate in hexane) gave the desired alcohol (67% yield). ^{1}H NMR (500 MHz, $CDCl_3$) δ 7.50 (d, *J* = 2.1 Hz, 1H), 7.41 (dd, *J* = 8.4, 2.1 Hz, 1H), 6.86 (d, *J* = 8.4 Hz, 1H), 4.91 (q, *J* = 6.5 Hz, 1H), 4.86 – 4.80 (m, 1H), 4.77 – 4.71 (m, 1H), 4.38 – 4.32 (m, 1H), 4.32 – 4.27 (m, 1H), 3.87 (s, 3H), 3.07 (br. s, 1H), 2.75 – 2.68 (m, 2H), 1.70 – 1.59 (m, 2H), 1.53 (s, 3H), 0.97 (t, *J* = 7.3 Hz, 3H). ^{13}C NMR (126 MHz, $CDCl_3$) δ 164.54, 154.98, 151.17, 148.07, 132.41, 126.91, 120.40, 111.78, 111.57, 82.57, 81.21, 68.59, 68.43, 64.52, 56.08, 27.96, 25.32, 24.48, 13.78. HRMS-ESI (m/z) $[M + H]^+$ calcd for $C_{17}H_{23}FNO_3S$, 340.1383; found 340.1398.

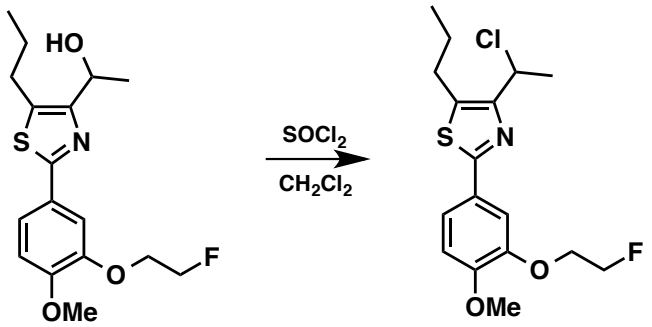

4-(1-chloroethyl)-2-(3-(2-fluoroethoxy)-4-methoxyphenyl)-5-propylthiazole (**9d**)**.** To a stirred solution of alcohol **9c** (25 mg, 0.074 mmol) in CH_2Cl_2 (0.5 mL) was added thionyl chloride (0.30 mL, 4.2 mmol) slowly at room temperature. The mixture was stirred for 2 hours under a balloon of nitrogen. The reaction was cooled to 0 °C, and cold saturated sodium bicarbonate (approximately 1.5 mL) was added. The product was mixed with water and extracted with dichloromethane. The organic fractions were dried with magnesium sulfate, the drying agent was filtered off, and the solvent was removed under reduced pressure. The crude product was used for the next step without further purification. ^{1}H NMR (500 MHz, $CDCl_3$) δ 7.55 (d, *J* = 2.1 Hz, 1H), 7.47 (dd, *J* = 8.4, 2.0 Hz, 1H), 6.90 (d, *J* = 8.4 Hz, 1H), 5.25 (q, *J* = 6.7 Hz, 1H), 4.90 – 4.84 (m, 1H), 4.80 – 4.75 (m, 1H), 4.42 – 4.37 (m, 1H), 4.37 – 4.31 (m, 1H), 3.91 (s, 3H), 2.89 – 2.75 (m, 2H), 2.00 (d, *J* = 6.7 Hz, 3H), 1.81 – 1.62 (m, 2H), 1.02 (t, *J* = 7.4 Hz, 3H). ^{13}C NMR (126 MHz, $CDCl_3$) δ 164.53, 151.74, 151.37, 148.14, 135.63, 127.02, 120.67, 111.89, 111.83, 82.66, 81.30, 68.70, 68.54, 56.19, 51.81, 28.36, 25.21, 24.77, 13.87. HRMS-ESI (m/z) $[M + H]^+$ calcd for $C_{17}H_{22}ClFNO_2S$, 358.1044; found 358.1046.

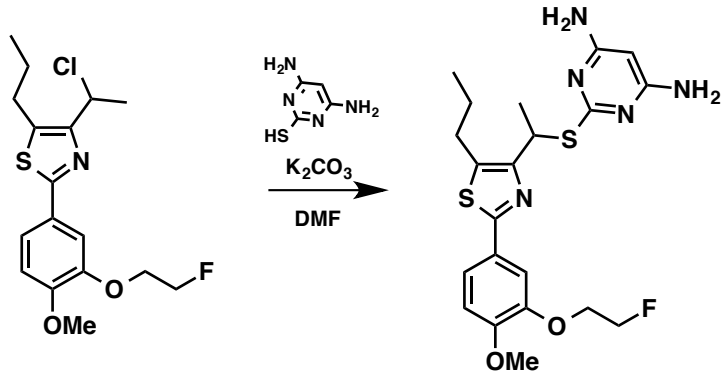

2-((1-(2-(3-(2-fluoroethoxy)-4-methoxyphenyl)-5-propylthiazol-4-yl)ethyl)thio)pyrimidine-4,6-diamine (**9**)**.** A mixture of chloride **9d** (25 mg) from the previous step, 4,6-diamino-2-mercaptopyrimidine (13.9 mg, 0.0977 mmol), and K_2CO_3 (38.6 mg, 0.279 mmol) in DMF (1.0 mL) was stirred at 50 °C for 1.5 hours while under a nitrogen atmosphere. The temperature of the reaction was increased to 80 °C, and the progress of the reaction was monitored via TLC. When the reaction was determined to be complete, the solution was concentrated under reduced pressure, water was added, and the product was extracted with dichloromethane. After drying with magnesium sulfate and filtering off the drying agent, the solvent was removed under reduced pressure. Column chromatography (silica gel, gradient elution: 1% to 5% methanol in dichloromethane) gave the desired product (20 mg, 0.043 mmol, 58% yield over two steps) as a white solid. ^{1}H NMR (500 MHz, $CDCl_3$) δ 7.55 (d, *J* = 2.1 Hz, 1H), 7.44 (dd, *J* = 8.4, 2.0 Hz, 1H), 6.88 (d, *J* = 8.4 Hz, 1H), 5.28 – 5.21 (m, 2H), 4.90 – 4.84 (m, 1H), 4.80 – 4.75 (m, 1H), 4.55 (s, 4H), 4.42 – 4.36 (m, 1H), 4.36 – 4.31 (m, 1H), 3.90 (s, 3H), 2.95 – 2.83 (m, 2H), 1.82 (d, *J* = 6.9 Hz, 3H), 1.71 – 1.63 (m, 2H), 1.00 (t, *J* = 7.3 Hz, 3H). ^{13}C NMR (126 MHz, $CDCl_3$) δ 170.91, 163.93, 163.29, 153.13, 151.03, 148.11, 133.12, 127.52, 120.45, 111.83, 111.72, 82.66, 81.31, 80.72, 68.62, 68.45, 56.21, 37.94, 28.65, 25.39, 22.52, 14.00. HRMS-ESI (m/z) $[M + H]^+$ calcd for $C_{21}H_{27}FN_5O_2S_2$, 464.1590; found 464.1567.

4.2.5 Experimental Procedures Relevant to Compound 10

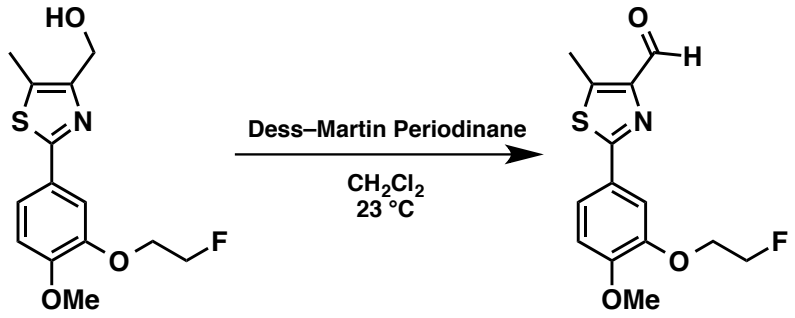

2-(3-(2-fluoroethoxy)-4-methoxyphenyl)-5-methylthiazole-4-carbaldehyde (**10b**). Dess-Martin Periodinane (171 mg, 0.403 mmol) was added to a solution of alcohol **10a** (74 mg, 0.25 mmol) in dry dichloromethane (4 mL) at room temperature while under a nitrogen atmosphere. After 1.75 hours, another 71 mg of DMP was added. The reaction was monitored via TLC, and after 1 hour it was diluted with ether, washed with aqueous sodium hydroxide (1 M), and washed with saturated sodium thiosulfate. The organic layer was washed with saturated sodium bicarbonate, washed with brine, and dried with magnesium sulfate. The drying agent was filtered off, and the solvent was removed under reduced pressure. Column chromatography (silica gel, gradient elution: 1% to 4% methanol in dichloromethane) afforded the aldehyde (70% yield). ^{1}H NMR (500 MHz, $CDCl_3$) δ 10.18 (s, 1H), 7.57 (d, *J* = 2.1 Hz, 1H), 7.45 (dd, *J* = 8.4, 2.2 Hz, 1H), 6.93 (d, *J* = 8.4 Hz, 1H), 4.90 – 4.84 (m, 1H), 4.81 – 4.74 (m, 1H), 4.44 – 4.36 (m, 1H), 4.35 (t, *J* = 4.2 Hz, 1H), 3.93 (s, 3H), 2.81 (s, 3H). ^{13}C NMR (126 MHz, $CDCl_3$) δ 186.53, 164.65, 151.95, 149.36, 148.43, 144.93, 125.95, 121.03, 111.90, 111.67, 82.61, 81.25, 77.16, 68.73, 68.57, 56.25, 12.50. HRMS-ESI (m/z) $[M + H]^+$ calcd for $C_{14}H_{15}FNO_3S$, 296.0757; found 296.0748.

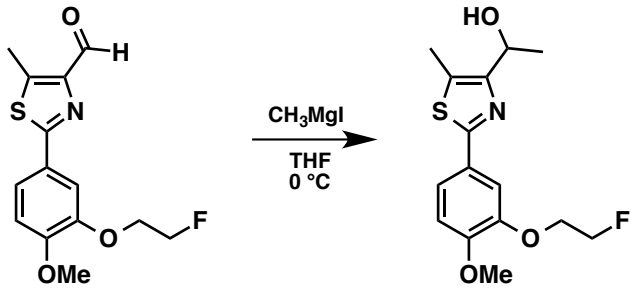

1-(2-(3-(2-fluoroethoxy)-4-methoxyphenyl)-5-methylthiazol-4-yl)ethan-1-ol (**10c**). Aldehyde **10b** (52 mg, 0.18 mmol) was stirred in 2 mL of tetrahydrofuran at 50 °C for 2 hours. Once dissolved, the solution was cooled to room temperature. While at room temperature, a solution of methyl magnesium iodide (3M, 0.19 mmol) was added. The reaction was heated to 50 °C and monitored via TLC (20% ethyl acetate in hexane). When the reaction was determined to be complete it was quenched via addition of acetic acid (80% in water, 0.05 mL) and 1 mL of water. Water (10 mL) was added, and the product was extracted with dichloromethane. The combined organic layers were dried with magnesium sulfate, the drying agent was filtered off, and the solvent was removed under reduced pressure. Column chromatography (silica gel, 50% ethyl acetate in hexane) gave the desired alcohol (68% yield). ^{1}H NMR (500 MHz, $CDCl_3$) δ 7.50 (d, *J* = 2.1 Hz, 1H), 7.41 (dd, *J* = 8.3, 2.1 Hz, 1H), 6.88 (d, *J* = 8.4 Hz, 1H), 4.93 (q, *J* = 6.5 Hz, 1H), 4.88 – 4.82 (m, 1H), 4.78 – 4.73 (m, 1H), 4.40 – 4.34 (m, 1H), 4.34 – 4.28 (m, 1H), 3.89 (s, 3H), 3.07 (s, 1H), 2.39 (s, 3H), 1.53 (d, *J* = 6.5 Hz, 3H). ^{13}C NMR (126 MHz, $CDCl_3$) δ 164.31, 155.31, 151.26, 148.15, 126.90, 126.14, 120.47, 111.87, 111.67, 82.63, 81.27, 77.16, 68.68, 68.51, 64.65, 56.17, 24.18, 10.98. HRMS-ESI (m/z) $[M + H]^+$ calcd for $C_{15}H_{19}FNO_3S$, 312.1070; found 312.1085.

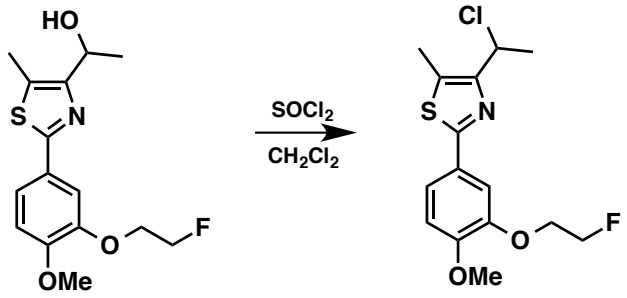

4-(1-chloroethyl)-2-(3-(2-fluoroethoxy)-4-methoxyphenyl)-5-methylthiazole (**10d**). To a stirred solution of alcohol **10c** (37 mg, 0.12 mmol) in CH_2Cl_2 (0.5 mL) was added thionyl chloride (50 equivalents) slowly at room temperature. The mixture was stirred for 2 hours under a balloon of nitrogen. The reaction was cooled to 0 °C, and cold saturated sodium bicarbonate (approximately 2.0 mL) was added. The product was mixed with water (5 mL) and extracted with dichloromethane. The organic fractions were dried with magnesium sulfate, the drying agent was filtered off, and the solvent was removed under reduced pressure. The crude product was used for the next step without further purification. ^{1}H NMR (300 MHz, $CDCl_3$) δ 7.55 (d, *J* = 2.0 Hz, 1H), 7.45 (dd, *J* = 8.4, 2.1 Hz, 1H), 6.90 (d, *J* = 8.4 Hz, 1H), 5.26 (q, *J* = 6.8 Hz, 1H), 4.95 – 4.85 (m, 1H), 4.79 – 4.67 (m, 1H), 4.46 – 4.39 (m, 1H), 4.39 – 4.27 (m, 1H), 3.91 (s, 3H), 2.49 (s, 3H), 2.00 (d, *J* = 6.8 Hz, 3H).

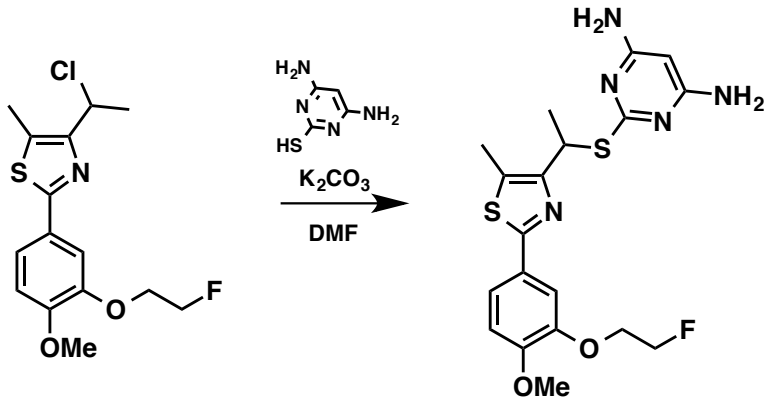

2-((1-(2-(3-(2-fluoroethoxy)-4-methoxyphenyl)-5-methylthiazol-4-yl)ethyl)thio)pyrimidine-4,6-diamine (**10**). A mixture of chloride **10d** (39 mg) from the previous step, 4,6-diamino-2-mercaptopyrimidine (23 mg, 0.17 mmol), and K_2CO_3 (65 mg, 0.47 mmol) in DMF (1.0 mL) was stirred at 80 °C for 1.5 hours while under a nitrogen atmosphere. The temperature of the reaction was increased to 80 °C and monitored via TLC. The mixture was concentrated on a Rotevap, and the residue was put under reduced pressure overnight. Water was added, and the product was extracted with dichloromethane. After drying with magnesium sulfate and filtering off the drying agent, the solvent was removed under reduced pressure. The crude product was dry-loaded onto silica gel, and column chromatography (silica gel, 5% methanol in dichloromethane) gave the desired product (33 mg, 0.0749 mmol, 63% yield over two steps) as a white solid. ^{1}H NMR (500 MHz, MeOD-d_4) δ 7.54 (d, J = 2.1 Hz, 1H), 7.44 (dd, J = 8.4, 2.1 Hz, 1H), 7.03 (d, J = 8.4 Hz, 1H), 5.37 – 5.29 (m, 2H), 4.84 – 4.78 (m, 1H), 4.74 – 4.69 (m, 1H), 4.35 (t, J = 4.0 Hz, 1H), 4.29 (t, J = 3.9 Hz, 1H), 3.89 (s, 3H), 2.52 (s, 3H), 1.76 (d, J = 7.0 Hz, 3H). ^{13}C NMR (126 MHz, MeOD-d_4) δ 170.42, 165.82, 165.22, 154.78, 152.72, 149.66, 128.54, 128.13, 121.50, 113.31, 112.84, 83.83, 82.49, 80.55, 70.13, 69.97, 56.52, 38.40, 22.21, 11.48. HRMS-ESI (m/z) $[M + H]^+$ calcd for $C_{19}H_{23}FN_5O_2S_2$, 436.1277; found 436.1245.

4.2.6 Experimental Procedures Relevant to Compound S22

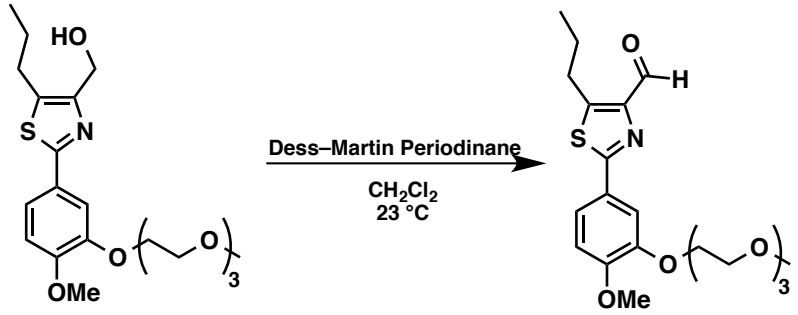

2-(4-methoxy-3-(2-(2-(2-methoxyethoxy)ethoxy)ethoxy)phenyl)-5-propylthiazole-4-carbaldehyde (**S22d**). Dess-Martin Periodinane (240 mg, 0.565 mmol) was added to a solution of alcohol **S22c** (164 mg, 0.385 mmol) in dry dichloromethane (8 mL) at room temperature while under a nitrogen atmosphere. The reaction was monitored via TLC, and after approximately 2 hours it was diluted with ether, washed with aqueous sodium hydroxide (1 M), and washed with saturated sodium thiosulfate. The organic layer was washed with saturated sodium bicarbonate, brine, and it was dried with magnesium sulfate. The drying agent was filtered off, and the solvent was removed under reduced pressure. Column chromatography (silica gel, 75% ethyl acetate in hexane) afforded the aldehyde (82% yield). ^{1}H NMR (500 MHz, $CDCl_3$) δ 10.17 (s, 1H), 7.56 (d, *J* = 2.1 Hz, 1H), 7.44 (dd, *J* = 8.3, 2.1 Hz, 1H), 6.90 (d, *J* = 8.4 Hz, 1H), 4.28 (dd, *J* = 5.7, 4.5 Hz, 2H), 3.93 (dd, *J* = 5.6, 4.5 Hz, 2H), 3.90 (s, 3H), 3.79 – 3.73 (m, 2H), 3.72 – 3.66 (m, 2H), 3.66 – 3.62 (m, 2H), 3.57 – 3.51 (m, 2H), 3.37 (s, 3H), 3.27 – 3.20 (m, 2H), 1.80 – 1.72 (m, 2H), 1.03 (t, *J* = 7.4 Hz, 3H). ^{13}C NMR (126 MHz, $CDCl_3$) δ 186.42, 164.95, 151.77, 151.03, 149.14, 148.80, 126.00, 120.41, 111.66, 111.40, 77.16, 72.07, 71.01, 70.80, 70.70, 69.72, 68.76, 59.17, 56.15, 28.72, 21.19, 14.33. HRMS-ESI (m/z) $[M + H]^+$ calcd for $C_{21}H_{30}NO_6S$, 424.1794; found 424.1784.

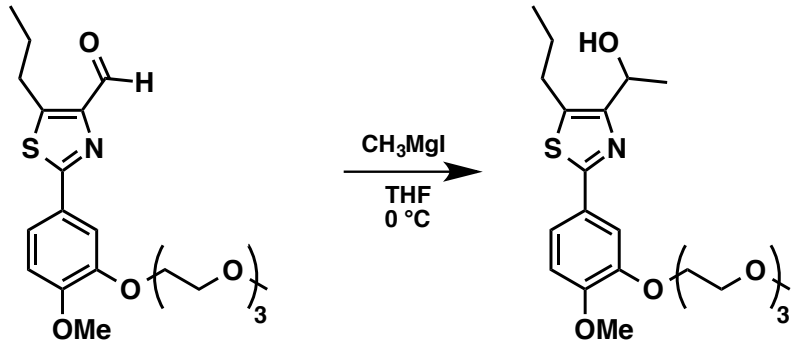

1-(2-(4-methoxy-3-(2-(2-(2-methoxyethoxy)ethoxy)ethoxy)phenyl)-5-propylthiazol-4-yl)ethan-1-ol (**S22e**). Aldehyde **S22d** (135 mg, 0.319 mmol) was stirred in 5 mL of tetrahydrofuran at room temperature, and a solution of methyl magnesium iodide (3M, 0.38 mmol) was added. The reaction was monitored via TLC, and another 1.8 equivalents of MeMgI needed to be added in order to complete the reaction. The reaction was quenched at 0 °C via addition of acetic acid (80% in water, 0.15 mL) in 1 mL of water. Water (10 mL) was added, and the product was extracted with dichloromethane. The combined organic layers were dried with magnesium sulfate, the drying agent was filtered off, and the solvent was removed under reduced pressure. Column chromatography (silica gel, 100% ethyl acetate) gave the desired alcohol (67% yield). ^{1}H NMR (500 MHz, $CDCl_3$) δ 7.53 – 7.48 (m, 1H), 7.41 (ddd, *J* = 8.3, 4.9, 2.1 Hz, 1H), 6.86 (dd, *J* = 8.4, 4.8 Hz, 1H), 4.90 (q, *J* = 6.5 Hz, 1H), 4.29 – 4.23 (m, 2H), 3.95 – 3.89 (m, 2H), 3.88 (d, *J* = 5.0 Hz, 2H), 3.78 – 3.72 (m, 2H), 3.71 – 3.61 (m, 4H), 3.56 – 3.50 (m, 2H), 3.36 (d, *J* = 4.2 Hz, 3H), 2.98 – 2.87 (m, 1H), 2.78 – 2.71 (m, 2H), 1.67 (qd, *J* = 7.3, 4.8 Hz, 2H), 1.54 (dd, *J* = 6.4, 3.4 Hz, 3H), 1.03 – 0.95 (m, 3H). ^{13}C NMR (126 MHz, $CDCl_3$) δ 164.75, 155.05, 151.12, 148.54, 132.20, 127.01, 119.91, 111.65, 111.41, 72.04, 70.97, 70.77, 70.66, 69.74, 68.68, 64.67, 59.14, 56.11, 28.05, 25.39, 24.68, 13.85. HRMS-ESI (m/z) $[M + H]^+$ calcd for $C_{22}H_{34}NO_6S$, 440.2107; found 440.2101.

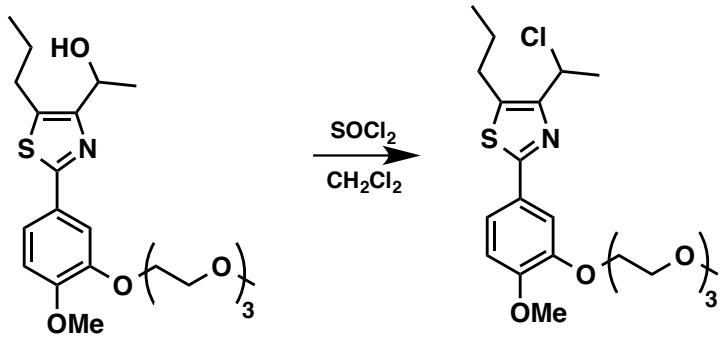

4-(1-chloroethyl)-2-(4-methoxy-3-(2-(2-(2-methoxyethoxy)ethoxy)ethoxy)phenyl)-5-propylthiazole (**S22f**). To a stirred solution of alcohol **S22e** (93 mg, 0.21 mmol) in CH_2Cl_2 was added thionyl chloride (50 equivalents) slowly at room temperature. The mixture was stirred for 2 hours under a balloon of nitrogen. The reaction was cooled to 0 °C, and cold saturated sodium bicarbonate (approximately 3.5 mL) was added. The product was mixed with water (10 mL) and extracted with dichloromethane. The organic fractions were dried with magnesium sulfate, the drying agent was filtered off, and the solvent was removed under reduced pressure. The crude product was used for the next step without further purification. ^{1}H NMR (300 MHz, $CDCl_3$) δ 7.54 (d, *J* = 2.1 Hz, 1H), 7.44 (dd, *J* = 8.4, 2.1 Hz, 1H), 6.87 (d, *J* = 8.4 Hz, 1H), 5.24 (q, *J* = 6.7 Hz, 1H), 4.27 (dd, *J* = 5.8, 4.5 Hz, 2H), 3.97 – 3.89 (m, 2H), 3.91 (s, 1H), 3.81 – 3.72 (m, 2H), 3.72 – 3.57 (m, 4H), 3.59 – 3.49 (m, 2H), 3.37 (s, 3H), 2.82 (td, *J* = 7.4, 1.1 Hz, 2H), 1.99 (d, *J* = 6.7 Hz, 3H), 1.84 – 1.59 (m, 2H), 1.01 (t, *J* = 7.3 Hz, 3H).

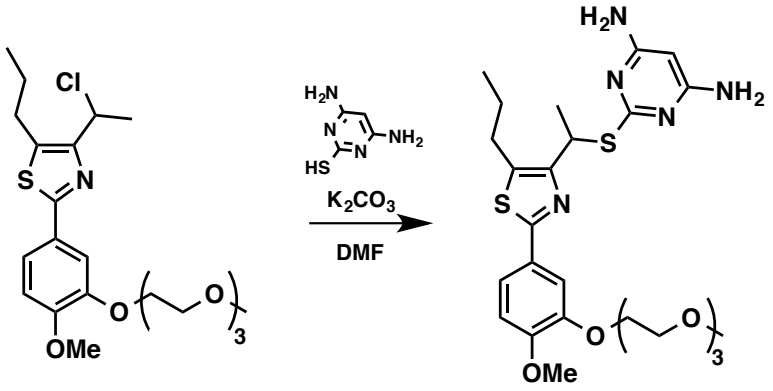

2-((1-(2-(4-methoxy-3-(2-(2-(2-methoxyethoxy)ethoxy)ethoxy)phenyl)-5-propylthiazol-4-yl)ethyl)thio)pyrimidine-4,6-diamine (**S22**). A mixture of chloride **S22f** (90 mg) from the previous step, 4,6-diamino-2-mercaptopyrimidine (41 mg, 0.29 mmol), and K_2CO_3 (111 mg, 0.803 mmol) in DMF (1.2 mL) was stirred at 80 °C while under a nitrogen atmosphere. The reaction was monitored via TLC (10% methanol in dichloromethane). When the reaction was determined to be complete, the mixture was concentrated on a Rotevap. Water (10 mL) was added, and the product was extracted with dichloromethane. More product was extracted by washing the aqueous layer with diethyl ether. After drying with magnesium sulfate and filtering off the drying agent, the solvent was removed under reduced pressure. Column chromatography (silica gel, gradient elution: 5% to 7% methanol in dichloromethane) gave the desired product (67 mg, 71% yield over two steps). ^{1}H NMR (500 MHz, $CDCl_3$) δ 7.53 (d, *J* = 2.0 Hz, 1H), 7.42 (dd, *J* = 8.3, 2.1 Hz, 1H), 6.85 (d, *J* = 8.4 Hz, 1H), 5.23 (s, 2H), 4.71 (s, 4H), 4.26 (dd, *J* = 5.7, 4.5 Hz, 2H), 3.91 (dd, *J* = 5.8, 4.4 Hz, 2H), 3.87 (s, 3H), 3.75 (dd, *J* = 5.8, 3.6 Hz, 2H), 3.68 (dd, *J* = 5.9, 3.6 Hz, 2H), 3.67 – 3.62 (m, 2H), 3.56 – 3.50 (m, 2H), 3.36 (s, 3H), 2.94 – 2.78 (m, 2H), 1.80 (d, *J* = 7.0 Hz, 3H), 1.73 – 1.60 (m, 2H), 0.98 (t, *J* = 7.3 Hz, 3H). ^{13}C NMR (126 MHz, $CDCl_3$) δ 170.57, 164.05, 163.34, 153.12, 150.89, 148.44, 133.00, 127.42, 119.91, 111.62, 111.53, 80.70, 72.04, 70.94, 70.75, 70.64, 69.73, 68.62, 59.11, 56.09, 37.85, 28.59, 25.35, 22.51, 13.96. HRMS-ESI (m/z) $[M + H]^+$ calcd for $C_{26}H_{38}N_5O_5S_2$, 564.2314; found 564.2311.

4.2.7 Experimental Procedures Relevant to Compound S23

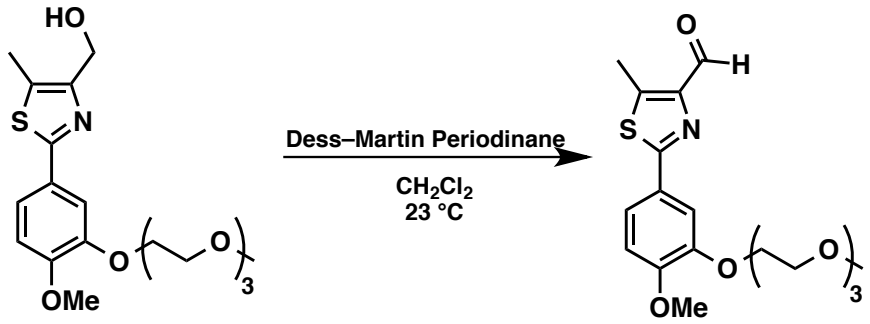

2-(4-methoxy-3-(2-(2-(2-methoxyethoxy)ethoxy)ethoxy)phenyl)-5-methylthiazole-4-carbaldehyde (**S23d**). Dess-Martin Periodinane (389 mg, 0.916 mmol) was added to a solution of alcohol **S23c** (237 mg, 0.596 mmol) in dry dichloromethane (10 mL) at room temperature while under a nitrogen atmosphere. The reaction was monitored via TLC, and after 40 minutes another 50 mg of DMP was added. After another 20 minutes, another 100 mg of DMP needed to be added. After approximately 2 hours, the reaction was diluted with ether, washed with aqueous sodium hydroxide (1 M, 30 mL), and washed with saturated sodium thiosulfate (20 mL). The organic layer was washed with saturated sodium bicarbonate (50 mL), washed with brine (50 mL), and dried with magnesium sulfate. The drying agent was filtered off, and the solvent was removed under reduced pressure. Column chromatography (silica gel, gradient elution: 75% ethyl acetate in hexane to 100% ethyl acetate) gave the aldehyde (93% yield). ^{1}H NMR (500 MHz, $CDCl_3$) δ 10.15 (s, 1H), 7.53 (d, *J* = 2.1 Hz, 1H), 7.40 (dd, *J* = 8.4, 2.1 Hz, 1H), 6.87 (d, *J* = 8.4 Hz, 1H), 4.26 (dd, *J* = 5.7, 4.5 Hz, 2H), 3.91 (dd, *J* = 5.7, 4.4 Hz, 2H), 3.88 (s, 3H), 3.87 (s, 3H), 3.79 – 3.71 (m, 2H), 3.70 – 3.65 (m, 2H), 3.65 – 3.58 (m, 2H), 3.55 – 3.47 (m, 2H), 3.35 (s, 3H), 2.78 (s, 3H). ^{13}C NMR (126 MHz, $CDCl_3$) δ 186.54, 164.72, 151.72, 149.25, 148.74, 144.70, 125.82, 120.35, 111.61, 111.32, 77.16, 72.00, 70.93, 70.73, 70.63, 69.66, 68.71, 59.10, 56.09, 12.42. HRMS-ESI (m/z) $[M + H]^+$ calcd for $C_{19}H_{26}NO_6S$, 396,1418; found 396.1470.

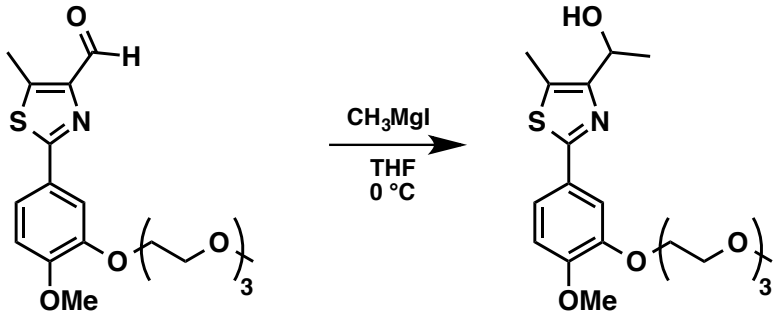

1-(2-(4-methoxy-3-(2-(2-(2-methoxyethoxy)ethoxy)ethoxy)phenyl)-5-methylthiazol-4-yl)ethan-1-ol (**S23e**). Aldehyde **S23d** (60 mg, 0.15 mmol) was stirred in 1.5 mL of tetrahydrofuran at 0 °C, and a solution of methyl magnesium iodide (3M, 0.46 mmol) was added. The reaction was stirred at 0 °C for 10 minutes and monitored via TLC. After 15 minutes, the reaction was quenched at 0 °C via addition of a solution of acetic acid (80% in water, 0.1 mL) in 0.5 mL of water. Water (5 mL) was added, and the product was extracted with dichloromethane. The combined organic layers were dried with magnesium sulfate, the drying agent was filtered off, and the solvent was removed under reduced pressure. Column chromatography (silica gel, 1% methanol in ethyl acetate) gave the desired alcohol (87% yield). ^{1}H NMR (500 MHz, $CDCl_3$) δ 7.50 (d, *J* = 2.1 Hz, 1H), 7.40 (dd, *J* = 8.4, 2.1 Hz, 1H), 6.86 (d, *J* = 8.4 Hz, 1H), 4.92 (p, *J* = 6.7 Hz, 1H), 4.26 (t, *J* = 5.1 Hz, 2H), 3.92 (dd, *J* = 5.8, 4.5 Hz, 2H), 3.88 (s, 3H), 3.75 (dd, *J* = 5.9, 3.7 Hz, 2H), 3.68 (dd, *J* = 5.9, 3.7 Hz, 2H), 3.66 – 3.62 (m, 2H), 3.56 – 3.50 (m, 2H), 3.36 (s, 3H), 2.94 (d, *J* = 7.6 Hz, 1H), 2.40 (s, 3H), 1.53 (d, *J* = 6.5 Hz, 3H). ^{13}C NMR (126 MHz, $CDCl_3$) δ 164.48, 155.34, 151.14, 148.56, 126.92, 125.91, 119.91, 111.66, 111.43, 72.05, 70.97, 70.77, 70.66, 69.75, 68.70, 64.71, 59.15, 56.12, 24.28, 11.00. HRMS-ESI (m/z) $[M + H]^+$ calcd for $C_{20}H_{30}NO_6S$, 412.1794; found 412.1784.

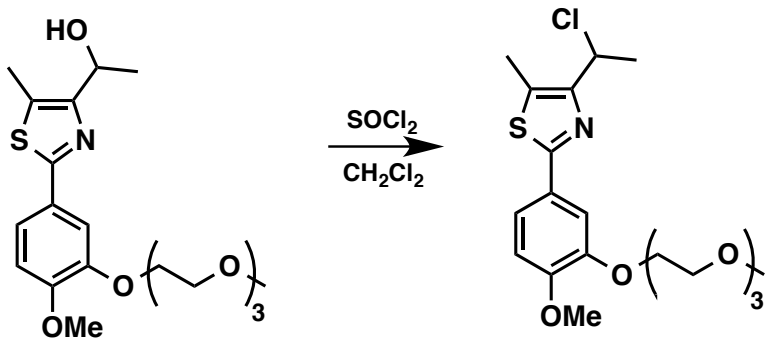

4-(1-chloroethyl)-2-(4-methoxy-3-(2-(2-(2-methoxyethoxy)ethoxy)ethoxy)phenyl)-5-methylthiazole (**S23f**). To a stirred solution of alcohol **S23e** (55 mg, 0.13 mmol) in CH_2Cl_2 (0.3 mL) was added thionyl chloride (0.49 mL, 6.7 mmol) slowly at room temperature. The mixture was stirred for 1.5 hours under a balloon of nitrogen. The reaction was cooled to 0 °C, and cold saturated sodium bicarbonate (approximately 1.5 mL) was added. The product was mixed with water (5 mL) and extracted with dichloromethane. The organic fractions were dried with magnesium sulfate, the drying agent was filtered off, and the solvent was removed under reduced pressure. The crude product was used for the next step without further purification. Mass spectrometry analysis was conducted in acetonitrile due to the product's instability in methanol. ^{1}H NMR (500 MHz, $CDCl_3$) δ 7.51 (d, *J* = 2.1 Hz, 1H), 7.41 (dd, *J* = 8.4, 2.1 Hz, 1H), 6.85 (d, *J* = 8.4 Hz, 1H), 5.24 (q, *J* = 6.8 Hz, 1H), 4.26 (dd, *J* = 5.7, 4.6 Hz, 2H), 3.95 – 3.87 (m, 2H), 3.87 (s, 3H), 3.78 – 3.71 (m, 2H), 3.71 – 3.65 (m, 2H), 3.65 – 3.61 (m, 2H), 3.56 – 3.49 (m, 2H), 3.35 (s, 3H), 2.46 (s, 3H), 1.98 (d, *J* = 6.8 Hz, 3H). ^{13}C NMR (126 MHz, $CDCl_3$) δ 164.25, 152.00, 151.18, 148.48, 129.47, 126.83, 120.01, 111.58, 111.55, 72.00, 70.91, 70.72, 70.61, 69.70, 68.66, 59.09, 56.06, 51.84, 24.51, 11.26. HRMS-ESI (m/z) $[M + H]^+$ calcd for $C_{20}H_{29}ClNO_5S$, 430.1455; found 430.1458.

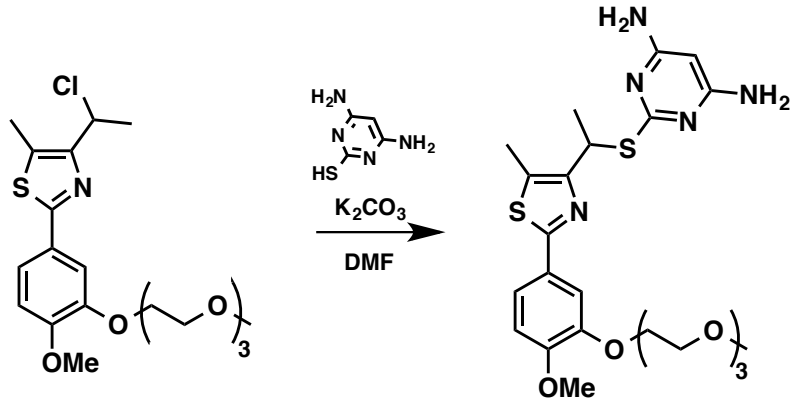

2-((1-(2-(4-methoxy-3-(2-(2-(2-methoxyethoxy)ethoxy)ethoxy)phenyl)-5-methylthiazol-4-yl)ethyl)thio)pyrimidine-4,6-diamine

ethoxy)phenyl)-5-propylthiazol-4-yl)ethyl)thio)pyrimidine-4,6-diamine (**S23**). A mixture of chloride **S23f** (60 mg) from the previous step, 4,6-diamino-2-mercaptopyrimidine (28 mg, 0.20 mmol), K_2CO_3 (77 mg, 0.56 mmol), and DMF (0.5 mL) was stirred at 80 °C while under a nitrogen atmosphere. After 2 hours, the mixture was concentrated on a Rotevap. A precipitate was filtered off, and the crude product was dry loaded onto silica gel. Column chromatography (silica gel, gradient elution: 5% to 10% methanol in dichloromethane) gave the desired product (45 mg, 0.084 mmol, 63% yield over two steps). ^{1}H NMR (300 MHz, $CDCl_3$) δ 7.51 (d, *J* = 2.0 Hz, 1H), 7.38 (dd, *J* = 8.4, 2.0 Hz, 1H), 6.84 (d, *J* = 8.5 Hz, 1H), 5.25 – 5.14 (m, 2H), 4.80 (s, 4H), 4.24 (dd, *J* = 5.8, 4.3 Hz, 2H), 3.89 (dd, *J* = 5.8, 4.3 Hz, 2H), 3.86 (s, 3H), 3.79 – 3.70 (m, 2H), 3.70 – 3.57 (m, 4H), 3.57 – 3.48 (m, 2H), 3.35 (s, 3H), 2.47 (s, 3H), 1.78 (d, *J* = 7.0 Hz, 3H). ^{13}C NMR (75 MHz, $CDCl_3$) δ 170.30, 163.81, 163.36, 153.49, 150.87, 148.43, 127.28, 126.93, 119.91, 111.63, 111.49, 80.72, 77.16, 71.99, 70.88, 70.70, 70.59, 69.71, 68.60, 59.06, 56.06, 37.70, 22.09, 11.65. HRMS-ESI (m/z) $[M + H]^+$ calcd for $C_{24}H_{34}N_5O_5S_2$, 536.2001; found 536.2017.

4.2.8 Experimental Procedures Relevant to Compound S28

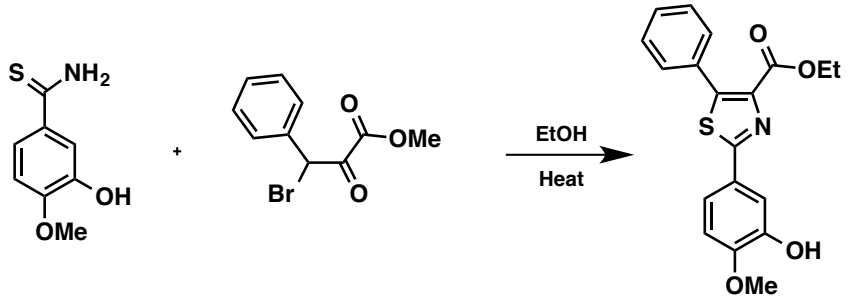

Ethyl 2-(3-hydroxy-4-methoxyphenyl)-5-phenylthiazole-4-carboxylate (**S28a**). Methyl 3-bromo-2-oxo-3-phenylpropanoate (347 mg, 1.35 mmol) and thioamide **12b** (137 mg, 0.75 mmol) were stirred in absolute ethanol (2 mL). The reaction was refluxed and monitored via TLC (50% ethyl acetate and hexane). When the reaction was determined to be complete, the solvent was removed on a rotary evaporator. Column chromatography (silica gel, gradient elution: 30% to 40% ethyl acetate in hexane) afforded a white solid (160 mg, 33% yield). ^{1}H NMR (500 MHz, $CDCl_3$) δ 7.58 – 7.47 (m, 4H), 7.47 – 7.38 (m, 3H), 6.93 – 6.87 (m, 1H), 5.73 (s, 1H), 4.29 (q, *J* = 7.1 Hz, 2H), 3.95 (s, 3H), 1.23 (t, *J* = 7.1 Hz, 3H). ^{13}C NMR (126 MHz, $CDCl_3$) δ 166.03, 162.51, 148.77, 145.98, 145.28, 141.32, 130.77, 130.04, 129.16, 128.27, 126.54, 119.33, 113.13, 110.78, 77.16, 61.39, 56.20, 14.14. HRMS-ESI (m/z) $[M + H]^+$ calcd for $C_{19}H_{18}NO_4S$, 356.0957; found 356.0952.

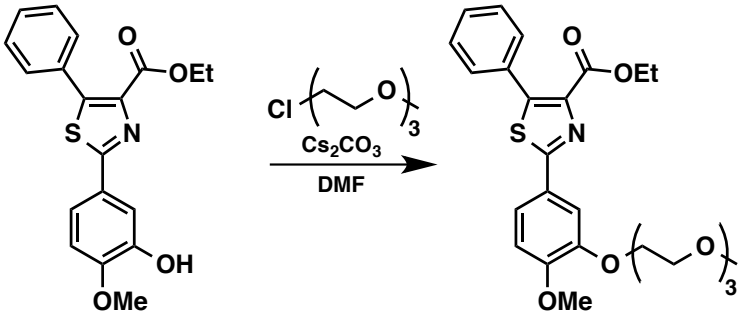

Ethyl-2-(4-methoxy-3-(2-(2-(2-methoxyethoxy)ethoxy)ethoxy)phenyl)-5-phenylthiazole-4-carboxylate (**S28b**). To a solution of phenol **S28a** (160 mg, 0.45 mmol) in DMF (3 mL) was added Cs_2CO_3 (293 mg, 0.900 mmol) and 13-chloro-2,5,8,11-tetraoxatridecane (293 mg, 1.60 mmol). The mixture was stirred for approximately 3 days at 50 °C. Water was added to the

reaction, and the product was extracted with ethyl acetate. The organic layer was dried with magnesium sulfate, the drying agent was filtered off, and the solvent was removed on a rotary evaporator. Column chromatography (silica gel, gradient elution: 30% to 100% ethyl acetate in hexane) was performed. The product from column chromatography was dissolved in toluene, and the toluene was removed on a rotary evaporator. The residue was placed under reduced pressure using a vacuum pump. (205 mg, 90% yield). ^{1}H NMR (500 MHz, $CDCl_3$) δ 7.60 (d, *J* = 2.1 Hz, 1H), 7.56 – 7.47 (m, 3H), 7.46 – 7.38 (m, 3H), 6.90 (d, *J* = 8.5 Hz, 1H), 4.33 – 4.25 (m, 4H), 3.93 (dd, *J* = 5.6, 4.5 Hz, 2H), 3.90 (s, 3H), 3.79 – 3.73 (m, 2H), 3.73 – 3.67 (m, 2H), 3.67 – 3.62 (m, 2H), 3.56 – 3.50 (m, 2H), 3.36 (s, 3H), 1.22 (t, *J* = 7.1 Hz, 3H). ^{13}C NMR (126 MHz, $CDCl_3$) δ 166.17, 162.51, 151.85, 148.68, 145.08, 141.32, 130.76, 129.99, 129.15, 128.25, 125.93, 120.64, 111.65, 111.58, 77.16, 72.05, 70.98, 70.78, 70.68, 69.74, 68.79, 61.38, 59.15, 56.12, 14.11. HRMS-ESI (m/z) $[M + H]^+$ calcd for $C_{26}H_{32}NO_7S$, 502.1899; found 502.1896.

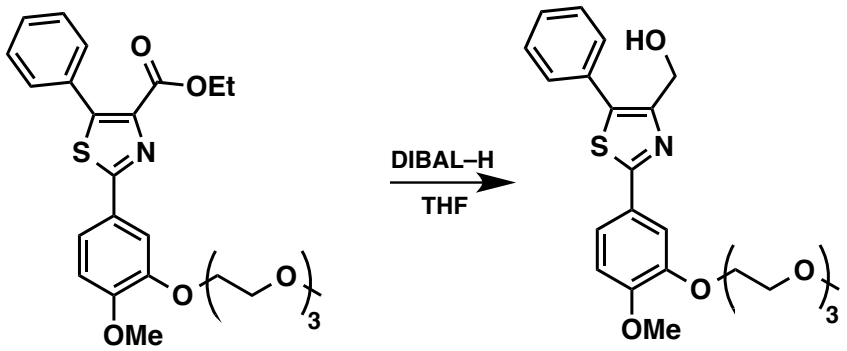

(2-(4-methoxy-3-(2-(2-(2-methoxyethoxy)ethoxy)ethoxy)phenyl)-5-phenylthiazol-4-yl)methanol (**S28c**). DIBAL-H (1.0 M in THF, 1.7 mL) was added to a solution of ester **S28b** (205 mg, 0.41 mmol) in dichloromethane (6 mL) at –78 °C over the course of 10 minutes. The reaction was stirred for 30 minutes then slowly warmed to room temperature. After 30 minutes, TLC (100% ethyl acetate) indicated that the reaction was complete. Saturated sodium potassium tartrate (1.5 mL) was added, followed by water. The product was extracted with ethyl acetate, and the organic fractions were dried with magnesium sulfate. The drying agent was

filtered off, and the solvent was removed under reduced pressure (89% yield). ^{1}H NMR (500 MHz, $CDCl_3$) δ 7.59 (d, *J* = 2.1 Hz, 1H), 7.52 – 7.34 (m, 6H), 6.89 (d, *J* = 8.4 Hz, 1H), 4.78 (d, *J* = 5.9 Hz, 2H), 4.32 – 4.26 (m, 2H), 3.96 – 3.91 (m, 2H), 3.90 (s, 3H), 3.79 – 3.74 (m, 2H), 3.74 – 3.67 (m, 2H), 3.67 – 3.63 (m, 2H), 3.57 – 3.51 (m, 2H), 3.36 (s, 3H), 3.06 – 3.00 (m, 1H). ^{13}C NMR (126 MHz, $CDCl_3$) δ 166.24, 151.52, 151.05, 148.68, 134.01, 131.28, 129.28, 129.03, 128.44, 126.54, 120.18, 111.69, 111.44, 72.07, 71.01, 70.80, 70.69, 69.77, 68.75, 59.28, 59.17, 56.15. HRMS-ESI (m/z) $[M + H]^+$ calcd for $C_{24}H_{29}NNaO_6S$, 482.1613; found 482.1604.

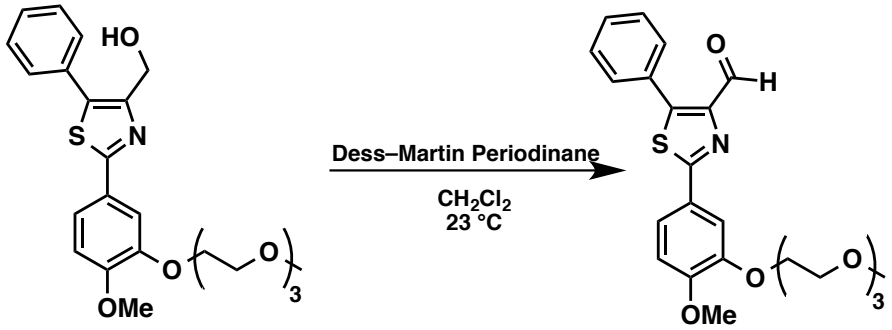

2-(4-methoxy-3-(2-(2-(2-methoxyethoxy)ethoxy)ethoxy)phenyl)-5-phenylthiazole-4-carbaldehyde (**S28d**). Dess-Martin Periodinane (212 mg, 0.501 mmol) was added to a solution of alcohol **S28c** (115 mg, 0.250 mmol) in dry dichloromethane (5 mL) at room temperature while under a nitrogen atmosphere. The reaction was monitored via TLC, and after approximately 30 minutes it was diluted with ether, washed with aqueous sodium hydroxide (1 M), and washed with saturated sodium thiosulfate. The organic layer was washed with saturated sodium bicarbonate, washed with brine, and dried with magnesium sulfate. The drying agent was filtered off, and the solvent was removed under reduced pressure. Column chromatography (silica gel, gradient elution: 50% to 100% ethyl acetate in hexane) gave the desired product (83% yield). ^{1}H NMR (500 MHz, $CDCl_3$) δ 9.96 (s, 1H), 7.64 (d, *J* = 2.1 Hz, 1H), 7.60 – 7.55 (m, 2H), 7.53 (dd, *J* = 8.4, 2.1 Hz, 1H), 7.51 – 7.44 (m, 3H), 6.90 (d, *J* = 8.4 Hz, 1H), 4.29 (dd, *J* = 5.7, 4.3 Hz, 2H), 3.95 – 3.91 (m, 2H), 3.90 (s, 3H), 3.78 – 3.73 (m, 2H), 3.73 – 3.66 (m, 2H),

3.66 – 3.62 (m, 2H), 3.56 – 3.50 (m, 2H), 3.36 (s, 3H). ^{13}C NMR (126 MHz, $CDCl_3$) δ 184.19, 166.93, 152.17, 150.65, 148.78, 148.51, 130.26, 130.13, 129.06, 129.01, 125.53, 120.94, 111.64, 111.56, 77.16, 72.02, 70.96, 70.75, 70.65, 69.69, 68.81, 59.12, 56.11. HRMS-ESI (m/z) $[M + H]^+$ calcd for $C_{24}H_{28}NO_6S$, 458.1637; found 458.1636.

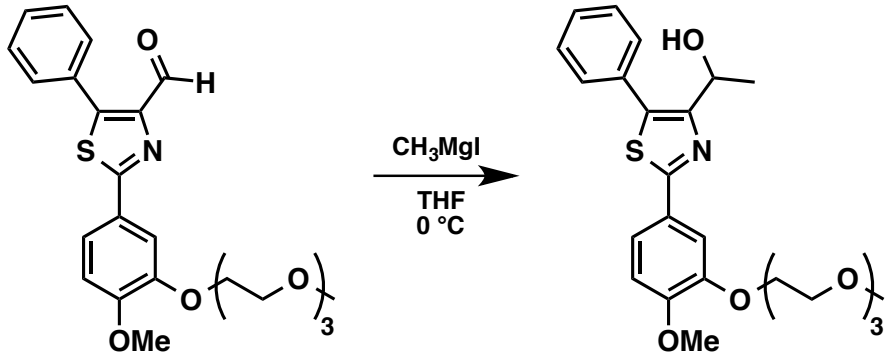

1-(2-(4-methoxy-3-(2-(2-(2-methoxyethoxy)ethoxy)ethoxy)phenyl)-5-phenylthiazol-4-yl)ethan-1-ol (**S28e**). Aldehyde **S28d** (95 mg, 0.21 mmol) was stirred in 1.5 mL of tetrahydrofuran at room temperature, and a solution of methyl magnesium iodide (3M, 0.14 mmol) was added. The reaction was stirred at 0 °C for 15 minutes, and then it was warmed to room temperature. After approximately 4.5 hours, the reaction was heated to reflux. The reaction was cooled to room temperature after 15 minutes of being at 70 °C, and another 0.14 mL of the MeMgI solution was added. After an additional 2 hours, another 2.4 mL of the MeMgI solution needed to be added. Shortly afterwards, the reaction was quenched at 0 °C via addition of acetic acid. Water was added, and the product was extracted with dichloromethane. The combined organic layers were dried with magnesium sulfate, the drying agent was filtered off, and the solvent was removed under reduced pressure. Column chromatography gave the desired alcohol (67% yield). ^{1}H NMR (500 MHz, $CDCl_3$) δ 7.59 (d, *J* = 2.1 Hz, 1H), 7.50 (ddd, *J* = 8.4, 2.1, 0.7 Hz, 1H), 7.48 – 7.34 (m, 5H), 6.90 (d, *J* = 8.4 Hz, 1H), 4.98 (dq, *J* = 8.2, 6.5 Hz, 1H), 4.30 (t, *J* = 5.1 Hz, 2H), 3.94 (dd, *J* = 5.6, 4.6 Hz, 2H), 3.91 (s, 3H), 3.77 (dd, *J* = 5.9, 3.8 Hz, 2H), 3.70 (ddd, *J* = 5.0, 3.8, 1.7 Hz, 2H), 3.69 – 3.63 (m, 2H), 3.54 (dd, *J* = 5.6, 3.7 Hz, 2H), 3.37 (d, *J* = 0.8 Hz, 3H), 1.96 (s, 1H), 1.62 (d, *J* = 6.0 Hz, 3H). ^{13}C NMR (126 MHz, $CDCl_3$) δ

166.34, 154.80, 151.47, 148.60, 131.99, 131.24, 129.57, 128.94, 128.39, 126.70, 120.20, 111.67, 111.56, 72.04, 70.98, 70.77, 70.66, 69.76, 68.74, 64.67, 59.14, 56.13, 24.49. HRMS-ESI (m/z) $[M + H]^+$ calcd for $C_{25}H_{32}NO_6S$, 474.1950; found 474.1943.

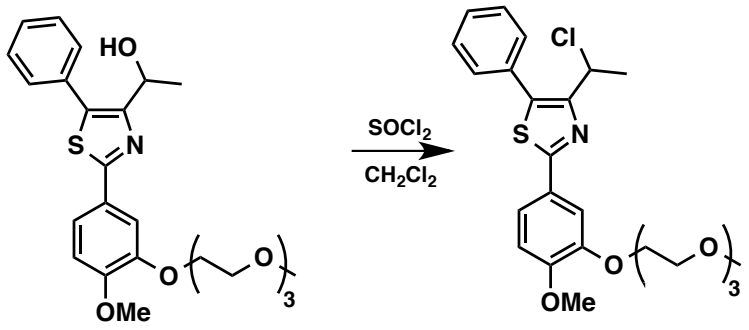

4-(1-chloroethyl)-2-(4-methoxy-3-(2-(2-(2-methoxyethoxy)ethoxy)ethoxy)phenyl)-5-phenylthiazole (**S28f**). To a stirring solution of alcohol **S28e** (65 mg, 0.14 mmol) in CH_2Cl_2 (0.2 mL) was added thionyl chloride (0.5 mL, 7 mmol) slowly at room temperature. The mixture was stirred for 3 hours under a balloon of nitrogen. The reaction was cooled to 0 °C, and cold saturated sodium bicarbonate (approximately 2 mL) was added. The product was mixed with water (5 mL) and extracted with dichloromethane. The organic fractions were dried with magnesium sulfate, the drying agent was filtered off, and the solvent was removed under reduced pressure. The crude product was used for the next step without further purification (66 mg crude yield). ^{1}H NMR (300 MHz, $CDCl_3$) δ 7.67 – 7.34 (m, 7H), 6.90 (d, *J* = 8.4 Hz, 1H), 5.23 (q, *J* = 6.7 Hz, 1H), 4.30 (dd, *J* = 5.8, 4.5 Hz, 2H), 3.99 – 3.93 (m, 2H), 3.91 (s, 3H), 3.83 – 3.74 (m, 2H), 3.74 – 3.59 (m, 4H), 3.59 – 3.49 (m, 2H), 3.37 (s, 3H), 1.99 (d, *J* = 6.7 Hz, 3H). ^{13}C NMR (75 MHz, $CDCl_3$) δ 166.48, 151.58, 151.31, 148.59, 134.12, 130.98, 129.56, 129.09, 128.69, 126.68, 120.34, 111.76, 111.64, 72.04, 70.98, 70.78, 70.67, 69.76, 68.77, 59.13, 56.12, 52.63, 24.88.

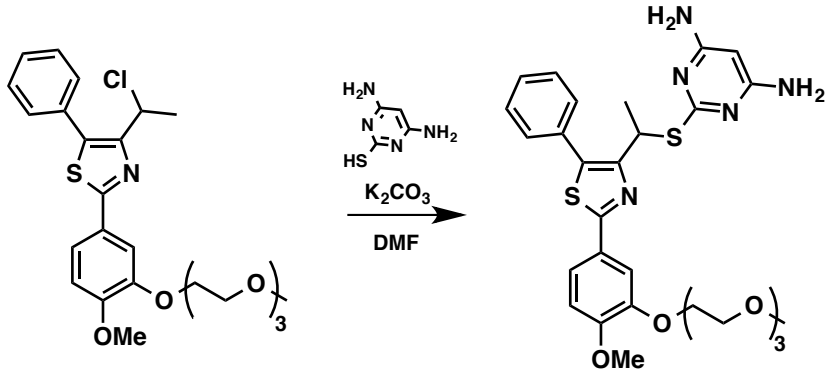

2-((1-(2-(4-methoxy-3-(2-(2-(2-methoxyethoxy)ethoxy)ethoxy)phenyl)-5-phenylthiazol-4-yl)ethyl)thio)pyrimidine-4,6-diamine (**S28**). A mixture of chloride **S28f** (65 mg) from the previous step, 4,6-diamino-2-mercaptopyrimidine (26 mg, 0.19 mmol), K_2CO_3 (73 mg, 0.53 mmol), and DMF (1.0 mL) was stirred at 80 °C while under a nitrogen atmosphere. The reaction was monitored via TLC. When the reaction was determined to be complete, the mixture was concentrated on a rotary evaporator. Water (5 mL) was added, and the product was extracted with dichloromethane. More product was extracted by washing the aqueous layer with ethyl acetate. After drying with magnesium sulfate and filtering off the drying agent, the solvent was removed under reduced pressure. The residue was placed under reduced pressure overnight using a vacuum pump. Column chromatography (silica gel, 5% methanol in dichloromethane) gave the desired product (37% yield over two steps). ^{1}H NMR (500 MHz, $CDCl_3$) δ 7.61 – 7.47 (m, 4H), 7.47 – 7.41 (m, 2H), 7.41 – 7.32 (m, 1H), 6.88 (d, *J* = 8.4 Hz, 1H), 5.40 (q, *J* = 7.1 Hz, 1H), 5.13 (s, 1H), 4.41 (s, 4H), 4.29 (dd, *J* = 5.7, 4.4 Hz, 2H), 3.96 – 3.90 (m, 2H), 3.89 (s, 3H), 3.80 – 3.74 (m, 2H), 3.74 – 3.68 (m, 2H), 3.68 – 3.63 (m, 2H), 3.57 – 3.51 (m, 2H), 3.36 (s, 3H), 1.84 (d, *J* = 7.1 Hz, 3H). ^{13}C NMR (126 MHz, $CDCl_3$) δ 170.20, 165.87, 163.16, 153.33, 151.22, 148.47, 132.50, 131.53, 129.86, 128.80, 127.84, 127.02, 120.19, 111.57, 80.47, 72.03, 70.94, 70.75, 70.65, 69.73, 68.63, 59.13, 56.09, 38.22, 22.44. HRMS-ESI (m/z) $[M + H]^+$ calcd for $C_{29}H_{36}N_5O_5S_2$, 598.2158; found 598.2159.

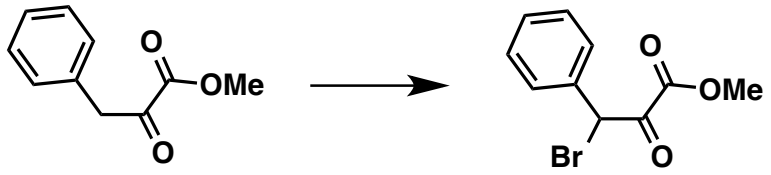

Methyl 3-bromo-2-oxo-3-phenylpropanoate. Methyl 2-oxo-3-phenylpropanoate (502 mg, 2.81 mmol) was stirred in 0.8 mL of chloroform at room temperature. To this solution was added Br_2 (2.5 mL, 1.06 M solution in carbon tetrachloride). When TLC indicated that the reaction was complete, approximately 2 mL of saturated sodium thiosulfate was added while at room temperature. The organic layer was separated, and more material was extracted with ethyl acetate. The organic solutions were dried with magnesium sulfate, the drying agent was filtered off, and the solvent was removed under reduced pressure. Column chromatography (silica gel, 20% ethyl acetate in hexane) improved the purity of the sample (347 mg crude yield). The crude product was taken onto the next step without further purification. ^{1}H NMR (500 MHz, $CDCl_3$) δ 7.48 – 7.44 (m, 2H), 7.42 – 7.37 (m, 3H), 6.22 (s, 1H), 3.89 (s, 3H). ^{13}C NMR (126 MHz, $CDCl_3$) δ 183.73, 160.58, 133.11, 129.87, 129.78, 129.18, 53.72, 49.69.

4.2.9 Additional Experimental Procedures Relevant to Compound S23

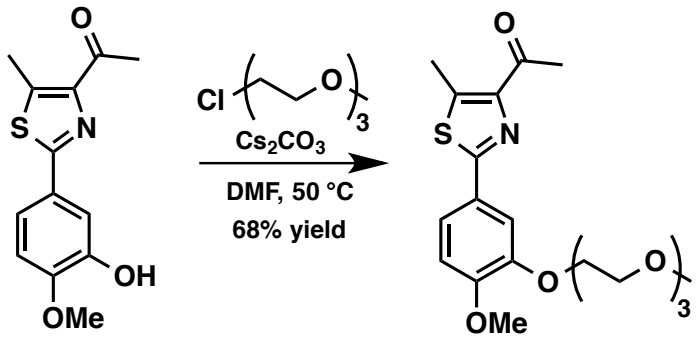

1-(2-(4-methoxy-3-(2-(2-(2-methoxyethoxy)ethoxy)ethoxy)phenyl)-5-methylthiazol-4-yl)ethan-1-one (**S23h**)**.** To a solution of thiazole intermediate **S23g** (633 mg, 2.40 mmol) in DMF (12 mL) was added Cs_2CO_3 (1.56 g, 4.81 mmol) and 13-chloro-2,5,8,11-tetraoxatridecane (886 mg, 4.85 mmol). The mixture was stirred for 24 h at 50 °C. The reaction was poured into

water, and the product was extracted with ethyl acetate. The organic layer was dried with magnesium sulfate, the drying agent was filtered off, and the solvent was removed under reduced pressure. Column chromatography (silica gel, gradient elution: 30% to 100% ethyl acetate in hexane) gave the purified ketone (**S23h**) (673 mg, 68% yield). ^{1}H NMR (500 MHz, $CDCl_3$) δ 7.52 (d, *J* = 2.1 Hz, 1H), 7.42 (dd, *J* = 8.4, 2.1 Hz, 1H), 6.89 (d, *J* = 8.4 Hz, 1H), 4.27 (dd, *J* = 5.7, 4.6 Hz, 2H), 3.93 (dd, *J* = 5.7, 4.6 Hz, 2H), 3.90 (s, 3H), 3.79 – 3.73 (m, 2H), 3.71 – 3.66 (m, 2H), 3.66 – 3.60 (m, 2H), 3.56 – 3.50 (m, 2H), 3.36 (s, 3H), 2.77 (s, 3H), 2.71 (s, 3H). HRMS-ESI (m/z) $[M + H]^+$ calcd for $C_{20}H_{28}NO_6S$, 410.1637; found 410.1623.

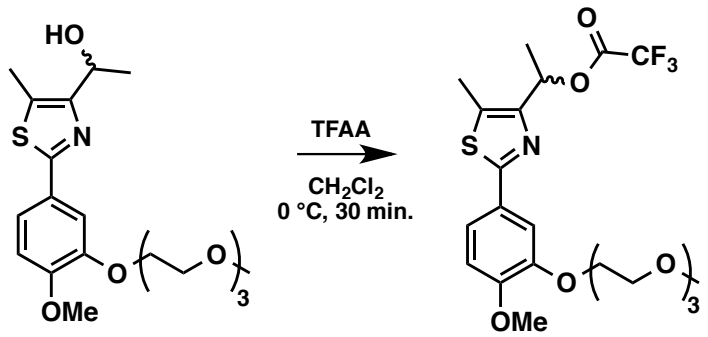

1-(2-(4-methoxy-3-(2-(2-(2-methoxyethoxy)ethoxy)ethoxy)phenyl)-5-methylthiazol-4-yl)ethyl 2,2,2-trifluoroacetate (**S23i**). Trifluoroacetic anhydride (0.045 mL, 0.32 mmol) was added dropwise to a solution of alcohol **S23e** (33 mg, 0.08 mmol) and dichloromethane (5 mL) at 0 °C. Another 5 microliters of trifluoroacetic anhydride was added. The reaction was kept at 0 °C for 30 minutes before being poured into 5 mL of cold saturated sodium bicarbonate. The product was extracted with dichloromethane (3 x 5 mL) and washed with water (1 x 5 mL). The organic fractions were dried with magnesium sulfate, the drying agent was filtered off, and the solvents were removed under reduced pressure. The crude product was used for the next step without further purification (38 mg crude yield). ^{1}H NMR (500 MHz, $CDCl_3$) δ 7.51 (d, *J* = 2.1 Hz, 1H), 7.41 (dd, *J* = 8.3, 2.1 Hz, 1H), 6.87 (d, *J* = 8.4 Hz, 1H), 6.16 (q, *J* = 6.6 Hz, 1H), 4.27 (dd, *J* = 5.8, 4.5 Hz, 2H), 3.93 (dd, *J* = 5.7, 4.6 Hz, 2H), 3.89 (s, 3H), 3.79 – 3.74 (m, 2H), 3.74 – 3.67 (m, 2H), 3.67 – 3.62 (m, 2H), 3.57 – 3.51 (m, 2H), 3.37 (s, 3H), 2.51 (s, 3H), 1.81 (d, *J* =

6.6 Hz, 3H). ^{13}C NMR (126 MHz, $CDCl_3$) δ 164.85, 157.66, 157.33, 156.99, 156.66, 151.35, 148.61, 148.45, 131.74, 126.74, 120.09, 118.09, 115.82, 113.55, 111.66, 111.54, 111.27, 72.06, 71.32, 70.99, 70.80, 70.69, 69.75, 68.73, 59.16, 56.14, 19.70, 11.19.

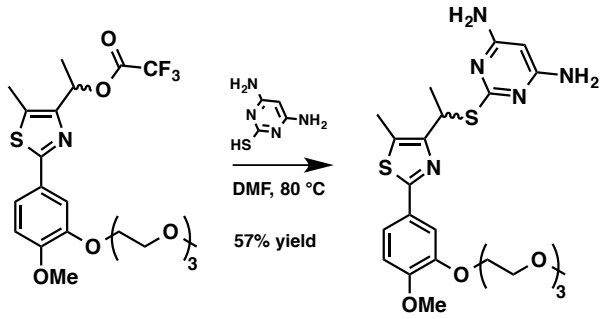

2-((1-(2-(4-methoxy-3-(2-(2-(2-methoxyethoxy)ethoxy)ethoxy)phenyl)-5-methylthiazol-4-yl)ethyl)thio)pyrimidine-4,6-diamine (**S23**). A mixture of crude ester **S23i** (73 mg) from the previous step, 4,6-diamino-2-mercaptopyrimidine (28 mg, 0.20 mmol), K_2CO_3 (79 mg, 0.58 mmol), and DMF (1.0 mL) was stirred at 80 °C while under a nitrogen atmosphere. The reaction was monitored via TLC (1% ethanol in ethyl acetate). After 2 hours, the mixture was concentrated on a rotary evaporator. Water (10 mL) was added, and the product was extracted with dichloromethane. After drying with magnesium sulfate and filtering off the drying agent, the solvent was removed under reduced pressure. Column chromatography (silica gel, gradient elution: 5% to 10% methanol in dichloromethane) gave the desired product (13 mg crude yield, 60% ee). Characterization for the purified compound is consistent with the structure of **S23**.

4.2.10 Experimental Procedures Relevant to Compound S15

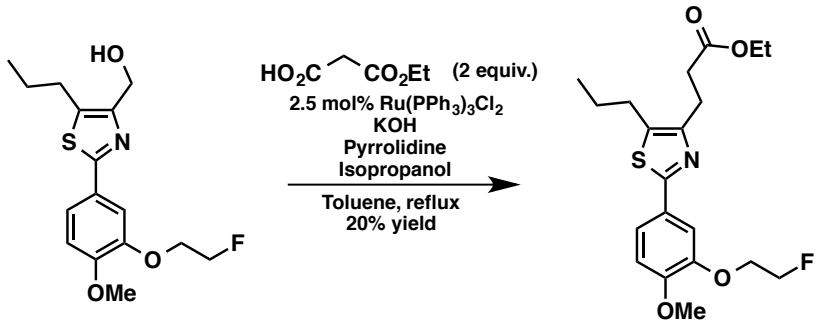

Ethyl 3-(2-(3-(2-fluoroethoxy)-4-methoxyphenyl)-5-propylthiazol-4-yl)propanoate (**S15a**). To a mixture of pyrrolidine (0.02 mL, 0.09 mmol), potassium hydroxide (3 mg, 0.05 mmol) , and $Ru(PPh_3)_3Cl_2$ (20 mg, 0.02 mmol) was added toluene (1.3 mL), alcohol **9a** (272 mg, 0.815 mmol), isopropanol (0.012 mL, 0.16 mmol) and monoethyl malonate (0.2 mL, 1.7 mmol). The reaction was heated to reflux under nitrogen and monitored via TLC (30% ethyl acetate/hexane). After 1 day, the reaction was poured into ethyl acetate and washed once with water. The organic layer was dried with magnesium sulfate, the drying agent was filtered off, and the solvent was removed under reduced pressure. Column chromatography (silica gel, 30% ethyl aceate/hexane) gave the targeted product (20% yield). ^{1}H NMR (500 MHz, $CDCl_3$) δ 7.49 (d, *J* = 2.0 Hz, 1H), 7.41 (dd, *J* = 8.4, 2.1 Hz, 1H), 6.87 (d, *J* = 8.4 Hz, 1H), 4.88 – 4.81 (m, 1H), 4.78 – 4.72 (m, 1H), 4.40 – 4.34 (m, 1H), 4.34 – 4.27 (m, 1H), 4.13 (q, *J* = 7.1 Hz, 2H), 3.88 (s, 3H), 2.97 (dd, *J* = 8.3, 7.0 Hz, 2H), 2.80 – 2.70 (m, 4H), 1.65 (q, *J* = 7.4 Hz, 2H), 1.23 (t, *J* = 7.2 Hz, 3H), 0.98 (t, *J* = 7.3 Hz, 3H). ^{13}C NMR (126 MHz, $CDCl_3$) δ 173.24, 163.64, 151.00, 150.75, 148.08, 132.72, 127.34, 120.25, 111.83, 111.54, 82.56, 81.20, 68.59, 68.42, 60.42, 56.10, 34.10, 28.31, 25.28, 24.43, 14.32, 13.76. HRMS-ESI (m/z) $[M + H]^+$ calcd for $C_{20}H_{27}FNO_4S$, 396.1645; found 396.1636.

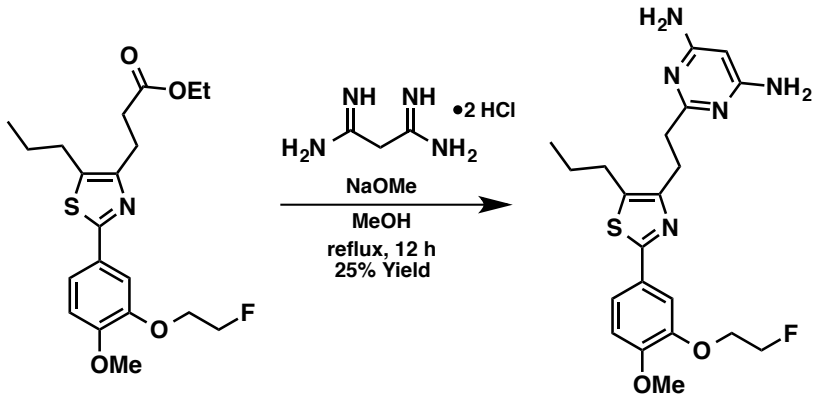

2-(2-(2-(3-(2-fluoroethoxy)-4-methoxyphenyl)-5-propylthiazol-4-yl)ethyl)pyrimidine-4,6-diamine (**S15**). Sodium methoxide (0.79 mmol, 0.5 M) was added to a solution of malonodiamidine (58 mg, 0.34 mmol) in methanol (0.8 mL) at room temperature. The resulting solution was heated to 50 °C for 30 min. After cooling to room temperature, a solution of ester **S15a** (78 mg, 0.20 mmol) in methanol (0.8 mL) was added dropwise. The reaction was heated to reflux, and upon evaporation of the solvent, the residue was heated at 85 °C overnight. The residue was mixed with water (15 mL) and extracted with ethyl acetate. The combined organic fractions were dried with magnesium sulfate, the drying agent was filtered off, and the solvent was removed under reduced pressure. Column chromatography (silica gel, 5% methanol in dichloromethane) gave compound **S15**. A second column (silica gel, 15% methanol in dichloromethane) was needed to fully purify **S15** (25% yield). ^{1}H NMR (500 MHz, $CDCl_3$) δ 7.56 (d, *J* = 2.1 Hz, 1H), 7.41 (dd, *J* = 8.4, 2.1 Hz, 1H), 6.89 (d, *J* = 8.4 Hz, 1H), 5.27 (s, 1H), 5.21 (s, 4H), 4.87 – 4.81 (m, 1H), 4.77 – 4.72 (m, 1H), 4.40 – 4.34 (m, 1H), 4.34 – 4.29 (m, 1H), 3.90 (s, 3H), 3.11 – 3.04 (m, 2H), 2.95 – 2.88 (m, 2H), 2.76 – 2.67 (m, 2H), 1.62 (h, *J* = 7.4 Hz, 2H), 0.96 (t, *J* = 7.3 Hz, 3H). ^{13}C NMR (126 MHz, $CDCl_3$) δ 169.74, 163.86, 163.78, 151.94, 151.02, 148.20, 132.84, 127.47, 120.45, 111.93, 111.50, 82.72, 81.93, 81.36, 68.67, 68.50, 56.19, 39.12, 28.36, 28.28, 25.45, 13.85. HRMS-ESI (m/z) $[M + H]^+$ calcd for $C_{21}H_{27}FN_5O_2S$, 432.1869; found 432.1855.

4.2.11 Experimental Procedures Relevant to Compound S32b

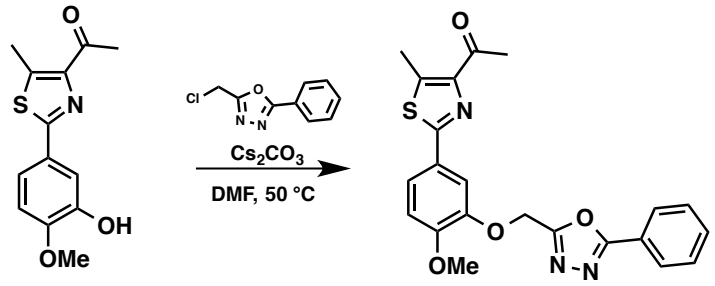

1-(2-(4-methoxy-3-((5-phenyl-1,3,4-oxadiazol-2-yl)methoxy)phenyl)-5-methylthiazol-4-yl)ethan-1-one (**S32b**). To a solution of thiazole intermediate **12c** (190 mg, 0.712 mmol) in DMF (3.5 mL) was added Cs_2CO_3 (approximately 420 mg, 1.29 mmol) and 2-(chloromethyl)-5-phenyl-1,3,4-oxadiazole (250 mg, 1.29 mmol). The mixture was stirred at 50 °C and monitored via TLC (75% ethyl acetate in hexane). When the reaction was determined to be complete, the reaction was worked up and subjected to column chromatography (silica gel, 5% methanol in dichloromethane). The product was used for the next step without further purification (177 mg, 65% yield). ^{1}H NMR (500 MHz, $CDCl_3$) δ 8.11 – 8.06 (m, 2H), 7.74 (d, *J* = 2.1 Hz, 1H), 7.58 – 7.47 (m, 4H), 6.96 (d, *J* = 8.4 Hz, 1H), 5.47 (s, 2H), 3.93 (s, 3H), 2.77 (s, 3H), 2.69 (s, 3H). ^{13}C NMR (126 MHz, $CDCl_3$) δ 195.96, 165.96, 162.32, 161.76, 152.01, 149.02, 147.25, 143.23, 132.17, 129.19, 127.23, 126.53, 123.62, 122.08, 114.14, 112.26, 61.90, 56.20, 29.53, 13.56. HRMS-ESI (m/z) $[M + H]^+$ calcd for $C_{22}H_{20}N_3O_4S$, 422.1175; found 422.1164.

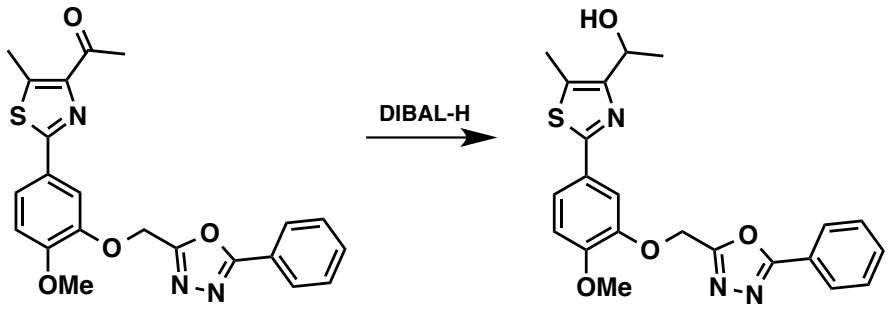

1-(2-(4-methoxy-3-((5-phenyl-1,3,4-oxadiazol-2-yl)methoxy)phenyl)-5-methylthiazol-4-yl)ethan-1-ol (**S32c**). DIBAL-H (1.0 M in THF, 1.0 mL) was slowly added to a solution of ketone **S32b** (177 mg, 0.42 mmol) in dichloromethane (4 mL) at –78 °C. The reaction was stirred for 30 minutes then slowly warmed to room temperature. After approximately 1.5 hours, the reaction was cooled to –78 °C and another 0.6 mL of the DIBAL solution was added. The reaction was monitored via TLC (5% methanol in dichloromethane), and after approximately 6 hours the reaction was cooled to 0 °C and quenched by the addition of water. The product was extracted with dichloromethane, and the organic fractions were dried with magnesium sulfate. The drying agent was filtered off, and the solvent was removed under reduced pressure. Column chromatography (silica gel, 5% methanol in dichloromethane) afforded a sample of product that was used for the next step without further purification (75 mg crude yield). ^{1}H NMR (500 MHz, $CDCl_3$) δ 8.11 – 8.03 (m, 2H), 7.68 (d, *J* = 2.1 Hz, 1H), 7.56 – 7.46 (m, 4H), 6.91 (d, *J* = 8.5 Hz, 1H), 5.43 (s, 2H), 4.93 (p, *J* = 6.6 Hz, 1H), 3.89 (s, 3H), 2.96 (d, *J* = 7.6 Hz, 1H), 2.40 (s, 3H), 1.53 (d, *J* = 6.5 Hz, 3H). ^{13}C NMR (126 MHz, $CDCl_3$) δ 165.92, 163.83, 162.34, 155.47, 151.56, 147.12, 132.11, 129.18, 127.23, 127.09, 126.39, 123.63, 121.74, 113.86, 112.19, 64.66, 61.81, 56.16, 24.22, 11.01. HRMS-ESI (m/z) $[M + H]^+$ calcd for $C_{22}H_{22}N_3O_4S$, 424.1331; found 424.1330.

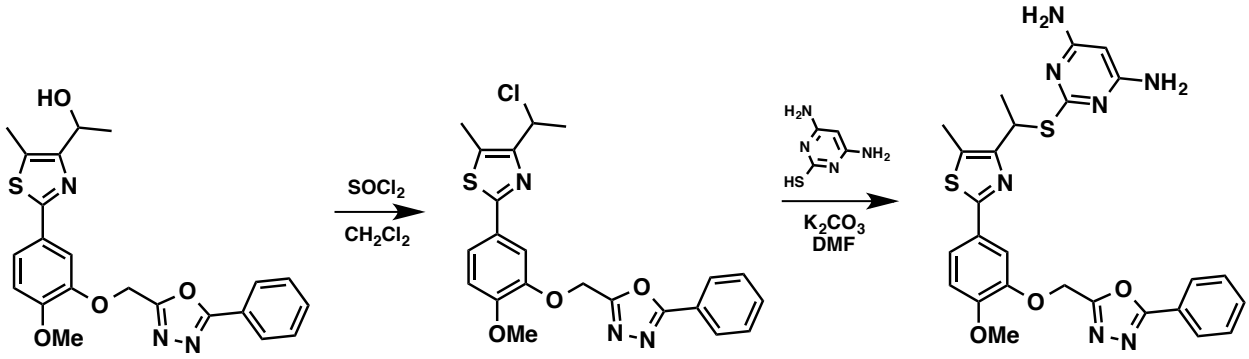

2-((1-(2-(4-methoxy-3-((5-phenyl-1,3,4-oxadiazol-2-yl)methoxy)phenyl)-5-methylthiazol-4-yl)ethyl)thio)pyrimidine-4,6-diamine (**S32**). Alcohol **S32c** (75 mg, 0.17 mmol) was stirred in dichloromethane (0.25 mL) at room temperature. To this solution was added thionyl chloride (0.65 mL, 8.9 mmol) at room temperature. After a few hours, 1 mL of cold saturated sodium bicarbonate was added at 0 °C. Water was added, and the product was extracted with dichloromethane. The organic layer was dried with magnesium sulfate, and the drying agent was filtered off. After removal of the solvent, the crude product was used for the next step without purification. A mixture of chloride **S32d** (73 mg, 0.16 mmol), 4,6-diamino-2-mercaptopyrimidine (40 mg, 0.28 mmol), K_2CO_3 (91 mg, 0.66 mmol), and DMF (0.6 mL) was stirred at 80 °C while under a nitrogen atmosphere. The reaction was monitored via TLC (10% methanol in dichloromethane). After 2.5 hours, the mixture was diluted with water, and the product was extracted with dichloromethane. The organic layer was dried with magnesium sulfate, the drying agent was filtering off, and the solvent was removed under reduced pressure. The crude product was triturated with ethyl acetate. The ethyl acetate layer was separated, and the solvent was removed under reduced pressure to yield a residue that was subjected to column chromatography (silica gel, 5% methanol in dichloromethane). The sample was submitted for biology experiments without further purification. ^{1}H NMR (500 MHz, DMSO-d_6) δ 8.05 – 8.00 (m, 2H), 7.69 – 7.58 (m, 4H), 7.50 (dd, J = 8.5, 2.1 Hz, 1H), 7.12 (dd, J = 8.6, 1.6 Hz, 1H), 6.12 (s, 4H), 5.54 (s, 2H), 5.22 (q, J = 7.0 Hz, 1H), 5.16 (d, J = 2.0 Hz, 1H), 3.82 (s, 3H), 2.47 (s, 3H), 1.67 (d, J = 7.0 Hz, 3H). ^{13}C NMR (126 MHz, DMSO) δ 168.05, 164.79,

163.51, 162.70, 162.56, 153.72, 151.04, 146.73, 132.33, 129.57, 126.83, 126.67, 126.16, 123.00, 120.88, 112.73, 112.62, 79.07, 60.91, 55.82, 39.52, 36.13, 22.16, 12.14. HRMS-ESI (m/z) $[M + H]^+$ calcd for $C_{26}H_{26}N_7O_3S_2$, 548.1539; found 548.1538.

APPENDIX ONE

Data Collection and Refinement Statistics Relevant to Part 1

Structure-Guided Development of Deoxycytidine Kinase Inhibitors with Nanomolar Affinity and Improved Metabolic Stability

Julian Nomme,* Zheng Li,* Raymond M. Gipson,* Jue Wang,* Amanda L. Armijo, Thuc Le,

Soumya Poddar, Tony Smith, Bernard D. Santarsiero, Hien-Anh Nguyen, Johannes Czernin,

Anastassia N. Alexandrova, Michael E. Jung, Caius G. Radu, and Arnon Lavie

J. Med. Chem. **2014**, *57*, 9480–9494

Table A1.1 Data Collection and Refinement Statistics.

	complex							
	4	**5**	**6**	**7**	**8**	**9**	**10**	**12R**
PDB code	4Q18	4Q19	4Q1A	4Q1B	4Q1C	4Q1D	4Q1E	4Q1F
				Data Collection Statistics				
X-ray source and detector	LS-CAT ID-G MARCCD 300	LS-CAT ID-G MARCCD 300	LS-CAT ID-G MARCCD 300	LS-CAT ID-G MARCCD 300	LS-CAT ID-G MARCCD 300	Rigaku RU-200 R-AXIS IV++	Rigaku RU-200 R-AXIS IV++	Rigaku RU-200 R-AXIS IV++
wavelength (Å)	0.9785	0.9785	0.9785	0.9785	0.9785	1.5418	1.5418	1.5418
temp (K)	100	100	100	100	100	93	93	93
resolution (Å) (*high res in parentheses*)	2.0 (2.1–2.0)	2.09 (2.21–2.09)	1.90 (2.01–1.90)	2.15 (2.28–2.15)	2.0 (2.12–2.00)	2.0 (2.12–2.00)	1.85 (1.96–1.85)	2.1 (2.23–2.10)
number of reflections								
observed	194 185	201 554	273 877	191 219	194 108	144 843	158 177	175 767
unique	38 119	32 496	43 643	30 472	36 902	37 712	46 762	32 727
completeness (%)	99.4 (99.9)	98.8 (93.9)	99.3 (98.4)	98.3 (97.4)	98.8 (96.1)	99.5 (98.5)	96.9 (82.8)	99.5 (98.7)
R_{sym} (%)	5.9 (54.7)	7.3 (67.9)	4.4 (62.9)	5.2 (55.2)	5.1 (71.6)	3.3 (67.1)	2.8 (40.4)	4.3 (75.6)
average $I/\sigma(I)$	13.6 (2.7)	14.2 (2.5)	20.64 (2.54)	17.42 (2.87)	16.57 (2.04)	19.38 (1.79)	21.62 (1.99)	21.66 (2.12)
space group	$P4_1$	$P4_1$	$P4_1$	$P4_1$	$P4_1$	$P4_1$	$P4_1$	$P4_1$
unit cell (Å): $a = b$, c	68.75, 122.45	68.53, 119.79	68.66, 120.36	68.97, 121.94	68.66, 119.27	68.73, 120.62	68.74, 122.20	68.78, 121.28
				Refinement Statistics				
refinement program	Refmac5	Refmac5	Refmac5	Refmac5	Refmac5	Refmac5	Refmac5	Phenix 1.8.4
twinning fraction	0.5	0.5	0.5	0.5	0.5	0.5	0.5	0.5
R_{cryst} (%)	18.3	22.9	20.2	17.3	20.5	19.1	17.4	20.3
R_{free} (%)	21.6	26.1	25.0	25.3	23.8	25.3	21.8	23.1
resolution range (Å)	30.0–2.0	30–2.09	30–1.9	30–2.15	30–2.0	30–2.0	30–1.85	30–2.1
protein molecules per au	2	2	2	2	2	2	2	2
number of atoms								
protein (protA, protB)	1921, 1902	1877, 1889	1890, 1904	1877, 1873	1897, 1870	1890, 1842	1905, 1904	1897, 1897
water molecule	88	103	105	92	109	92	185	170
inhibitor	32 × 4	27 × 2	30 × 2	32 × 2	32 × 2	31 × 2	29 × 4	33 × 2
UDP	25 × 2	25 × 2	25 × 2	25 × 2	25 × 2	25 × 2	25 × 2	25 × 2
rms deviation from ideal								
bond length (Å)	0.012	0.013	0.011	0.012	0.012	0.011	0.013	0.006
bond angles (deg)	1.66	1.84	1.65	1.70	1.72	1.68	1.67	1.03
average *B*-factors (Å^2)								
protein (protA, protB)	47.0, 46.9	30.1, 30.1	40.6, 40.7	53.8, 54.6	29.5, 29.5	51.8, 51.8	37.6, 39.2	47.8, 48.7
water molecules	39.8	29.8	39.3	45.4	29.3	46.8	38.4	44.2
inhibitor								
protA (301, 302)	46.6, 45.8	29.9, –	39.7, –	58.7, –	29.4, –	55.8, –	43.1, 44.5	47.3, –
protB (301, 302)	53.4, 41.2	30.0, –	40.1, –	58.3, –	29.5, –	52.8, –	40.0, 48.5	54.5, –
UDP (protA, protB)	51.6, 49.0	30.1, 30.3	41.4, 39.9	58.4, 58.5	29.6, 29.5	53.3, 53.6	38.5, 39.4	49.8, 51.2
Ramachandran plot (%)								
most favored regions	90.0	88.7	91.9	87.3	91.6	89.2	90.3	88.6
additionally allowed regions	9.5	10.8	7.6	12.3	8.4	10.3	9.2	10.9
generously allowed/disallowed regions	0.5	0.5	0.5	0.4	0.5	0.5	0.5	0.5

APPENDIX TWO

In Vitro Biological Data Relevant to Part 1

Structure-Guided Development of Deoxycytidine Kinase Inhibitors with Nanomolar Affinity and Improved Metabolic Stability

Julian Nomme,* Zheng Li,* Raymond M. Gipson,* Jue Wang,* Amanda L. Armijo, Thuc Le,

Soumya Poddar, Tony Smith, Bernard D. Santarsiero, Hien-Anh Nguyen, Johannes Czernin,

Anastassia N. Alexandrova, Michael E. Jung, Caius G. Radu, and Arnon Lavie

J. Med. Chem. **2014**, *57*, 9480–9494

Table A2.1 In vitro biological data in CEM cells for compounds **1**–**12** and **S1**–**S32**.

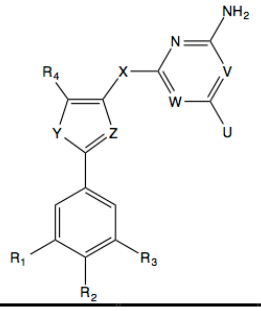

Compound	R_1	R_2	R_3	R_4	U	V	W	Y	Z	X	IC_{50} (nM)
1	H	OCH_3	$OCH_2C(CH_3)_2OH$	$CH_2CH_2CH_3$	NH_2	C	N	S	N	CH_2S	1.4
2	H	OCH_3	$OCH_2CH_2NHSO_2Me$	$CH_2CH_2CH_3$	NH_2	C	N	S	N	CH_2S	4.9
3	H	OCH_3	$OCH_2C(CH_3)_2OH$	$CH_2CH_2CH_3$	H	C	N	S	N	CH_2S	21.8
4	H	OCH_3	$OCH_2C(CH_3)_2OH$	$CH_2CH_2CH_3$	NH_2	N	C	S	N	CH_2S	395 (±14.2)
5	H	OCH_3	OH	$CH_2CH_2CH_3$	NH_2	C	N	S	N	CH_2S	18.6
6	H	OCH_3	OCH_2CH_2OH	$CH_2CH_2CH_3$	NH_2	C	N	S	N	CH_2S	1.15
7	H	H	$OCH_2CH_2NHSO_2Me$	$CH_2CH_2CH_3$	NH_2	C	N	S	N	CH_2S	11.6
8	H	$O(CH_2)_2OH$	OCH_2CH_2OH	$CH_2CH_2CH_3$	NH_2	C	N	S	N	CH_2S	0.9
9	H	OCH_3	OCH_2CH_2F	$CH_2CH_2CH_3$	NH_2	C	N	S	N	$CH(CH_3)S$	10.0
10	H	OCH_3	OCH_2CH_2F	CH_3	NH_2	C	N	S	N	$CH(CH_3)S$	7.0
11 R	H	Note[c]	OCH_2CH_3	CH_3	NH_2	C	N	S	N	$CH(CH_3)S$	1.25
11 S	H	Note[c]	OCH_2CH_3	CH_3	NH_2	C	N	S	N	$CH(CH_3)S$	429.5 (±34.1)
12 R	H	OCH_3	$OCH_2CH_2NHSO_2Me$	CH_3	NH_2	C	N	S	N	$CH(CH_3)S$	3.7 (±0.8)
12 S	H	OCH_3	$OCH_2CH_2NHSO_2Me$	CH_3	NH_2	C	N	S	N	$CH(CH_3)S$	94.0 (±14.4)
S1 DI-47	H	OCH_3	$OCH_2C(CH_3)_2OH$	$CH_2CH_2CH_3$	NH_2	C	N	S	N	CD_2S	4.0 (±2.2)
S2 DI-50	H	Note[d]	$OCH_2CH_2NHSO_2Me$	$CH_2CH_2CH_3$	NH_2	C	N	S	N	CH_2S	1,200(±312)
S3 DI-51	H	OCH_3	$OCH_2CH_2CH_2F$	$CH_2CH_2CH_3$	NH_2	C	N	S	N	CH_2S	2.5 (±0.35)
S4 DI-52	H	OCH_2CH_2F	OCH_2CH_3	$CH_2CH_2CH_3$	NH_2	C	N	S	N	CH_2S	2.8 (±1.6)
S5 DI-53	H	F	$OCH_2CH_2CH_2F$	$CH_2CH_2CH_3$	NH_2	C	N	S	N	CH_2S	31.7(±11.9)
S6 DI-54	H	F	OCH_2CH_2F	$CH_2CH_2CH_3$	NH_2	C	N	S	N	CH_2S	23.3 (±13)
S7 DI-55	H	N/A[e]	OCH_2CH_2F	$CH_2CH_2CH_3$	NH_2	C	N	S	N	CH_2S	6.8 (±1.7)
S8 DI-56	H	N/A[e]	OCH_2CH_2F	$CH_2CH_2CH_3$	NH_2	C	N	S	N	CD_2S	30 (±4)
S9 DI-57	H	OCH_3	OCH_2CH_2F	$CH_2CH_2CH_3$	NH_2	C	N	S	N	CD_2S	3.1 (±1.1)
S10 DI-58	H	OCH_3	$O(CH_2)_2O(CH_2)_2O(CH_2)_2X$[f]	$CH_2CH_2CH_3$	NH_2	C	N	S	N	CH_2S	4.7 (±1.6)

S11 DI-59	H	OCH_3	$O(CH_2)_2O(CH_2)_2O(CH_2)_2OH$	$CH_2CH_2CH_3$	NH_2	C	N	S	N	CH_2S	1.06 (±0.15)
S12 DI-60	H	OCH_3	OCH_2CH_2F	CH_3	NH_2	C	N	O	C	CH_2S	13,840(±280)
S13 DI-61	H	OCH_3	$OCH_2CH_2NHSO_2Me$	$CH_2CH_2CH_3$	NH_2	C	N	S	N	CD_2S	3.04 (±0.704)
S14 DI-62	H	OCH_2CH_2F	OCH_3	CH_3	NH_2	C	N	O	C	CH_2S	276 (±179)
S15 DI-64	H	OCH_3	OCH_2CH_2F	$CH_2CH_2CH_3$	NH_2	C	N	S	N	CH_2CH_2	664 (±360)
S16 DI-65	H	OCH_3	$O(CH_2)_2O(CH_2)_2O(CH_2)_2F$	$CH_2CH_2CH_3$	NH_2	C	N	S	N	CH_2S	4.22 (±1.98)
S17 DI-66	H	H	$O(CH_2)_2O(CH_2)_2O(CH_2)_2F$	$CH_2CH_2CH_3$	NH_2	C	N	S	N	CH_2S	69.08 (±46.41)
S18 DI-67	H	OCH_2CH_2F	OCH_3	CH_3	NH_2	C	N	S	C	CH_2S	262 (±150)
S19 DI-69	F	H	$O(CH_2)_2O(CH_2)_2O(CH_2)_2F$	$CH_2CH_2CH_3$	NH_2	C	N	S	N	CH_2S	33.68 (±3.59)
S20 DI-70	H	OCH_3	$O(CH_2)_2O(CH_2)_2O(CH_2)_2OCH_3$	$CH_2CH_2CH_3$	NH_2	C	N	S	N	CH_2S	3.31 (±0.44)
S21 DI-71	H	Note[c]	OCH_2CH_3	$CH_2CH_2CH_3$	NH_2	C	N	S	N	CH_2S	2.37 (±0.44)
S22 DI-73	H	OCH_3	$O(CH_2)_2O(CH_2)_2O(CH_2)_2OCH_3$	$CH_2CH_2CH_3$	NH_2	C	N	S	N	$CH(CH_3)S$	6.0 (±2.4)
S23 DI-74	H	OCH_3	$O(CH_2)_2O(CH_2)_2O(CH_2)_2OCH_3$	CH_3	NH_2	C	N	S	N	$CH(CH_3)S$	8.03 (±3.16)
S24 DI-76	H	Note[c]	OCH_3	CH_3	NH_2	C	N	S	N	$CH(CH_3)S$	6.1 (±3.2)
S25 DI-77	H	OCH_3	$O(CH_2)_2O(CH_2)_2O(CH_2)_2OCH_3$	Cpr[g]	NH_2	C	N	S	N	CH_2S	23 (±20)
S26 DI-79	H	OCH_3	$O(CH_2)_2O(CH_2)_2O(CH_2)_2OCH_3$	CH_3	NH_2	C	N	S	N	CH_2S	9.1 (n=1)
S27 DI-80	H	OCH_3	$O(CH_2)_2O(CH_2)_2O(CH_2)_2OCH_3$	Cpr[g]	NH_2	C	N	S	N	$CH(CH_3)S$	3.7 (n=1)
S28 DI-81	H	OCH_3	$O(CH_2)_2O(CH_2)_2O(CH_2)_2OCH_3$	Phenyl	NH_2	C	N	S	N	$CH(CH_3)S$	98.9 (n=1)
S29 DI-83	H	Note[h]	$O(CH_2)_2O(CH_2)_2O(CH_2)_2OCH_3$	CH_3	NH_2	C	N	S	N	$CH(CH_3)S$	61.4 (n=1)
S30 DI-84	H	Note[h]	$OCH_2CH_2NHSO_2Me$	CH_3	NH_2	C	N	S	N	$CH(CH_3)S$	200.3(n=1)
S31 DI-85	F	H	$OCH_2CH_2NHSO_2Me$	CH_3	NH_2	C	N	S	N	$CH(CH_3)S$	9.07 (±2.24)
S32 DI-86	H	OCH_3	OCH_2–R–Ph[i]	CH_3	NH_2	C	N	S	N	$CH(CH_3)S$	—

[a]Inhibition activity measured by ^{3}H-deoxycytidine (dCyd) uptake in CEM cells. Values reported are the mean ± SD of at least n = 2 independent experiments. [b]Value reported for n = 1. [c]$R_2=O(CH_2)_2O(CH_2)_2O(CH_2)_2OCH_3$. [d]$R_2=N(SO_2Me)(CH_2CH_2NHSO_2Me)$. [e]2,4-disubstituted pyridine ring. [f]3,5-diaminopyrimidine thiol. [g]Cpr=cyclopropyl. [h] $R_2=OCH_2CH_2NHSO_2Me$. [i]R=1,3,4-oxadizole

APPENDIX THREE

Spectra Relevant to Part 1

Structure-Guided Development of Deoxycytidine Kinase Inhibitors with Nanomolar Affinity and Improved Metabolic Stability

Julian Nomme,* Zheng Li,* Raymond M. Gipson,* Jue Wang,* Amanda L. Armijo, Thuc Le,

Soumya Poddar, Tony Smith, Bernard D. Santarsiero, Hien-Anh Nguyen, Johannes Czernin,

Anastassia N. Alexandrova, Michael E. Jung, Caius G. Radu, and Arnon Lavie

J. Med. Chem. **2014**, *57*, 9480–9494

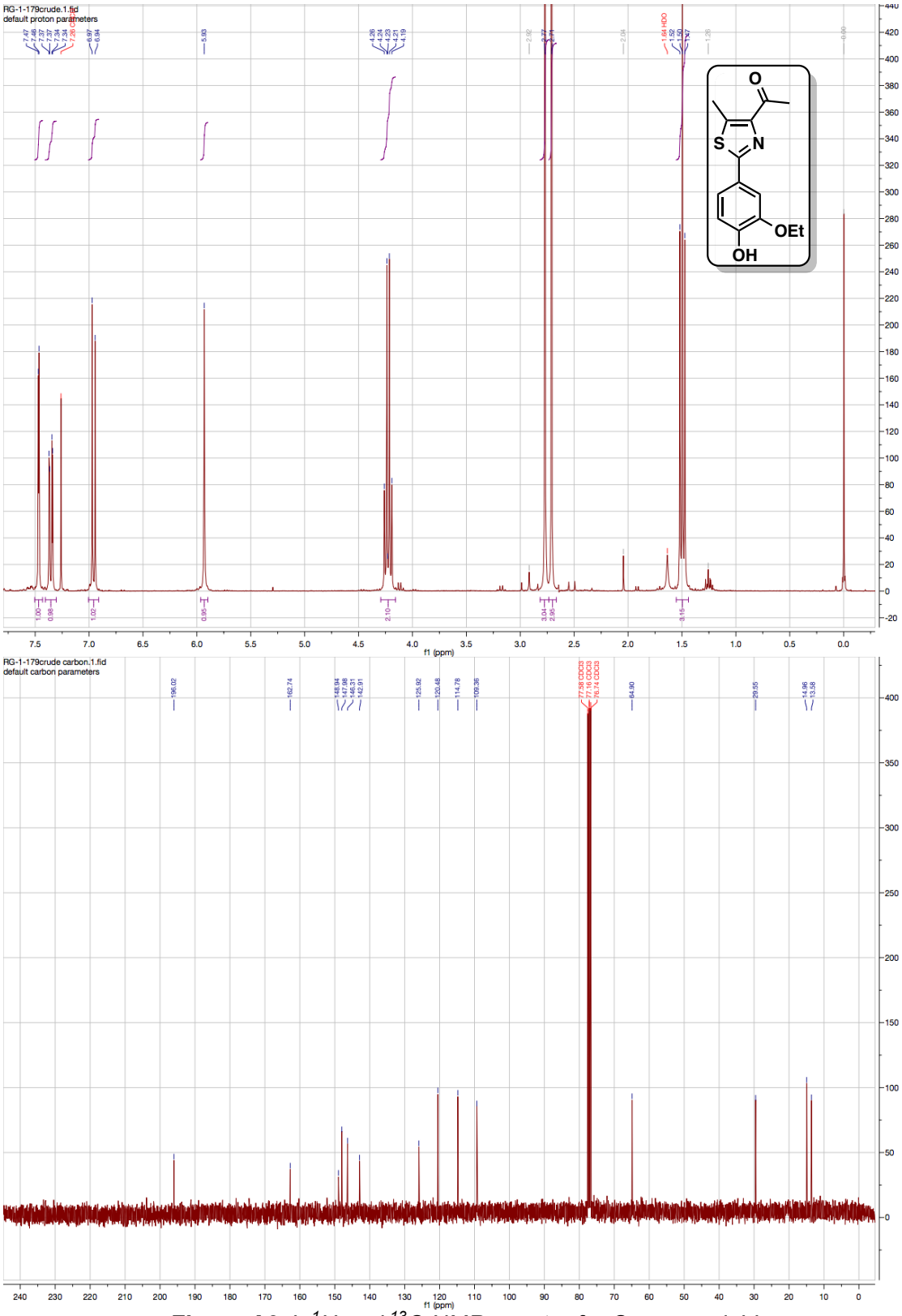

Figure A3.1. *^{1}H and ^{13}C NMR spectra for Compound* ***11c***

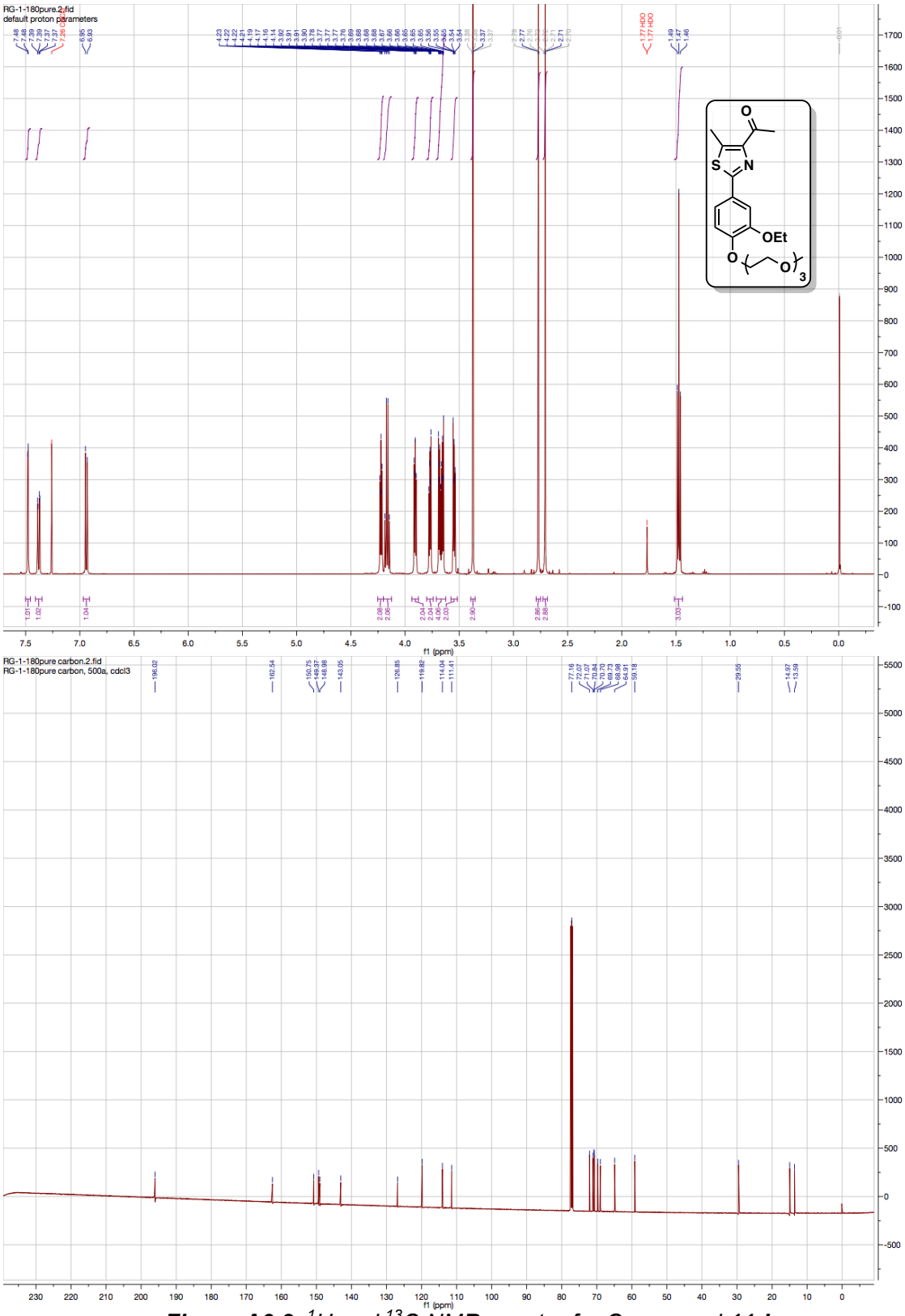

Figure A3.2. *^{1}H and ^{13}C NMR spectra for Compound* ***11d***.

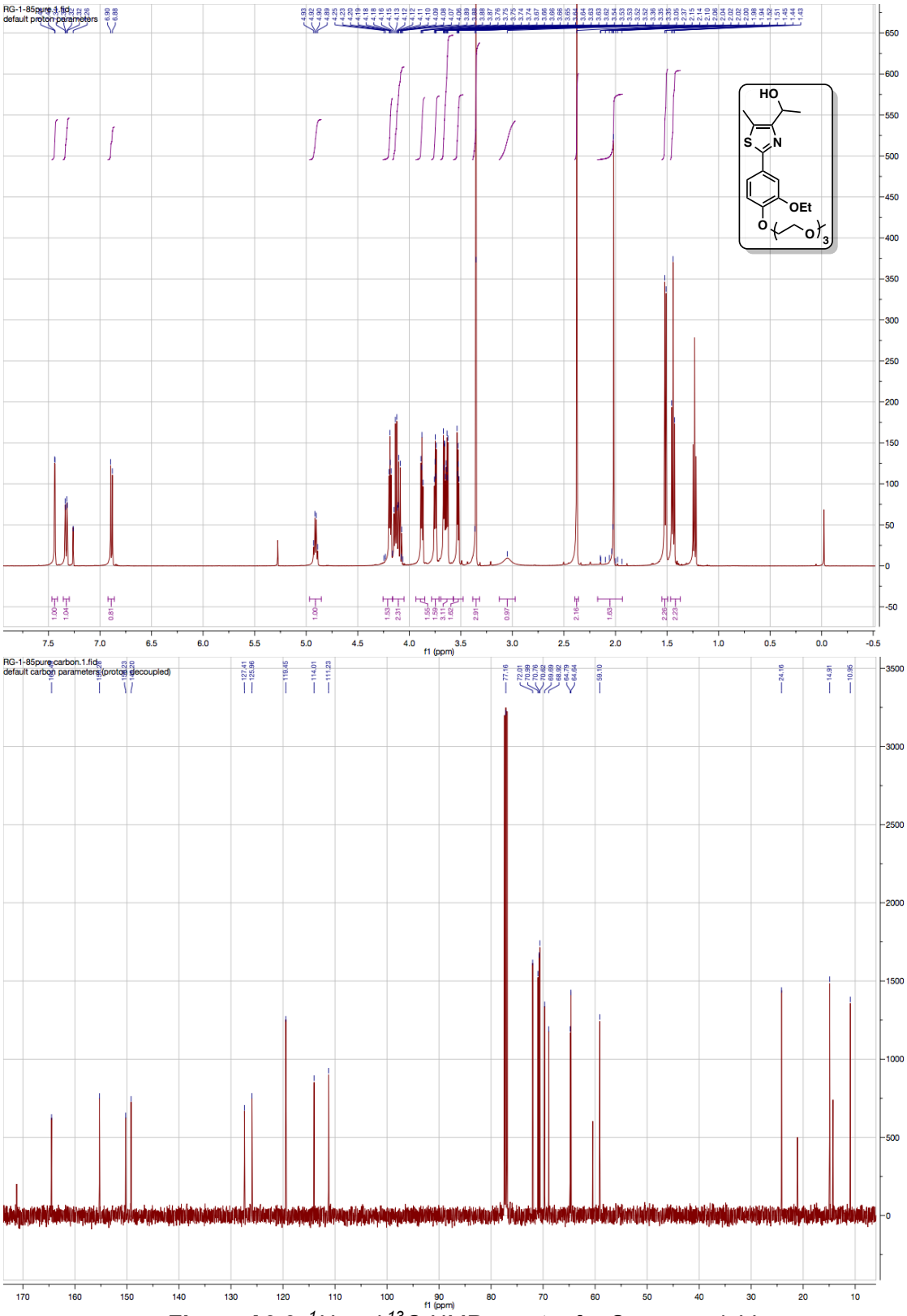

Figure A3.3. *^{1}H and ^{13}C NMR spectra for Compound* ***11e***.

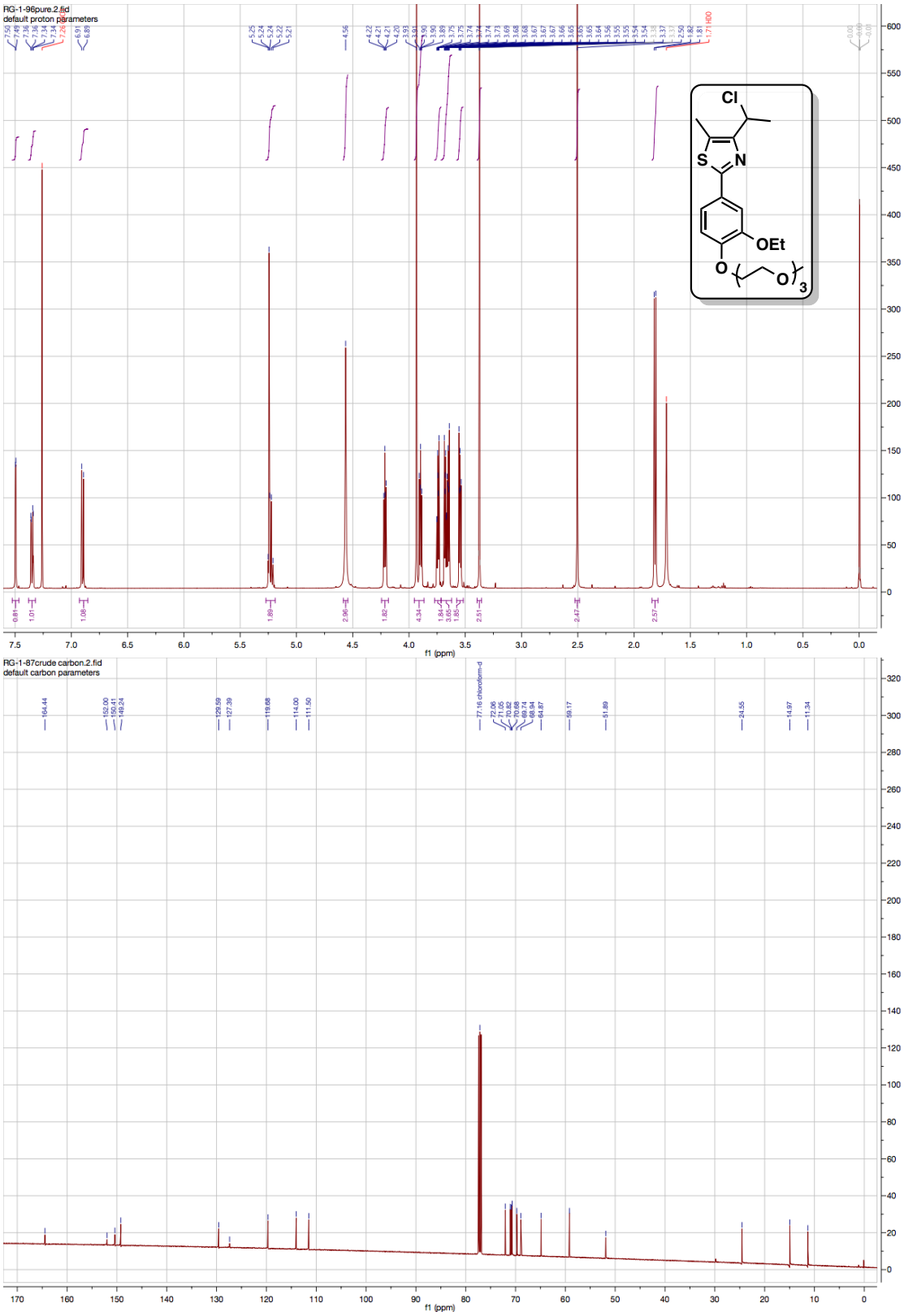

***Figure A3.4**. ^{1}H and ^{13}C NMR spectra for Compound **11f**.*

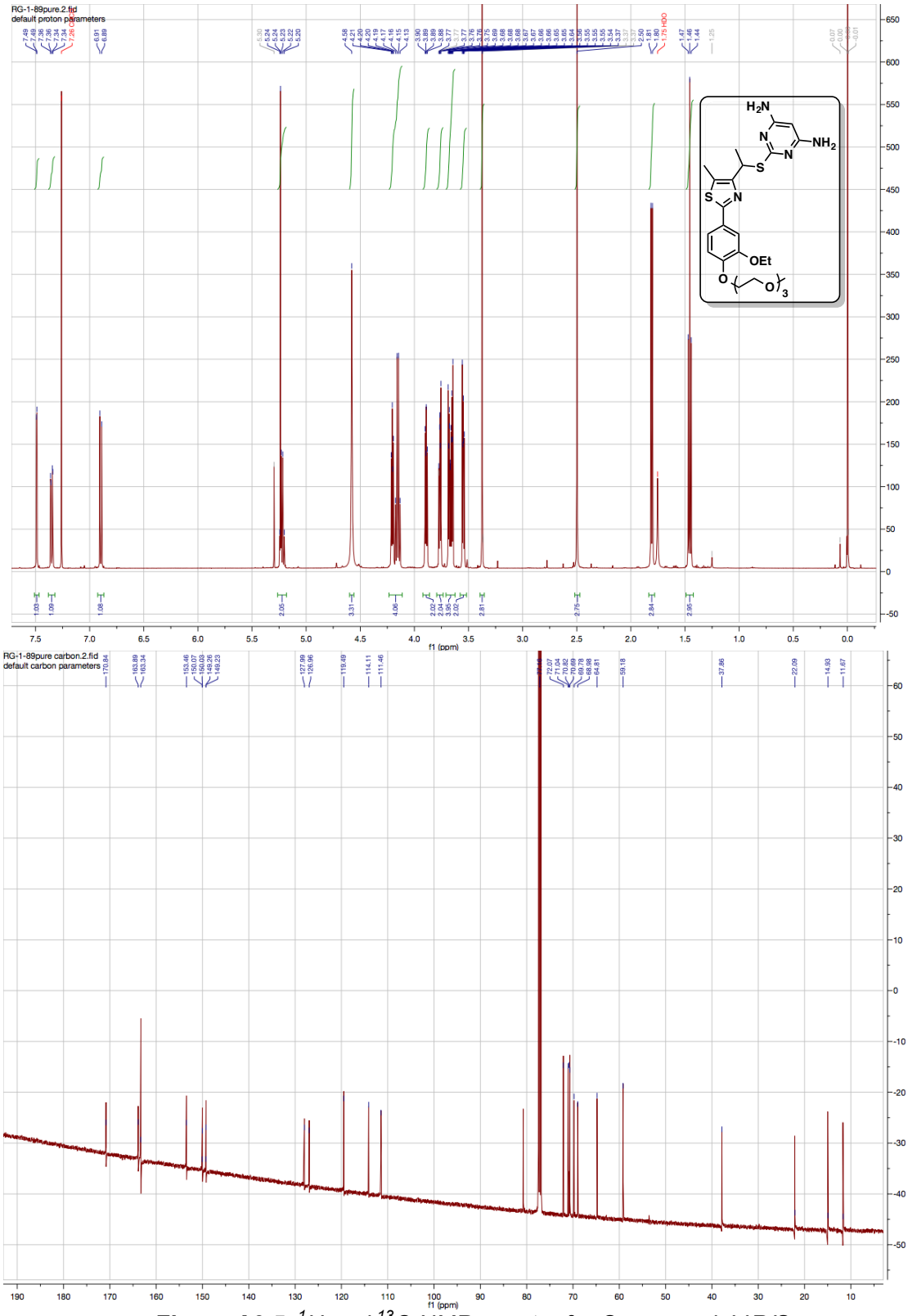

Figure A3.5. *^{1}H and ^{13}C NMR spectra for Compound* ***11R/S****.*

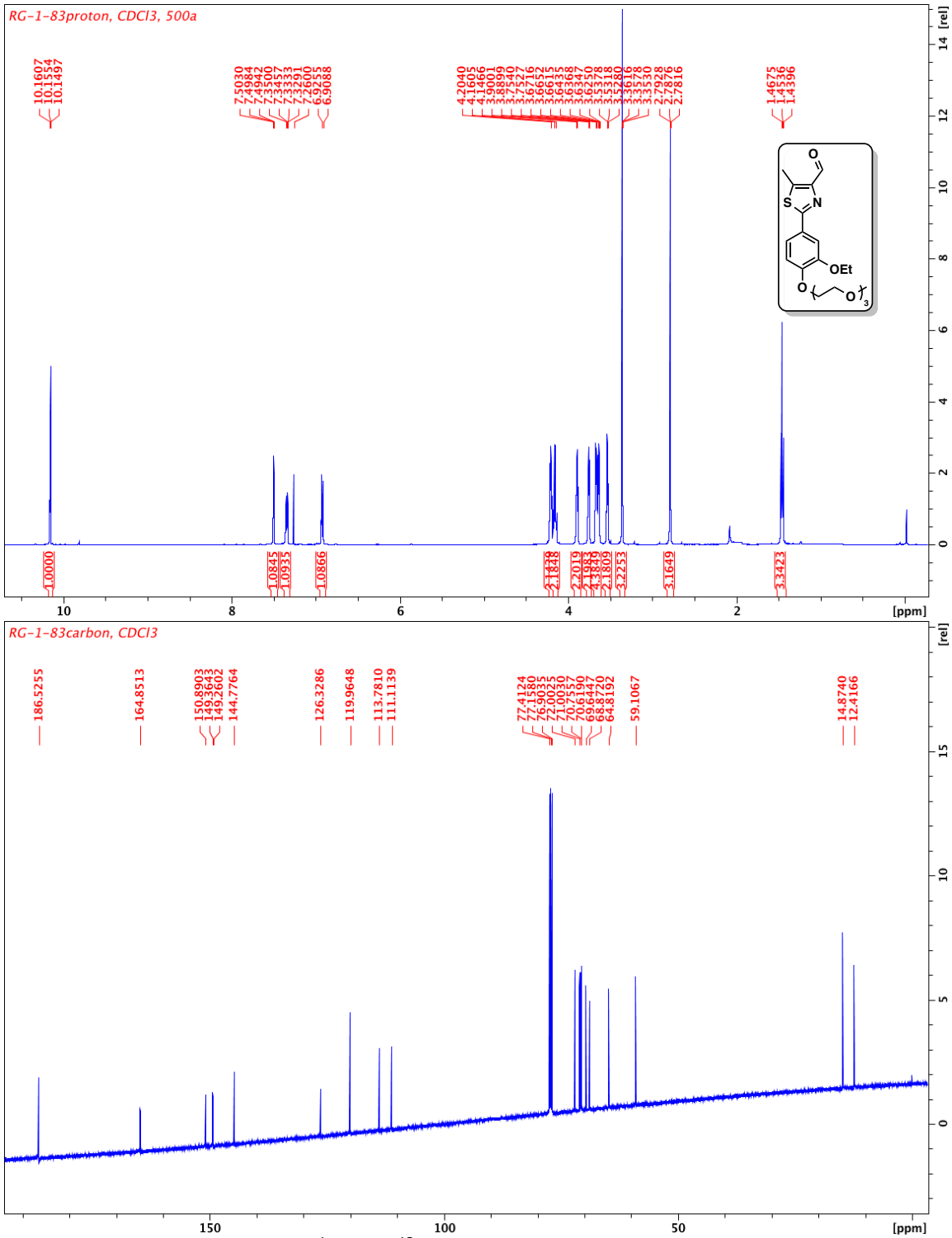

Figure A3.6. *^{1}H and ^{13}C NMR spectra for Compound **11j**.*

Figure A3.7. *^{1}H NMR spectrum for 4-bromo-2,3-dione*

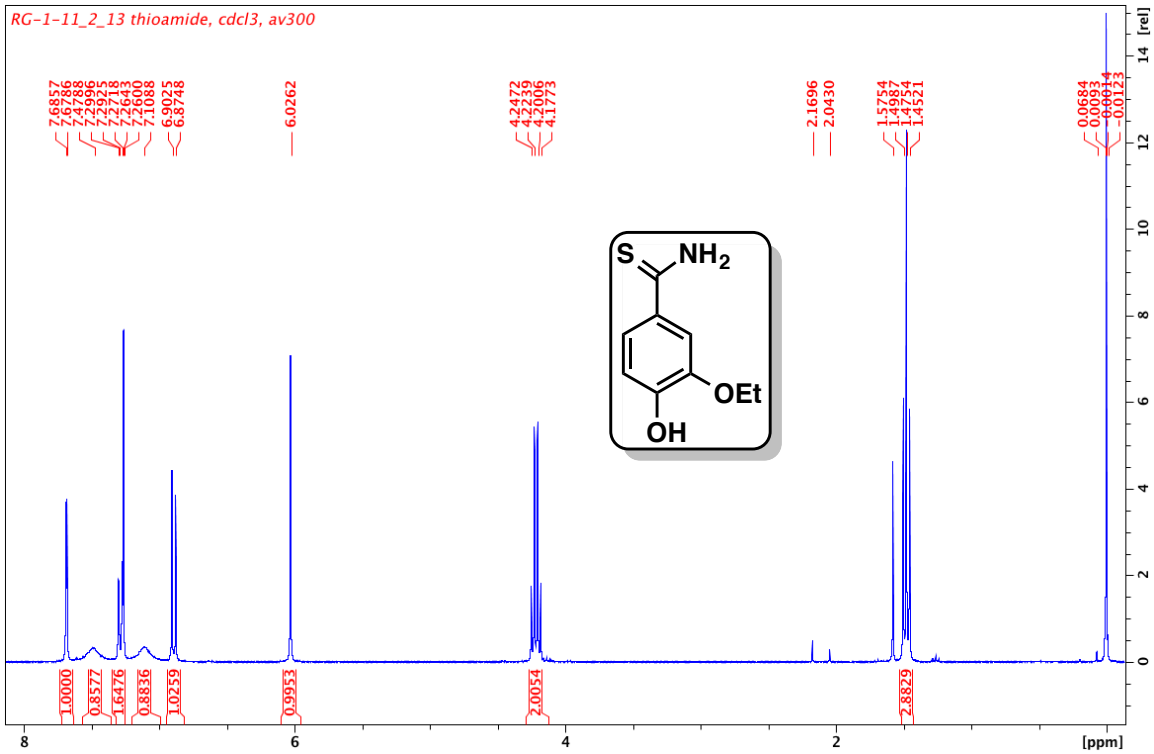

Figure A3.8. *^{1}H NMR spectrum for Compound* ***11b***

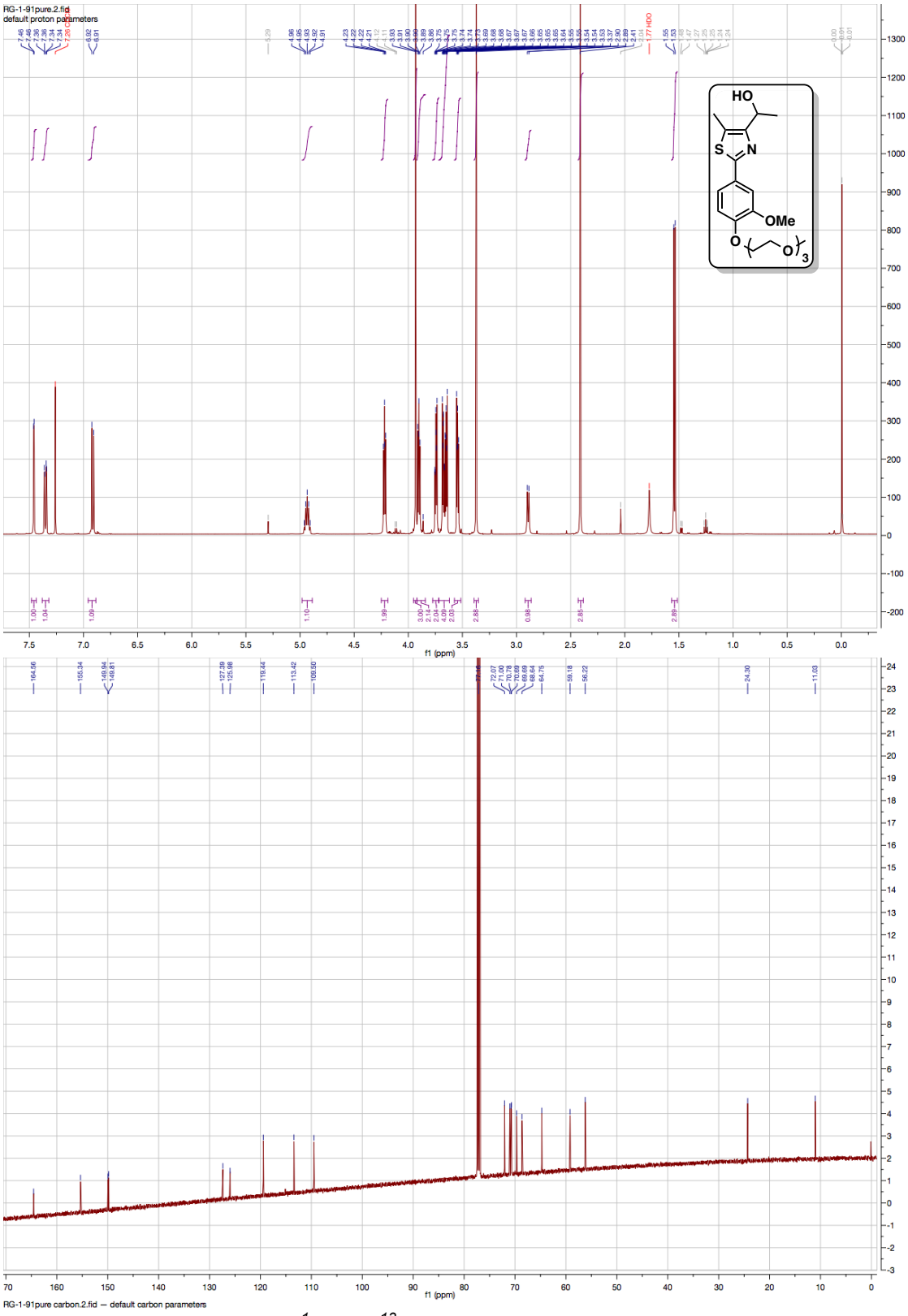

Figure A3.9. *^{1}H and ^{13}C NMR spectra for Compound* ***S24e***.

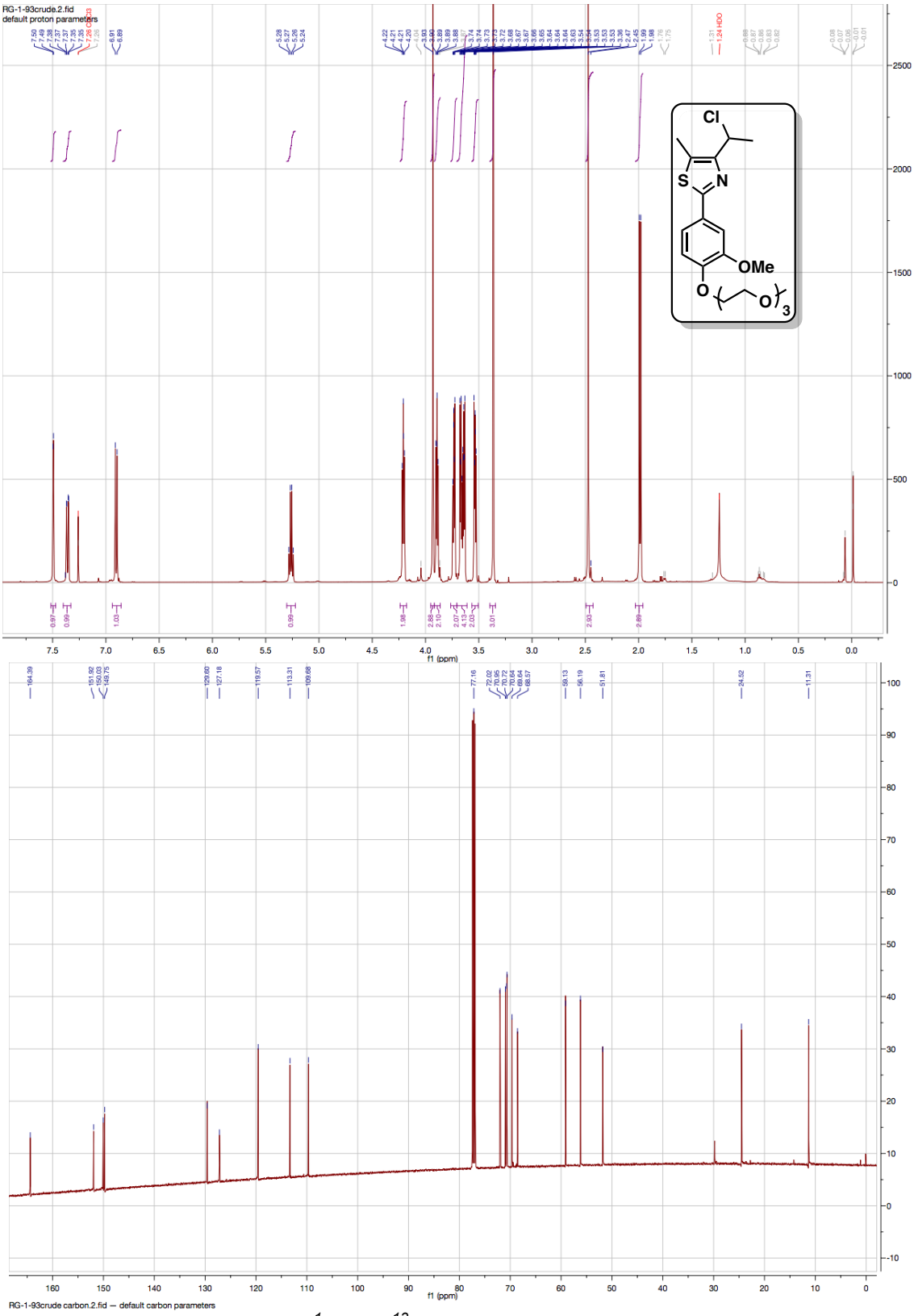

Figure A3.10. *^{1}H and ^{13}C NMR spectra for Compound* ***S24f****.*

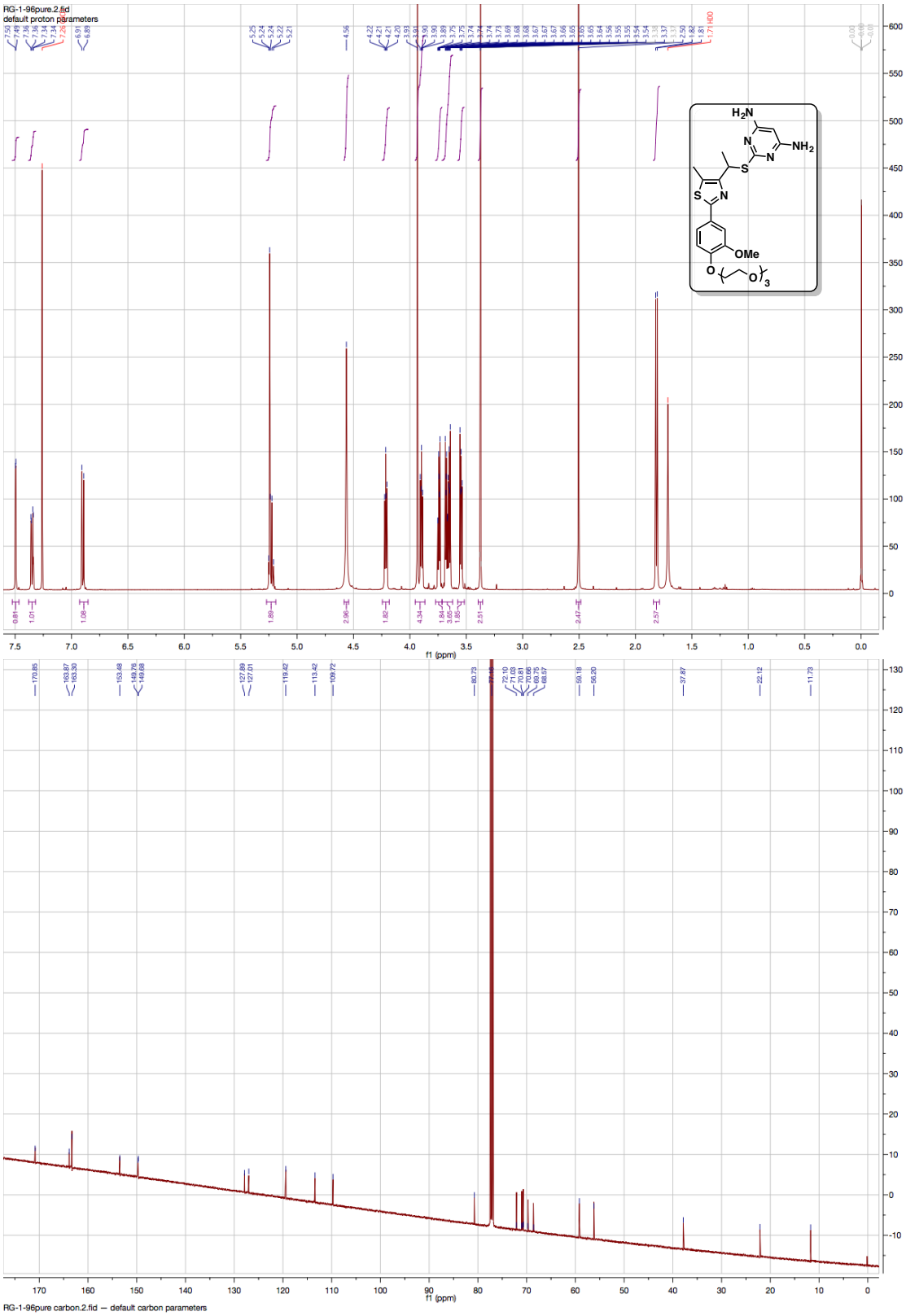

Figure A3.11. *^{1}H and ^{13}C NMR spectra for Compound **S24**.*

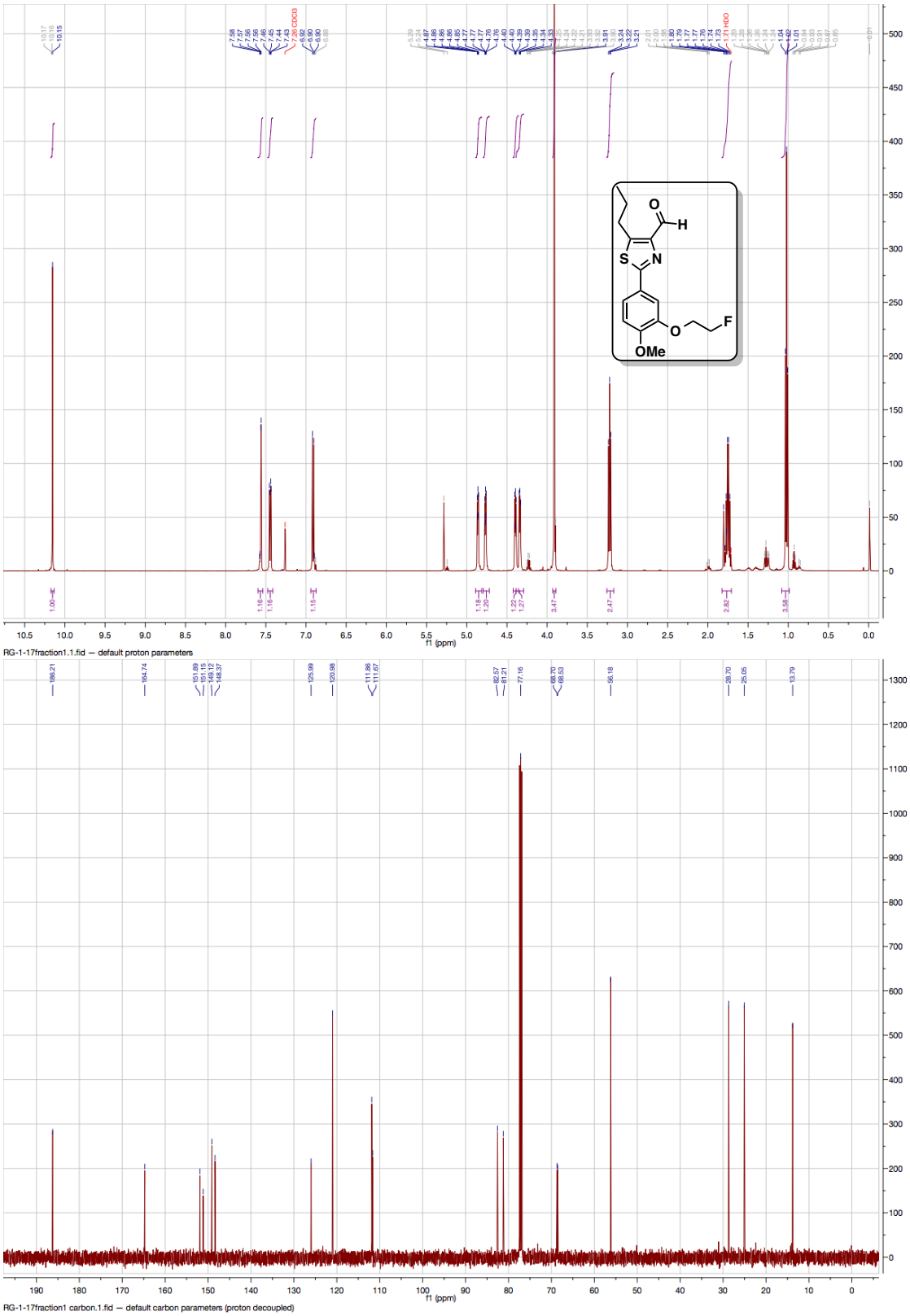

Figure A3.12. *^{1}H and ^{13}C NMR spectra for Compound* ***9b***.

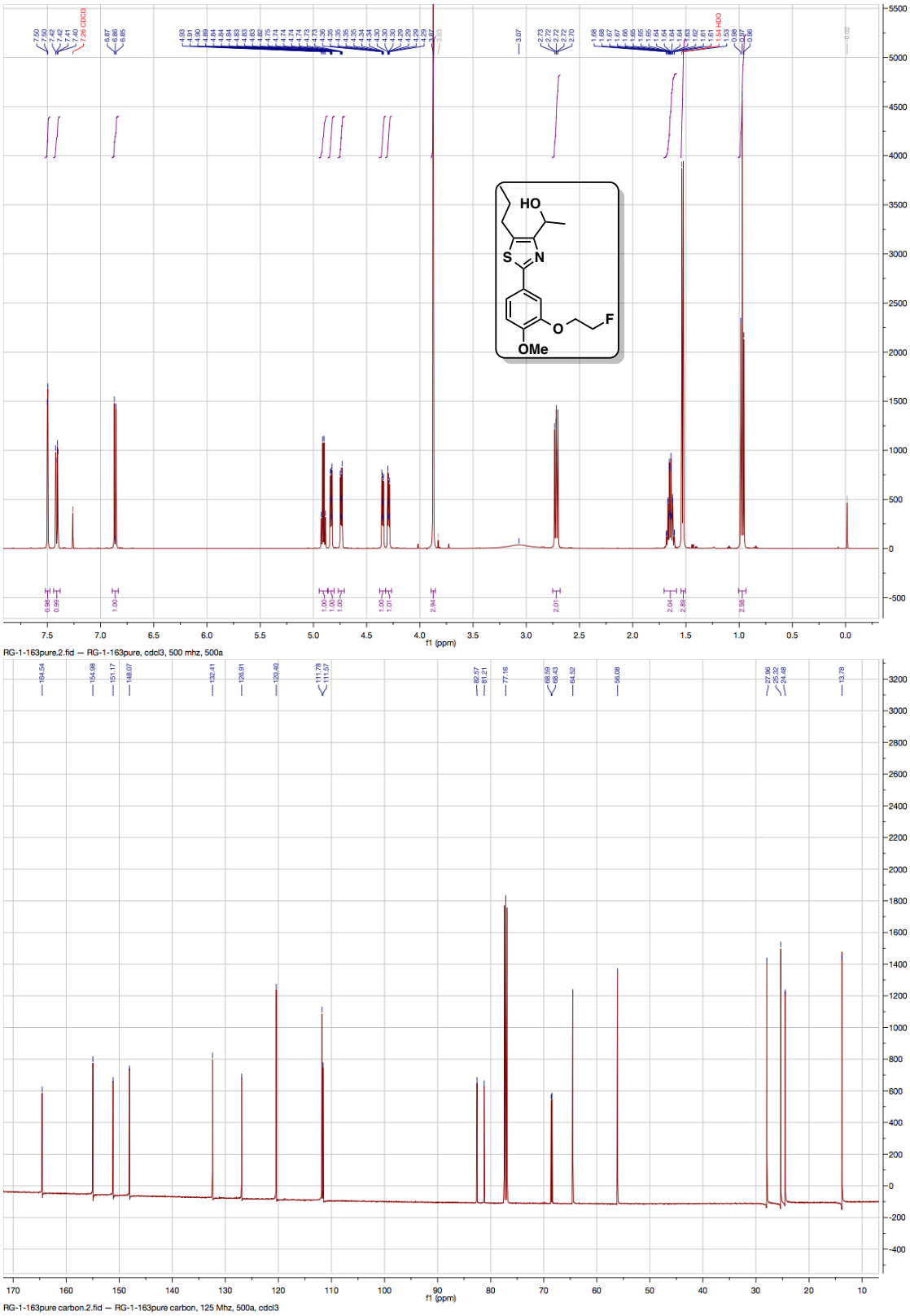

Figure A3.13. *^{1}H and ^{13}C NMR spectra for Compound* ***9c***.

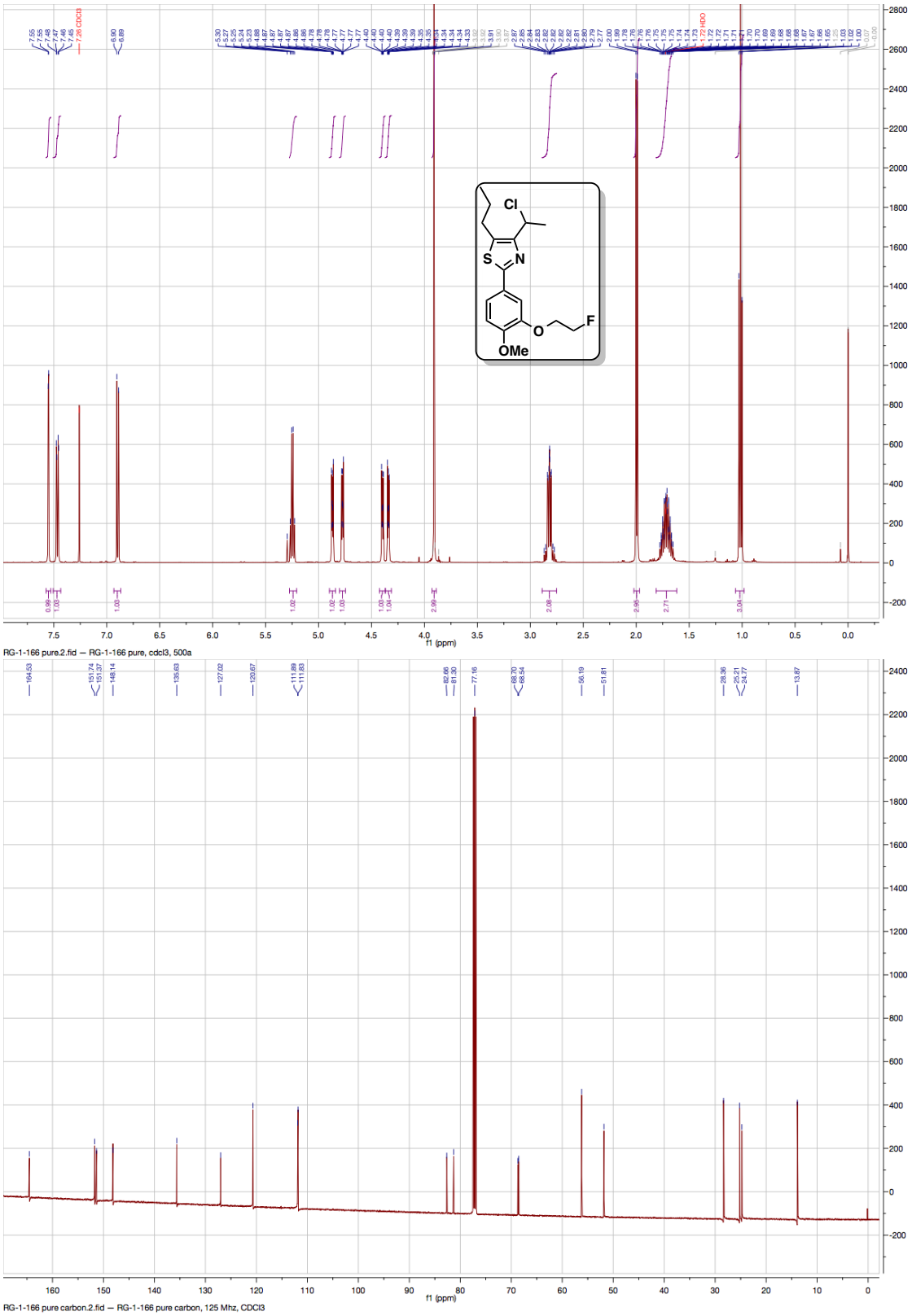

Figure A3.14. *^{1}H and ^{13}C NMR spectra for Compound* ***9d***.

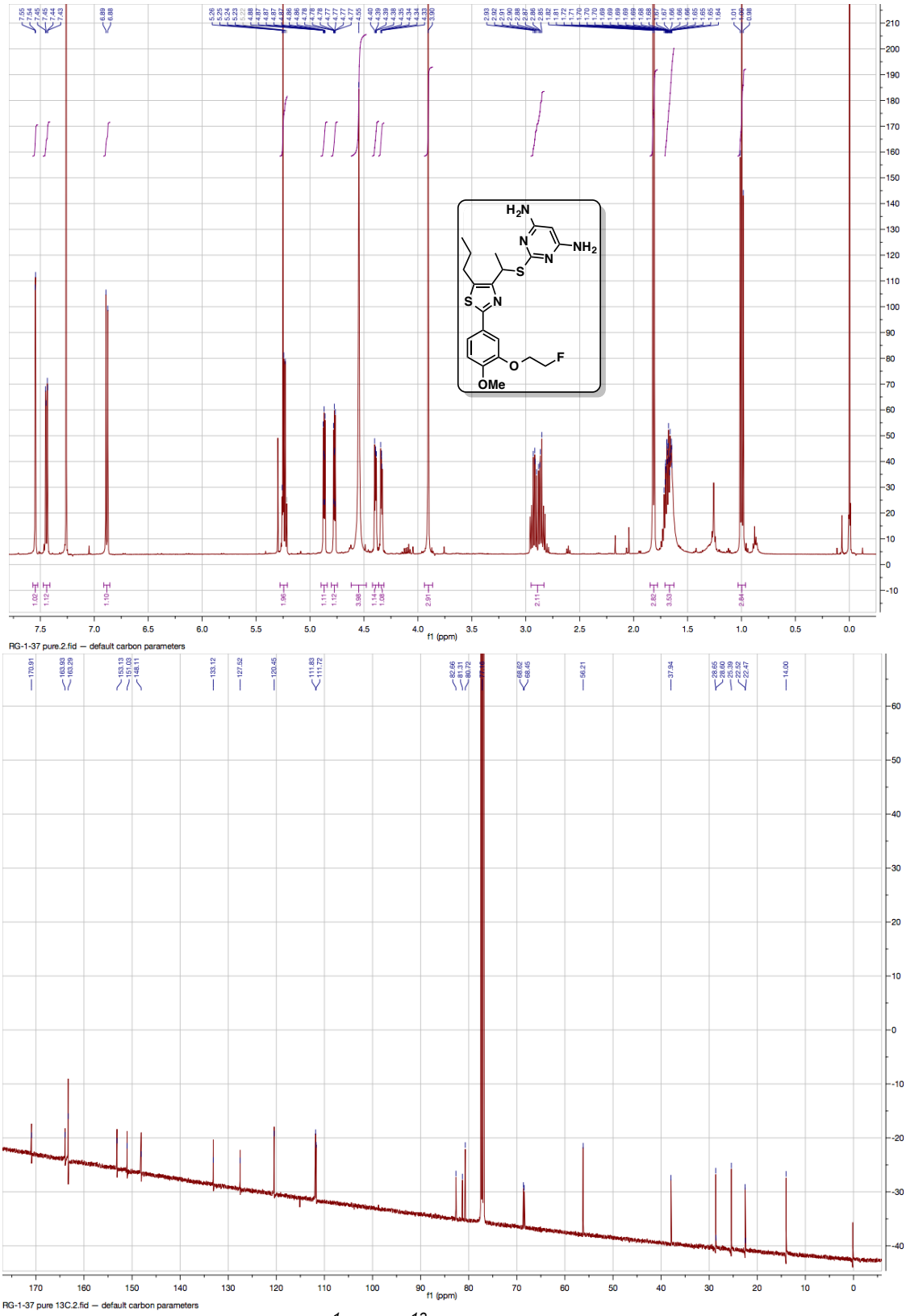

***Figure A3.15**. ^{1}H and ^{13}C NMR spectra for Compound **9**.*

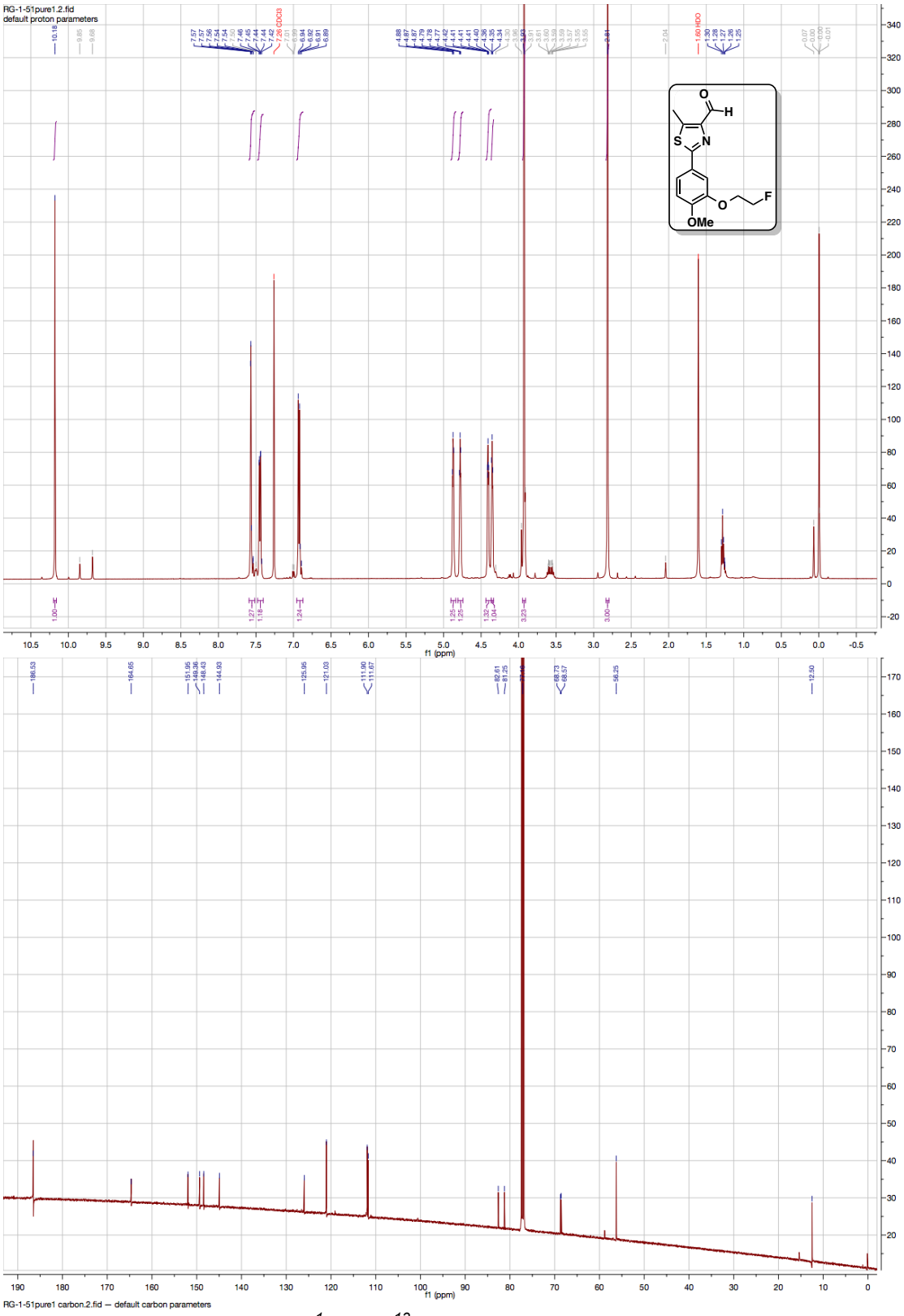

***Figure A3.16**. ^{1}H and ^{13}C NMR spectra for Compound **10b**.*

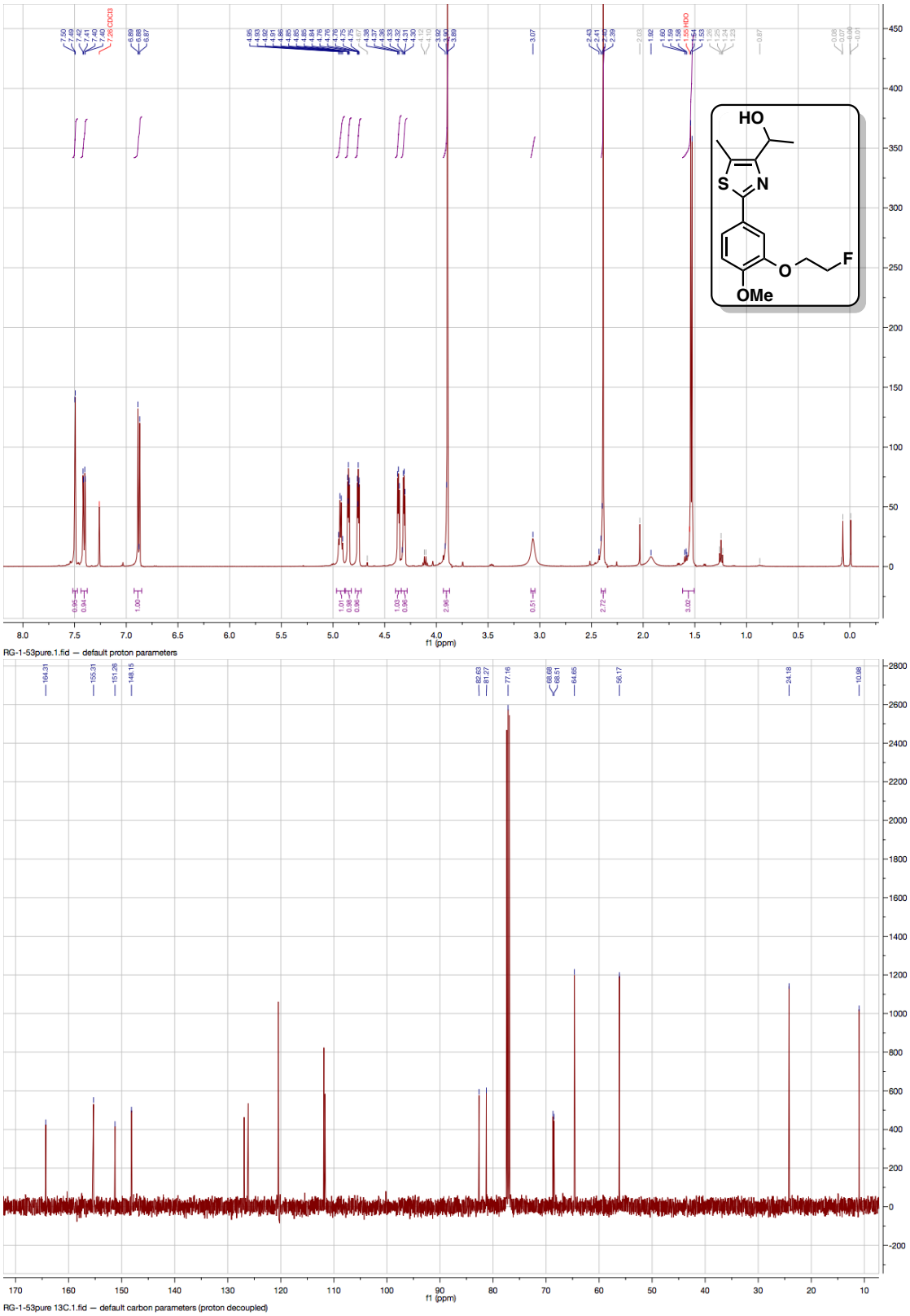

***Figure A3.17**. ^{1}H and ^{13}C NMR spectra for Compound **10c**.*

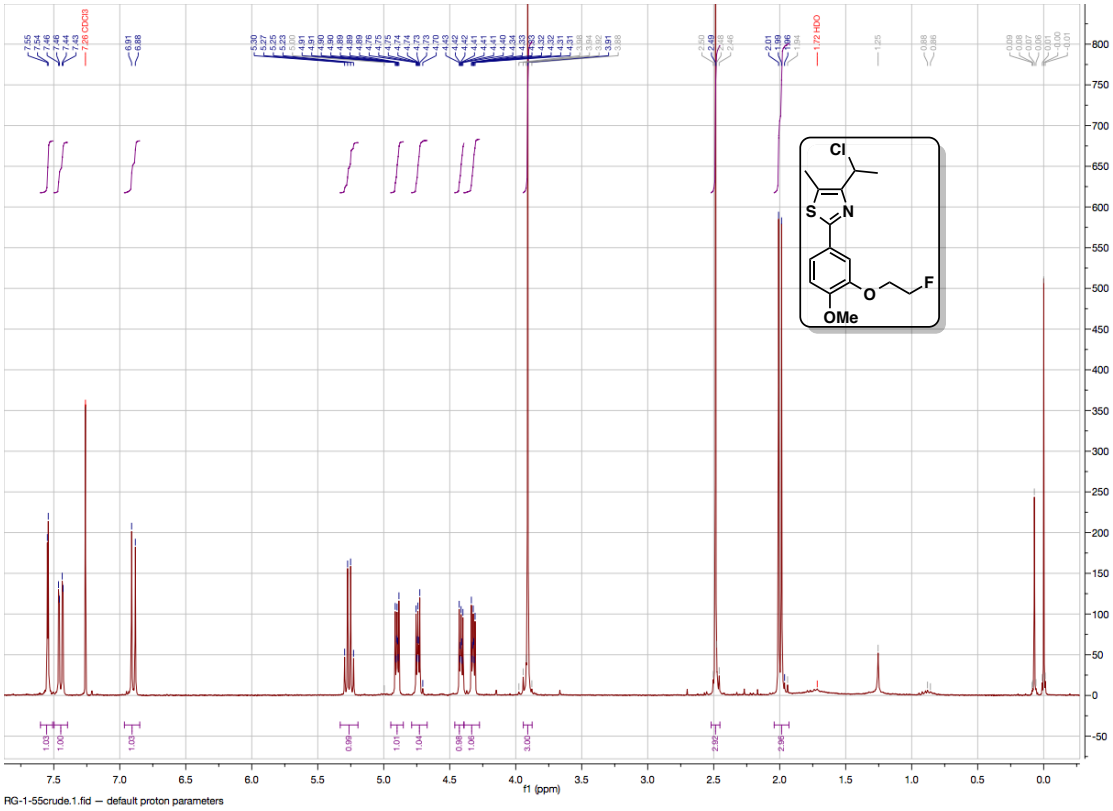

***Figure A3.18**. ^{1}H NMR spectrum for Compound **10d**.*

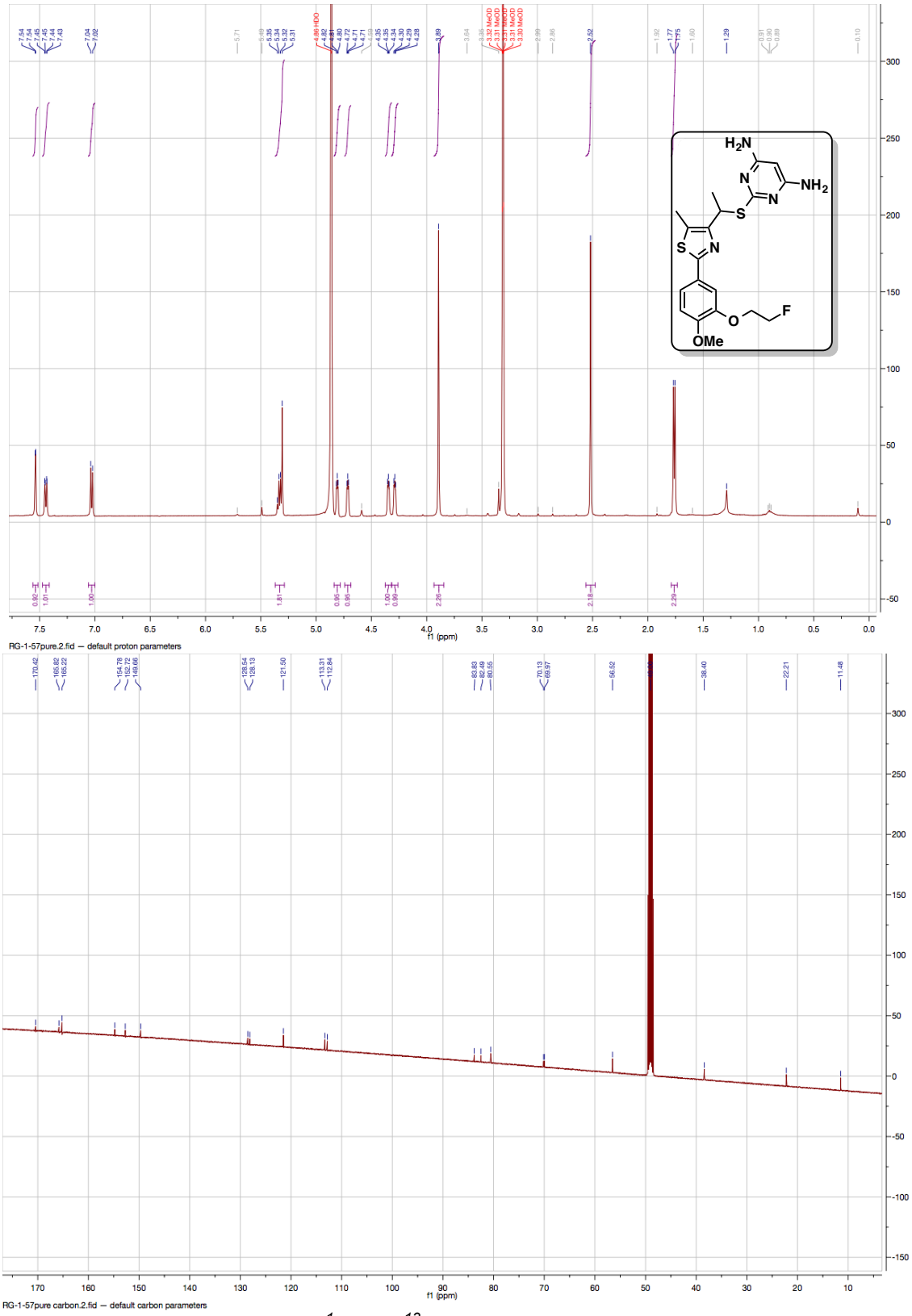

Figure A3.19. *^{1}H and ^{13}C NMR spectra for Compound **10**.*

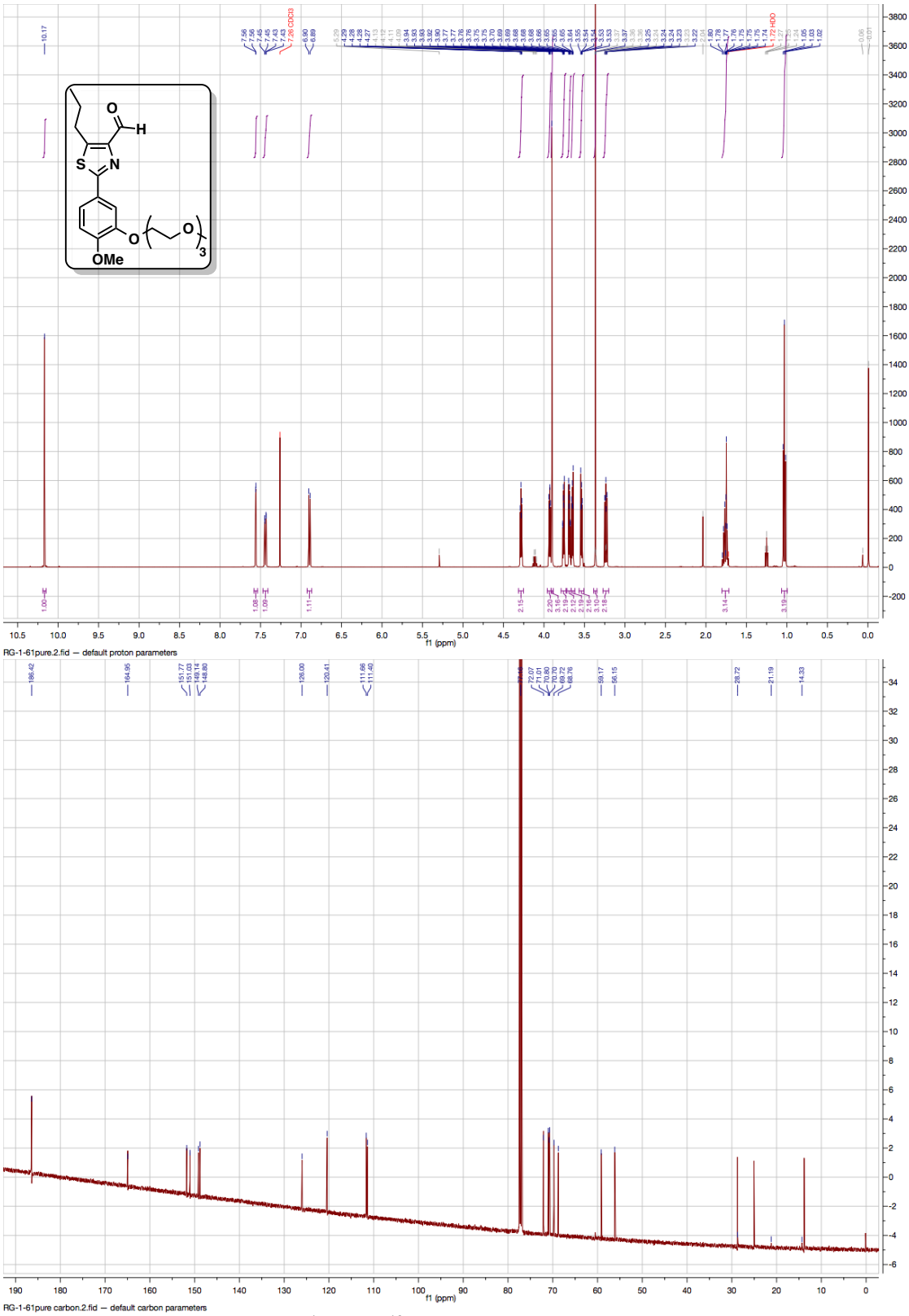

Figure A3.20. *^{1}H and ^{13}C NMR spectra for Compound* ***S22d***.

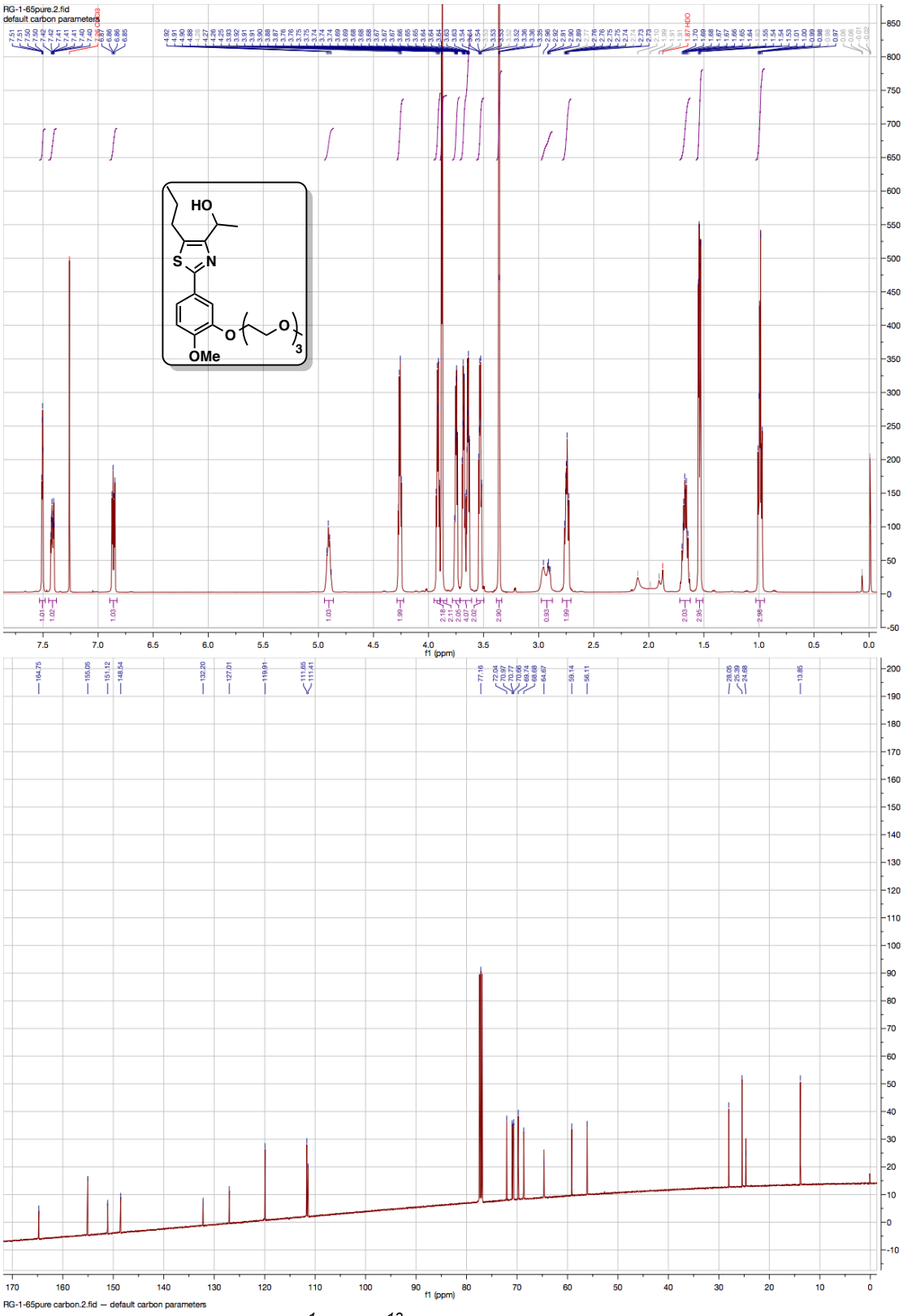

Figure A3.21. *^{1}H and ^{13}C NMR spectra for Compound* ***S22e***.

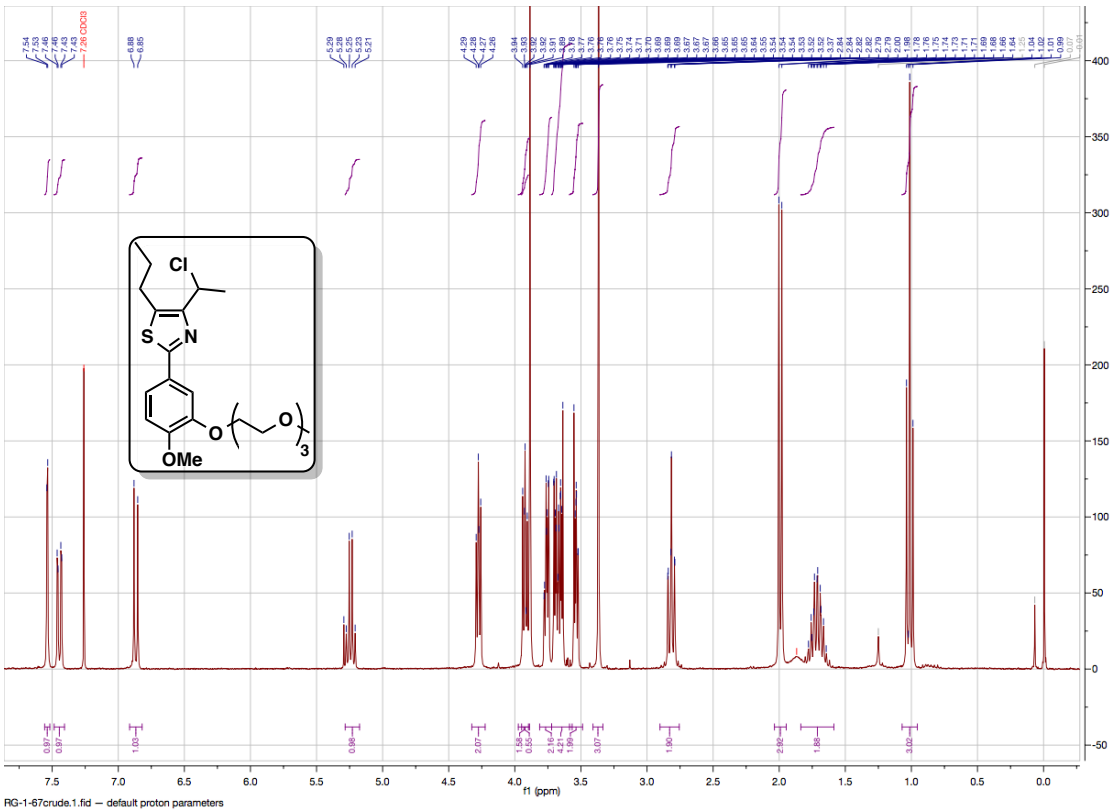

Figure A3.22. *^{1}H NMR spectrum for Compound **S22f**.*

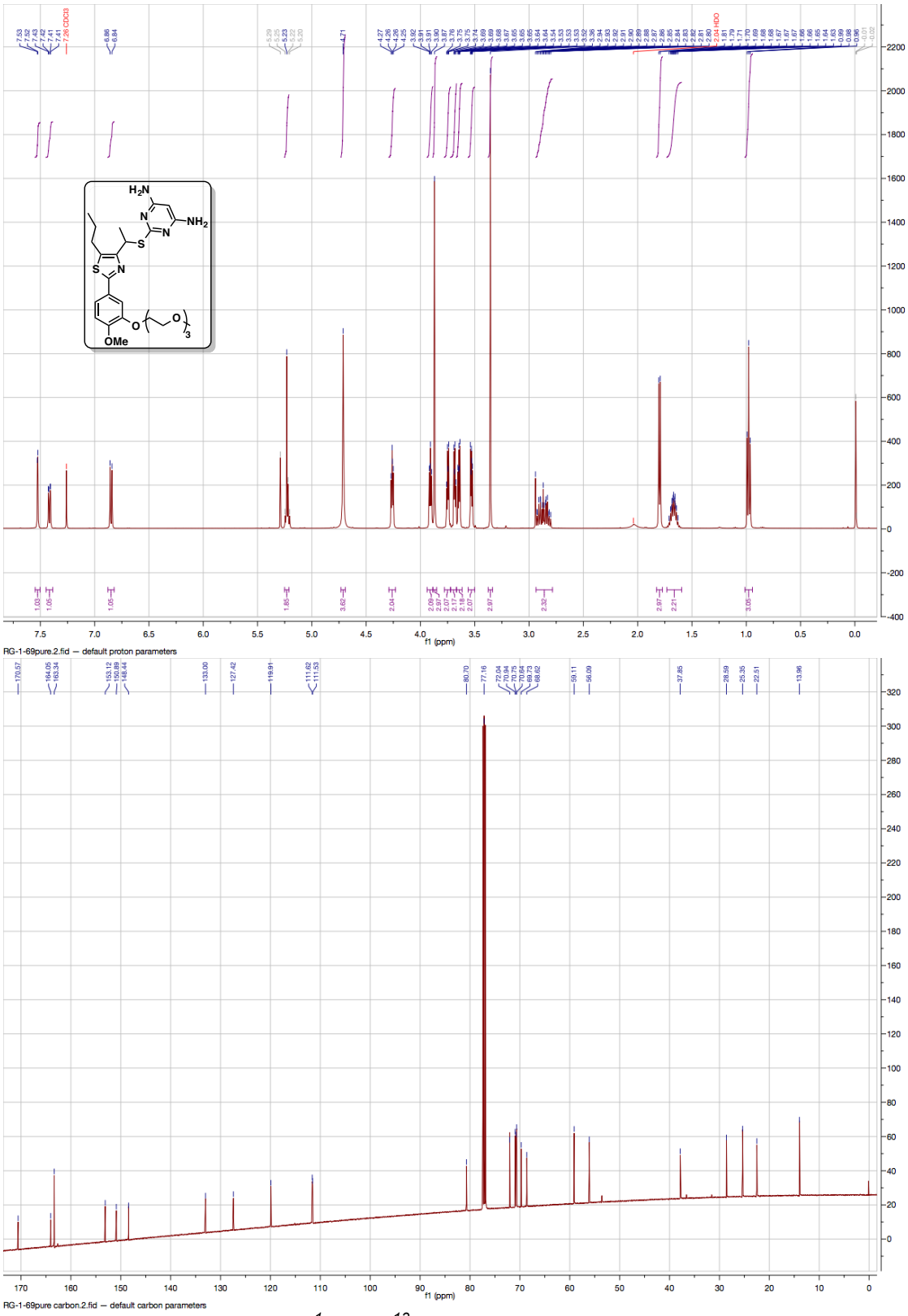

***Figure A3.23**. ^{1}H and ^{13}C NMR spectra for Compound **S22**.*

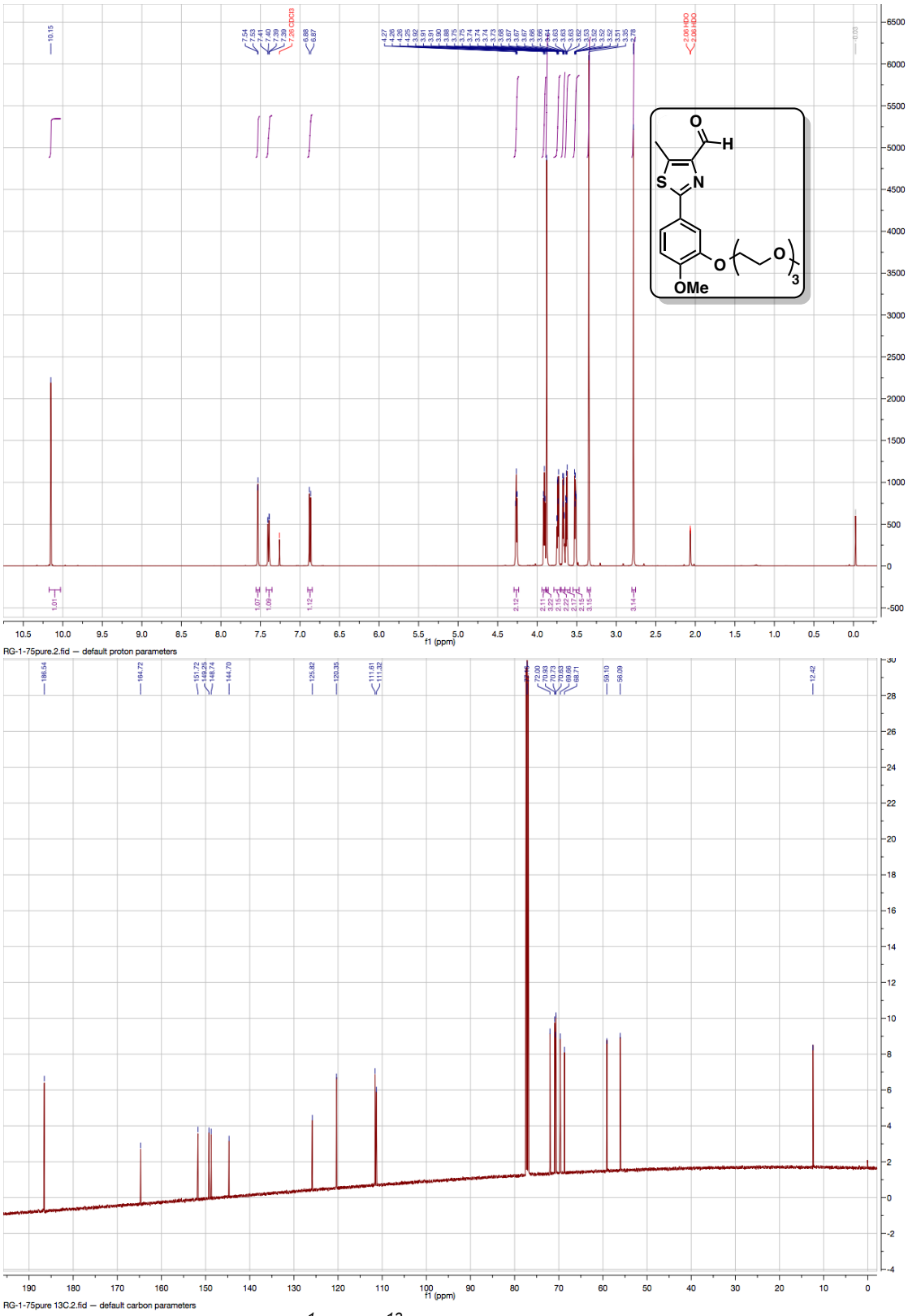

Figure A3.24. *^{1}H and ^{13}C NMR spectra for Compound* ***S23d****.*

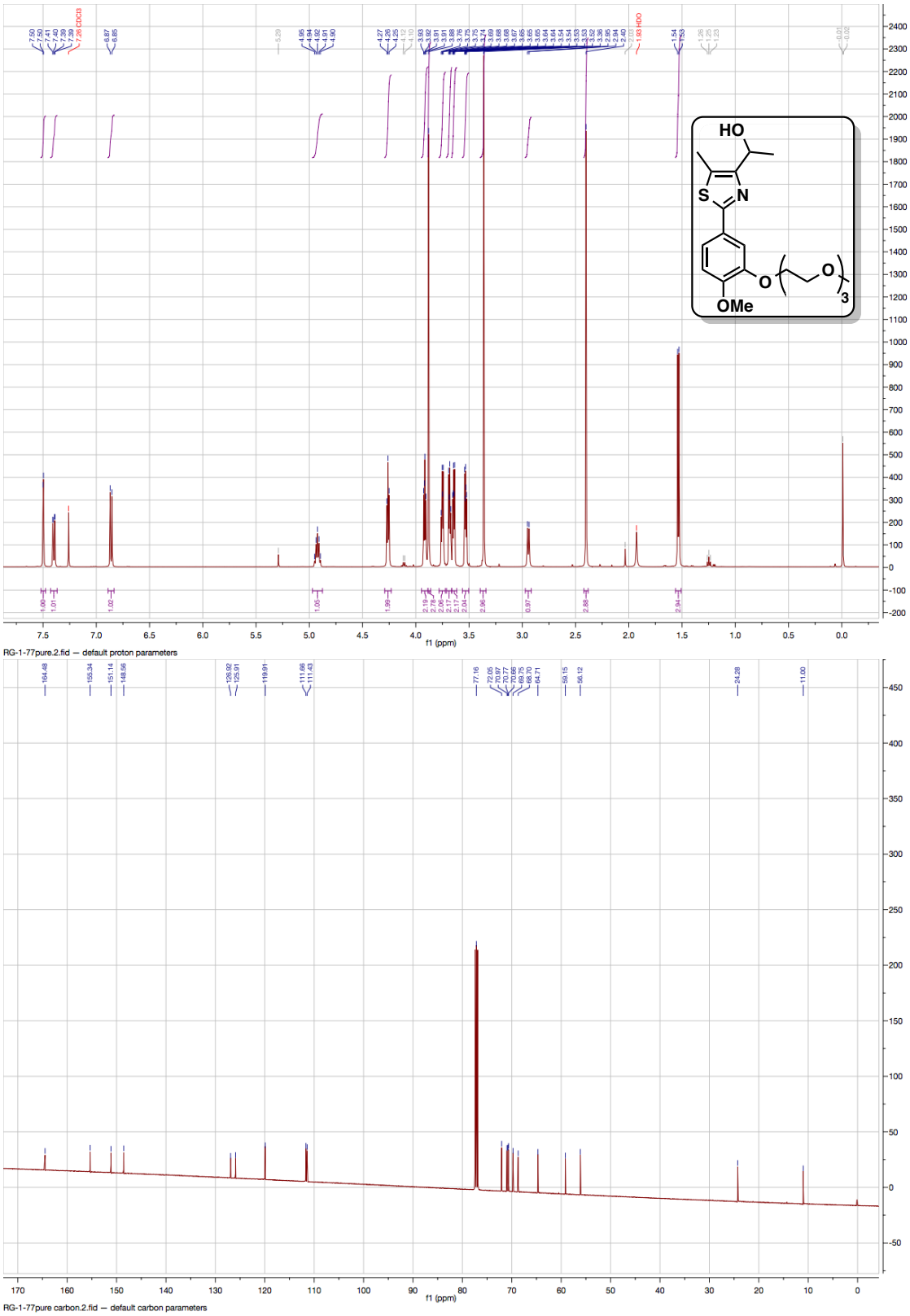

***Figure A3.25**. ^{1}H and ^{13}C NMR spectra for Compound **S23e**.*

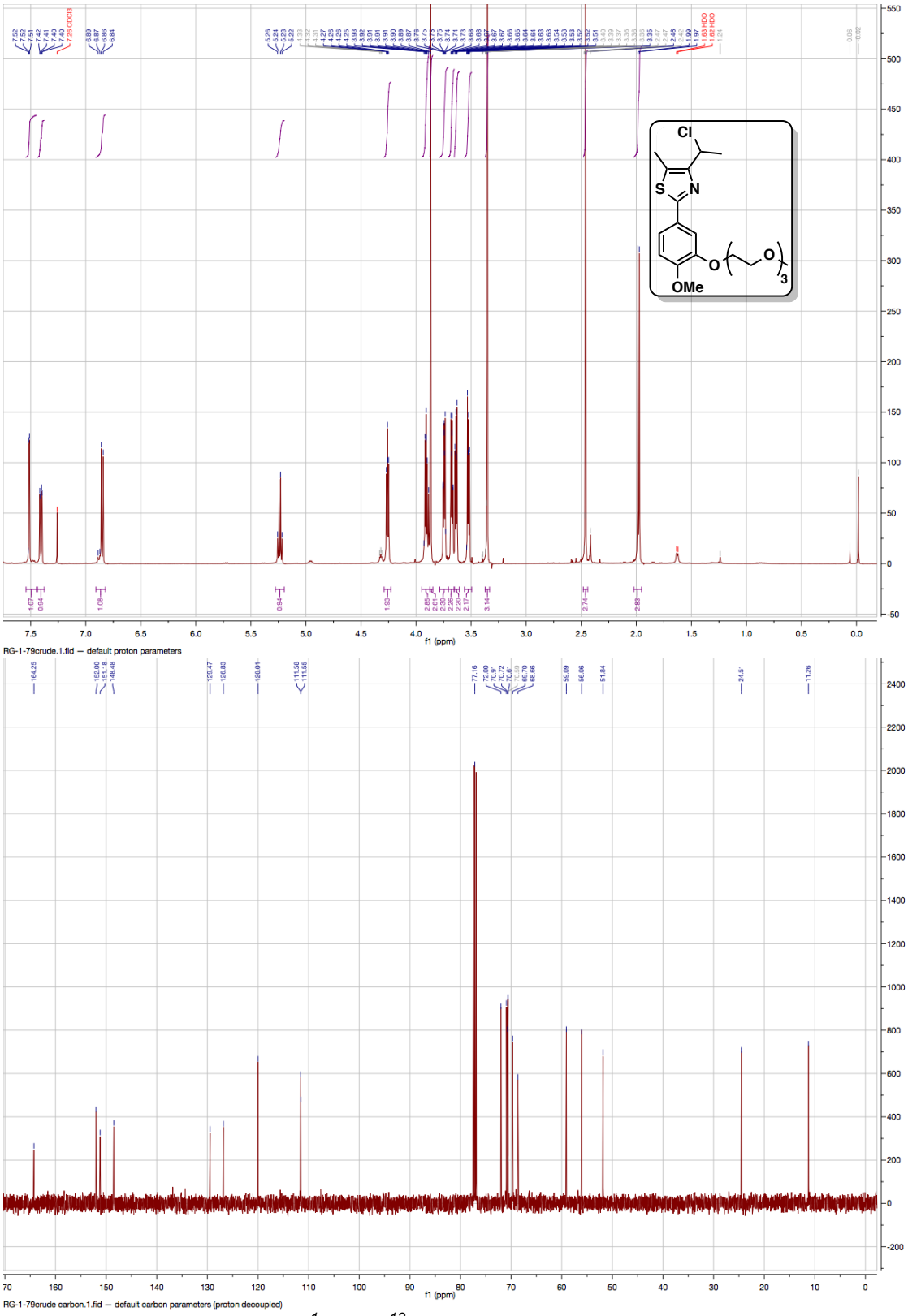

***Figure A3.26**. ^{1}H and ^{13}C NMR spectra for Compound **S23f**.*

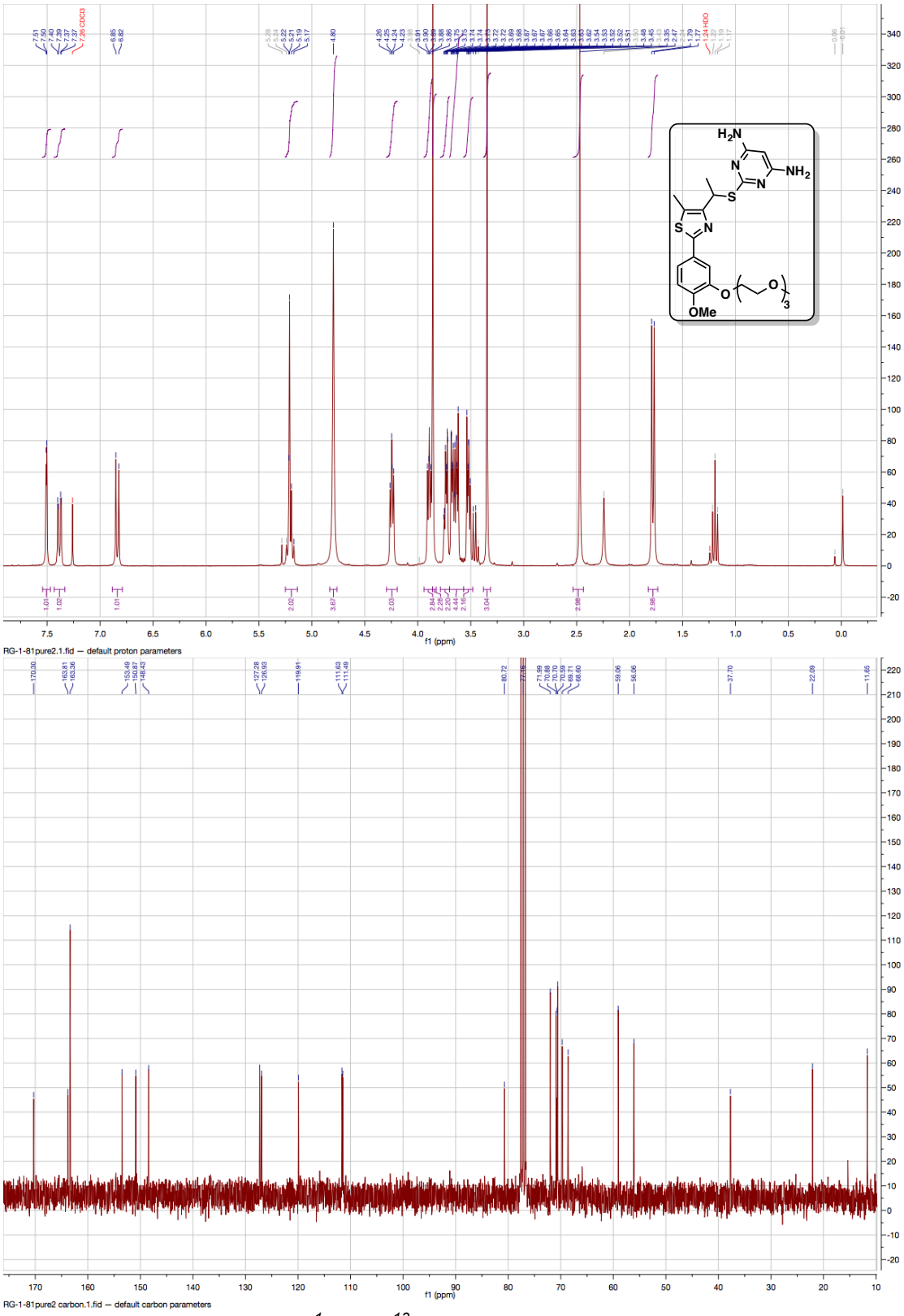

Figure A3.27. *^{1}H and ^{13}C NMR spectra for Compound **S23**.*

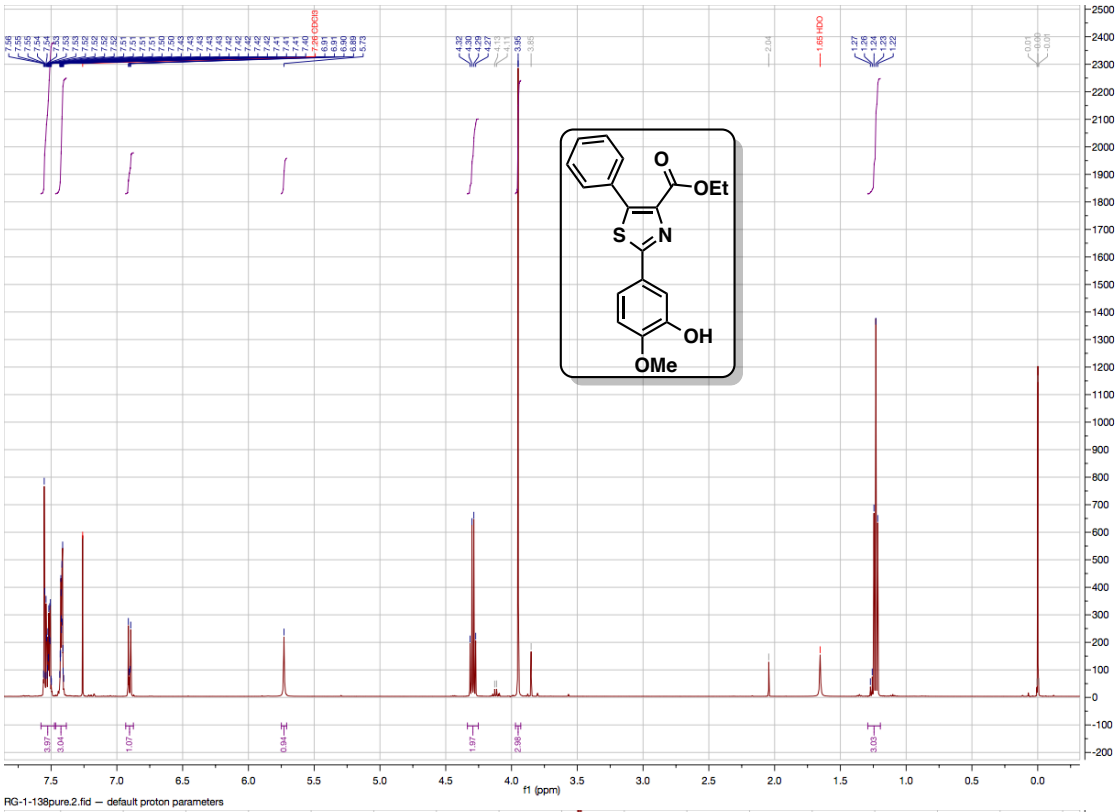

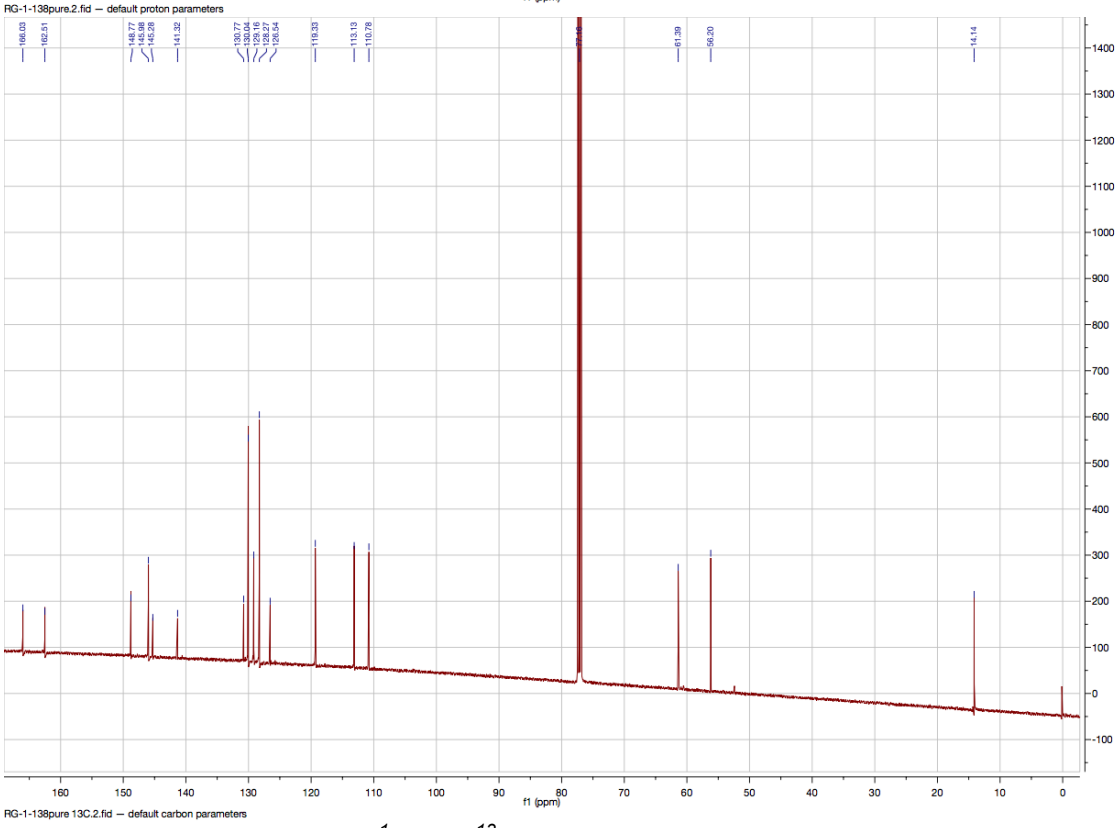

Figure A3.28. *^{1}H and ^{13}C NMR spectra for Compound* ***S28a***.

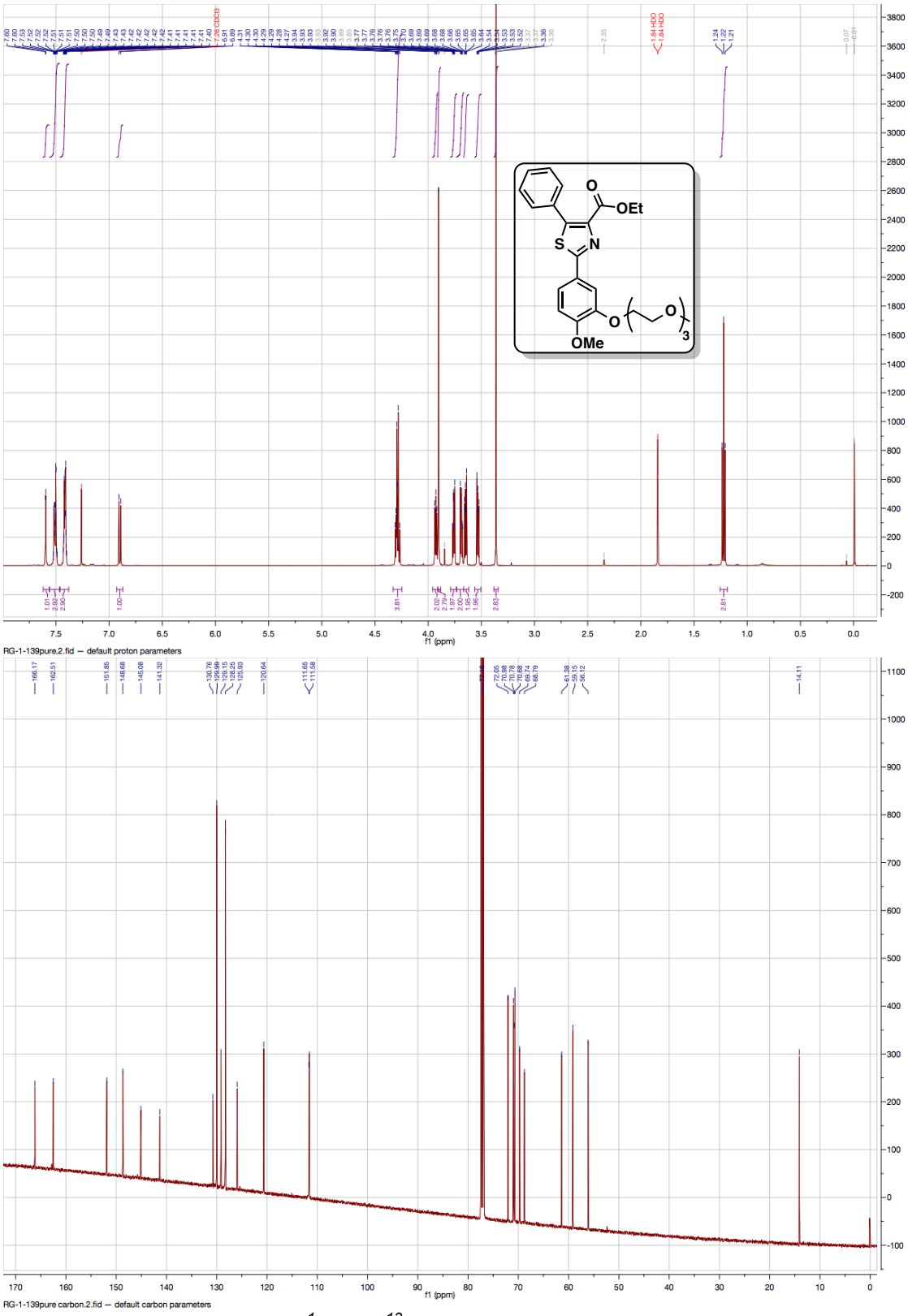

Figure A3.29. *^{1}H and ^{13}C NMR spectra for Compound* ***S28b***.

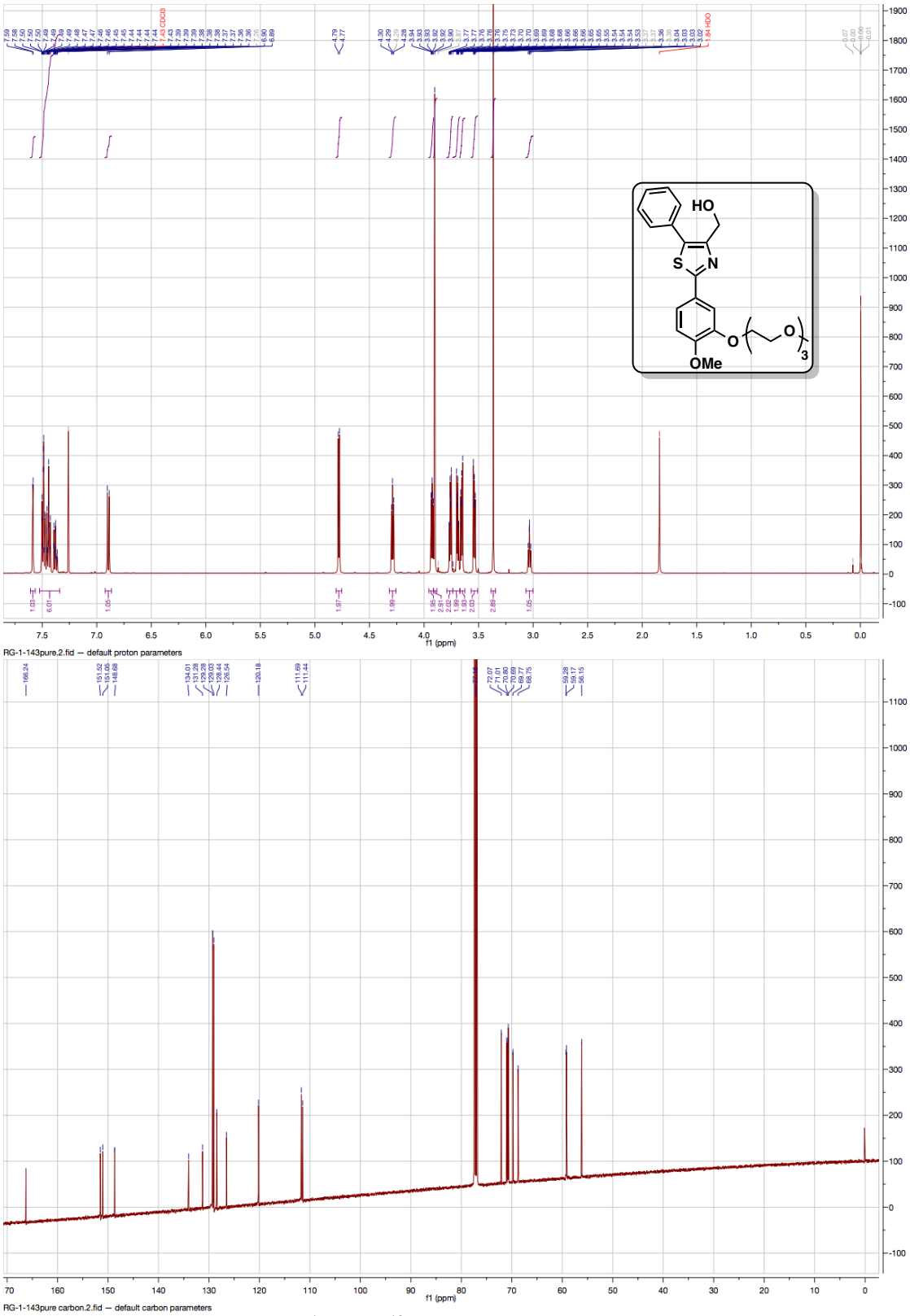

Figure A3.30. *^{1}H and ^{13}C NMR spectra for Compound* ***S28c***.

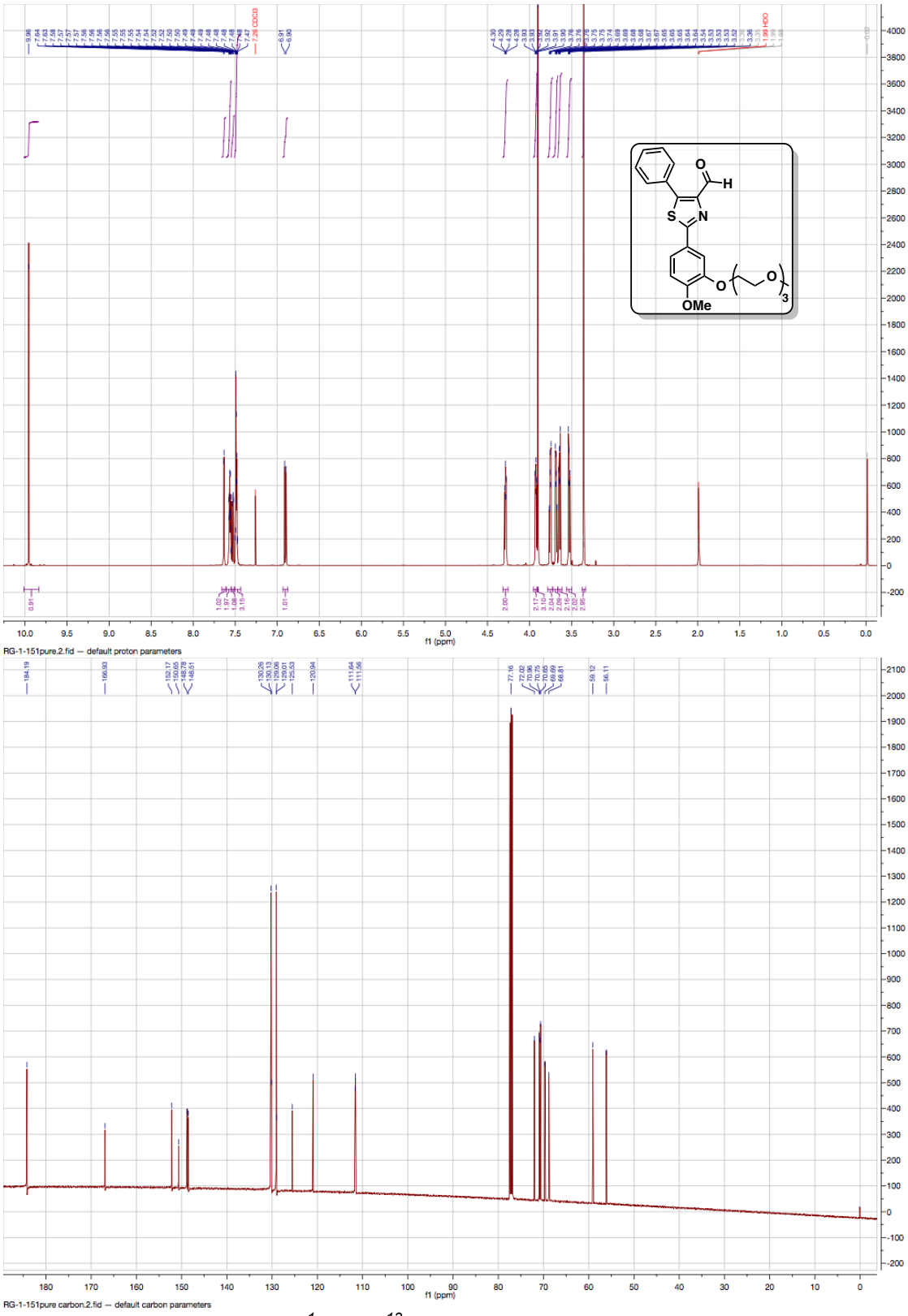

Figure A3.31. *^{1}H and ^{13}C NMR spectra for Compound* ***S28d***.

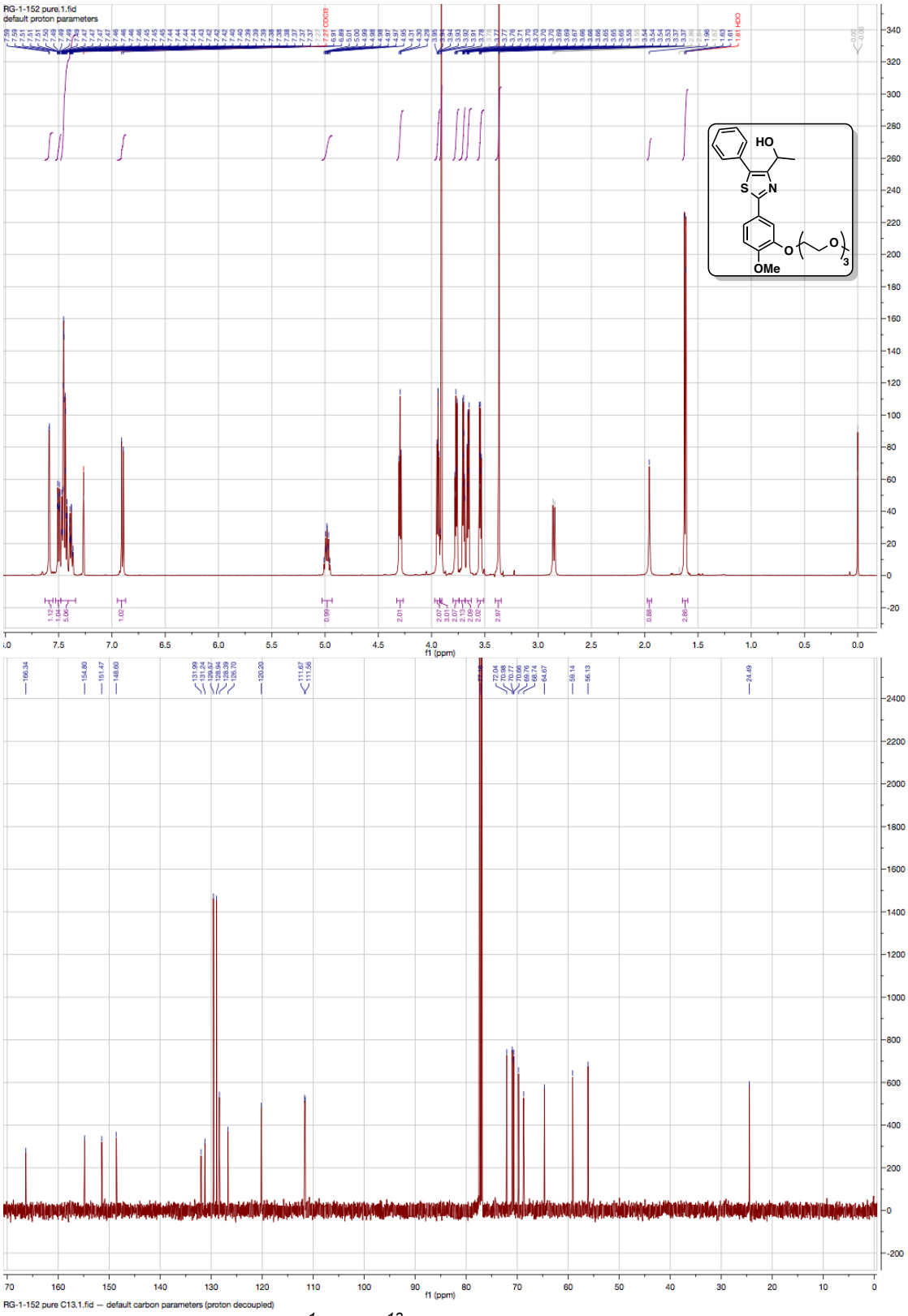

***Figure A3.32**. ^{1}H and ^{13}C NMR spectra for Compound **S28e**.*

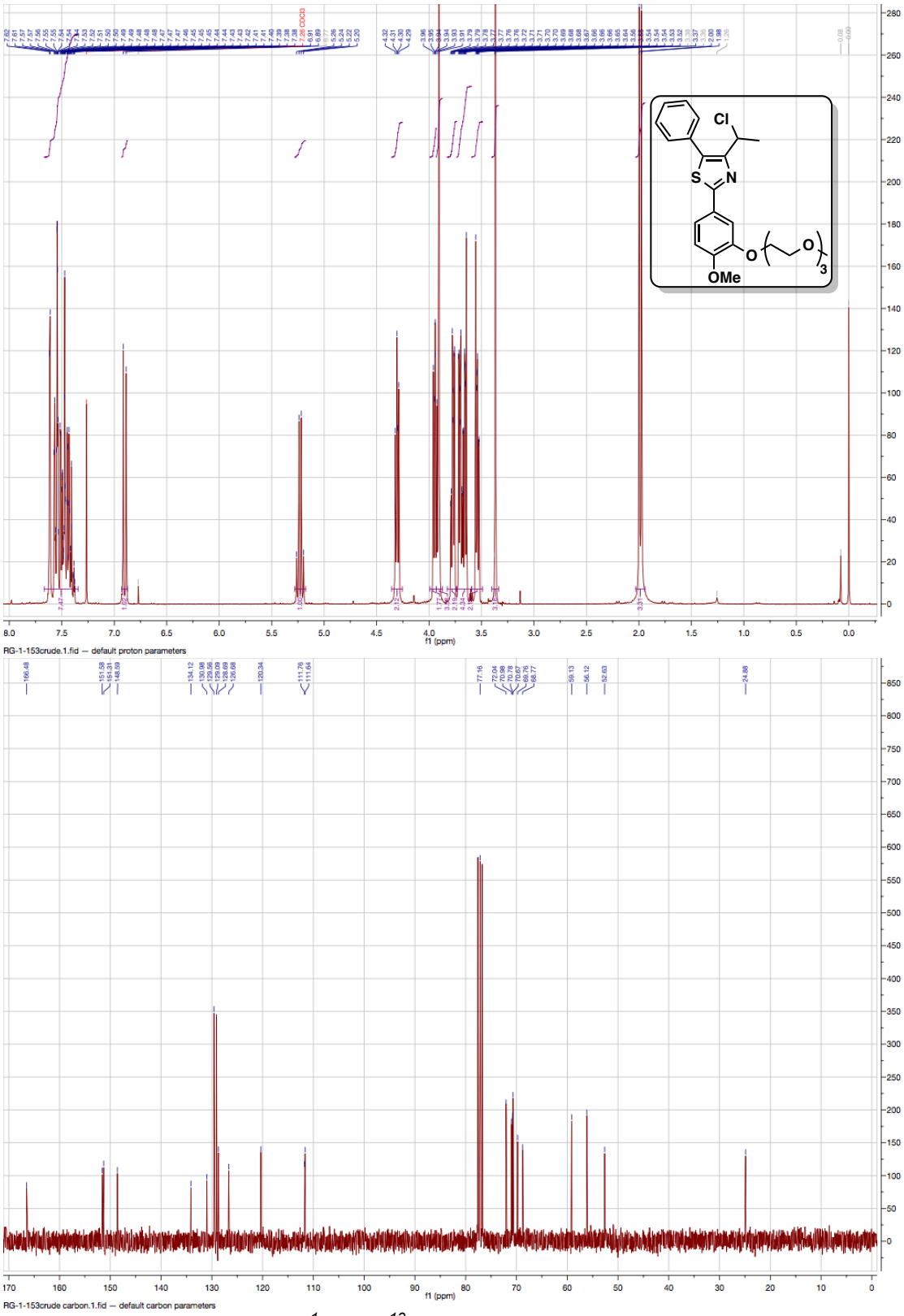

Figure A3.33. *^{1}H and ^{13}C NMR spectra for Compound* ***S28f***.

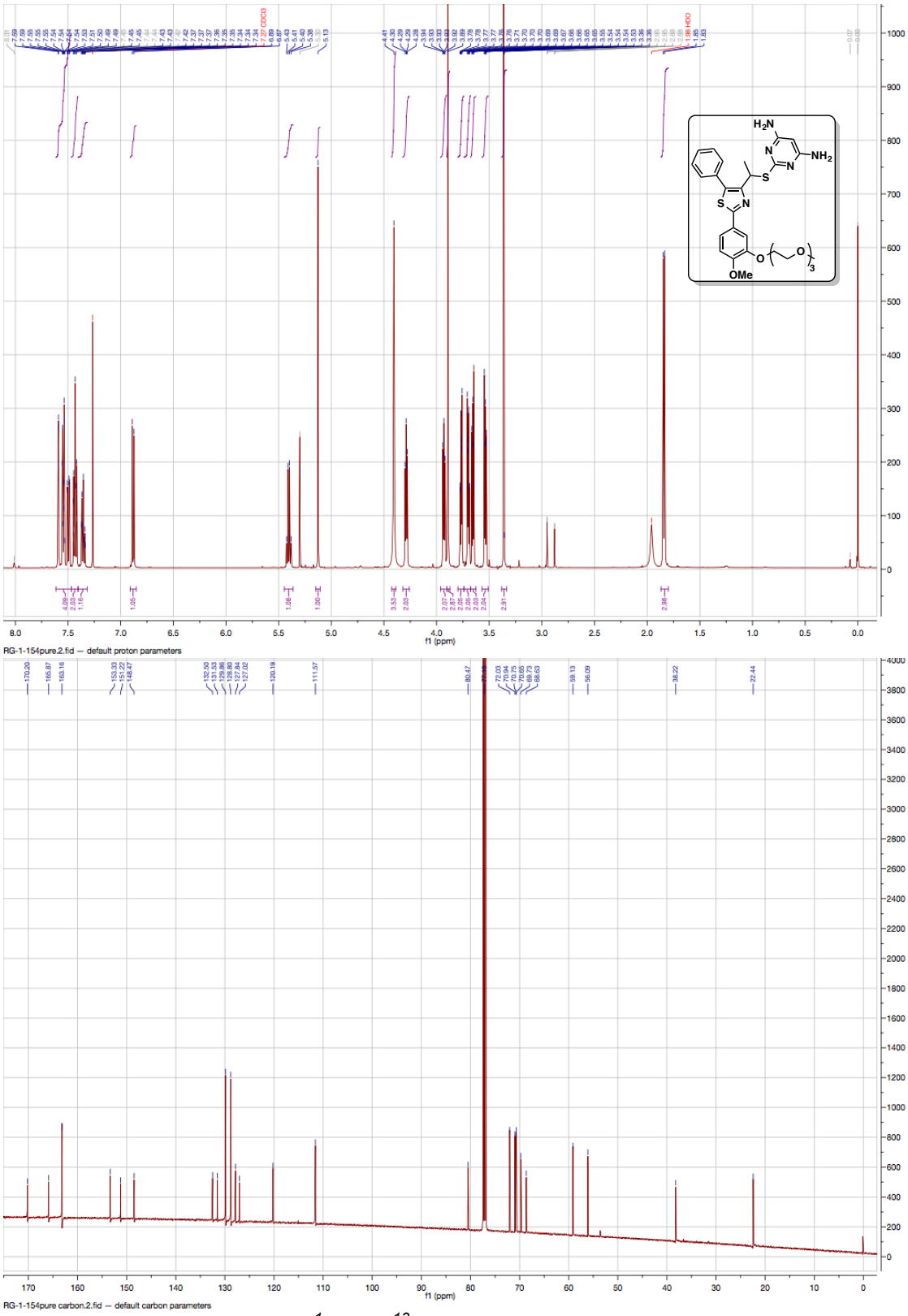

Figure A3.34. *^{1}H and ^{13}C NMR spectra for Compound **S28**.*

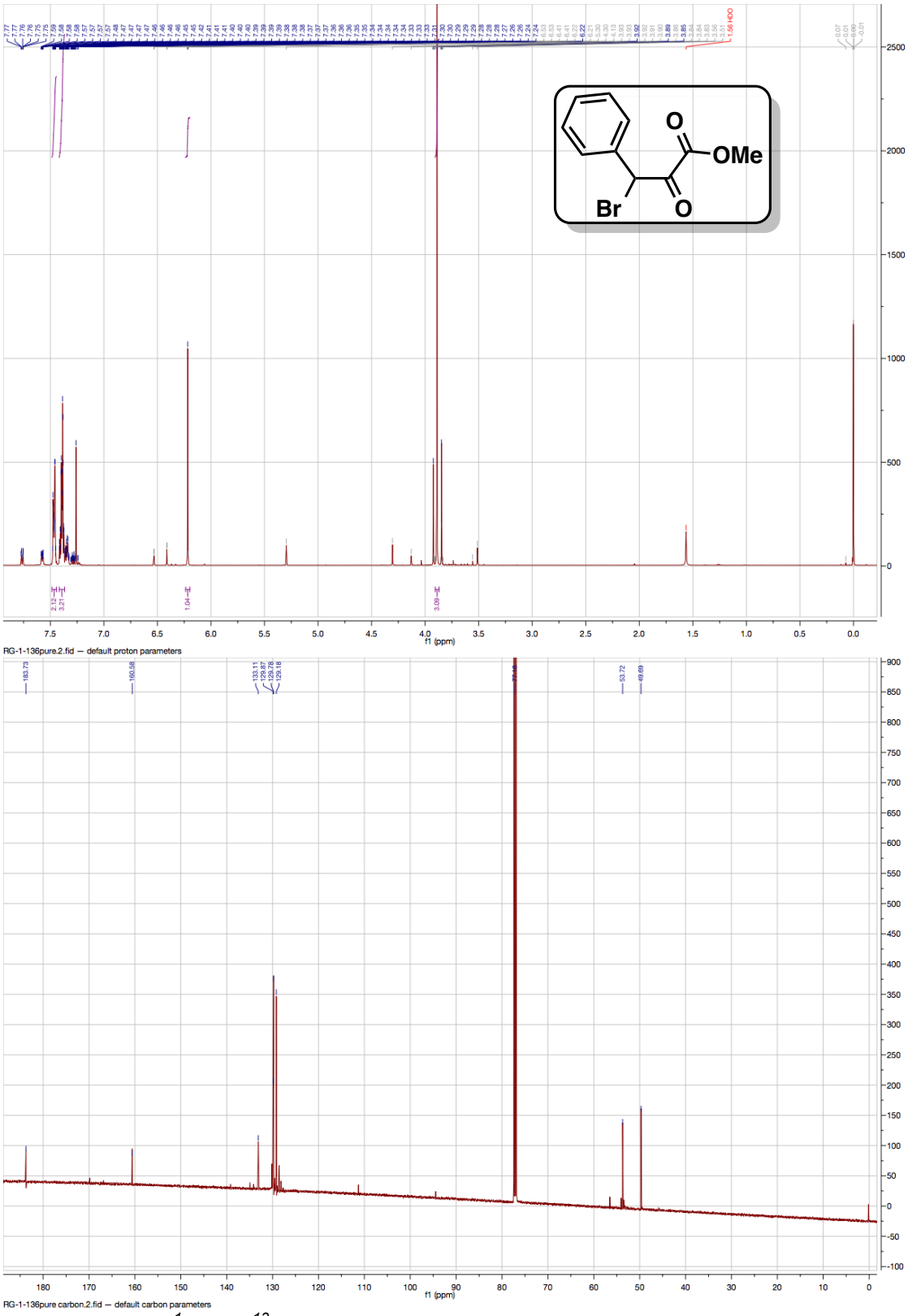

***Figure A3.35**. ^{1}H and ^{13}C NMR spectra for Methyl 3-bromo-2-oxo-3-phenylpropanoate*

Figure A3.36. *^{1}H NMR spectrum for Compound **S23h**.*

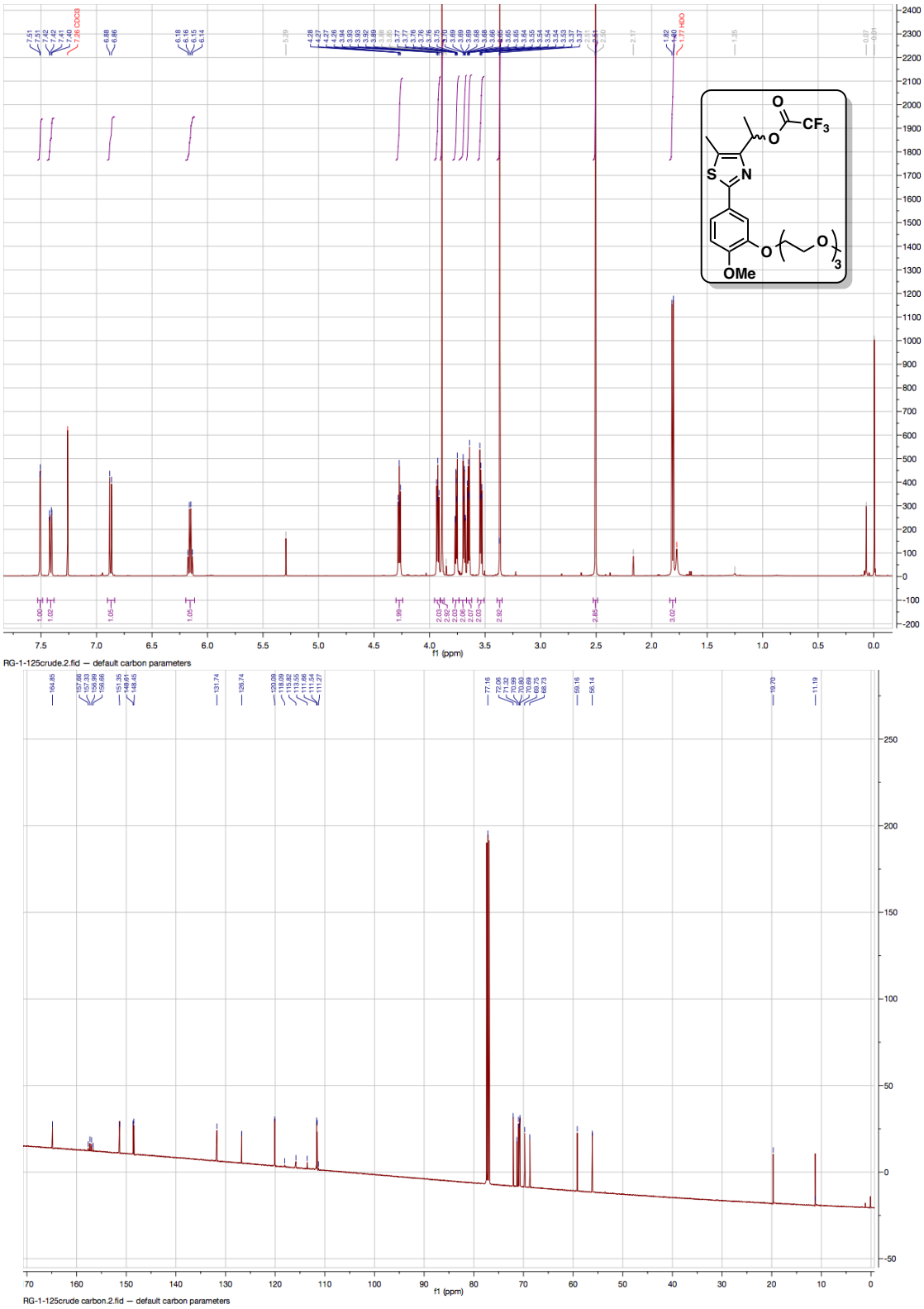

Figure A3.37. *^{1}H and ^{13}C NMR spectra for Compound* ***S23i***.

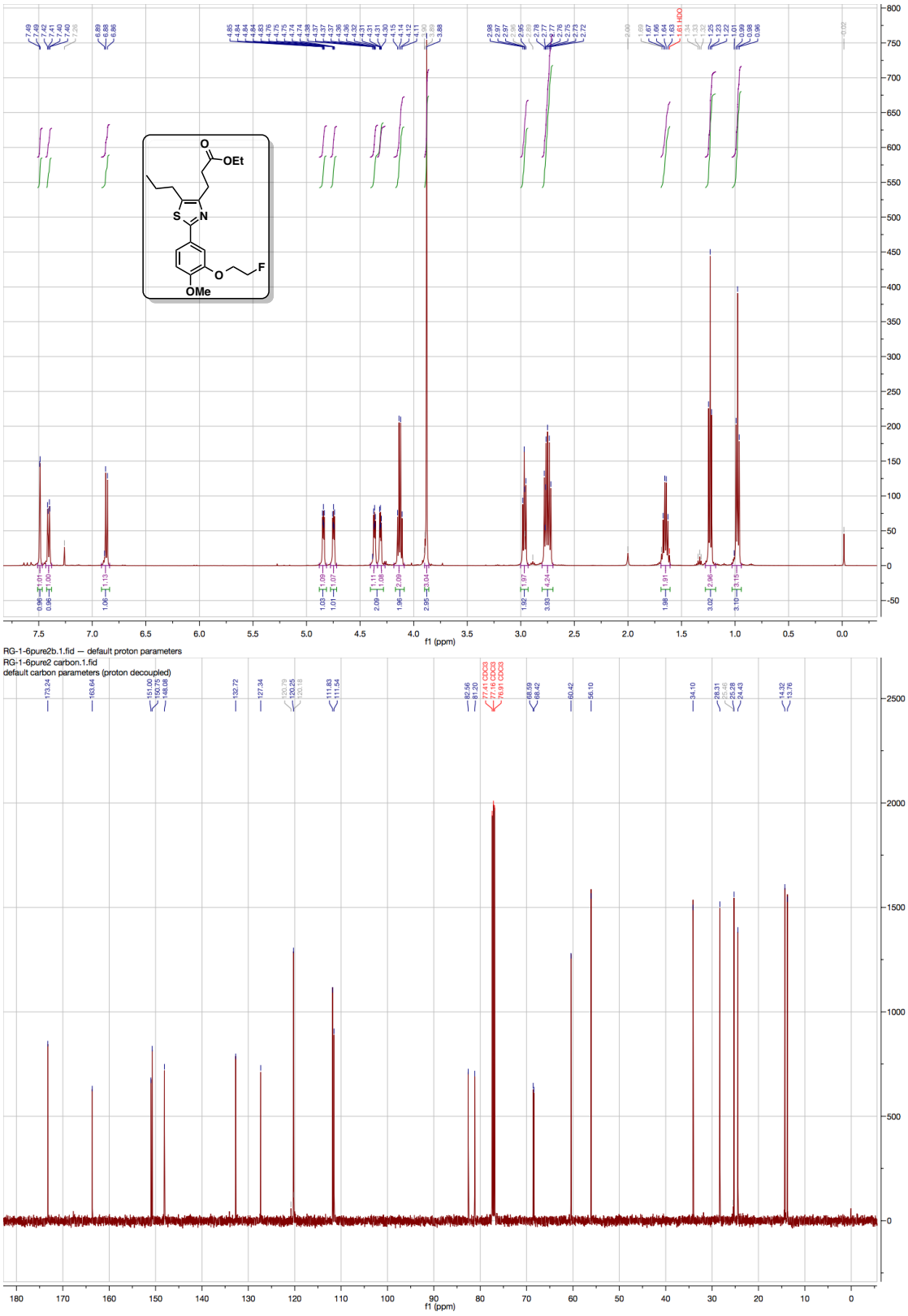

Figure A3.38. *^{1}H and ^{13}C NMR spectra for Compound* ***S15a***.

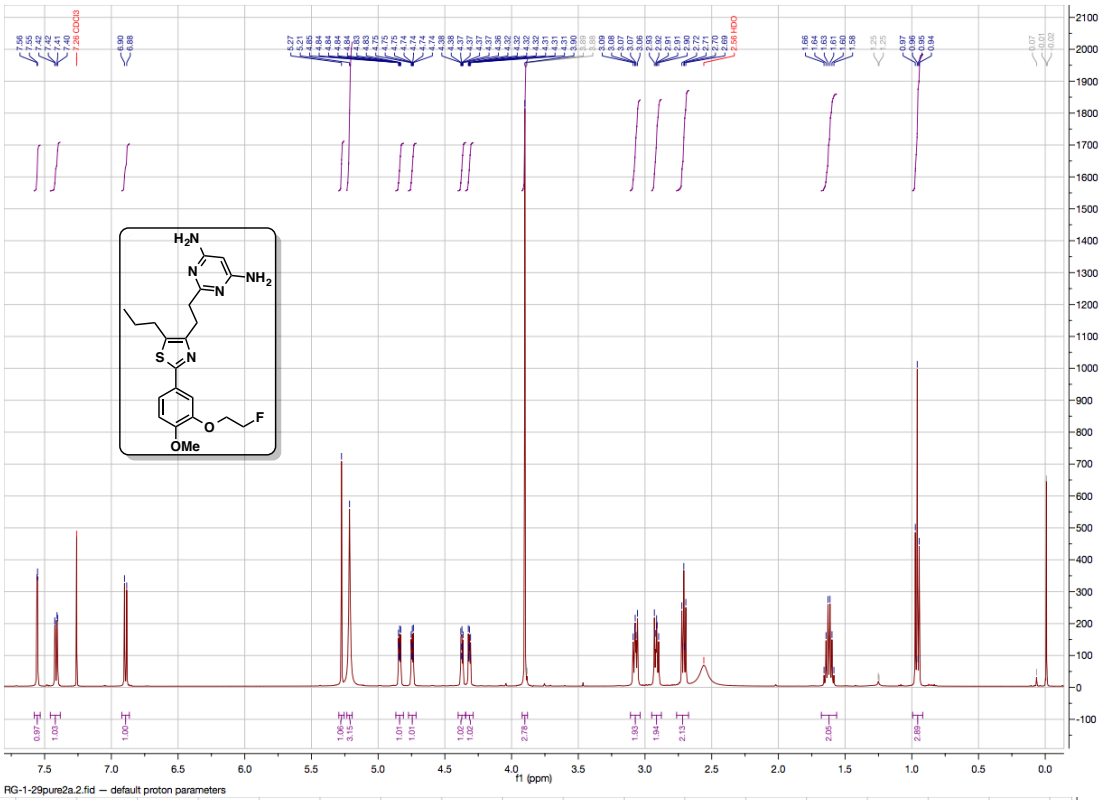

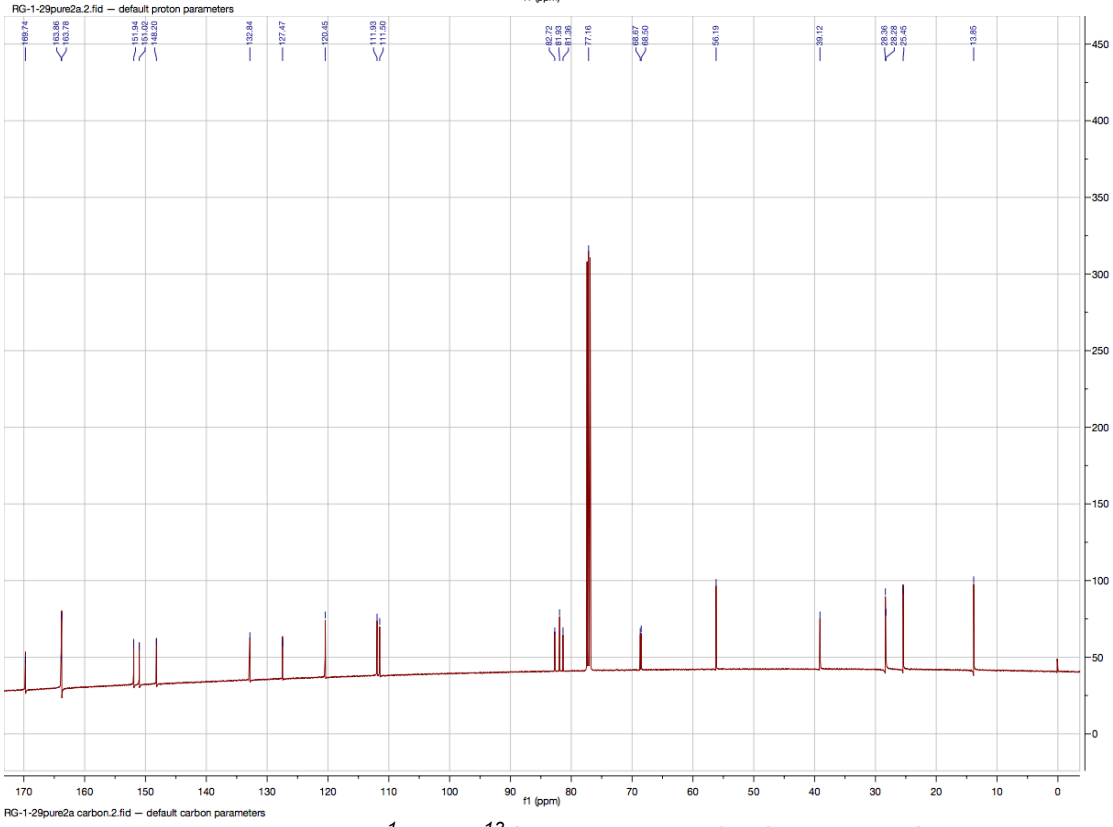

***Figure A3.39**. ^{1}H and ^{13}C NMR spectra for Compound **S15**.*

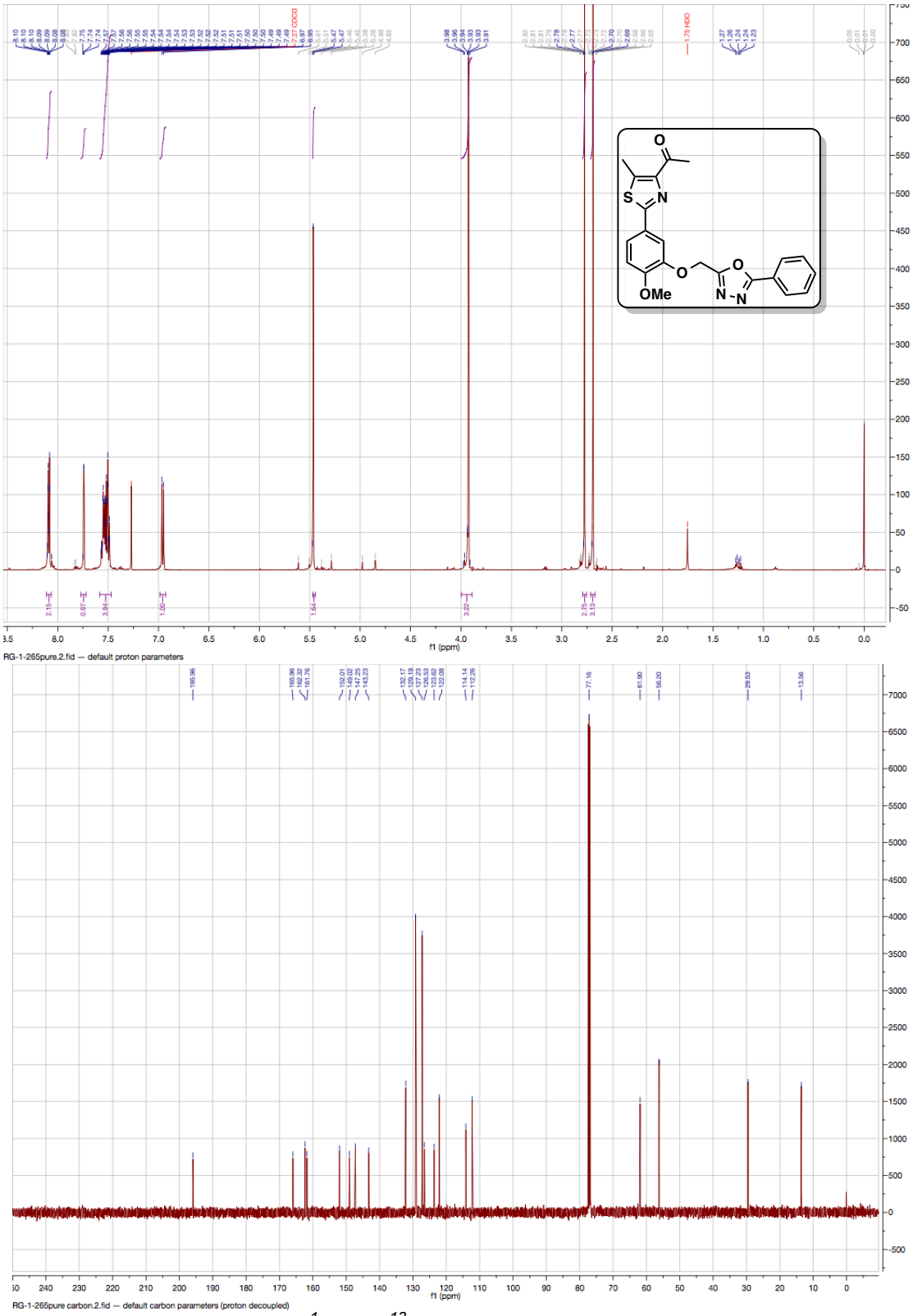

Figure A3.40. *^{1}H and ^{13}C NMR spectra for Compound* ***S32b***.

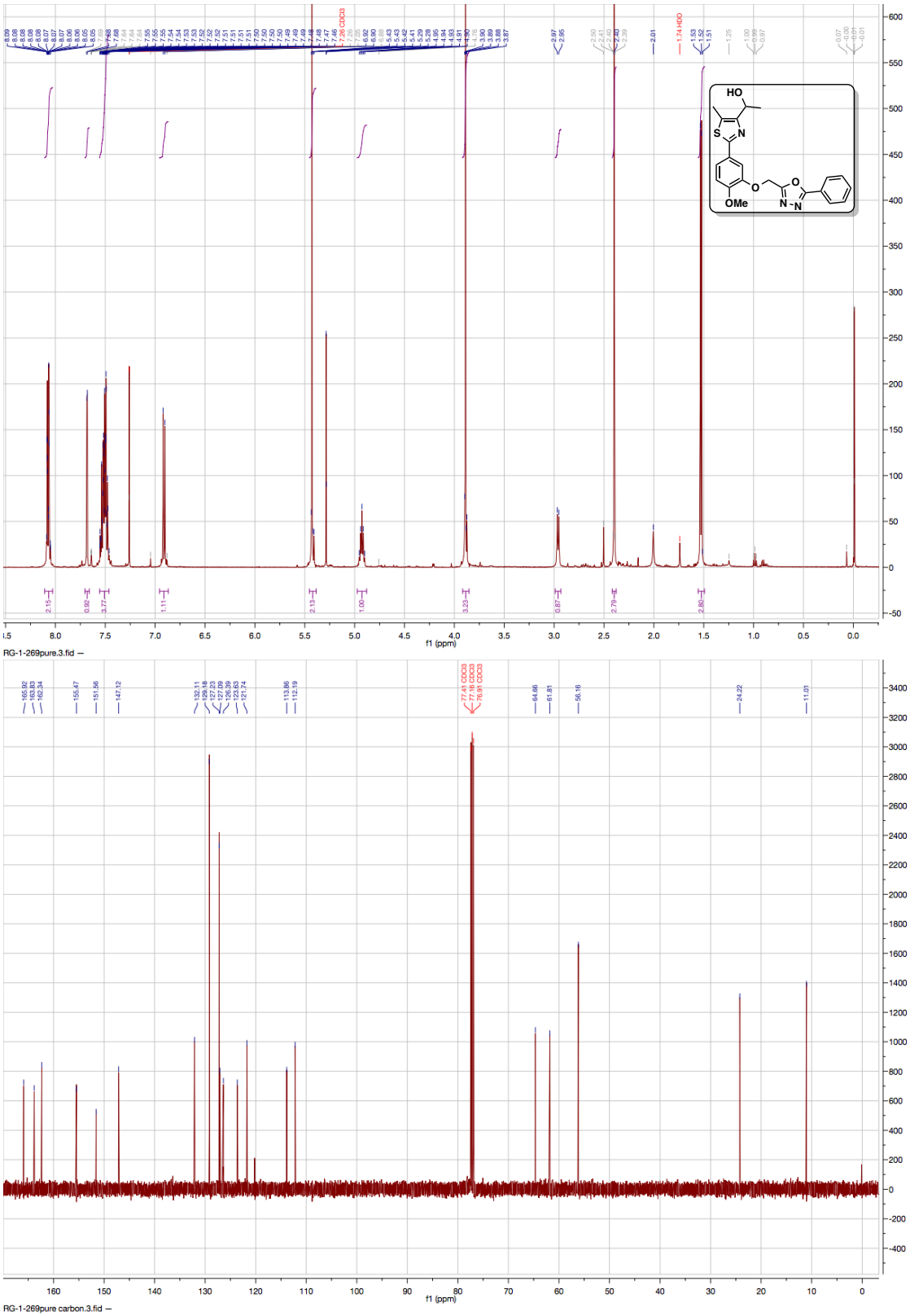

Figure A3.41. *^{1}H and ^{13}C NMR spectra for Compound* ***S32c***.

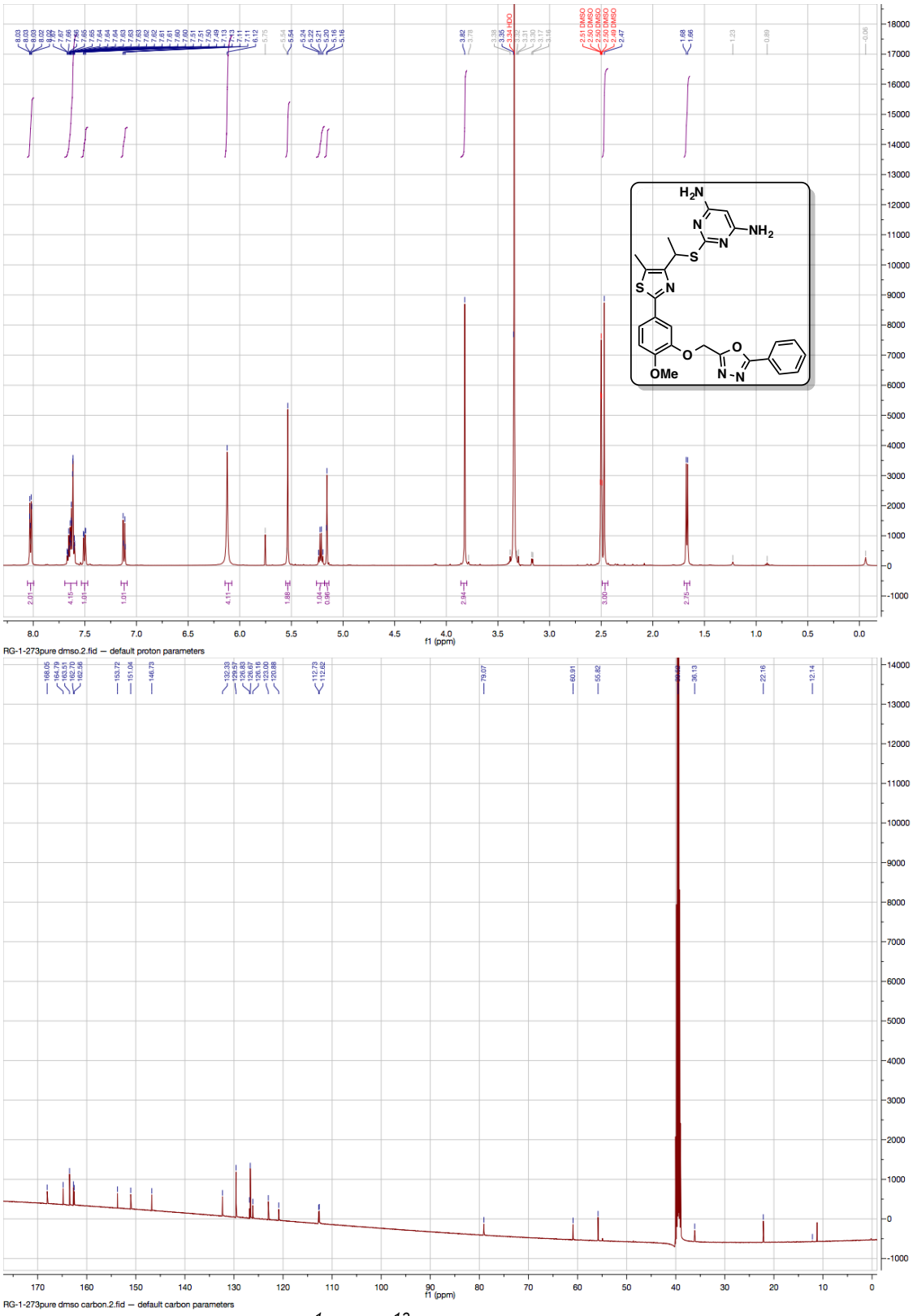

***Figure A3.42**. ^{1}H and ^{13}C NMR spectra for Compound **S32**.*

REFERENCES FOR PART ONE

(1) Eriksson, S.; Munch-Petersen, B.; Johansson, K.; Eklund, H. *Cell. Mol. Life. Sci.* **2002**, *59*, 1327–1346.

(2) Sabini, E.; Ort, S.; Monnerjahn, C.; Konrad, M.; Lavie, A. *Nat. Struct. Biol.* **2003**, *10*, 513–519.

(3) Toy, G.; Austin, W. R.; Liao, H. I.; Cheng, D. H.; Singh, A.; Campbell, D. O.; Ishikawa, T. O.; Lehmann, L. W.; Satyamurthy, N.; Phelps, M. E.; Herschman, H. R.; Czernin, J.; Witte, O. N.; Radu, C. G. *P. Natl. Acad. Sci. USA* **2010**, *107*, 5551–5556.

(4) Austin, W. R.; Armijo, A. L.; Campbell, D. O.; Singh, A. S.; Hsieh, T.; Nathanson, D.; Herschman, H. R.; Phelps, M. E.; Witte, O. N.; Czernin, J.; Radu, C. G. *J. Exp. Med.* **2012**, *209*, 2215–2228.

(5) Choi, O.; Heathcote, D. A.; Ho, K. K.; Muller, P. J.; Ghani, H.; Lam, E. W. F.; Ashton-Rickardt, P. G.; Rutschmann, S. *J. Immunol.* **2012**, *188*, 3920–3927.

(6) Yang, C. Y.; Lee, M.; Hao, J. W.; Cui, X. L.; Guo, X. J.; Smal, C.; Bontemps, F.; Ma, S. M.; Liu, X. D.; Engler, D.; Parker, W. B.; Xu, B. *Nucleic Acids Res.* **2012**, *40*, 9621–9632.

(7) Nathanson, D. A.; Armijo, A. L.; Tom, M.; Li, Z.; Dimitrova, E.; Austin, W. R.; Nomme, J.; Campbell, D. O.; Ta, L.; Le, T. M.; Lee, J. T.; Darvish, R.; Gordin, A.; Wei, L.; Liao, H. I.; Wilks, M.; Martin, C.; Sadeghi, S.; Murphy, J. M.; Boulos, N.; Phelps, M. E.; Faull, K. F.; Herschman, H. R.; Jung, M. E.; Czernin, J.; Lavie, A.; Radu, C. G. *J. Exp. Med.* **2014**, *211*, 473–486.

(8) Murphy, J. M.; Armijo, A. L.; Nomme, J.; Lee, C. H.; Smith, Q. A.; Li, Z.; Campbell, D. O.; Liao, H. I.; Nathanson, D. A.; Austin, W. R.; Lee, J. T.; Darvish, R.; Wei, L.; Wang, J.; Su, Y.; Damoiseaux, R.; Sadeghi, S.; Phelps, M. E.; Herschman, H. R.; Czernin, J.; Alexandrova, A. N.; Jung, M. E.; Lavie, A.; Radu, C. G. *J. Med. Chem.* **2013**, *56*, 6696–6708.

(9) Nomme, J.; Murphy, J. M.; Su, Y.; Sansone, N. D.; Armijo, A. L.; Olson, S. T.; Radu, C.; Lavie, A. *Acta. Crystallogr. D* **2014**, *70*, 68–78.

(10) Godsey, M. H.; Ort, S.; Sabini, E.; Konrad, M.; Lavie, A. *Biochemistry-Us* **2006**, *45*, 452–461.

(11) Sabini, E.; Hazra, S.; Ort, S.; Konrad, M.; Lavie, A. *J. Mol. Biol.* **2008**, *378*, 607–621.

(12) Shu, Y. Z.; Johnson, B. M.; Yang, T. J. *AAPS J.* **2008**, *10*, 178–192.

(13) Mikhailovskii, D. I.; Mikhailovskaya, V. N. *Izv. Vuz. Khim. Kh. Tekh.* **1987**, *30*, 29–31.

(14) Gudipati, V.; Curran, D. P.; Wilcox, C. S. *J. Org. Chem.* **2006**, *71*, 3599–3607.

(15) Jorgensen, W. L.; Chandrasekhar, J.; Madura, J. D.; Impey, R. W.; Klein, M. L. *J. Chem. Phys.* **1983**, *79*, 926–935.

(16) Jorgensen, W. L.; Maxwell, D. S.; TiradoRives, J. *J. Am. Chem. Soc.* **1996**, *118*, 11225–11236.

(17) Jorgensen, W. L.; Tirado-Rives, J. *J. Comput. Chem.* **2005**, *26*, 1689–1700.

(18) Jorgensen, W. L.; Ulmschneider, J. P.; Tirado-Rives, J. *J. Phys. Chem. B.* **2004**, *108*, 16264–16270.

(19) Repasky, M. P.; Chandrasekhar, J.; Jorgensen, W. L. *J. Comput. Chem.* **2002**, *23*, 1601–1622.

(20) Still, W. C.; Tempczyk, A.; Hawley, R. C.; Hendrickson, T. *J. Am. Chem. Soc.* **1990**, *112*, 6127–6129.

(21) Pridmore, S. J. W., J. M. *Tetrahedron Lett* **2008**, *49*, 7413–7415.

(22) Schirok, H. M.; Stasch, J. P.; Wunder, F. *PCT Int. Appl. Bayer Healthcare AG: Germany* **2008**, *WO 2008061657*, 59.

(23) Alajarin, M. C., J.; Pastor, A.; Sanchez-Andrada, P.; Bautista, D. *J. Org. Chem.* **2006**, *71*, 5328–5339.

(24) Walter, M. V. C., Y.; Isensee, K.; Sandler, K.; Stark, H.; Ligneau, X.; Camelin, J.-C.; Schwartz, J.-C. *Bioorg. Med. Chem. Lett.* **2010**, *20*, 5879–5882.

(25) Tamiaki, H. M., S.; Mizutani, K. *J. Org. Chem.* **2012**, *77*, 4751–4758.

(26) Sabini, E.; Hazra, S.; Konrad, M.; Lavie, A. *J. Med. Chem.* **2007**, *50*, 3004–3014.

(27) Agarwal, K. C.; Miech, R. P.; Parks, R. E., Jr. *Methods Enzymol.* **1978**, *51*, 483–490.

(28) Bourne, D. W. A. *Comput. Meth. Prog. Bio.* **1986**, *23*, 277–281.

(29) Bourne, D. W. *Comput. Methods Programs Biomed.* **1989**, *29*, 191–195.

(30) Kabsch, W. *Acta. Crystallogr. D* **2010**, *66*, 125–132.

(31) Vagin, A.; Teplyakov, A. *Acta. Crystallogr. D* **2010**, *66*, 22–25.

(32) Murshudov, G. N.; Skubak, P.; Lebedev, A. A.; Pannu, N. S.; Steiner, R. A.; Nicholls, R. A.; Winn, M. D.; Long, F.; Vagin, A. A. *Acta Crystallogr. D* **2011**, *67*, 355–367.

(33) Emsley, P.; Lohkamp, B.; Scott, W. G.; Cowtan, K. *Acta Crystallogr. D* **2010**, *66*, 486–501.

(34) Schuttelkopf, A. W.; van Aalten, D. M. F. *Acta Crystallogr. D* **2004**, *60*, 1355–1363.

(35) Repasky, M. P.; Chandrasekhar, J.; Jorgensen, W. L. *J. Comput. Chem.* **2002**, *23*, 498–510.

PART TWO

Synthesis of Ferrocene-Containing Monomers and Biodegradable Polymers

Adapted from: Brianna M. Upton, Raymond M. Gipson, Selma Duhović, Brian R. Lydon, Nicholas M. Matsumoto, Heather D. Maynard and Paula L. Diaconescu

Inorg. Chem. Front. **2014**, *1*, 271–277.

CHAPTER 1: INTRODUCTION

1.1 Background

Ferrocene's discovery in 1951 captured the attention of many chemists,[1] and to this day ferrocene continues to be the subject of extensive scientific research. Ferrocene's unique properties have resulted in its incorporation into polymers, nanotubes, molecular machines, multimetallic complexes, olefin polymerization catalysts, and ligands for metal catalysis.[2-5] In addition, ferrocene has been utilized for numerous biological applications. For example, ferrocene can be found in anticancer and antimalarial agents such as ferrocifin[6-8] and ferroquine (Figure 1).[9] Ferrocene-containing polymers have been researched extensively, but ferrocene-derivatized biodegradable polymers have received far less focus.[2-5]

Figure 1. A few biologically active substrates containing ferrocene.

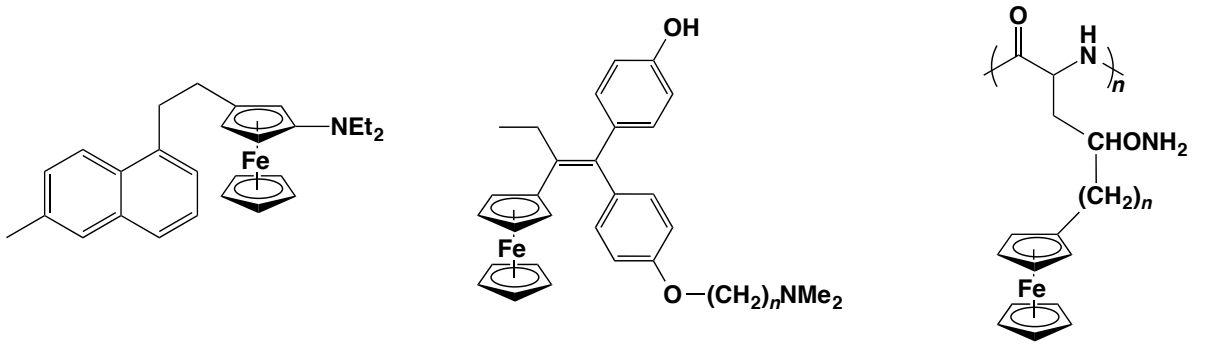

Ferroquine
Malaria

Ferrocene Derivatized Tamoxifen
Breast cancer

Polyaspartamide
Bioactive Copolymer

Because of the biological properties attributed to ferrocene, ferrocene-containing polymers have great potential for use in medicinal chemistry. Ferrocene's redox activity, also known as Fenton reactivity, is related to the biological properties of ferrocene-containing compounds.[10-14] Ferrocene can become oxidized to the ferrocenium radical cation. In turn, the ferrocenium radical can generate both superoxides and hydroxyl radicals (Figure 2).[15] The incorporation of functional groups on ferrocene can allow for additional mechanisms for biological activity.

Figure 2. The Fenton reactivity of Ferrocene. Ferrocene can generate hydroxyl radicals in a mechanism involving a ferrocenium intermediate.

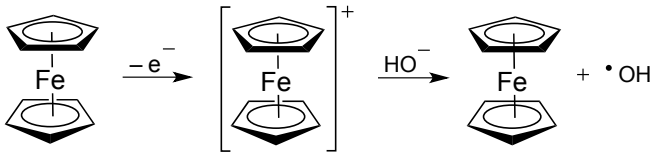

The presence of alcohol or thiol appendages on ferrocene substrates permits reactions with free radicals.[16-18] Ferrocene analogues bearing alcohol functionalities (Figure 3) can also become oxidized during metabolism. The oxidized intermediates can proceed to transform organic appendages into electrophilic *o*-quinones, quinone methides, or carbocations that proceed to damage DNA, GSH, or proteins.[14] Thiols are also active in the quenching of free radicals (Figure 4). Compounds displaying these properties are of interest because current radioprotectors such as Amifostine (Figure 4) are associated with acute and chronic side effects.[19,20] In fact, many small molecule drugs have limitations, and this makes the discovery of improved drugs a necessity.

Figure 3. Hydroxyferrocene redox chemistry

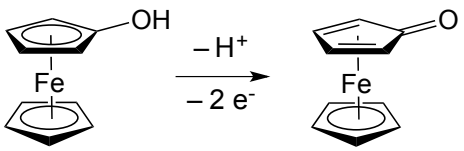

Figure 4. Sulfur-containing free-radical scavengers for use in radiation therapy.

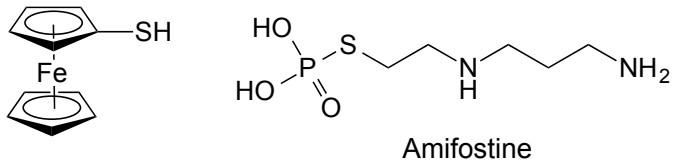

Amifostine

Functionalized biodegradable polymers have been employed in biological studies, but the controlled synthesis of these polymers is challenging. One synthetic approach towards a bioactive ferrocene-containing biodegradable polymer involved *post-polymerization* functionalization of a polyaspartamide copolymer with a ferrocene moiety.[21] This post-polymerization approach resulted in incomplete side-chain functionalization, increased polydispersity indices (PDI) and number-average molecular weights (M_n), and problematic purification procedures.[22] Therefore, to avoid the complications associated with post-polymerization functionalization, our goal was to functionalize monomers with ferrocene, develop a method for the polymerization of these ferrocene-containing monomers, and to characterize the ferrocene containing biodegradable polymers.

1.2 Reactions of Ferrocene

For the research presented in Part Two, several key substrates were prepared directly from ferrocene according to known procedures. Formylferrocene **1** was prepared using two separate routes (Scheme 1A). In the first strategy, ferrocene was deprotonated by *tert*-butyllithium, and the lithioferrocene intermediate was reacted with DMF.[23] In the second strategy, formylferrocene could be synthesized via aluminum (III) chloride mediated electrophilic substitution.[24] The former approach is favored due to its relative ease and high yield. The latter is less attractive due to the need for a large excess of aluminum chloride. Ferrocene was acylated according to a well-known procedure (Scheme 1B). Although challenging, bromoferrocene (**9**) was prepared by reacting an *in situ* generated lithioferrocene intermediate

with an electrophilic source of bromine (Scheme 1C). Finally, carboxylic acid **11** was synthesized in a similar manner using a reported procedure (Scheme 1D).[25]

Scheme 1. Synthetic routes for several useful ferrocene derivatives.[a]

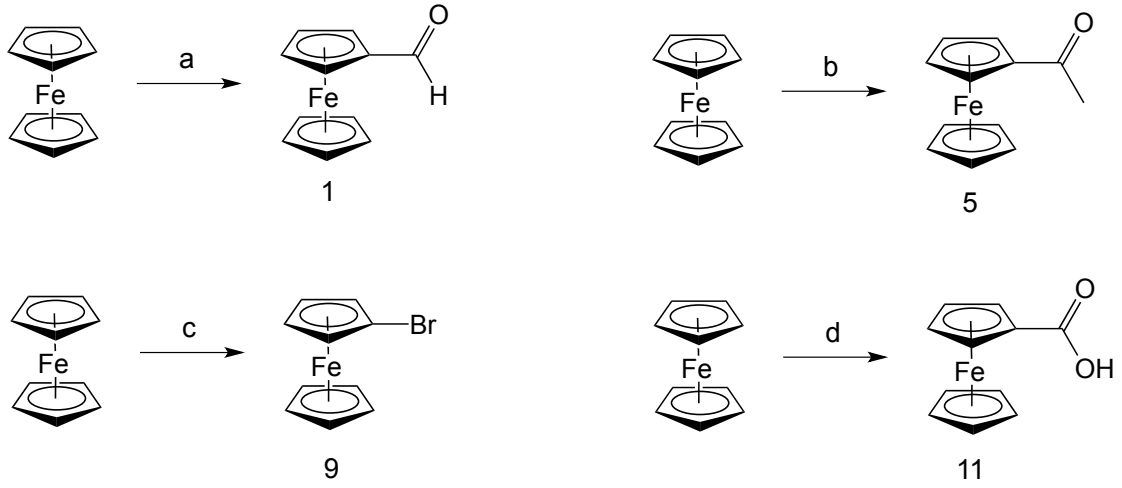

[a]Reagents and conditions: (a) *i. Tert*-butyllithium, potassium *tert*-butoxide; *ii. N,N'*-dimethylformamide, tetrahydrofuran, 88% yield. Or triethyl orthoformate, aluminum trichloride, dichloromethane, 80% yield; (b) Acetic anhydride, phosphoric acid, 62% yield; (c) *i. Tert*-butyllithium, potassium *tert*-butoxide; *ii.* Tetrabromoethane; (d) *i. Tert*-butyllithium, potassium *tert*-butoxide; *ii.* Carbon dioxide.

Formylferrocene (**1)** was converted to azide **3** and compound **4** through an alcohol intermediate (Scheme 2). Reduction of aldehyde **1** with lithium aluminum hydride (LAH) affords alcohol **2** in a scalable reaction that has a high percent yield.[26] Next, the alcohol functionality was reacted with sodium azide[24,26] or acetic anhydride to yield azide **3** and acetate **4**, respectively. Azide **3** could be purified via flash column chromatography on silica gel.

Scheme 2. Formylferrocene (**1**) was used as a building block for the preparation of alcohol **2**, azide **3**, and acetate **4**.[a]

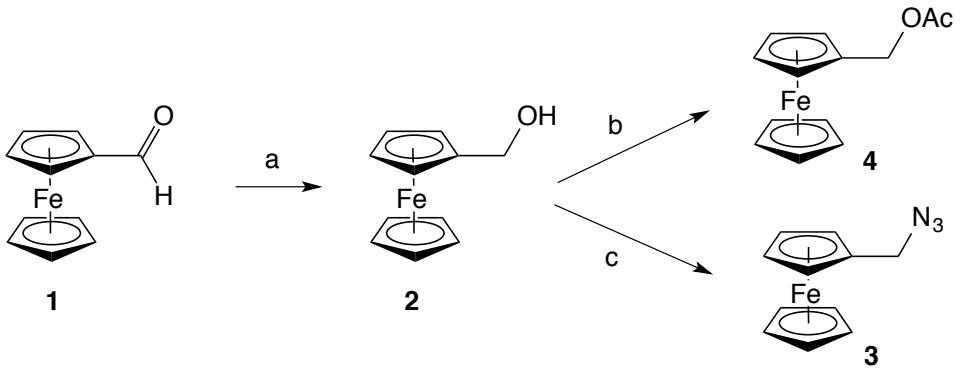

[a]Reagents and conditions: (a) Lithium aluminum hydride, diethyl ether, 95% yield; (b) Acetic anhydride, pyridine, quantitative yield; (c) Sodium azide, acetic acid, 85% yield.

Acetylferrocene **5** undergoes the same types of transformations that were shown for compound **1** (Scheme 3). Reduction of ketone **5** with LAH affords secondary alcohol **6** with a high percent yield.[27] The synthesis for compounds **7** and **8** proceeds almost identically to the transformations described for compound **1**.[24,26] Unfortunately, products **7** and **8** could not undergo purification via column chromatography due to their chemical instability.

Scheme 3. Acetylferrocene (**5**) as a building block for the synthesis of alcohol **6**, azide **7**, and acetate **8**.[a]

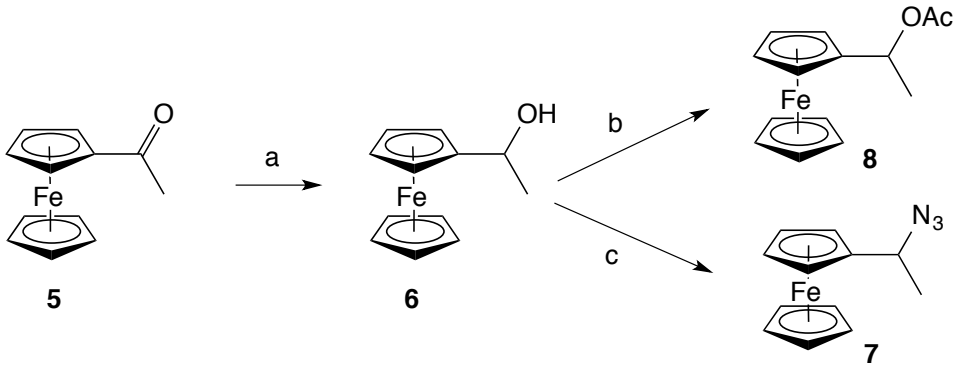

[a]Reagents and conditions: (a) Lithium aluminum hydride, diethyl ether, 95% yield; (b) Acetic anhydride, pyridine; (c) Sodium azide, acetic acid.

Azidoferrocene **10** was synthesized in two steps from ferrocene according to a combination of literature reported procedures (Scheme 4).[28] The yield for azidoferrocene was reported over two steps because bromoferrocene could not be isolated in pure form. Both steps for the synthesis of azidoferrocene proceeded slowly, and the conversion of bromoferrocene to azidoferrocene often required an excess of sodium azide and copper chloride.

Scheme 4. The two step synthesis of azidoferrocene from ferrocene.[a]

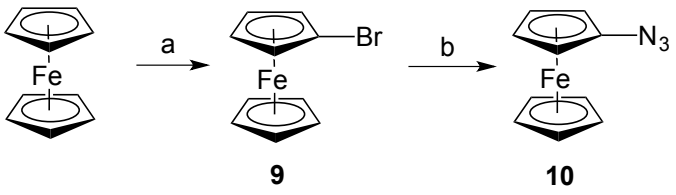

[a]Reagents and conditions: (a) *i. Tert*-butyllithium, potassium *tert*-butoxide, tetrahydrofuran, –78 °C to 23 °C. *ii.* Tetrabromoethane, tetrahydrofuran, –78 °C to 23 °C; (b) Sodium azide, copper chloride, degassed ethanol.

Ferrocene was deprotonated with *t*-BuLi at –78 °C, and the lithioferrocene intermediate was reacted with carbon dioxide to give ferrocene carboxylic acid (**11)** with a fairly high yield (Scheme 5).[25] When carboxylic acid **11** was treated with thionyl chloride, the resulting acid chloride (**12)** could be isolated in a quantitative yield.[29] Full conversion of the starting material to acid chloride **12** was confirmed by crude ^{1}H NMR. Due to its instability, compound **12** was often used immediately for subsequent steps without purification.

Scheme 5. The conversion of ferrocene to compound **12** in two steps.[a]

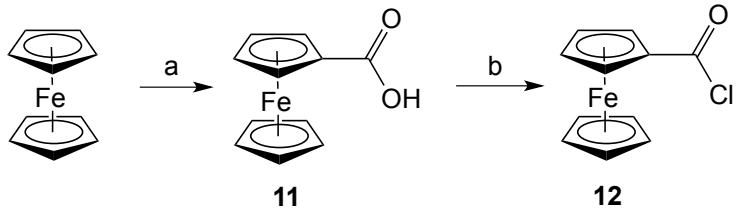

[a]Reagents and conditions: (a) *i. Tert*-butyllithium, potassium *tert*-butoxide, tetrahydrofuran; *ii.* Carbon dioxide, tetrahydrofuran; (b) Thionyl chloride, chloroform.

CHAPTER 2: MONOMER SYNTHESIS

2.1 Synthesis of Cyclic Carbonate Monomers

Cyclic carbonate monomers were first accessed by way of an azide-alkyne click cycloaddition between an alkyne-containing cyclic carbonate **13** and azidoferrocene. α-Propargyl-5-methyl-2-oxo-1,3-dioxane-5-carboxylate (**13**) was first synthesized according to a reported procedure (Scheme 6, path 1).[30] According to this route, commercially available 2,2-bis(methylol)propionic acid (bis-MPA) reacts with benzyl bromide to yield a benzyl protected diol. Triphosgene serves the role of installing the carbonate functional group, giving a cyclic carbonate in high yield. Afterwards, hydrogenolysis of the benzyl group, followed by esterification with propargyl alcohol gave the desired alkyne substrate (**13**). We envisioned an alternative route for this synthesis (Scheme 6, path 2), and successful application resulted in an un-optimized 40% overall yield. Luckily, this route (Path 1) for the synthesis of **13** was more efficient.

Scheme 6. The two routes for the synthesis of alkyne containing monomer **13**. Path 1: The precedented route. Path 2: The novel route.[a]

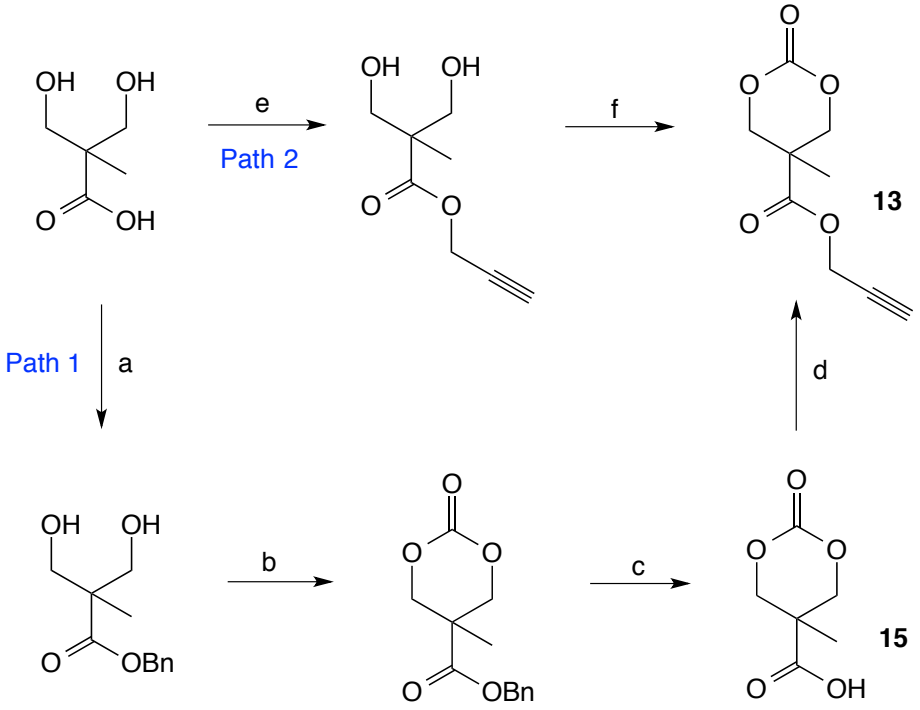

[a]Reagents and conditions: (a) Potassium hydroxide, *N,N'*-dimethylformamide, benzyl bromide, 60% yield; (b) Triphosgene, pyridine, dichloromethane, 97% yield; (c) Pd/C, hydrogen, ethyl acetate, 99% yield; (d) *i.* Oxalyl chloride, *N,N'*-dimethylformamide, tetrahydrofuran, *ii.* Propargyl alcohol, triethylamine; (e) Potassium hydroxide, propargyl bromide, *N,N'*-dimethylformamide, 100 °C, 50% yield; (f) Triphosgene, pyridine, dichloromethane, 80% yield.

With the appropriate alkyne substrate in hand, "click" cycloaddition reactions gave cyclic carbonate monomers containing ferrocene appendage. In the first experiment, cyclic carbonate **13** was coupled to azidoferrocene to yield monomer **14a** (Scheme 7). Monomer **14a** was air stable, and the crude product was purified using a combination of column chromatography and recrystallization from ethyl acetate. Although **14a** was initially obtained in low yields, time spent towards optimization resulted in a yield increase from approximately 50% to 70%. Coupling of carbonate **13** to ferrocenemethylazide (**3**) gave a second cyclic carbonate (**14b**). A third cyclic carbonate monomer was also synthesized by coupling cyclic carbonate **13** and azide **7** (data not shown).

Scheme 7. Ferrocene-containing cyclic carbonate monomers were synthesized via cycloaddition between alkyne **13** and azides **3** and **10**.[a]

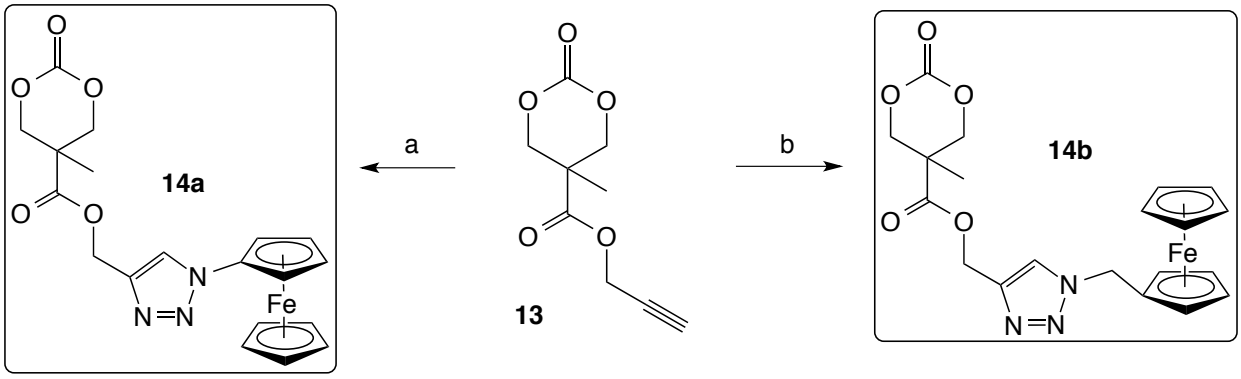

[a]Reagents and conditions: (a) Compound **10**, sodium ascorbate, copper sulfate pentahydrate, tetrahydrofuran, 23 °C, 71% yield; (b) Compound **3**, sodium ascorbate, copper sulfate pentahydrate, tetrahydrofuran, 23 °C, 45% yield.

Another route towards cyclic carbonate monomers was envisioned prior to our use of click chemistry. Instead of esterifying carboxylic acid **15** with propargyl alcohol, **15** was esterified with ferrocene methanol (**2**) (Scheme 8). The esterification was successful, however, the product could not be isolated in pure form. Minutes after exposure to air, the crude product (**16**) turned green likely due to oxidation. Also, column chromatography of the ester on silica gel resulted in decomposition, and the compound decomposed when it was heated during recrystallization.

Scheme 8. Esterification as a route to carbonate monomers.[a]

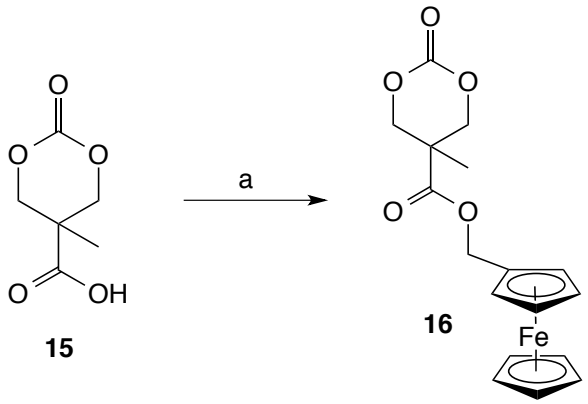

[a]Reagents and conditions: (a) *i.* Oxalyl chloride, tetrahydrofuran, *N,N'*-dimethylformamide; *ii*. Compound **2**, triethylamine.

2.2 Synthesis of δ-Valerolactone Monomers

After successfully preparing cyclic carbonates, we planned to synthesize additional types of monomers. One type of monomer that we pursued was a derivatized δ-valerolactone. Once again, our strategy was to prepare an alkyne-containing substrate that could be used as a reagent in a click cycloaddition reaction. α-Propargyl δ-valerolactone (**17**) was synthesized in one step from δ-valerolactone using a reported procedure (Scheme 9).[31] Although **17** could be purified by a combination of silica gel chromatography and vacuum distillation, **17** could not be stored for prolonged periods of time at 0 °C. Freezing the purified product in degassed anhydrous benzene at –30 °C prolonged the lifetime of **17** dramatically.

Scheme 9. The synthesis of α-propargyl-δ-valerolactone from δ-valerolactone.[a]

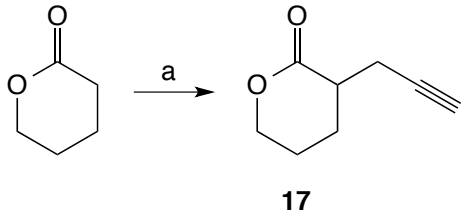

[a]Reagents and conditions: (a) *i.* Lithium diisopropylamide; *ii*. Propargyl bromide, –78 °C to 23 °C, 60% yield.

Two additional monomers containing the ferrocene moiety were constructed from α-propargyl-δ-valerolactone (**17**) using the azide-alkyne cycloaddition method (Scheme 10). The experimental procedures were nearly identical to the conditions used to make carbonate monomers **14a** and **14b**. Lactones **18a** and **18b** were also stable to both air and heat. Initial yields of both lactones were low (40–50% yield), but optimization of the workup and purification conditions increased yields for **18b** by 30%.

Scheme 10. Click reactions to make monomers from α-propargyl-δ-valerolactone.[a]

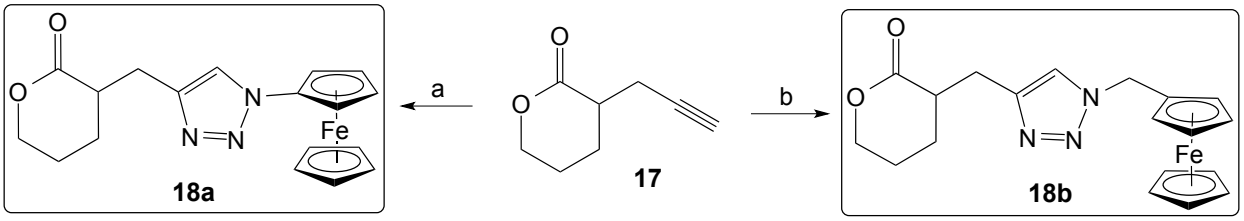

[a]Reagents and conditions: (a) Sodium ascorbate, copper sulfate pentahydrate, tetrahydrofuran, 23 °C, 40% yield; (b) Sodium ascorbate, copper sulfate pentahydrate, tetrahydrofuran, 23 °C, 47% yield.

2.3 Synthesis of ε-Caprolactone Monomers

Initial attempts to synthesize ε-caprolactone monomers began with esterification between acid chloride **12** and 1,4-cyclohexanediol (Scheme 11). The acid chloride component (**12**) was prepared from ferrocene carboxylic acid immediately before reacting with the diol. Unfortunately, ester **19** could only be isolated as a minor side product. Attempts to oxidize the alcohol functional group of **19** with manganese dioxide failed to afford the corresponding ketone.

Scheme 11. The efforts towards the synthesis of a ε-caprolactone monomer.

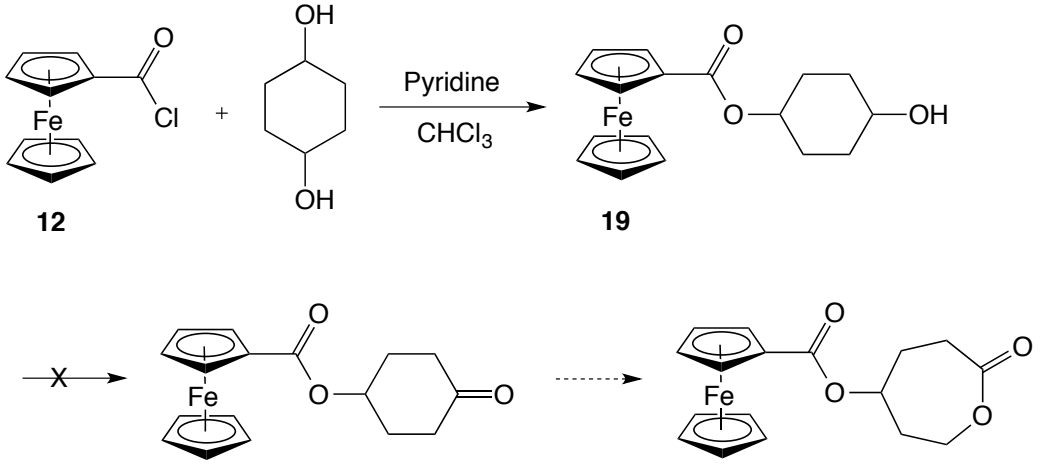

We desired to retry the synthesis of ε-caprolactone monomers using a click reaction. Following published procedures,[32] α-propargyl-cyclohexanone (**20**) was readily prepared from cyclohexane (Scheme 12). Afterwards, Baeyer–Villiger oxidation gave an inseparable mixture of alkyne functionalized ε-caprolactone isomers. ^{1}H NMR analysis of the chromatographed and distilled oil revealed that the mixture consisted of approximately 70% **21b** and 30% **21a**. Nevertheless, the mixture was carried onto the next stage without further purification.

Scheme 12. The synthesis of propargyl-ε-caprolactones **21a** and **21b** in two steps from cyclohexanone.[a]

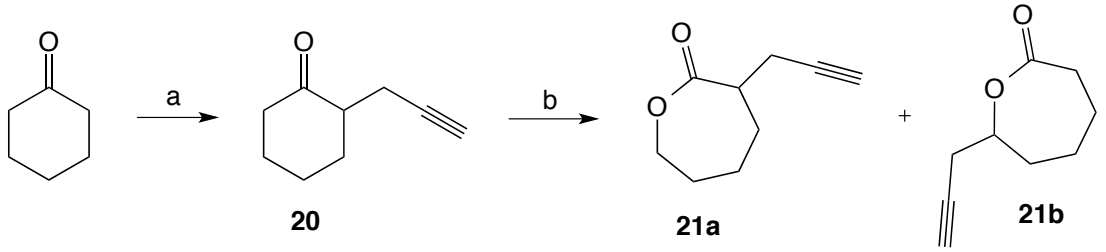

[a]Reagents and conditions: (a) *i.* Lithium diisopropylamide; *ii*. Propargyl bromide, –78 °C to 23 °C. (b) *meta*-chloroperoxybenzoic acid, dichloromethane.

The mixture of **21a** and **21b** was carried forward in order to synthesize monomers **22a** and **22b** via the azide-alkyne click reaction (Scheme 13). The cycloaddition products (**22a** and **22b**) were prepared in an approximate 1:1 ratio. Surprisingly, the mixture of compounds **22a** and **22b** could be separated via column chromatography. Both ferrocene containing caprolactones were also stable to both air and heat.

Scheme 13. ε-Caprolactone monomers were prepared from caprolactones **21a** and **21b** using a click reaction.[a]

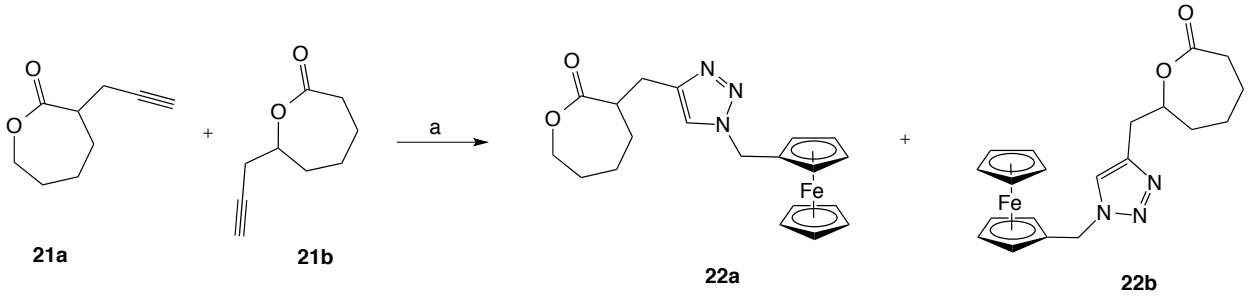

[a]Reagents and conditions: (a) Compound **3**, sodium ascorbate, copper sulfate pentahydrate, tetrahydrofuran, water.

2.4 Synthesis of Additional Monomers

Lactide monomers are relatively easy to polymerize, and polylactides are biodegradable. For these reasons we attempted to prepare a lactide that contains a ferrocene group. Esterifications between ferrocene methanol **2** and L-malic acid derivatives **23a**-**23c**[33] resulted in yields of up to 89% (Scheme 14). However, extensive efforts to deprotect the ester's acetonide functional group failed. It is speculated that the acidic reaction conditions required for acetonide deprotection resulted in the generation of a ferrocenium cation.

Scheme 14. Our failed attempt to prepare a lactide monomer.[a]

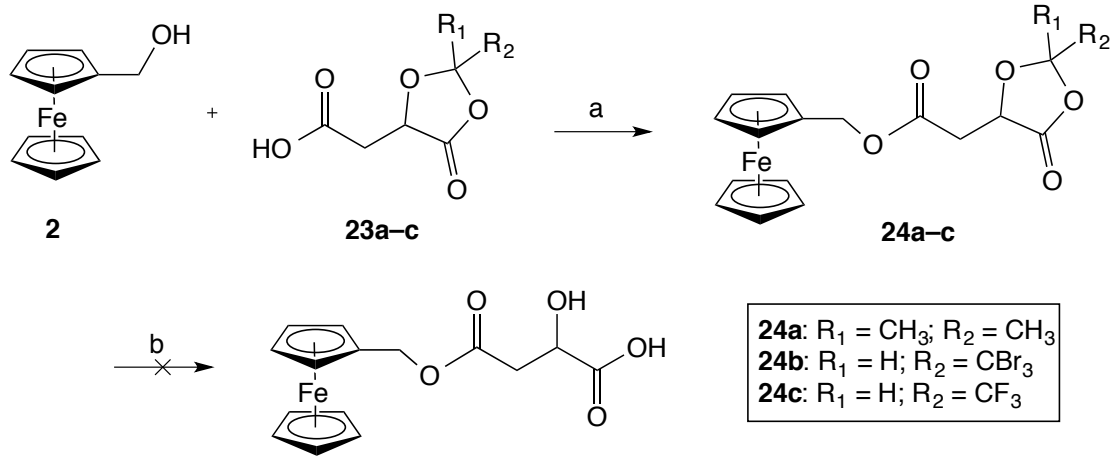

[a]Reagents and conditions: (a) *N,N'*-Dicyclohexylcarbodiimide, dimethylaminopyridine, dichloromethane. (b) Various deprotection conditions.

Early progress in this project involved the synthesis γ-butyrolactone monomers (Scheme 15). Tetramethyl silyl enol ether **25** was prepared from γ-butyrolactone in one step following a reported procedure.[26] Ferrocene-derivatized γ-butyrolactones were then prepared by reacting silyl enol ether nucleophile **25** with ferrocene electrophiles **4** and **8**. However, the reactions proceeded in low yield.

Scheme 15. Coupling of silyl enol ether **25** with ferrocene electrophiles.

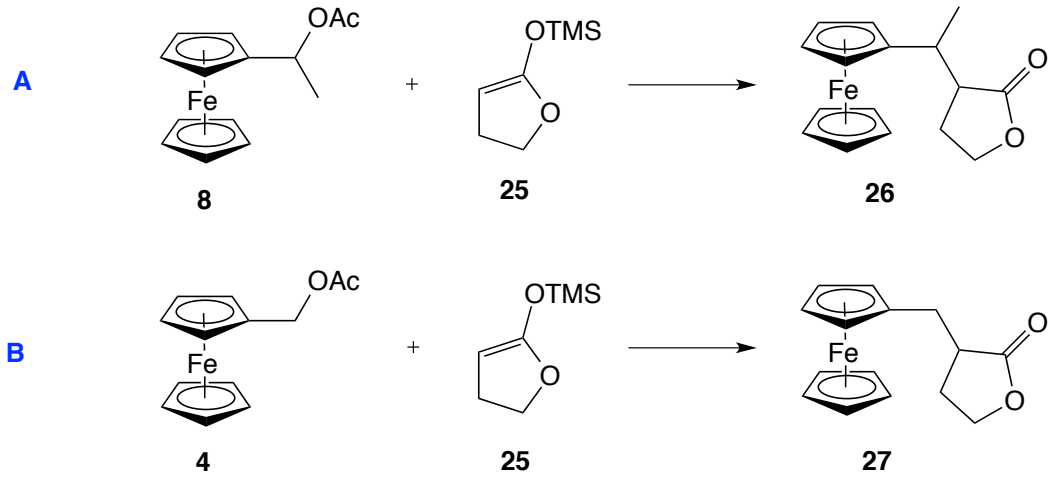

Another approach for making ferrocene-γ-butyrolactone conjugates was to perform an esterification between α-hydroxymethyl-γ-butyrolactone **28** and ferrocene carboxylic acid **11** (Scheme 16). The γ-butyrolactone nucleophile (**28**) was prepared, although in low yield according to a known procedure (Scheme 16, A).[33] Attempts to esterify **28** with **11** failed, but the reaction produced what appeared to be ferrocenyl anhydride (Scheme 16, B). Formation of this anhydride is a reasonable conclusion due to the enhanced nucleophilicity of ferrocene compounds.

Scheme 16. Coupling of ferrocene carboxylic acid and butyrolactone **28**.[a]

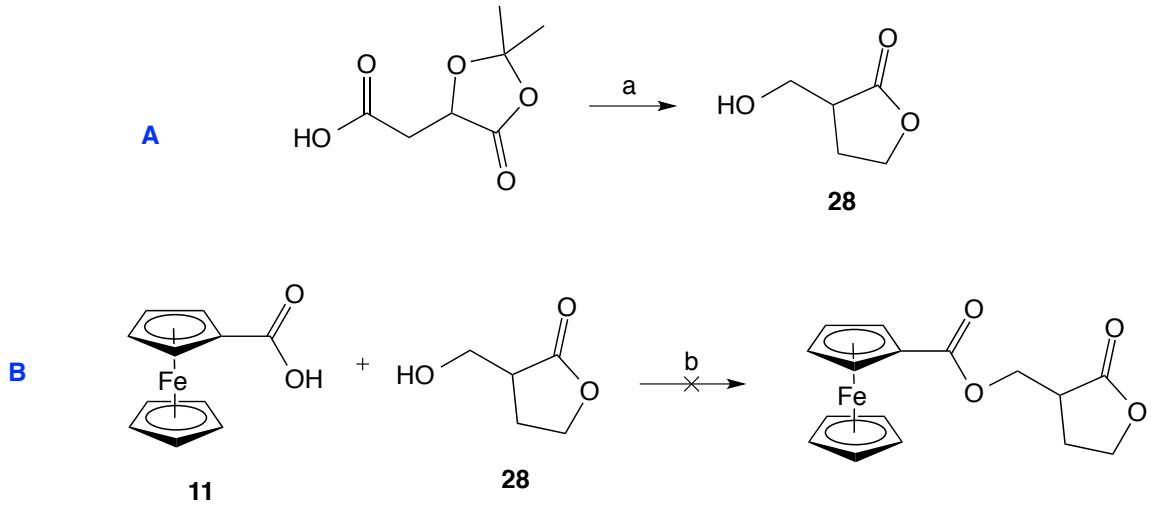

[a]Reagents and conditions: (a) *i.* Borane tetrahydrofuran complex, tetrahydrofuran; *ii.* *p*-TsOH, benzene; (b) Esterification conditions.

CHAPTER 3: THE SYNTHESIS OF FERROCENE-FUNCTIONALIZED POLYMERS

3.1 Polycarbonate Synthesis

With the cyclic carbonate and valerolactone monomers in hand, ring opening polymerization (ROP) experiments were performed with the objective of obtaining polycarbonates and polylactones. Lewis acidic metals are well known for their ability to perform ROP of cyclic carbonates and lactones.[34-36] Therefore, we attempted polymerization with tin, titanium, and aluminum catalysts. Yttrium catalysts (Figure 5) were also employed for polymerization studies. Despite being known for their high reactivity, polymerization of our novel carbonate monomers using these catalysts was not observed. These reactions would not proceed even at high temperatures. These results may be related to the Lewis basic nature of the triazole ring.

Figure 5. Organic and yttrium catalysts.

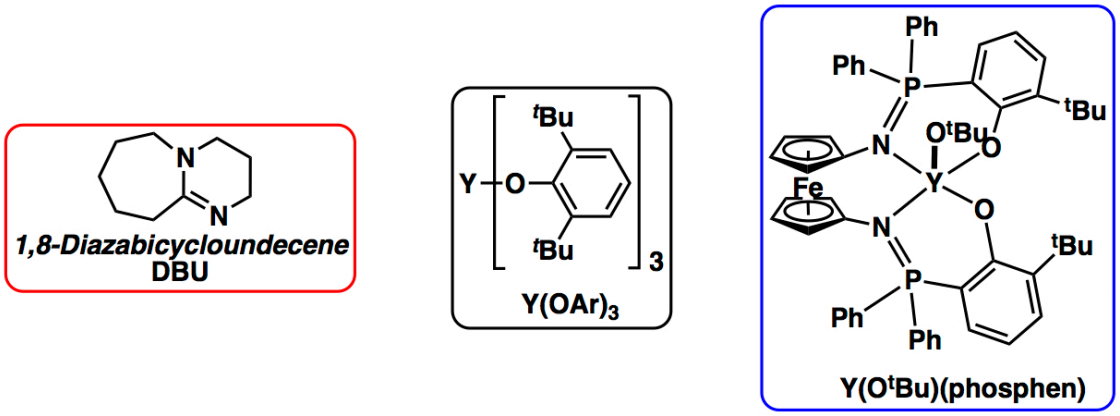

The use of 1,8-diazabicycloundec-7-ene (DBU) as an organic catalyst and benzyl alcohol (BnOH) as an initiator resulted in polymerization of carbonate **14a.** These reactions proceeded at room temperature in dichloromethane (Scheme 17). The poor solubility of **14a** and **14b** limited polymerization studies to solvents such as CH_2Cl_2. Polycarbonate **29a** was purified by precipitation from dichloromethane with cold methanol. Subsequent gel permeation chromatography (GPC) analysis revealed number average molecular weight (M_n) values as high as 20,300 g/mol (89% conversion) and low PDIs of 1.23. Polymerization of polycarbonate **14b**

under the same conditions gave comparable GPC results (M_n = 9,100 – 16,000 g/mol, PDI ≥ 1.35). Data collected via ^{1}H NMR spectroscopy provides evidence that there is retention of the ferrocene appendage on each repeating unit of the polycarbonate.

Scheme 17. Organocatalytic ROP for the synthesis of polycarbonates **29a** and **29b**.

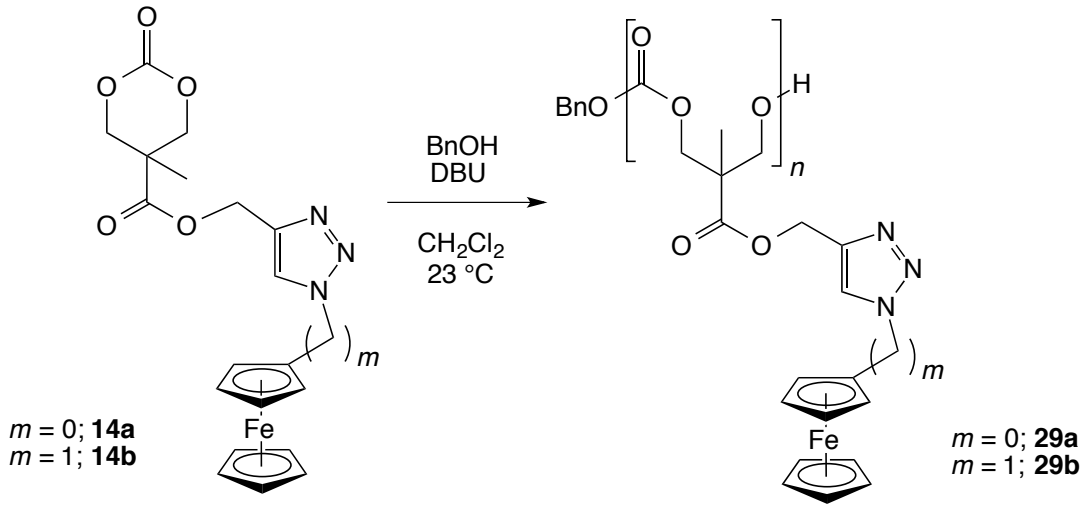

3.2 Attempts to Polymerize Lactones

After finding a successful method for the polymerization of the ferrocene-derivatized cyclic carbonate monomers, our next objective was to identify reaction conditions for the polymerization of our δ-valerolactone derivatives. Attempts to polymerize valerolactone **18a** with DBU and BnOH under conditions identical to the conditions for polycarbonate synthesis gave no reaction. Increasing the molar ratio of DBU and BnOH still failed to result in polymerization. Replacing dichloromethane with 1,2-dichloroethane followed by heating at 80 °C also failed to give a reaction. Therefore, we turned to organic catalysts known for their high activity (Figure 6).[37] Replacing DBU with 1,5,7-triazabicyclo[4.4.0]dec-5-ene (TBD), a highly active δ-valerolactone and ε-caprolactone ROP catalyst, still resulted in no reaction. Addition of a thiourea (TU) cocatalyst to the DBU/BnOH catalyst system is known to polymerize valerolactone monomers. However, applying this cocatalyst system failed to permit polymerization.

Figure 6. Highly active catalysts TBD (left) and cocatalyst TU (right).

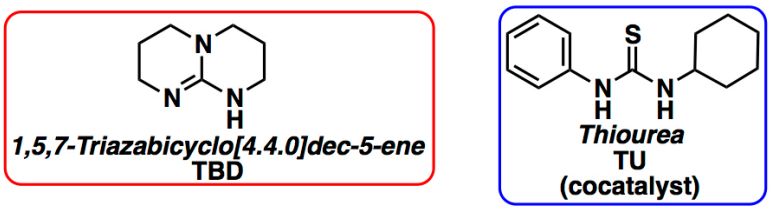

However, α-propargyl-δ-valerolactone[31] underwent ROP upon heating in the presence of tin octanoate and benzyl alcohol (Scheme 18). Subsequent GPC analysis revealed a degree of polymerization (DP ≈ 100) much higher than the DP reported in the literature (M_n of 13,000 g/mol and a PDI of 1.57). Although less controlled, carrying out Click reactions between polymer **30** and azidoferrocene derivatives may be the best route to obtaining a ferrocene-containing poly(δ-valerolactone).

Scheme 18. Ring opening polymerization of α-propargyl-δ-valerolactone.

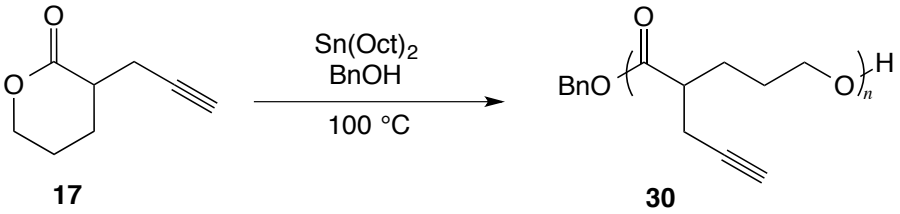

CHAPTER 4: CHARACTERIZATION OF MONOMERS AND POLYMERS

4.1 Cyclic Voltammetry

Electrochemical properties of monomers and polymers were investigated using cyclic voltammetry in THF with tetraisopropylammonium tetrakis(3,5-trifluoromethyl)phenylborate (TPABArF) as the supporting electrolyte (Figure 7). Cyclic carbonate monomers were found to have higher redox potentials than lactone monomers. In addition, the cyclic carbonates have electrochemically reversible redox events, which is apparent because the peak currents increase linearly with the square root of the scan rate. However, the peak potentials of the cyclic carbonate monomers and polycarbonates separates with increasing scan rates, indicating a slow electron transfer.

Figure 7. Cyclic voltammograms of lactone and cyclic carbonate monomers in THF with TPABArF as the supporting electrolyte at a 2 mm platinum disk electrode (10 mV/s scan rate, referenced to the ferrocene/ferrocenium couple).

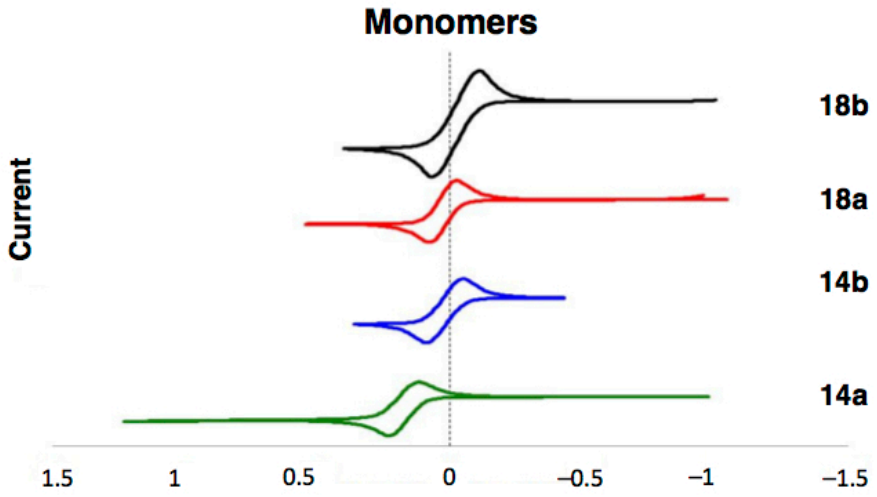

The redox potentials of the cyclic carbonate and lactone monomers decrease upon the introduction of a methylene group between the ferrocene and the triazole rings. The same decrease in redox potential is observed for the polycarbonates after introducing the methylene spacer (Table 1, and Figure 8). Such shifts of the redox potentials in the positive direction are known to result from the introduction of electron donating methylene groups.[38]

Table 1. Redox potentials of lactone monomers, cyclic carbonate monomers, and polycarbonates, 10 mV/s scan rate.

	Compound	$E_{1/2}$ (V vs $Fc^{0/+}$)	ΔE(V)
Carbonate Monomers	**14a**	0.020	0.14
	14b	0.372	0.11
Lactone Monomers	**18a**	–0.015	0.17
	18b	0.045	0.12
Carbonate Polymers	**29a**	0.367	0.17
	29b	0.100	0.15

Figure 8. Cyclic voltammograms of polycarbonates in THF with TPABArF as the supporting electrolyte at a 2 mm platinum disk electrode (10 mV/s scan rate).

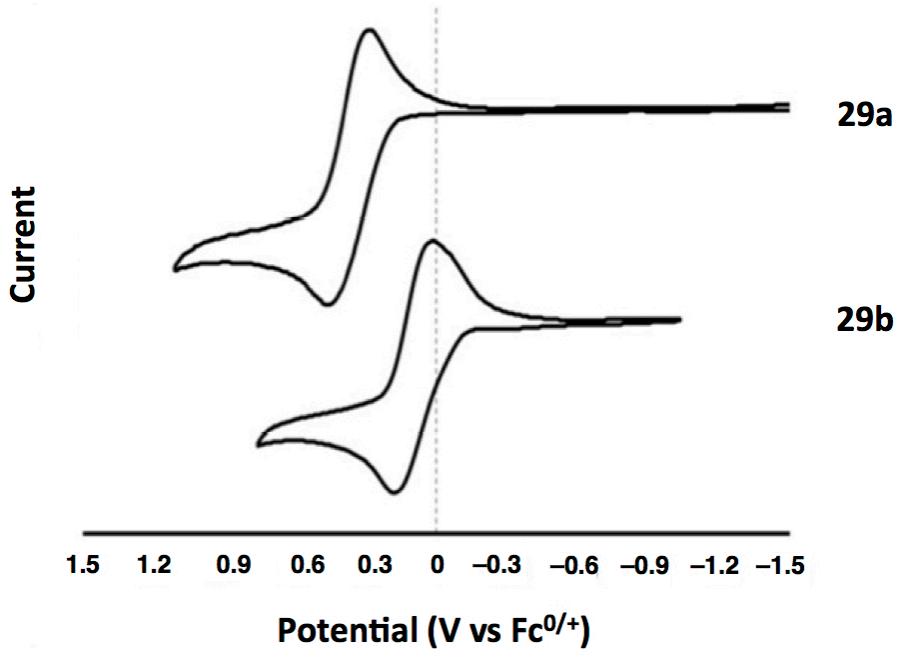

4.2 Chronoamperometry of Polycarbonates

Transient and steady state electrochemical methods were used when characterizing polycarbonates **29a** and **29b** (Table 2).[39-41] The number of electrons consumed in the oxidation of **29a** was calculated to be 44.2, while the number calculated for **29b** was 18.3. These values were obtained using equation 1. In comparison to the GPC determined degree of polymerization, the number of electrons obtained by chronoamperometry appears to be slightly lower than expected.

Table 2. Chronoamperometry data

Sample	Slope of Cottrell plot, **s** ($x10^6$)	Steady-state current, **i** ($x10^9$)	Concentration, **c** ($x10^3$)
ferrocene	–38.05	–14.11	14.79
29a	–6.07	–1.06	0.11
29b	–3.96	–0.389	0.08

The number of electrons transferred per molecule is often associated with a large amount of uncertainty.[42] This conclusion can be supported by previous work on polymer diffusion coefficients. The uncertainty is known to arise from uneven distributions in polymer molecular weight, interaction between iron centers, solvation, ion-pairing, adsorption or precipitation of oxidized species, and conformational changes occurring upon oxidation.[43]

Equation 1. The equation used for the calculation of the number of electrons consumed during oxidation of polycarbonates.

$$\frac{n_{polymer}}{n_{fc}} = \frac{s^2_{polymer} \times i_{fc} \times c_{fc}}{s^2_{fc} \times i_{polymer} \times c_{polymer}}$$

4.3 Thermal Analysis of Polycarbonate 29A

Thermogravimetric analysis (TGA) of polycarbonate **29a** exhibits three thermal events corresponding to the pyrolysis of the carbonate linkage, the polycarbonate backbone, and the ferrocene moiety (Figure 9). The results are consistent with the lability of carbonate linkages. In addition, preliminary differential scanning calorimetry (DSC) data suggests that the polymer undergoes decomposition prior to any other heat-induced event.

Figure 9. TGA thermogram for polycarbonate **29a**.

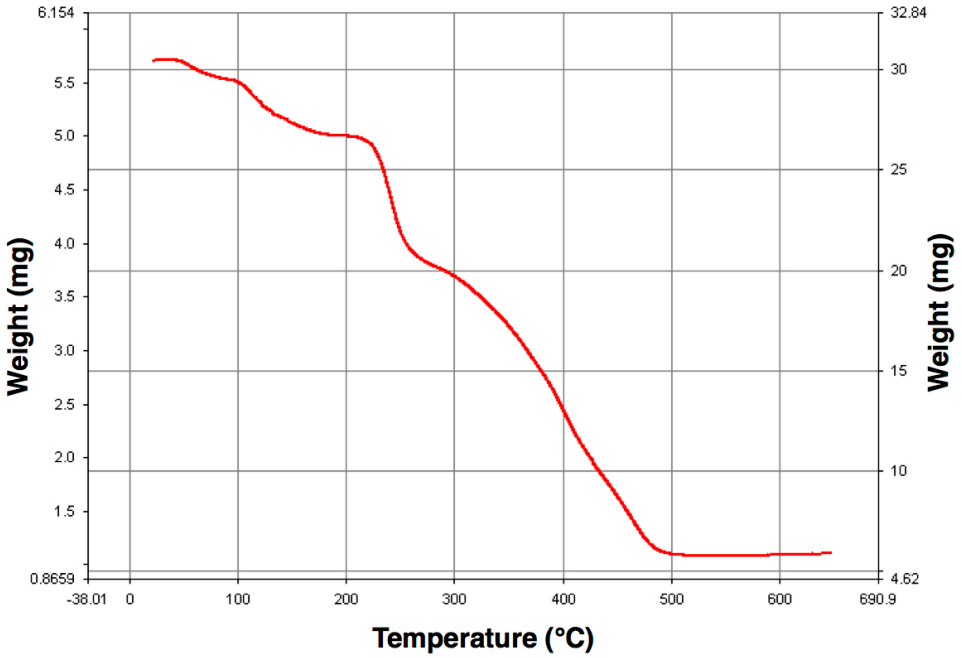

4.4 Density Functional Theory Calculations for Monomers

The thermodynamics of the polymerization reactions were investigated with density functional theory (DFT) calculations. The ring strain energy was calculated for carbonate and lactone monomers. Lactone monomers displayed larger free energy values (dG = 6.89 kcal/mol), whereas the cyclic carbonate monomers were found to have much lower free energy values (dG = 0.03–0.7 kcal/mol).

CHAPTER 5: CONCLUSION

In conclusion, the preparation of ferrocene-labeled monomers works best via azide-alkyne Huisgen “click” cycloaddition. Two ferrocene-containing cyclic carbonate monomers were synthesized according to this method, and organocatalytic ROP gave polycarbonates. These polycarbonates were characterized by GPC, NMR spectroscopy, electrochemical methods, and thermal analysis. The strategy of functionalizing with ferrocene prior to polymerization avoids the complications associated with current post-polymerization modification. Future studies will investigate the biological properties of the newly developed polymers.

CHAPTER 6: EXPERIMENTAL DATA

6.1 Methods and Materials

Unless stated otherwise, reactions were conducted in flame-dried glassware or in a glovebox under an atmosphere of nitrogen using anhydrous solvents (either freshly distilled or passed through activated alumina columns). All commercially obtained reagents were used as received unless otherwise specified. Benzyl alcohol and 1,8-diazabicycloundec-7-ene (DBU) were dried over calcium hydride, distilled, and degassed before being brought into a glovebox. Thin-layer chromatography (TLC) was conducted with silica gel plates and visualized using a combination of UV, iodine, and potassium permanganate staining. EMD silica gel 60 (particle size 40 – 63μm) was used for flash column chromatography. ^{1}H NMR spectra were recorded on Bruker spectrometers (at 300 MHz, 400 MHz, or 500 MHz) and are reported relative to deuterated solvent signals. Data for ^{1}H NMR spectra are reported as follows: chemical shift (δ ppm), multiplicity, coupling constant (Hz) and integration. ^{13}C NMR spectra were recorded on Bruker Spectrometers (at 125 MHz). Data for ^{13}C NMR spectra are reported in terms of chemical shift. Electrochemical measurements were carried out at room temperature under an inert atmosphere in anhydrous THF with TPABArF as the supporting electrolyte using a CHI630D potentiostat.[44] The electrochemical cell consisted of a platinum disk (2 mm) as the working electrode, glassy carbon disk (3 mm) as the counter electrode, and silver wire (0.25 mm) as the pseudo-reference electrode. Steady-state experiments were conducted with a platinum disk microelectrode (0.25 um). All potentials are reported versus a ferrocene internal standard, which was added to the electrochemical cell at the end of each measurement. Gel permeation chromatography (GPC) was conducted on a Shimadzu HPLC system equipped with a refractive index detector RID-10A, one Polymer Laboratories PLgel guard column, and two Polymer Laboratories PLgel 5 μm mixed D columns. LiBr (0.1 M) in DMF at 40 °C was used as an eluent (flow rate: 0.60 mL/min). Calibration was performed using near-monodisperse poly(methyl methacrylate) (PMMA) standards from Polymer Laboratories. Chromatograms were

analyzed using EZStart 7.2 chromatography software.

6.2 Experimental Procedures

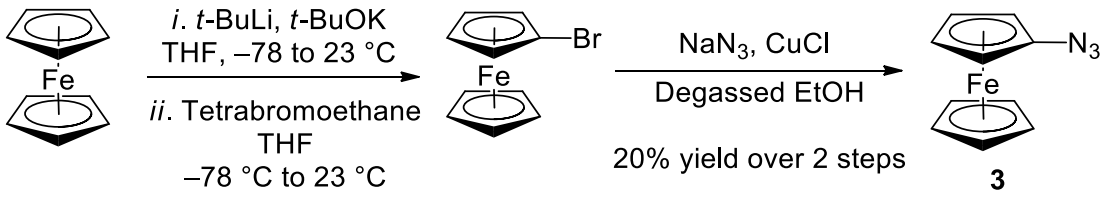

Ferroceneazide (**3**). Ferrocene (1.00 g, 5.38 mmol), *t*-BuOK (74 mg, 0.66 mmol) and dry THF (80 mL) were cooled to –78 °C under a nitrogen atmosphere, and *t*-BuLi (7.2 mL, 10.8 mmol, 1.5 M in hexane) was added over a course of 40 minutes. The reaction was kept at –78 °C for 1 hour, then at room temperature for 1 hour. The solution was then cooled to –78 °C, and tetrabromoethane (0.8 mL, 6.87 mmol) was added over a course of 30 minutes. After stirring at room temperature for 12 hours, the solvent was removed under reduced pressure. The resulting solid was dissolved in dichloromethane (100 mL). The mixture was washed with water (2 x 50 mL) and brine (50 mL), dried with $MgSO_4$, and concentrated under reduced pressure. The crude product was passed through a plug of silica and used for the next step without further purificiation. Characterization was consistent with literature reported values.[45] The sample was dissolved in 30 mL of degassed ethanol. Copper chloride (0.937 g, 5.5 mmol) was added, followed by the dropwise addition of a solution of sodium azide (0.627 g, 9.64 mmol) in water (3 mL). The mixture was stirred at room temperature for 48 hours then filtered through celite. The brown suspension was diluted with diethyl ether (100 mL), and was washed with water (4 x 50 mL). The solvent was removed under reduced pressure, and the crude product was purified via column chromatography (silica gel, hexane) to give an orange solid (20% yield over two steps). Characterization was consistent with literature reported values.[46]

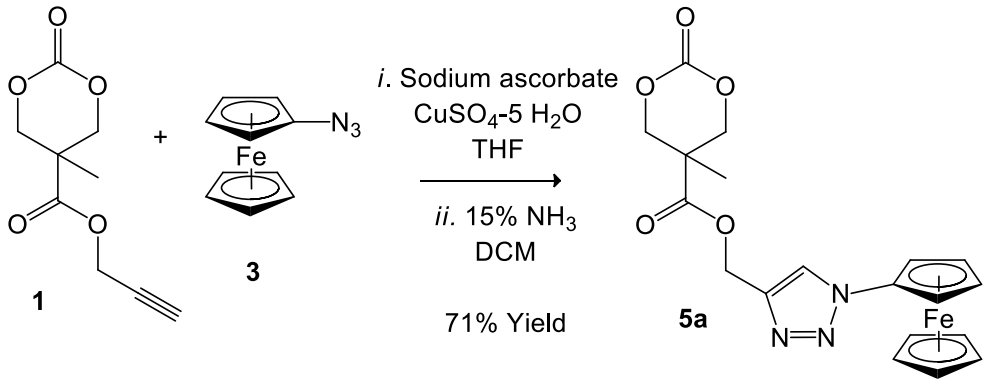

Cyclic carbonate 5a. A solution of copper sulfate pentahydrate (0.971 g, 3.88 mmol) in water (10 mL) was added to a room temperature solution of azidoferrocene (0.883 g, 3.87 mmol), alkyne **1** (0.766 g, 3.87 mmol), in THF (40 mL) and water (10 mL). A solution of sodium ascorbate (0.437 g, 2.21 mmol) in water (5 mL) was added dropwise, and the reaction was stirred for 2 hour at room temperature. Dichloromethane (100 mL) and 15% NH_3 solution (300 mL) were added to the reaction, and the mixture was stirred for 10 minutes in order to remove the Cu(I) derivative. The organic portion was washed with water (2 x 150 mL) and dried over magnesium sulfate. Filtration and concentration under reduced pressure gave **5a** as an orange oil that slowly solidified. The product was purified with column chromatography (20% ethyl acetate in dichloromethane). Yield = 1.17 g, 2.75 mmol, 71% yield. Material for polymerization was recrystallized from ethyl acetate. ^{1}H NMR (500 MHz, $CDCl_3$) δ 1.30 (s, 3H), 4.20–4.26 (m, 9H) 4.68 (d, *J* = 10.4 Hz, 2H), 4.84 (s, 2H), 5.38 (s, 2H), 7.85 (s, 2H); ^{13}C NMR (125 MHz, $CDCl_3$) δ 17.4, 40.6, 59.4, 62.3, 67.0, 70.4, 73.1, 93.5, 123.4, 141.9, 147.5, 171.3; HRMS-ESI (*m/z*) $[M + Na]^+$calcd for $C_{19}H_{19}FeN_3NaO_5$, 448.0572; found, 448.0619. Anal. Calcd for $C_{19}H_{19}FeN_3O_5$: C, 53.67; H, 4.50; N, 9.88. Found: C, 53.12; H, 4.04; N, 9.49.

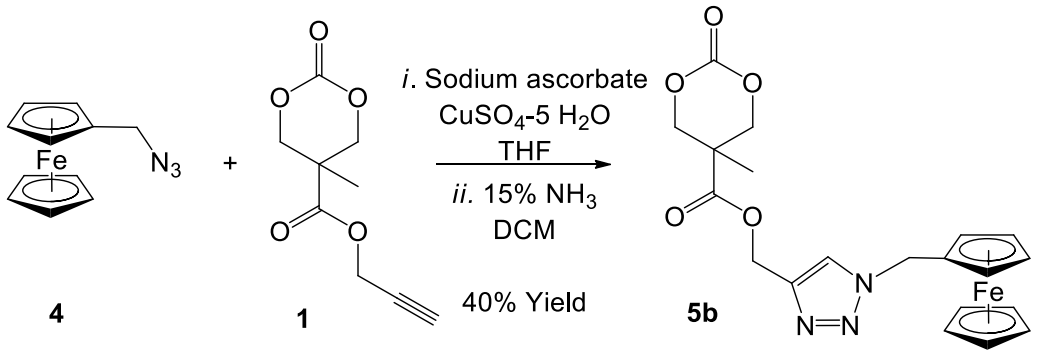

Cyclic carbonate 5b*.* To a solution of cyclic carbonate **1** (313 mg, 1.58 mmol), **4** (253 mg, 1.05 mmol), THF (11 mL) and water (2 mL) was added a solution of copper sulfate pentahydrate (262 mg, 1.05 mmol) in water (3.5 mL). A solution of sodium ascorbate (417 mg, 2.11 mmol) in water (2 mL) was added dropwise, and the reaction was stirred for 5 hours at room temperature. Dichloromethane (40 mL) and 15% NH_3 solution (40 mL) were added to the reaction, and the mixture was stirred for 10 minutes in order to remove the Cu(I) derivative. The organic portion was dried with magnesium sulfate. Filtration and concentration under reduced pressure gave **5b** as a yellow solid. The product was purified with column chromatography (20% ethyl acetate in dichloromethane). Yield = 206 mg, 0.469 mmol, 45% yield. Material for polymerization was recrystallized twice from ethyl acetate. ^{1}H NMR (500 MHz, $CDCl_3$) δ1.28 (s, 3H), 4.14–4.42 (m, 7H), 4.22 (s, 2H), 4.30 (s, 2H), 4.64 (d, *J* = 10.7 Hz, 2H), 5.29 (s, 4H), 7.51 (s, 1H).^{13}C NMR (125 MHz, $CDCl_3$) δ 17.4, 40.4, 50.3, 59.3, 69.0, 69.1, 69.3, 73.0, 80.7, 123.3, 141.7, 147.5, 171.1. Anal. Calcd for $C_{20}H_{21}FeN_3O_5$: C, 54.69; H, 4.82; N, 9.57. Found: C, 54.15; H, 4.45; N, 9.29.

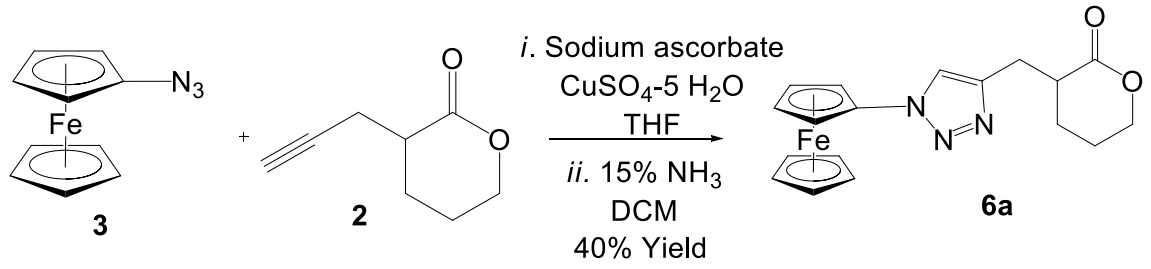

Lactone 6a. To a solution of lactone **2** (65 mg, 0.47mmol), azidoferrocene (90 mg, 0.40 mmol), THF (2.5 mL), and water (0.4 mL) was added copper sulfate pentahydrate (99 mg, 0.396 mmol). A solution of sodium ascorbate (157 mg, 0.79 mmol) in water (0.7 mL) was added dropwise, and the reaction was stirred for 1.5 hours at room temperature. Dichloromethane (14 mL) and 15% NH_3 solution (14 mL) were added to the reaction, and the mixture was stirred for 10 minutes in order to remove the Cu(I) derivative. The organic portion was washed with water (1 x 50 mL) and dried over magnesium sulfate. Filtration and concentration under reduced pressure gave **6a**. The product was purified with column chromatography (20% ethyl acetate in dichloromethane). Yield = 59 mg, 0.16 mmol, 40%. ^{1}H NMR (500 MHz, $CDCl_3$) δ 1.58–1.73 (m, 1H), 1.80–1.93 (m, 2H), 2.08–2.20 (m, 1H), 2.86–3.07 (m, 2H), 3.12–3.22 (m, 1H), 4.10–4.32 (m, 9H), 4.78 (s, 2H), 7.66 (s, 1H).^{13}C NMR (125 MHz, $CDCl_3$) δ 22.0, 24.2, 27.0, 39.9, 61.7, 66.6, 68.4, 70.1, 93.7, 122.3, 144.9, 174.2. HRMS-ESI (*m/z*) [M + Na]$^+$calcd for $C_{18}H_{19}FeN_3NaO_2$, 388.0724; found, 388.0715.

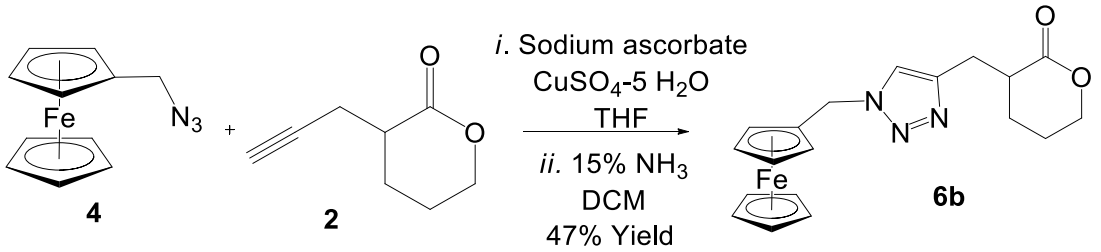

Lactone 6b. To a solution of lactone **2** (166 mg, 1.20 mmol), ferrocenemethylazide (241 mg, 1.00 mmol), THF (6 mL), and water (1 mL) was added copper sulfate pentahydrate (249 mg, 1.00 mmol). A solution of sodium ascorbate (396 mg, 2.00 mmol) in water (1.8 mL) was added dropwise, and the reaction was stirred for 3 hours at room temperature. Dichloromethane (40 mL) and 15% NH_3 solution (40 mL) were added to the reaction, and the mixture was stirred for 10 minutes in order to remove the Cu(I) derivative. The organic portion was washed with water (1 x 100 mL) and dried over magnesium sulfate. Filtration and concentration under reduced pressure gave **6b**. The product was purified with column chromatography (20% ethyl acetate in dichloromethane). Yield = 177 mg, 0.47 mmol, 47%. ^{1}H NMR (500 MHz, $CDCl_3$) δ 1.57–1.68 (m, 1H), 1.80–1.93 (m, 2H), 2.07–2.16 (m, 1H), 2.84–2.98 (m, 2H), 3.09–3.17 (m, 1H), 4.13–4.29 (m, 11H), 5.25 (s, 2H), 7.36 (s, 1H).^{13}C NMR (125 MHz, $CDCl_3$) δ 22.1, 24.3, 27.1, 40.0, 50.0, 68.4, 67.0, 69.05, 69.08, 81.2, 122.0, 144.9, 174.3. Anal. Calcd for $C_{19}H_{21}FeN_3O_2$: C, 60.17; H, 5.58; N, 11.08. Found: C, 60.07; H, 5.28; N, 10.78.

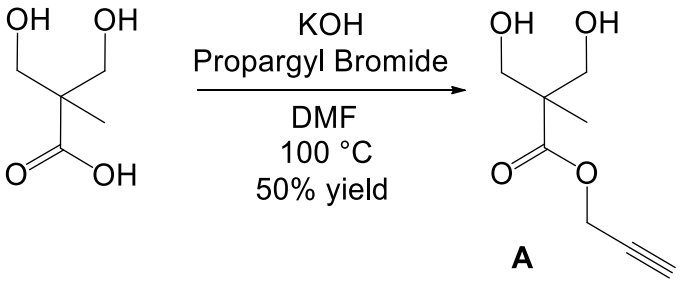

Alkyne modified 2,2-bis(methylol)propionic acid (**A**). Bis-MPA (4.00 g, 29.9 mmol), KOH (2.07 g, 31.3 mmol, 85% assay), and DMF (20 mL) were heated to 100 °C until dissolved. Propargyl bromide (4.45 g, 80% in toluene, 29.9 mmol) was added directly. After 24 hours, the solvent was removed under reduced pressure. The crude product was diluted in ethyl acetate (50 mL) and washed with water (3 x 25 mL). The combined organic layers were dried with magnesium sulfate, the drying agent was filtered off, and the solvent was removed under reduced pressure. Diol **A** was obtained as a colorless oil (50% yield). Characterization is consistent with the literature reported values.[47]

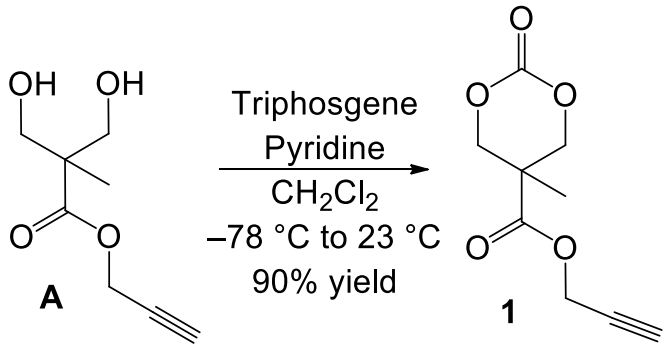

Propargyl 5-methyl-2-oxo-1,3-dioxane-5-carboxylate (**1**)**.** Alkyne **A** (0.500 g, 2.90 mmol) was stirred in pyridine (1.38 mL, 17.1mmol) and DCM (10 mL) at –78 °C. A solution of triphosgene (0.430 g, 1.45 mmol) in 5 mL of DCM was added dropwise over a course of 1 hour. The temperature was allowed to rise to 23 °C, and the reaction was allowed to stir for an additional 1 hour. The reaction was quenched by the addition of sat. NH_4Cl (5 mL). The organic layer was washed with 1M HCl (3 x 5 mL), washed with saturated $NaHCO_3$ (5 mL), and then washed with

water (5 mL). The organic layer was dried with $MgSO_4$, and the solvent was removed under reduced pressure. Product **1** was isolated as a white solid (90% yield) and was used without further purification. Characterization is consistent with literature reported values[30]

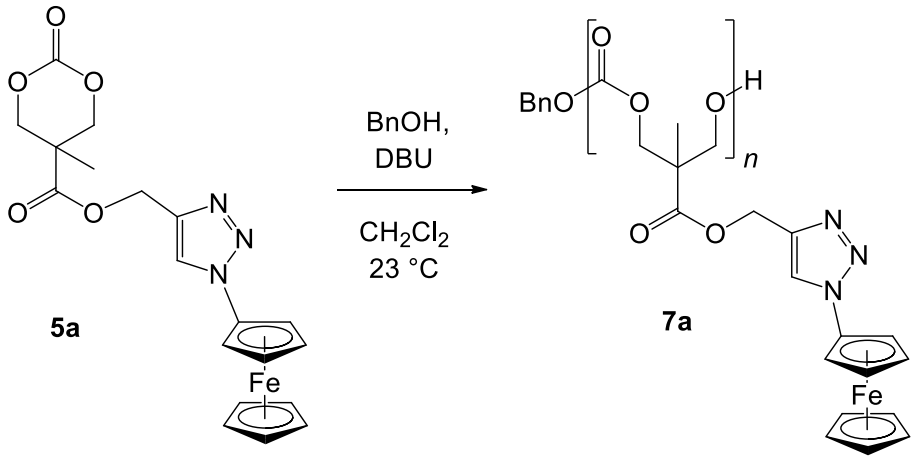

Polycarbonate 7a. Monomer **5a** (250 mg, 0.59 mmol) was stirred in DCM (1 mL), benzyl alcohol (1 mol%, 0.63 mg) and DBU (1 mol%, 0.89 mg) for 24 hours (conversion ~89%). The reaction was quenched by the addition of benzoic acid (5 mg, 0.04 mmol). The polymer was precipitated by the addition of cold methanol and filtered through celite. (Yield = 216 mg, 86%). ^{1}H NMR (500 MHz, $CDCl_3$) δ 1.21 (s, 3H), 4.19 (s, 5H), 4.25 (m, 6H), 4.85 (s, 2H), 5.28 (s, 2H), 7.90 (s, 1H); ^{13}C NMR (125 MHz, $CDCl_3$) δ 17.5, 46.8, 58.7, 62.3, 66.9, 68.7, 70.3, 93.6, 123.8, 142.3, 154.4, 172.1; GPC (DMF): M_n 20329, PDI 1.23

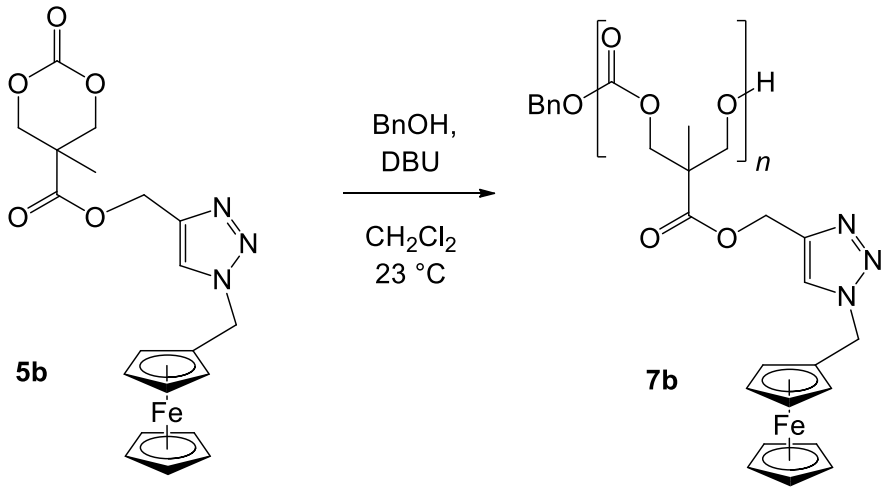

Polycarbonate 7b. Monomer **5b** (57 mg, 0.13 mmol) was stirred in DCM (0.6 mL), benzyl alcohol (1 mol%, 0.14 mg) and DBU (1 mol%, 0.20 mg) for 48 hours (conversion ~77%). The reaction was quenched by the addition of benzoic acid (~1 mg). The polymer was diluted in DCM (0.5 mL), precipitated by the addition of cold methanol, and filtered through celite. (Yield = 37 mg, 65%). ^{1}H NMR (500 MHz, $CDCl_3$) δ 1.18 (s, 3H), 4.17–4.27 (m, 13H), 5.20 (s, 2H), 5.28 (s, 2H), 7.57 (s, 1H); ^{13}C NMR (125 MHz, $CDCl_3$) δ 17.5, 46.7, 50.2, 58.8, 68.6, 69.0, 69.1, 69.2, 81.1, 123.6, 142.1, 154.4, 172.0; GPC (DMF): M_n 12434, PDI 1.34

APPENDIX FOUR

Spectra Relevant to Part 2

Synthesis of Ferrocene-Containing Monomers and Biodegradable Polymers

Brianna M. Upton, Raymond M. Gipson, Selma Duhović, Brian R. Lydon, Nicholas M. Matsumoto, Heather D. Maynard and Paula L. Diaconescu

Inorg. Chem. Front. **2014**, *1*, 271–277.

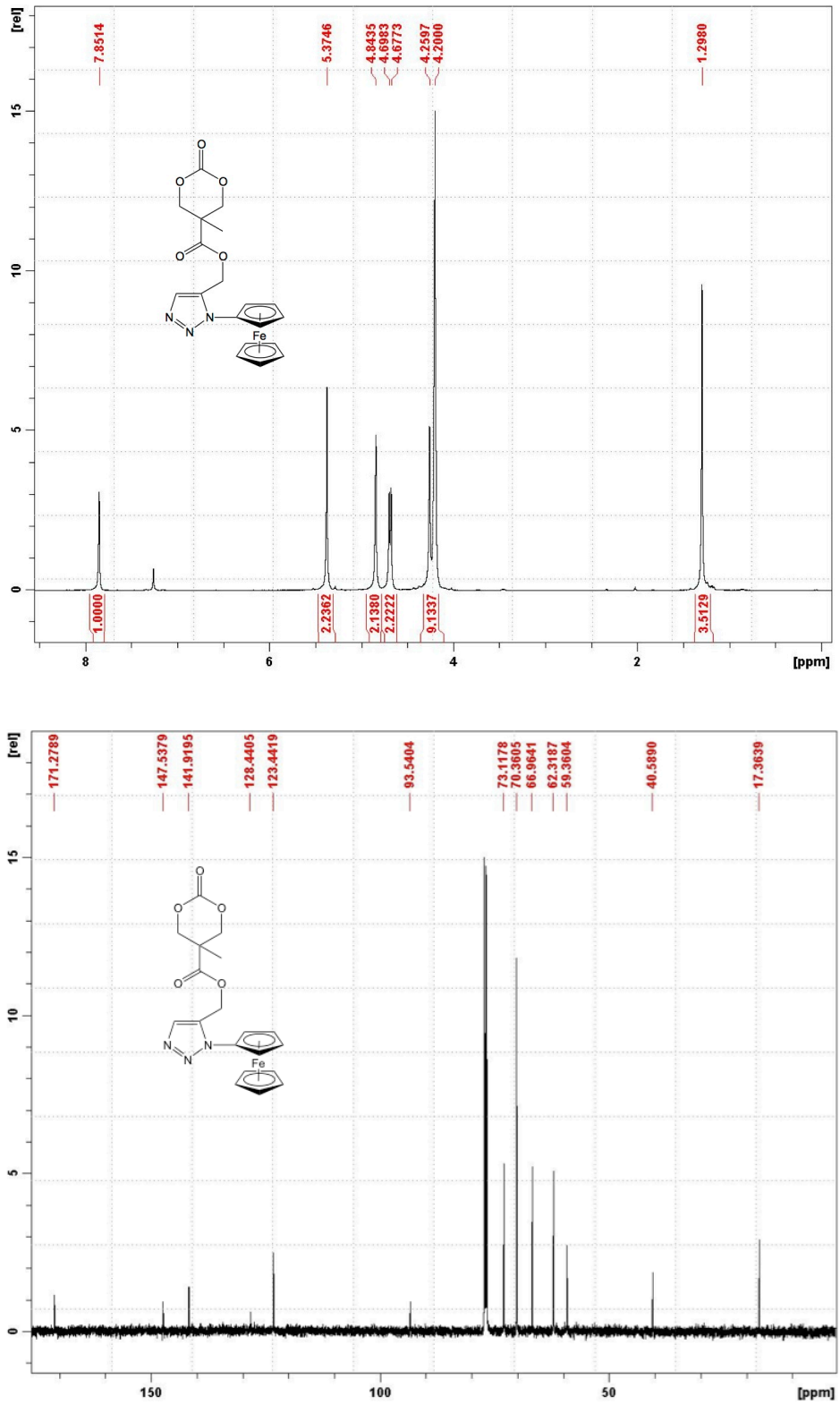

Figure A4.1. *^{1}H and ^{13}C NMR spectra for Compound* ***5a***

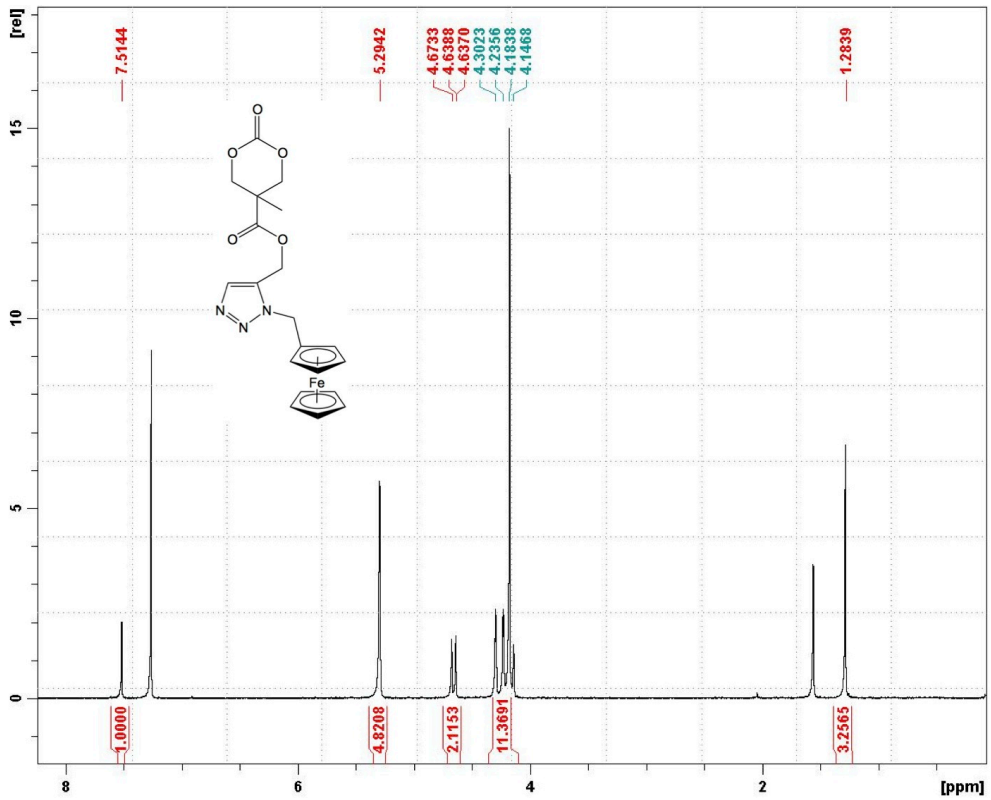

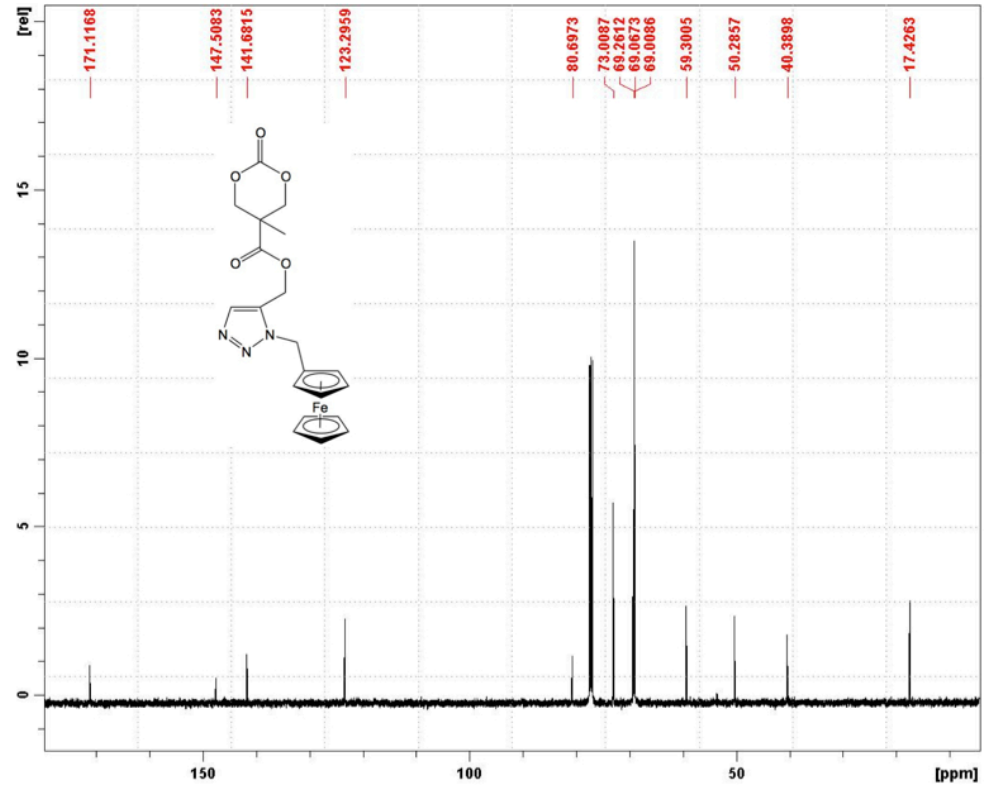

Figure A4.2**. ^{1}H and ^{13}C NMR spectra for Compound **5b

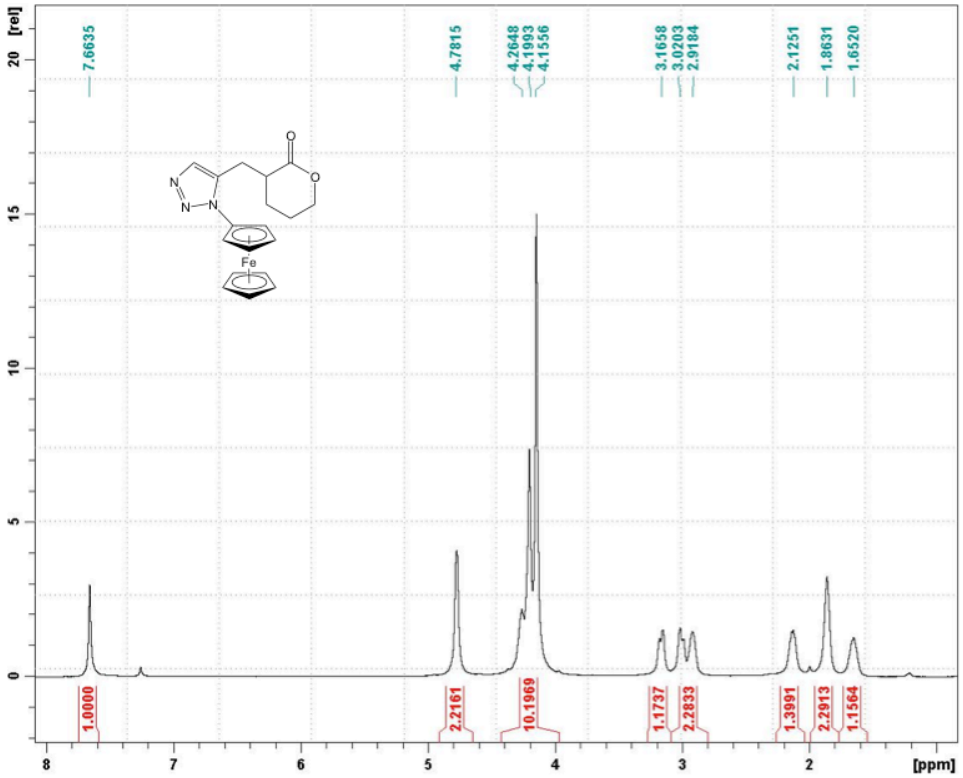

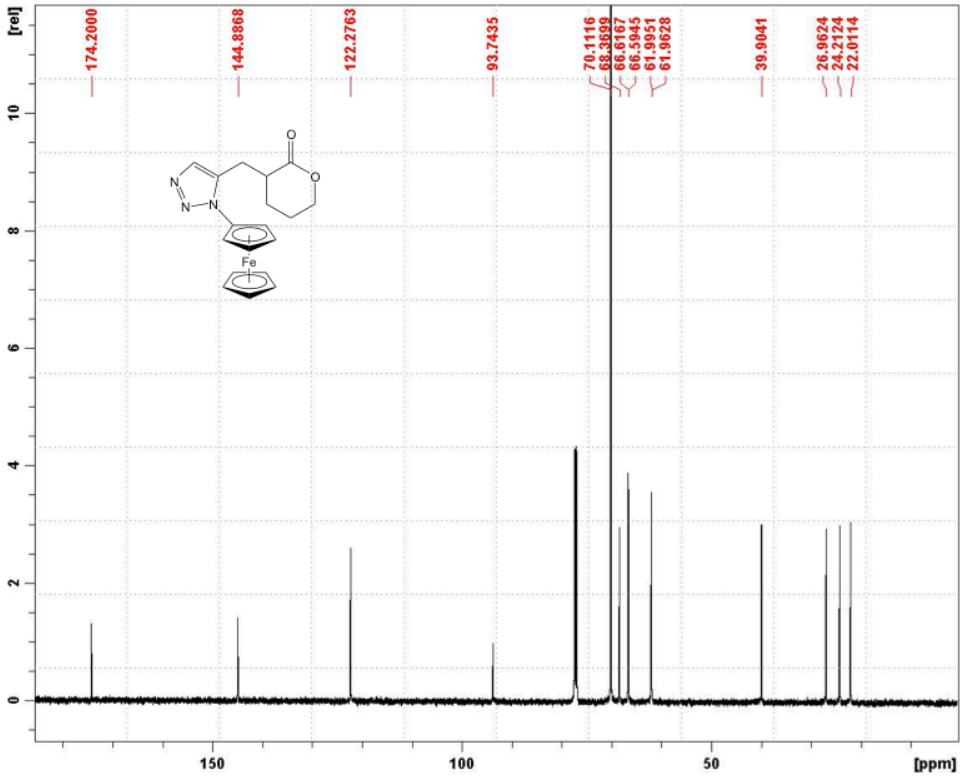

Figure A4.3. *^{1}H and ^{13}C NMR spectra for Compound* ***6a***

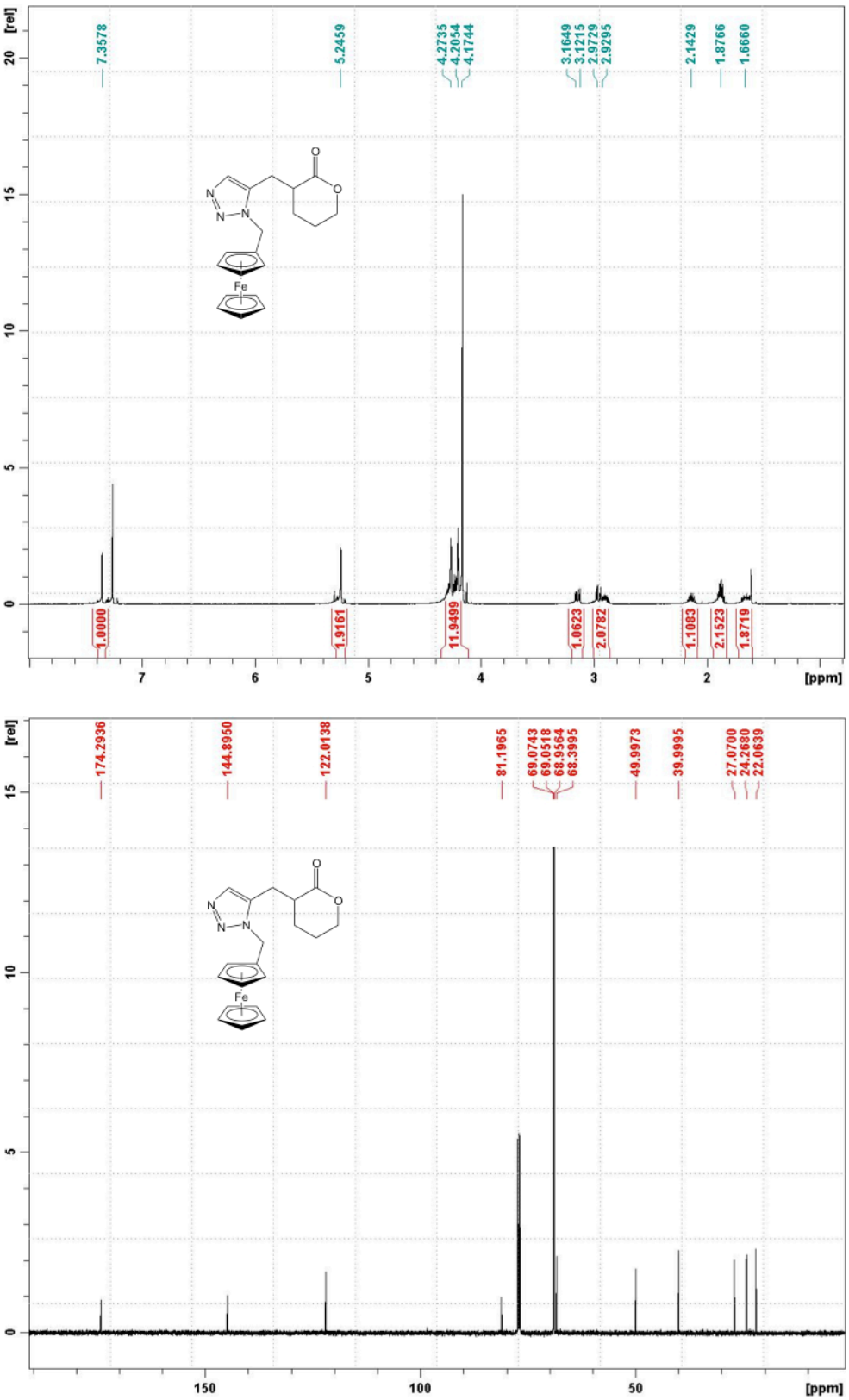

Figure A4.4**. ^{1}H and ^{13}C NMR spectra for Compound **6b

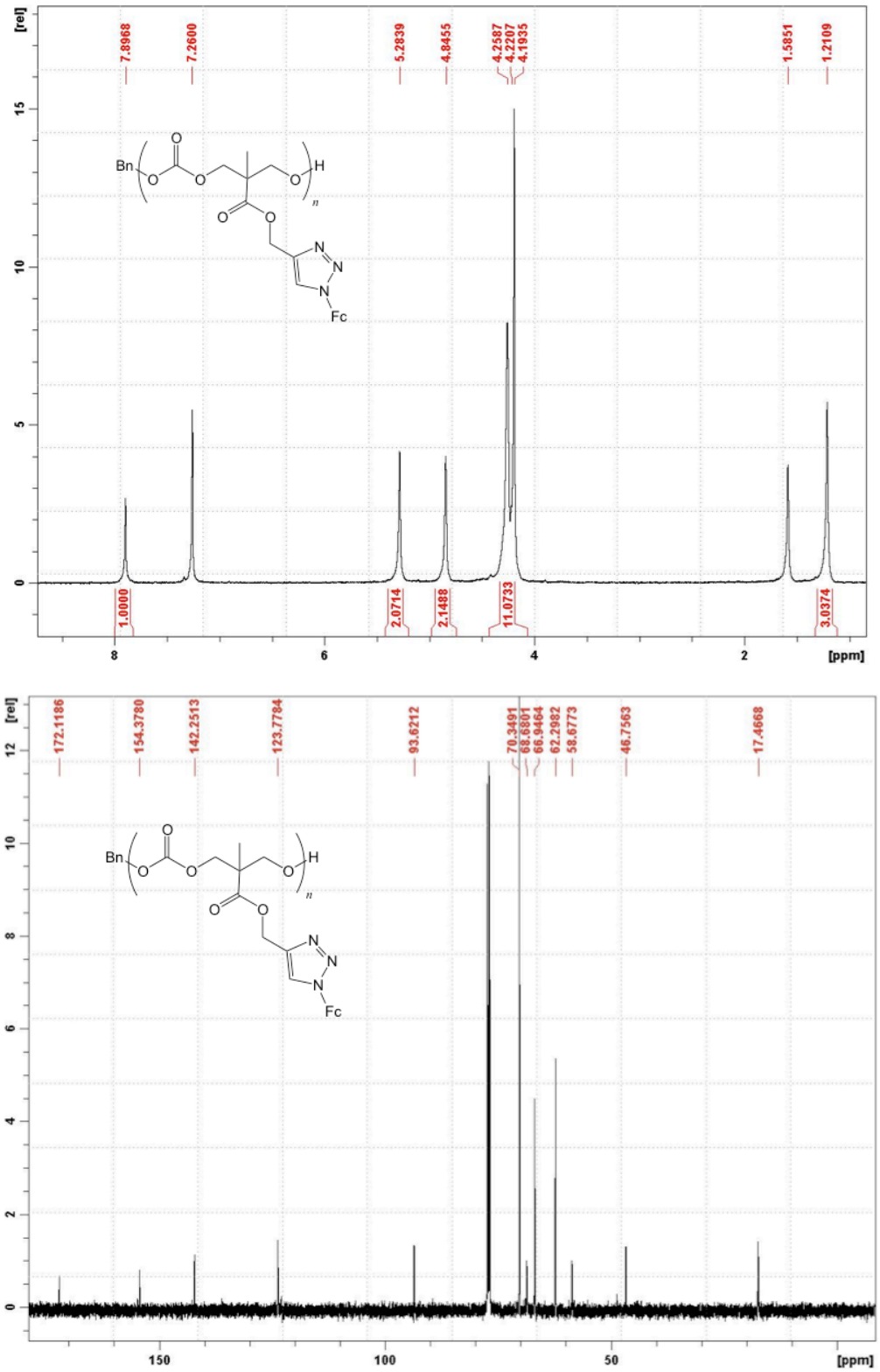

Figure A4.5. *^{1}H and ^{13}C NMR spectra for Compound* ***7a***

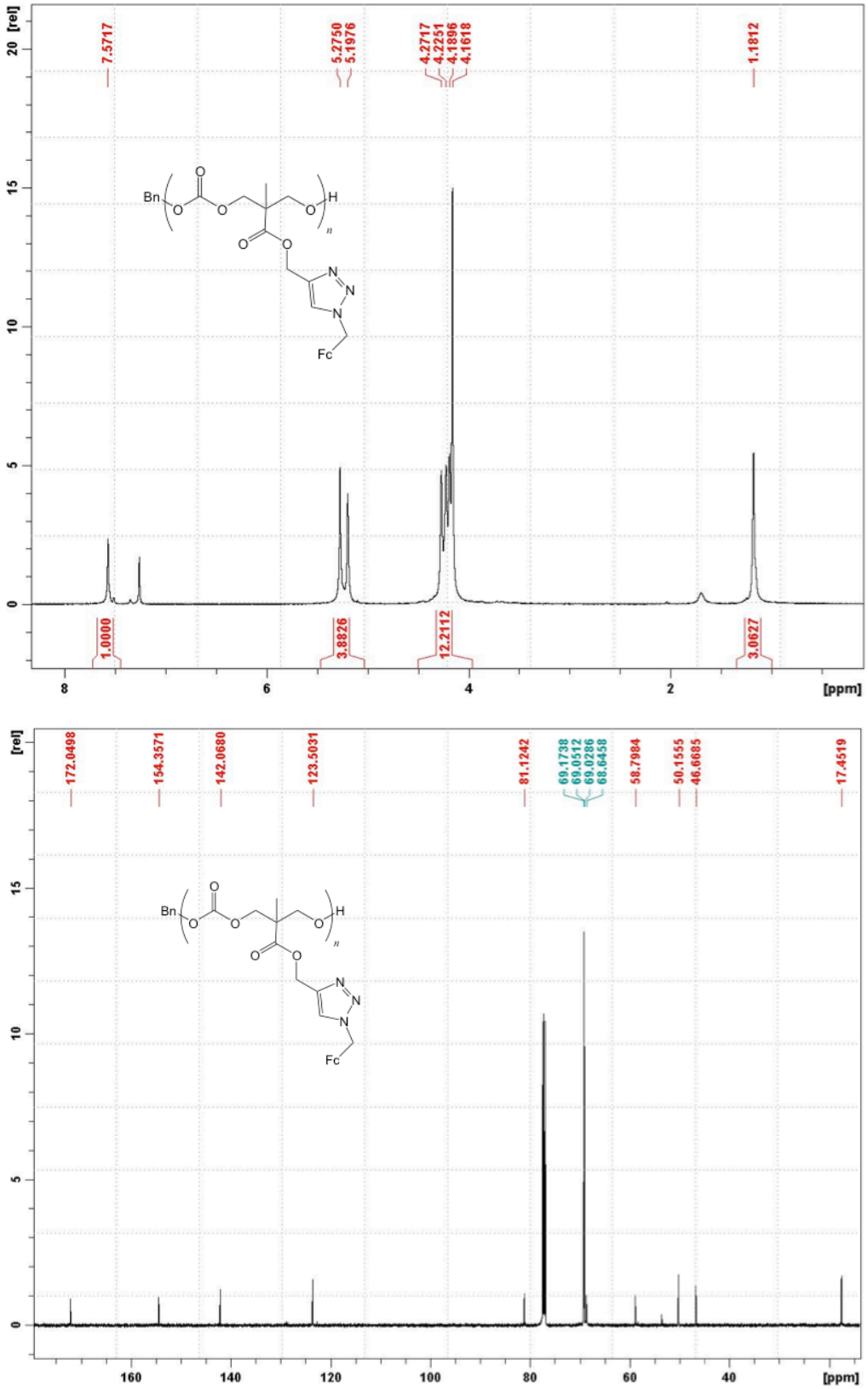

Figure A4.6**. ^{1}H and ^{13}C NMR spectra for Compound **7b

APPENDIX FIVE

Cyclic Voltammetry and Chronoamperometry Data Relevant to Part 2

Synthesis of Ferrocene-Containing Monomers and Biodegradable Polymers

Brianna M. Upton, Raymond M. Gipson, Selma Duhović, Brian R. Lydon, Nicholas M. Matsumoto, Heather D. Maynard and Paula L. Diaconescu

Inorg. Chem. Front. **2014**, *1*, 271–277.

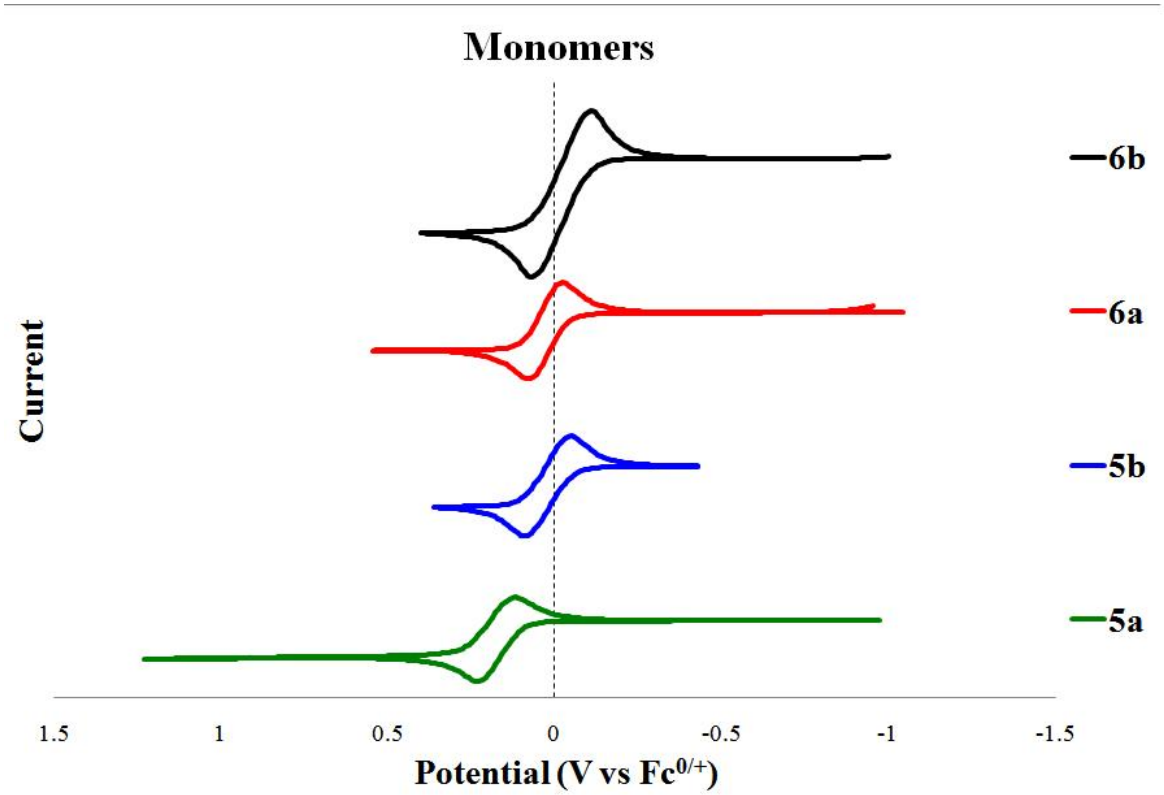

Figure A5.1. Cyclic voltammograms of lactone and cyclic carbonate monomers in THF with TPABArF as the supporting electrolyte at a 2 mm Pt disk electrode, 10 mV/s scan rate. (Referenced to the ferrocene/ferrocenium couple).

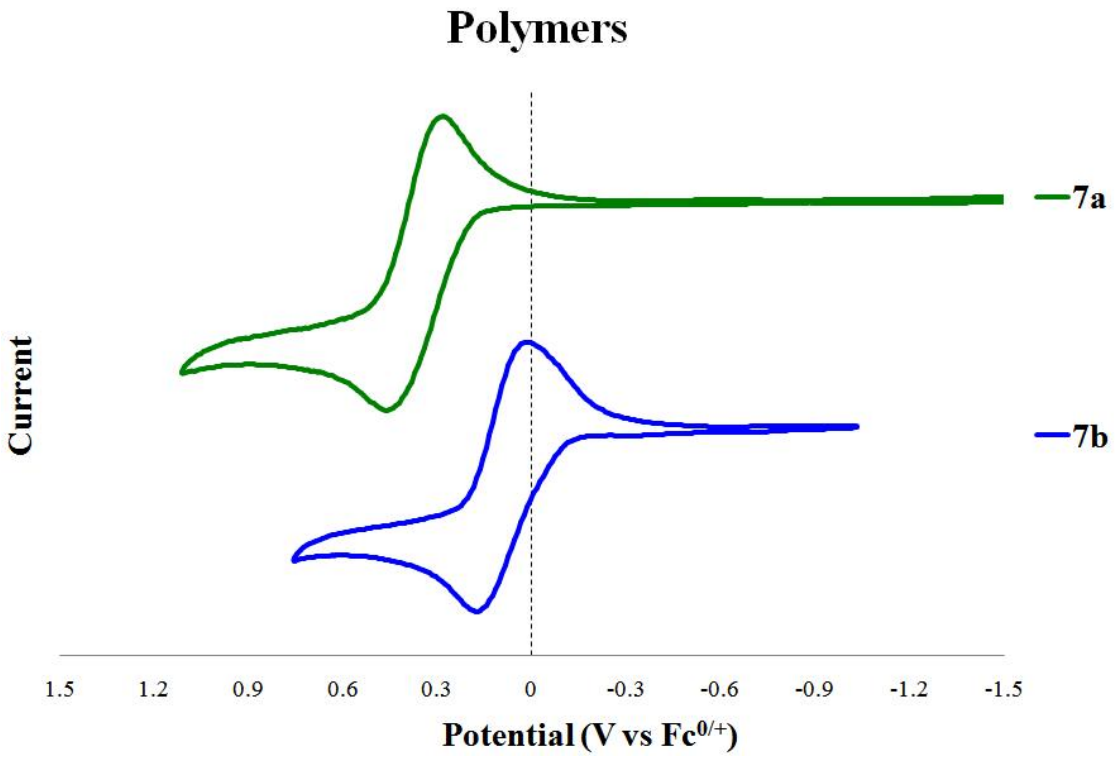

Figure A5.2. Cyclic voltammograms of cyclic carbonate polymers in THF with TPABArF as the supporting electrolyte at a 2 mm Pt disk electrode, 10 mV/s scan rate. (Referenced to the ferrocene/ferrocenium couple).

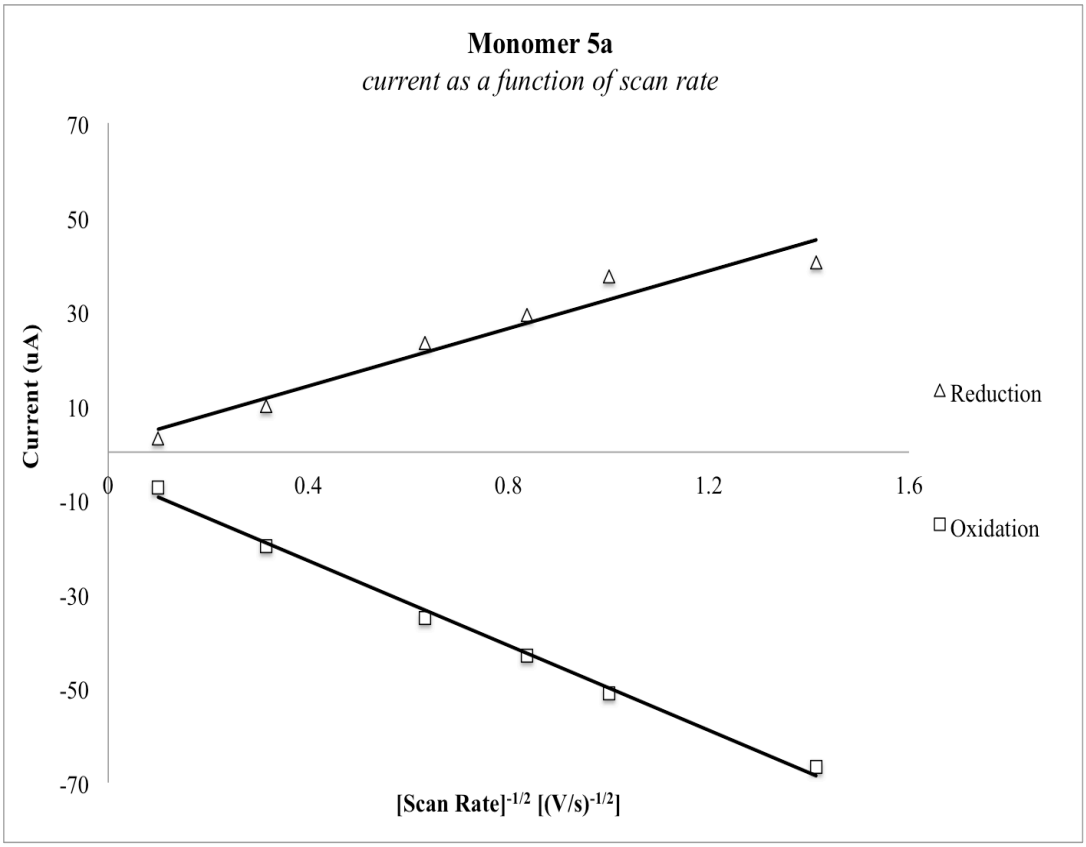

Figure A5.3. Current as a function of scan rate for monomer **5a**.

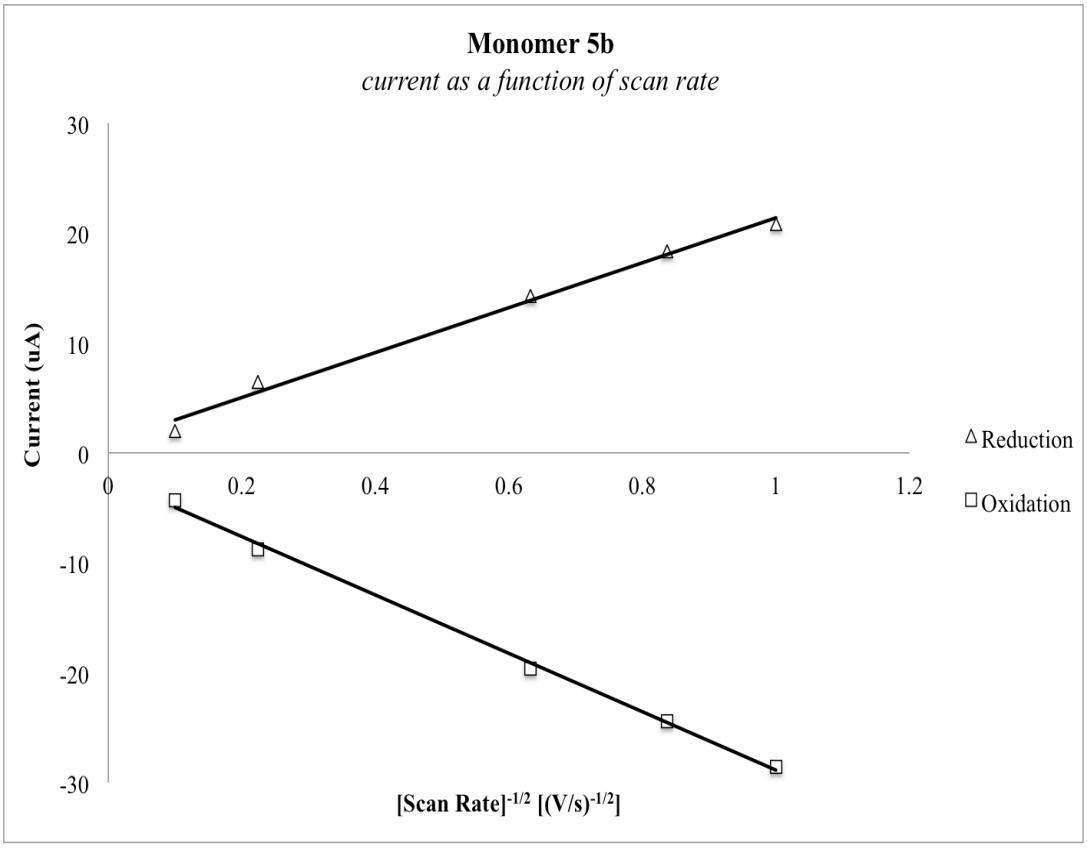

Figure A5.4. Current as a function of scan rate for monomer **5b**.

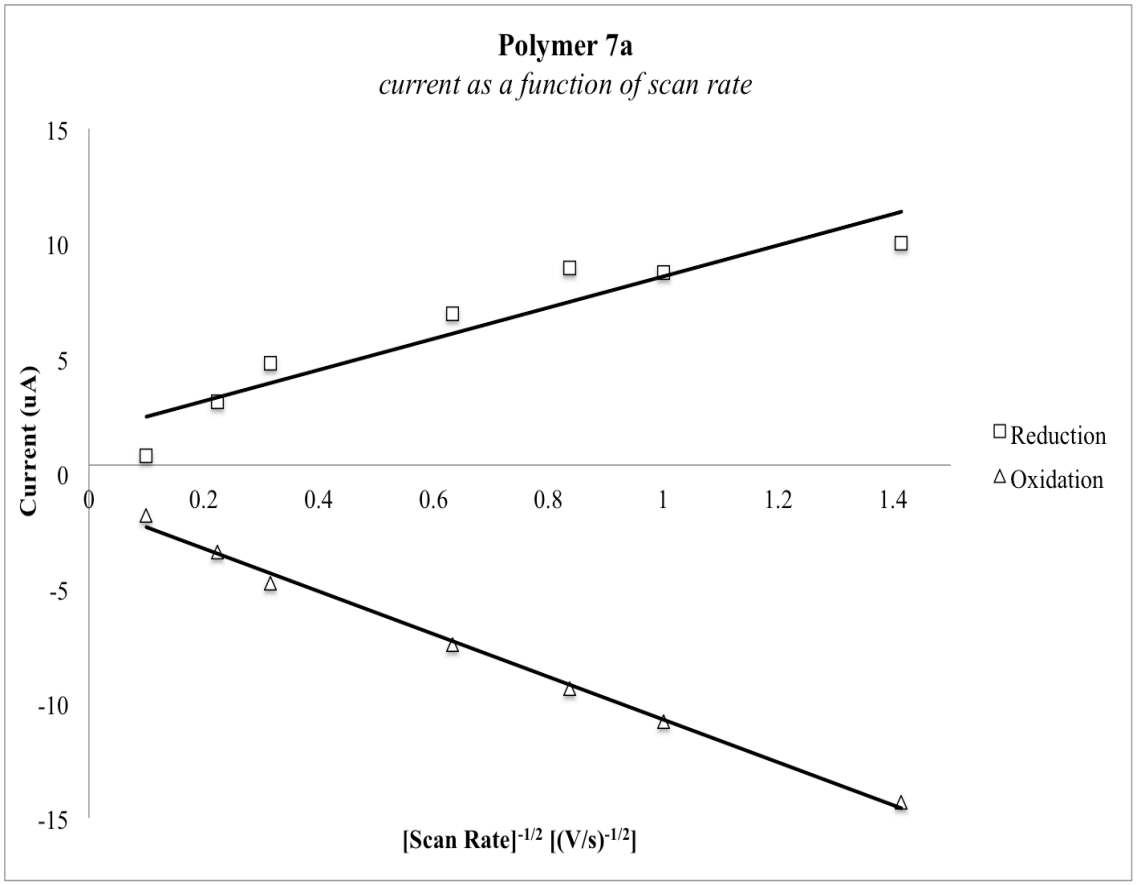

Figure A5.5. Current as a function of scan rate for polymer **7a**.

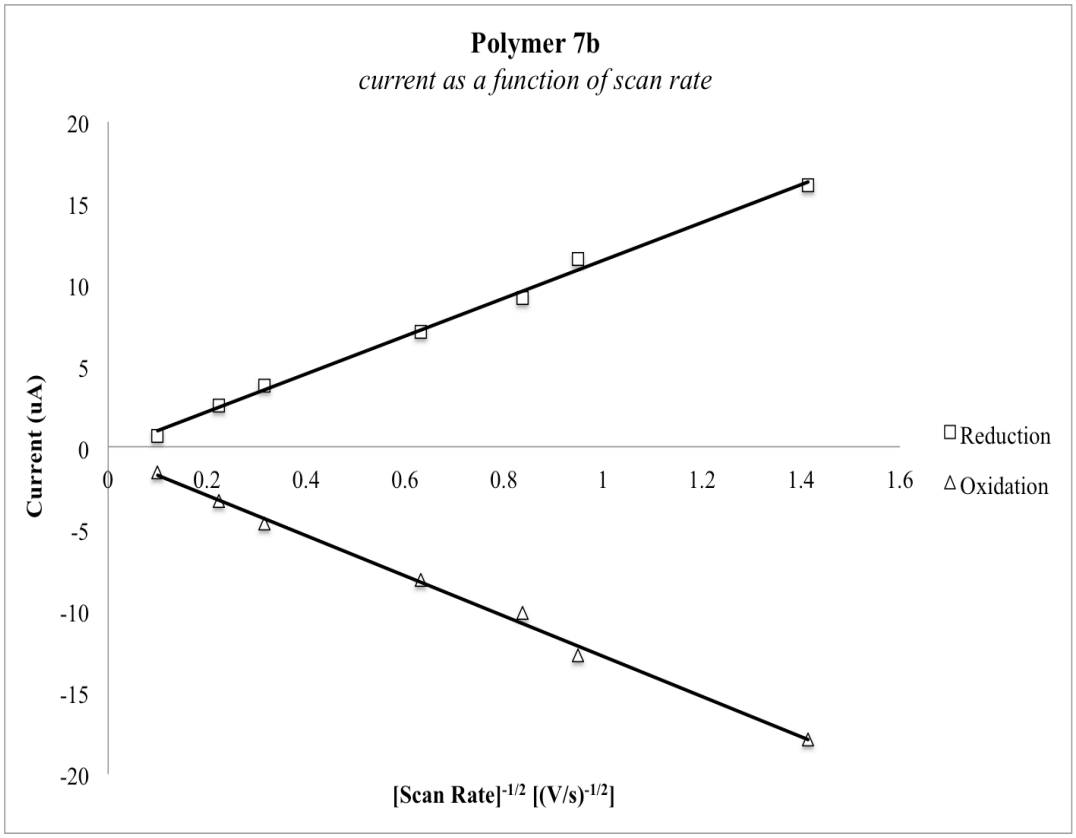

Figure A5.6. Current as a function of scan rate for polymer **7b**.

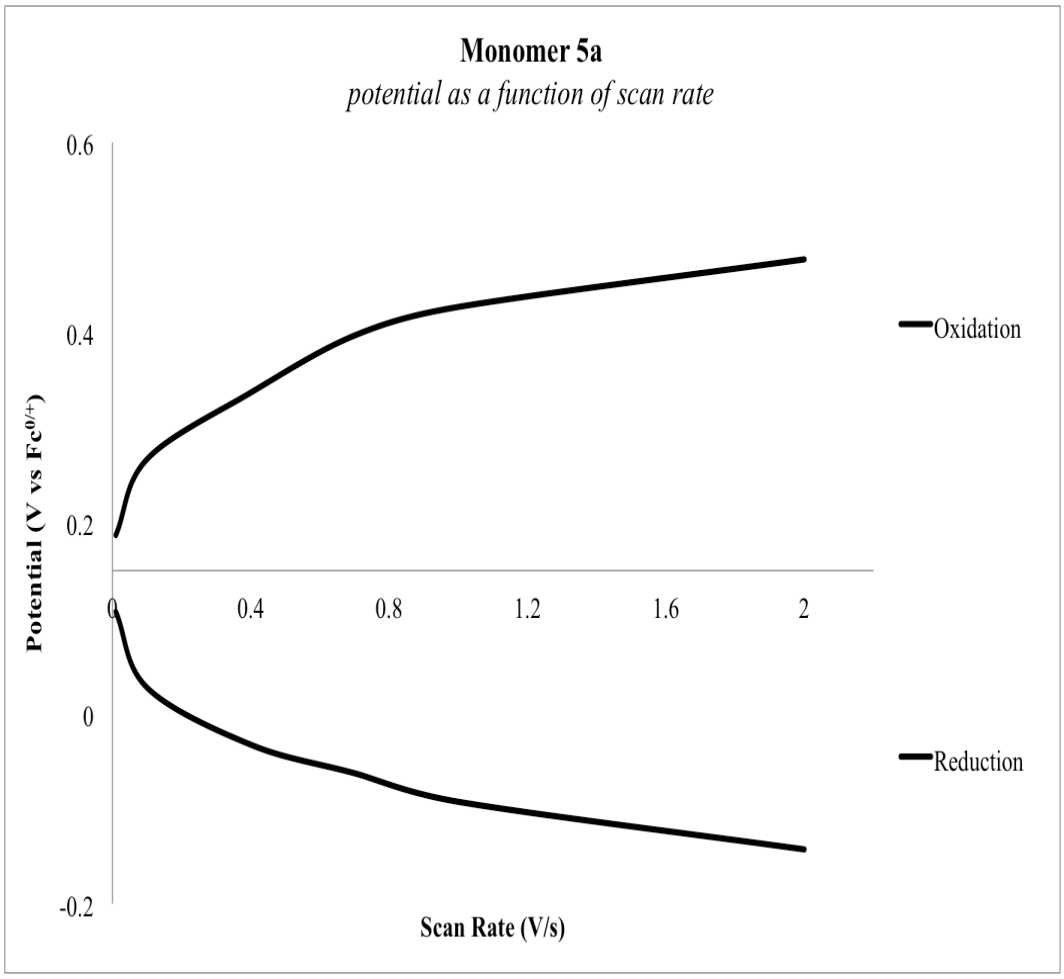

Figure A5.7. Potential as a function of scan rate for monomer **5a**

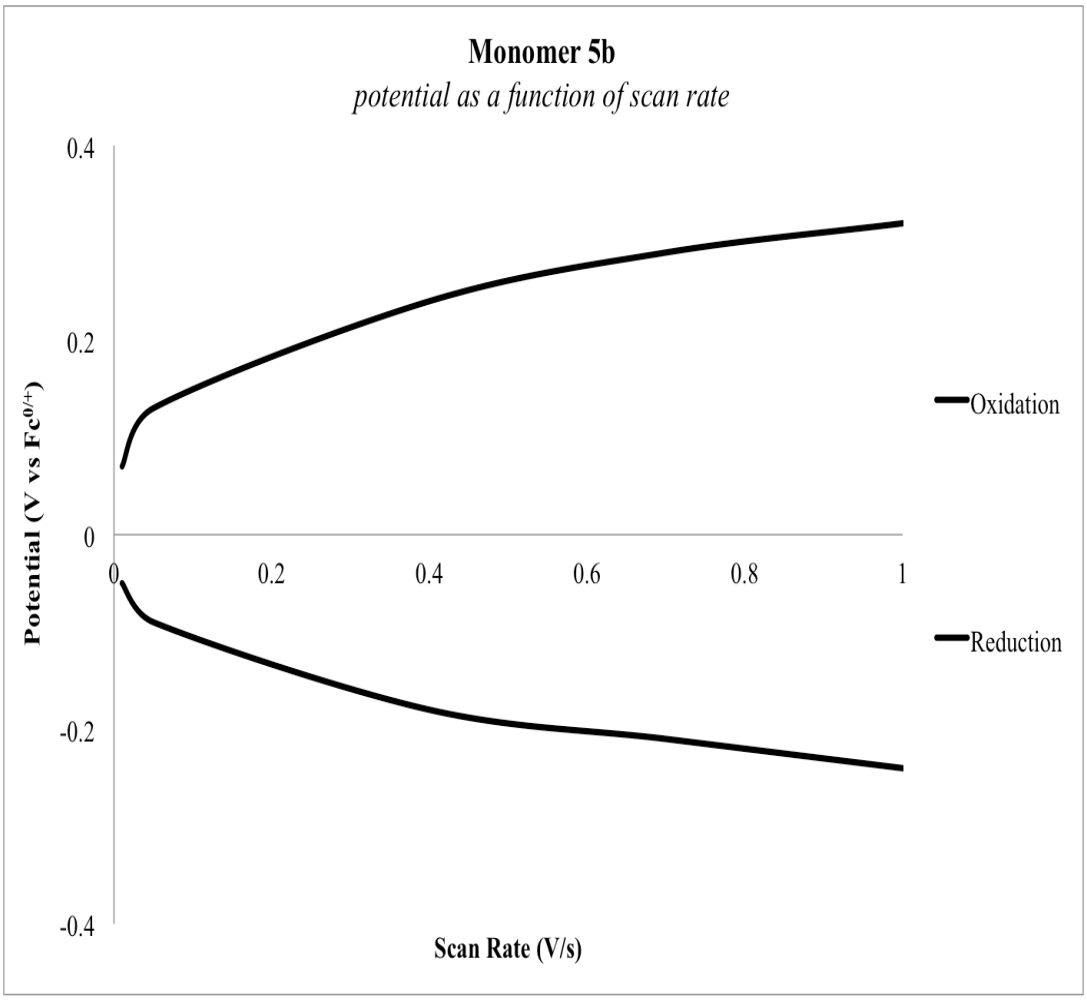

Figure A5.8. Potential as a function of scan rate for monomer **5b**.

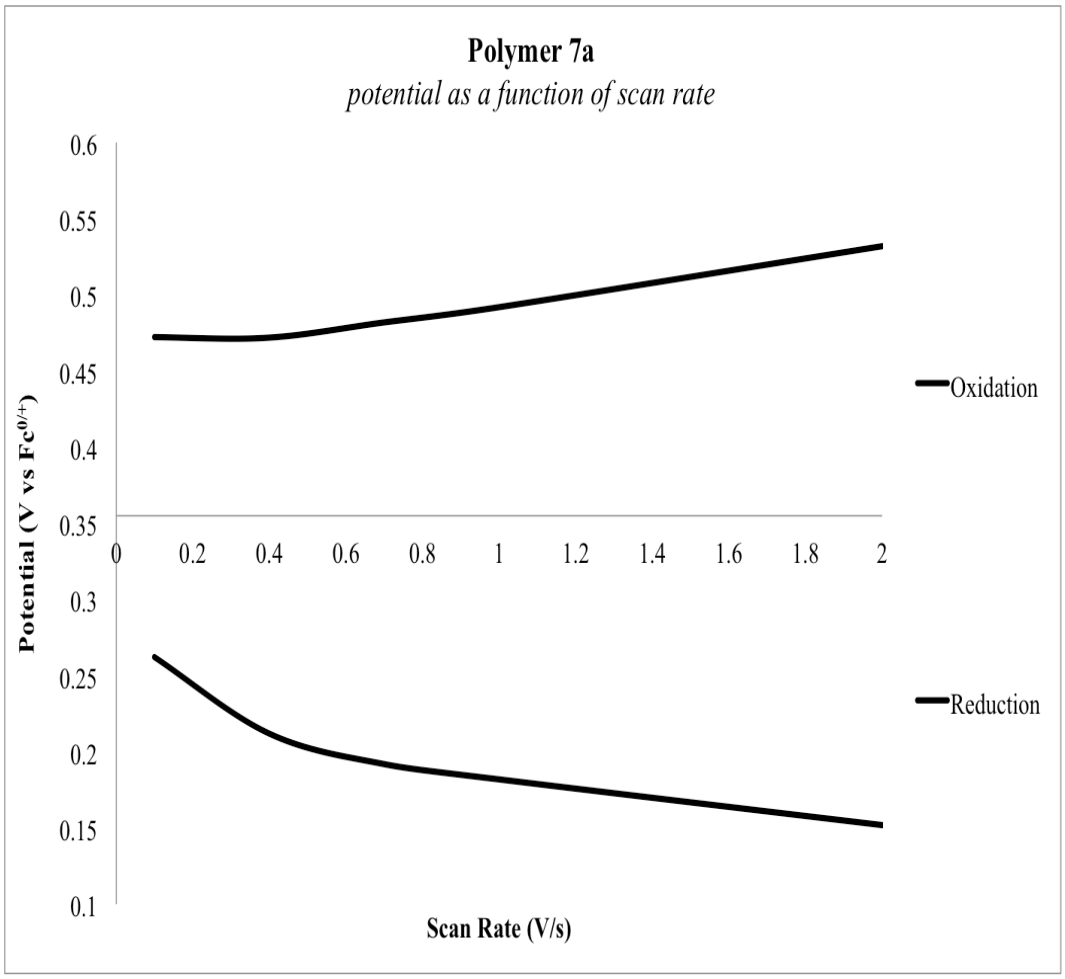

Figure A5.9. Potential as a function of scan rate for polymer **7a**.

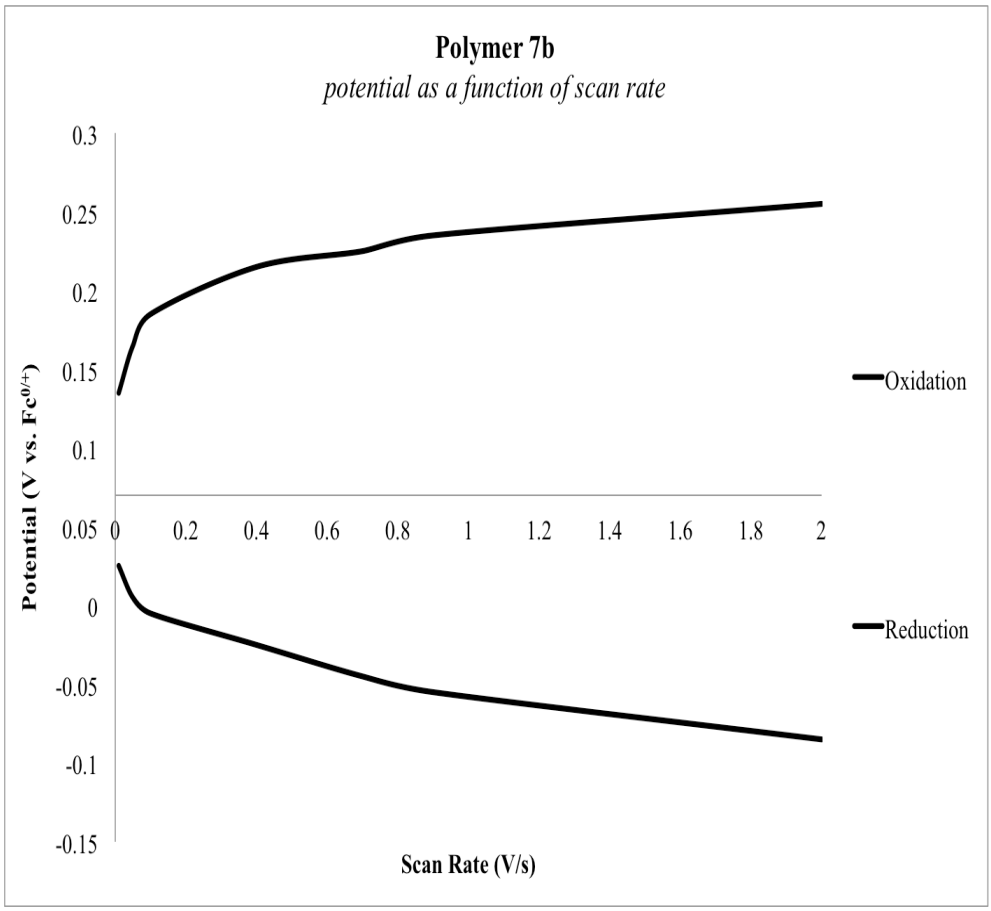

Figure A5.10. Potential as a function of scan rate for **7b**.

	Compound	$E_{1/2}$ (V vs $Fc^{0/+}$)	ΔE(V)
Carbonate Monomers	**5a**	0.020	0.14
	5b	0.372	0.11
Lactone Monomers	**6a**	–0.015	0.17
	6b	0.045	0.12
Carbonate Polymers	**7a**	0.367	0.17
	7b	0.100	0.15

Table A5.1. Redox potentials of lactone monomers and cyclic carbonate monomers and polymers, 10 mV/s scan rate.

$$\frac{n_x}{n_{fc}} = \frac{s_x^2 \times i_{fc} \times c_{fc}}{s_{fc}^2 \times i_x \times c_x}$$

Sample	Slope of Cottrell plot, **s**($x10^6$)	Steady-state current, **i**($x10^9$)	Concentration, **c**($x10^3$)
ferrocene	-38.05	-14.11	14.79
7a	-6.07	-1.06	0.11

Table A5.2. Chronoamperometry Data.

REFERENCES FOR PART TWO

(1) Kealy, T. J.; Pauson, P. L. *Nature* **1951**, *168*, 1039–1040.

(2) Masato, N.; Cyr, P. W.; Kun, L.; Sargent, E. H.; Manners, I. *Adv. Funct. Mater.* **2008**, *18*, 470–477.

(3) Cyr, P. W.; Klem, E. J. D.; Sargent, E. H.; Manners, I. *Chem. Mat.* **2005**, *17*, 5770–5773.

(4) Cyr, P. W.; Tzolov, M.; Hines, M. A.; Manners, I.; Sargent, E. H.; Scholes, G. D. *J. Mater. Sci.* **2003**, *13*, 2213–2219.

(5) Kulbaba, K.; Manners, I. *Macromol. Rapid. Commun.* **2001**, *22*, 711–724.

(6) Meegan, M. J.; Lloyd, D. G. *Curr. Med. Chem.* **2003**, *10*, 181–210.

(7) Musa, M. A.; Khan, M. O.; Cooperwood, J. S. *Curr. Med. Chem.* **2007**, *14*, 1249–1261.

(8) Leclercq, G.; Lacroix, M.; Laios, I.; Laurent, G. *Curr. Cancer Drug Targets* **2006**, *6*, 39–64.

(9) Blackie, M. A.; Beagley, P.; Croft, S. L.; Kendrick, H.; Moss, J. R.; Chibale, K. *Bioorg. Med. Chem.* **2007**, *15*, 6510–6516.

(10) Golan, S.; Aytar, B. S.; Muller, J. P. E.; Kondo, Y.; Lynn, D. M.; Abbott, N. L.; Talmont, Y. *Langmuir* **2011**, *27*, 6615–6621.

(11) Fouda, M. F. R.; Abd-Elzaher, M. M.; Abdelsamaia, R. A.; Labib, A. A. *Appl. Organomet. Chem.* **2007**, *21*, 613–625.

(12) Kovjazin, R.; Eldar, T.; Patya, M.; Vinichkin, A.; Lander, H. M.; Novogrodsky, A. *FASEB J.* **2003**, *17*, 467–511.

(13) Caldwell, G.; G., M. M.; Neuse, E. W.; van Rensburg, C. E. J. *Appl. Organomet. Chem.* **1998**, *12*, 793–799.

(14) Hillard, E. *Angew. Chem. Int. Ed.* **2006**, *45*, 285–290.

(15) Nikula, K. J.; Sun, J. D.; Barr, E. B.; Bechtold, W. E.; Haley, P. J.; Benson, J. M.; Edison, A. F.; Burt, D. G.; Dahl, A. R.; Henderson, R. F.; Chang, I. Y.; Mauderly, J. L.; Diter, M. P.; Hobbs, C. H. *Fundam. Appl. Toxicol.* **1993**, *21*, 127–139.

(16) Ward, J. F. *Prog. Nucleic. Acid Res. Mol. Biol.* **1988**, *35*, 95–125.

(17) Preston, R. J. *Health Physics* **2005**, *88*, 545–556.

(18) Wallace, S. S. *Free Radic. Biol. Med.* **2002**, *33*, 1–14.

(19) Marguiles, B. S.; Damron, T. A.; Allen, M. J. *J. Orthop. Res.* **2008**, *26*, 1512–1519.

(20) Mell, L. K.; Movasas, B. *Expert Opin. Drug Met.* **2008**, *4*, 1341–1350.

(21) Caldwell, G.; Meirim, M. C.; Neuse, E. W.; Beloussow, K.; Shen, W.-C. *J. Inorg. Organomet. Polym.* **2000**, *10*, 93–101.

(22) Cooper, B. M.; Chan-Seng, D.; Samanta, D.; Zhang, X.; Parelkar, S.; Emrick, T. *Chem. Commun.* **2009**, 815–817.

(23) Sanders, R.; Mueller-Westerhoff, U. T. *J. Organomet. Chem* **1996**, *512*, 219–224.

(24) Tang, T.; Liu, X. F.; Zhang, L. Y.; Xu, X. L.; Zhan, P. R. *Synth. Commun.* **2000**, *30*, 1657–1660.

(25) Breit, B.; Breuninger, D. *Synthesis* **2005**, *16*, 2782–2786.

(26) Graham, P. J.; Lindsey, R. V.; Parshall, G. W.; Peterson, M. L.; Whitman, G. M. *J. Am. Chem. Soc.* **1957**, *79*, 3416–3420.

(27) Hamilton, D. E. *J. Chem. Educ.* **1991**, *68*, A143–A144.

(28) Ciampi, S.; Eggers, P. K.; Guillaume, L. S.; James, M.; Harper, J. B.; Gooding, J. J. *Langmuir* **2009**, *25*, 2530–2539.

(29) Aguilar-Aguilar, A.; Allen, A. D.; Cabrera, E. P.; Fedorov, A.; Fu, N.; Henry-Riyad, H.; Leuninger, J.; Schmid, U.; Tidwell, T. T.; Verma, R. *J. Org. Chem.* **2005**, *70*, 9556–9561.

(30) Pratt, R. C.; Nederberg, F.; Waymouth, R. M.; Hedrick, J. L. *Chem. Commun.* **2008**, 114–116.

(31) Parrish, B.; Breitenkamp, R. B.; Emrick, T. *J. Am. Chem. Soc.* **2005**, *127*, 7404–7410.

(32) Jazkewitsch, O.; Mondrzyk, A.; Staffel, R.; Ritter, H. *Macromolecules* **2011**, *44*, 1365–1371.

(33) Denmark, S. E.; Yang, S. M. *J. Am. Chem. Soc.* **2004**, *126*, 12432–12440.

(34) Kricheldorf, H. R.; Kreiser-Saunders, I.; Boettcher, C. *Polymer* **1995**, 1253–1259.

(35) Zhu, K. J.; Hendren, R. W.; Jensen, K.; Pitt, C. G. *Macromolecules* **1991**, *24*, 1736–1740.

(36) Rokick, G. *Prog. Polym. Sci.* **2000**, 259–342.

(37) Lohmeijer, B. G. G.; Pratt, R. C.; Leibfarth, F.; Logan, J. W.; Long, D. A.; Dove, A. P.; Nederberg, F.; Choi, J.; Wade, C.; Waymouth, R. M.; Hedrick, J. L. *Macromolecules* **2006**, *39*, 8574–8583.

(38) Sudhit, V. S.; Venkateswarlu, C.; Muhammet-Musthafa, O. T.; Sampath, S.; Chandrasekaran, S. *Eur. J. Org. Chem.* **2009**, *13*, 2120–2129.

(39) Lingane, P. J. *Anal. Chem.* **1964**, *36*, 1723–1726.

(40) Brown, O. R. *J. Electroanal. Chem.* **1972**, *34*, 419–423.

(41) A. S. Fawcett, W. R.; Gilbert, C. M. *Anal. Chem.* **1985**, *57*, 166–170.

(42) Crumbliss, A. L.; Cooke, D.; Castillo, J.; Wisian-Neilson, P. *Inorg. Chem.* **1993**, *32*, 6088–6094.

(43) Flanagan, J. B.; Margel, S.; Bard, A. J.; Anson, F. C. *J. Am. Chem. Soc.* **1978**, *100*, 4248–4253.

(44) Thomson, R. K.; Scott, B. L.; Morris, D. E.; Kiplinger, J. L. *Cr. Chim.* **2010**, *13*, 790.

(45) Bildstein, B.; Malaun, M.; Kopacka, H.; Wurst, K.; Mitterbock, M.; Ongania, K.-H.; Opromolla, G.; Zanello, P. *Organometallics* **1999**, *18*, 4325–4336.

(46) Tennyson, A. G.; Khramov, D. M.; Varnado, C. D.; Creswell, P. T.; Kamplain, J. W.; Lynch, V. M.; Bielawski, C. W. *Organometallics* **2009**, *28*, 5142–5147.

(47) Wu, P.; Malkoch, M.; Hunt, J. N.; Vestberg, R.; Kaltgrad, E.; Finn, M. G.; Fokin, V. V.; Sharpless, K. B.; Hawker, C. J. *Chem. Commun.* **2005**, 5775–5777.